UNIVERSITY OF BIRMINGHAM

The Processing and Characterisation of Recycled NdFeB based Magnets

By

Salahadin Muhammed Ali Adrwish

A thesis submitted to the University of Birmingham for the degree of

Doctor of Philosphy

Supervisors

Prof. I.R. Harris

Dr. A.J. Williams

School of Metallurgy and materials

University of Birmingham

B15 2TT

CONTENTS

Chapter 10

Appendix A

References

Acknowledgement

My sincere thanks go to Prof. Rex Harris and to Dr Andrew Williams for having the confidence in me to complete this project. Further thanks go to my friend Dr Miha Zakotnik for his academic advice and for being patient to accommodate my technical needs.

My thanks also go to Drs Alex Bevan, Allan Walton and all the members of the Applied Alloy Chemistry (AACG) Group. The group had provided me with an occasional tranquil time which was not available in any of my previous working environments.

I could not forget about my wife Samira and my children: Hajer, Mosab, Amena, Nada and Amira who have given up so much and received very little. This work is dedicated to them and to the fallen heroes of Libya. For all of those people who helped me even with a smile, I am eternally grateful and I won't forget them. I have to thank my Mother and Father whom I love dearly and for their constant encouragement and they supported me in their "unique way" throughout the years.

Finally, a great gratitude go to Dr Winson KUO and my friend Maggie Harris for their endless help throughout.

List of Abbreviations

B_r	remanence	mT
BH_{max}	maximum energy product	kJ/m^3
${}_jH_c$	intrinsic coercivity	kA/m
${}_bH_c$	inductive coercivity	kA/m
at%	atomic weight percentage	
wt%	weight percentage	
LPPS	low pressure packing sublimation	
ρ	Density	g/cm^3
C	China magnets	
P	Philips magnets	
U	USA magnets	
N	Neomax Alloy/magnets	
I	IPMni magnets (Japan)	
HD	Hydrogen Decrepitation	
CSP	concentrated solar power	
Cixi	a Chinese electronic product- made in Cixi City	
HDD	Hard Disc Drive	
HRSEM	High resolution secondary electron microscope	
EDX	Energy Dispersive X-ray	
IMS	Industrial Methanol Spirit	
DSC	Differential Scanning Calorimetry	
HTP	Heat treatment Process	
H	hours	

Synopsis

The main aims of this work presented here were to develop viable methods of recycling NdFeB– based permanent magnet and to characterise the final products.
The starting permanent magnets were supplied by several magnet producers/suppliers and the hydrogen decrepitation (HD) process has been used as the main method of recycling the magnets. Conventional sintering was used to produce recycled magnets, the magnetic properties of which were compared with those of the corresponding magnets produced by commercial means. The main conditions, to be optimised at this stage of the work, were the milling and the sintering times.

The magnets were turned into a powder using the HD process. Then the powder was milled for specific times (conditions) and then sintered (1-3 h) at 1090 ºC. The resultant magnet samples were measured using a permeameter to determine their magnetic properties. Cross sections of these samples were also mounted in bakelite and metallographic studies carried out using SEM on a JOEL 6060 and 7000.

Some of the recycled magnets achieved magnetic properties close to those of the starting magnets. It was shown that the nature of the starting magnets determines the appropriate sintering conditions adopted during recycling. Sintering for 3 h proved to be effective for magnets with a high oxygen content but was too long for the non-oxidised material and for magnets with a lower oxygen content.

Because of the lean rare-earth content some magnets were studied further. These were subjected to various heat treatments and other techniques (such as grain boundary diffusion) and with the addition of various additives such as Dy, Co, Nd, Nb and Tb. In the case of the earth metals, the additives were often in the form of hydrides.

To characterise their corrosion resistance, a study was made of how the recycled magnets behaved in a 3% salt solution and these were compared with that of the starting magnets. The corrosion study was conducted over a period of 20 weeks and, generally, the results indicated that the recycled magnets exhibited better corrosion resistance than that of the original material. These studies also revealed the anisotropic nature of the corrosion process under these conditions with accelerated

reactions along the c-axis of the magnets. The data also indicated accelerated corrosion rates in the magnetised state. It was shown that the corrosion reaction initiated at the Nd rich phase and propagates further with time. Furthermore, the magnetic properties decrease over the period, as expected.

Further work is required to optimise the sintering conditions in order to produce lower oxygen content in the recycled magnets. Alternative processing routes, e.g. hot pressing/spark plasma sintering, should be investigated as a means of recycling the scrap magnets, perhaps under the same conditions regardless of composition.

1. Aims of the Project

The goal of this work is to investigate the optimisation of the Hydrogen Decrepitation (HD) process, applied to the re-cycling of high-energy product sintered magnets based on NdFeB. The project could lead to a cost-effective process for the recycling of sintered NdFeB-type magnets by producing powders with high coercivities suitable for use in the production of sintered or bonded magnets with acceptable magnetic properties.

The research utilises a range of techniques available within the School of Metallurgy and Materials at Birmingham University, including:

a) **Metallography**- employed to study the microstructure and phase analysis of the recycled sintered magnets;

b) **Density measurements**- to indicate the effectiveness of the sintering process;

d) **Magnetic characterisation**- to determine the magnetic properties of the recycled products;

c) **Addition of rare earth elements** (Dy, Nd, Tb) and niobium (Nb) to the recycled powder;

d) **Corrosion studies** using a 3% NaCl solution

Outside the School, the chemical analyses of the sintered products were measured by **Inductive Coupled Plasma Analysis (ICP)** in order to study the magnet composition. Less Common Metals, Liverpool UK, conducted these measurements.

This project seeks to develop further the existing work on the hydrogen decrepitation of rare-earth magnets, which has been proposed as a means of recycling NdFeB magnets by Rivoirard. et al., (2000), (Burns, et al. (2000) and by Zakotnik et al., (2006). Their work reports very encouraging results on the production of anisotropic powder from degassed hydrogen decrepitated (HD) powder obtained from sintered

NdFeB magnets. A flow chart of the process developed in the course of this project is shown in Figure 1-1 below.

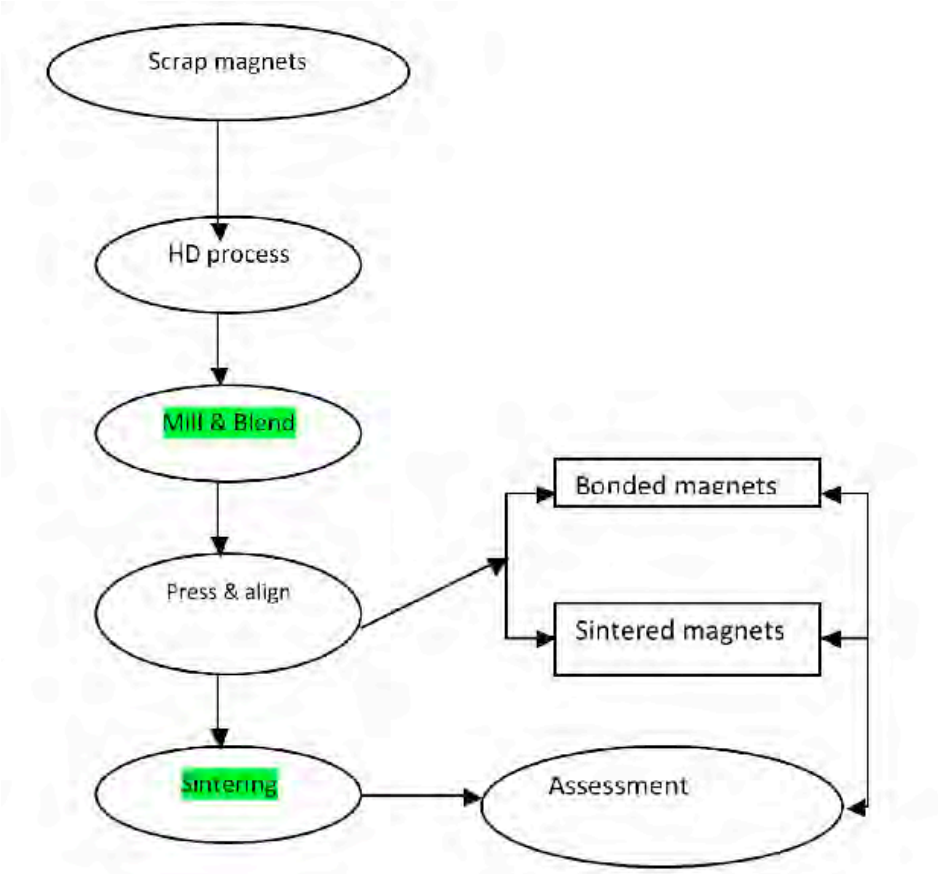

Figure 1-1: Flow chart of process of magnet recycling used in this project.

The recycling of NdFeB-type magnets in this manner is of growing importance due to their application in the expanding field of electric vehicles and an increased emphasis on materials and energy conservation. By optimising the recycling process, it is possible to produce an energy efficient material, which may be effectively recycled, and this is particularly true for hard drive applications where “end of life” rules apply (Harris et al., 1995).

An optimised recycling process can be justified further by considering the environmental impact of reducing metal contamination at landfill sites, reducing CO_2 emissions and counter-acting resource depletion (particularly for the less common rare earth elements such as dysprosium (Dy)).

This project aims to optimise the HD process for a range of recycled magnets and compare and contrast to a reference material. These magnets (and their suppliers) are summarised in Table 1- 1.

Table 1- 1 Table of Materials and Suppliers

Material	**Source**	**Referred to in text**
China magnets	Precision Magnetics Ltd, Rotherham, UK (now known as Arnolds).	China or C
USA Magnets	Val Pareiso of Indiana, USA (Philips)	USA or U
European Magnets	Philips, Southport, Lancashire (now closed)	Philips or P
IPM Magnets	by Shen-Etsu Chemical Ltd, Echizen City, Fukui, Japan	IPM or I
Cast Alloy (reference material)	Less Common Metals, Liverpool, UK	Neomax or N

By studying the different sintering and magnetic performance of each type of magnet recycled, it is possible to establish the individual optimum processing conditions for each composition. The optimum processing conditions are established for each

magnet type in terms of the sintering time, sintering temperature and milling time. The possibility of adding another rare earth element such as Dy, Nd or Tb in order to improve the magnetic properties is also explored and an explanation as to why these recycled magnets are subject to different optimum conditions is attempted with particular reference to the effect of oxygen.

The final objective of this project is to study the reaction of the starting material in comparisons with the recycled magnets through the corrosion testing using saline liquid designed to mimic sea water environment.

An evaluation attempt as to what the cost of recycling process of scrap magnets is considered so that this may become a cost effective method of conserving vital raw materials and of reducing the overall energy consumption.

2.0 Commercial use of NdFeB magnets

2.1 Development of NdFeB-type magnets:

A big leap in the development of permanent magnet production came with the discovery of $Nd_{15}Fe_{77}B_8$ (trade name "Neomax") in 1984 by Sumitomto Special Metals of Japan. Magnets of this type offer good coercivity and high remanence values, and possess the highest energy product available. Recent developments (Kaneko et al. 2006) have resulted in magnets with an energy product of 460 kJ/m^3 and Br value 1.533 T corresponding to almost 96% of the theoretical value of the $Nd_2Fe_{14}B$ system. However, the world record for energy product was established in 2006 at 474 kJ/m^3 by NEOMAX Co. Ltd. (Matsuura, 2006). Figure 2- 1 shows the trend of the improvement of permanent magnet properties (Zakotnik, 2008) against time and suggests how the properties may improve in the future. (The red square is the projected BH_{max} in the future).

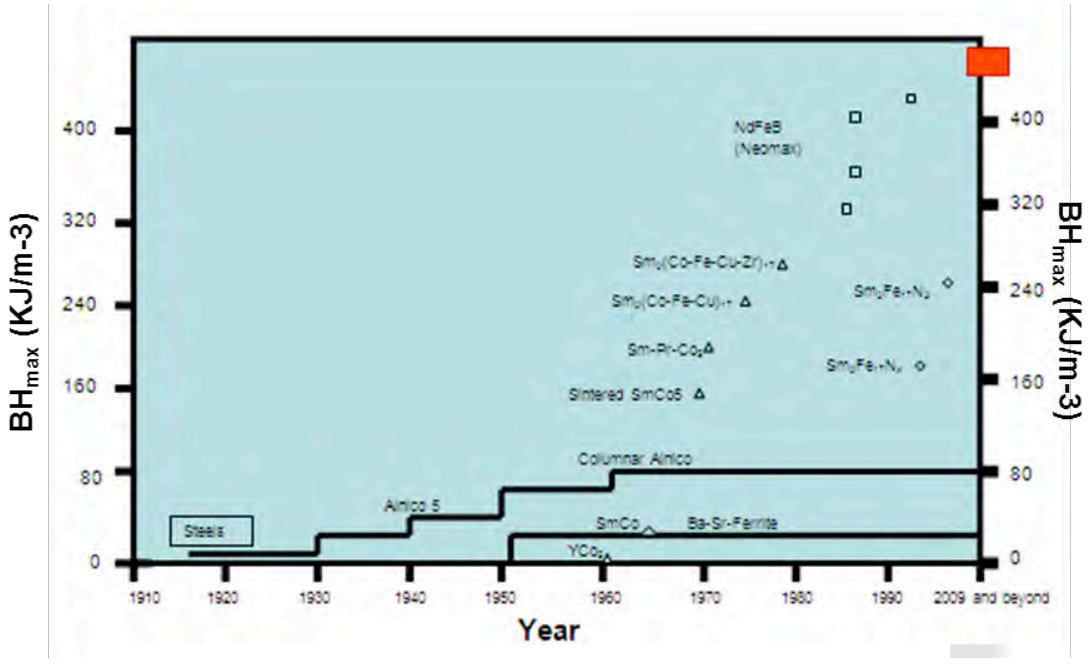

Figure 2- 1 Improvements in the energy product of permanent magnet. (adapted from Zakotnik, 2008)

Although the NdFeB permanent magnets have superior magnetic properties at room temperature when compared to other magnetic materials, application of these magnets are limited to relatively low operating temperatures (e.g. 150 ^{o}C to 200 ^{o}C), because of the low Curie temperature (312 ^{o}C), poor corrosion resistance and poor temperature coefficient of coercivity and remanence. On the other hand, SmCo ($SmCo_5$ and $Sm_2(Co,Fe,Cu,Zr)_{17}$) magnets can be employed in more demanding environments and high temperature (e.g. 250 ^{o}C and 350 ^{o}C) as their Curie temperatures approach ≈ 800 ^{o}C which is significantly higher than NdFeB (Zakotnik, 2008).

2.2 Global NdFeB Market

Since the discovery of NdFeB permanent magnets in the early 1980's, the annual global NdFeB output has risen dramatically from just 1 tonne per annum in 1983 to nearly 40,000 tonnes in 2005 (Yang, 2006). This rise in global production is clearly shown in Figure 2- 2 which plots total global production of sintered NdFeB magnets over 20 years.

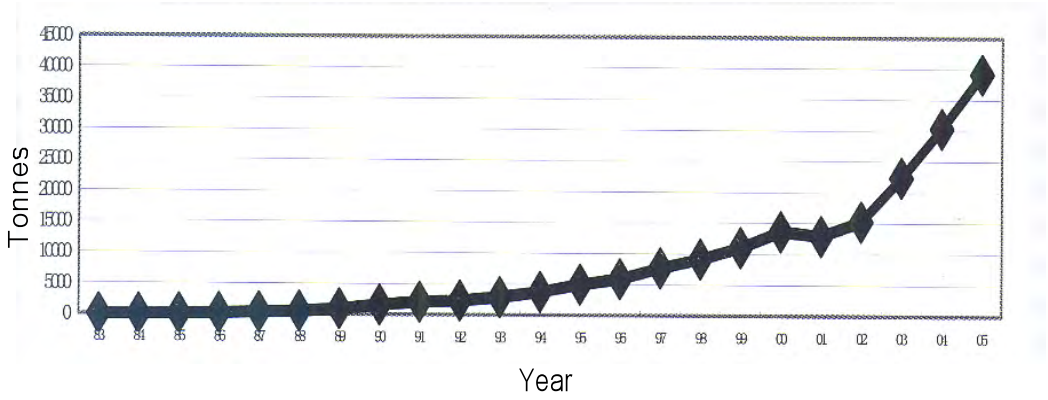

Figure 2- 2 Global output of sintered NdFeB between 1983 and 2005 (in tonnes) (taken from: L. Yang, 2006)

This variation shows that, up to 1988, the production was quite stable and at the beginning of the 1990's, the production rose dramatically with an annual increase of ~ 50%. The slight dip was due to the economic recession in that period. This caused the USA to halt production by 2003. There is now, very little production in Europe left and only China and to lesser extent, Japan, are the largest producers of NdFeB sintered magnets. The global output at the present day is much higher at about 100,000 tonnes ***(not shown in figure 2-3)***.

Global output has continued to rise and data from 2010 suggests that the most recent annual global production figures of 100,000 tonnes per annum are quite credible) (China RE report 2010).

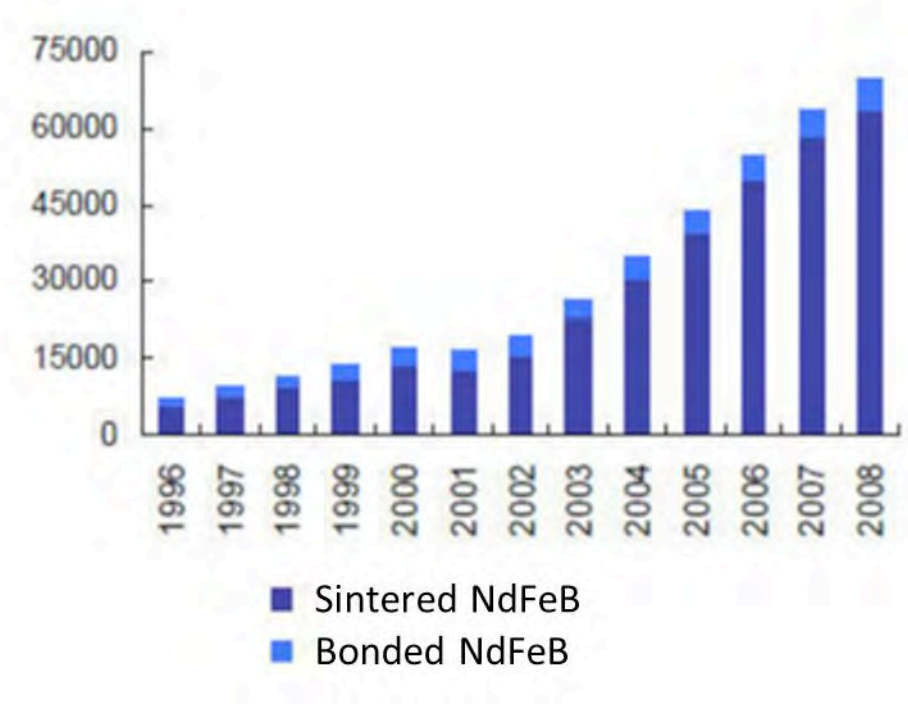

Figure 2- 3 Global Output of Nd-Fe-B Magnet between 1996-2008 (in tonnes). ***(Adapted from China Rare Earth Permanent Magnet Industry report, 2009-2010)***

Following the recession (Global : 2001-2, 2008-2009 (IMF)), global sintered NdFeB output volume saw a reduced annual average growth rate of 26.5% (China Rare Earth Permanent Magnet Industry report, 2009-2010). The sustained production growth is

attributed to breakthroughs in production technology, including the use of airflow grinders instead of the wet granulation system although most manufacturers still use locally made strip casting and hydrogen decrepitation (HD) equipment (China Rare Earth Permanent Magnet Industry report, 2009-2010).

2.3 Major NdFeB Producers

Due to the sharp rise in the production costs in the West and a reduction in the sales price in the international market, magnet production in the developed countries has become unsustainable. Japan experienced a decrease in 2001 and although they have managed a recovery of 10% of their annual production rate, in 2005, they still only produce 3.5 times less than their nearest competitor, China. The majority of magnets imported by the USA and Europe are now of Chinese origin and their dominance is shown in Figure 2- 4 which details annual production (in tonnes), % total production and % market share for the major NdFeB producers. The global production in 2005 was estimated at 40,000 tonnes of which around 30,000 tonnes (currently around 100,000 tonnes) were produced by China. About 9000 tonnes was Japan's share and the remainder was Europe and other countries. The total sale value of the NdFeB market for 2005 was $1.7 billion US. As discussed earlier, the USA had ceased to produce NdFeB by this date.

	Output, ton	%	Average Price, $/kg	Sales Value, $*10^6	%
China	30,160	77.1	32	965.12	56.2
Japan	8,500	21.7	84	714	41.6
USA	-	-	-	-	-
Europe	450	1.2	82	36.9	2.2
Global Total	39,110	100	43.5	1716.02	100

Figure 2- 4 Output (in tonnes) and Market share (in $ x10^6 and %) of major NdFeB producers in 2005 (taken from: L. Yang, (2006))

The challenge of contracting the Chinese dominance of the market has prompted Japan to concentrate on its fine quality magnets and open the door for the

miniaturisation of magnets production (less than 25 mm thickness) which can be used in more specialist industries such as automotive and medical applications. Indeed, Japan imports considerable amounts of NdFeB alloy from China to process into magnets, compliant with the standards within Japan. (L. Yang, 2006).

Due to a rise in production costs, increased taxation in the West and a general global decline in the sale of magnets, many western manufacturers have folded or merged with other partners. Many of the manufacturers still operating have opted to transfer their plants to mainland China where the cost of running a business is much lower than in the West and, as a result, since 2001 China has became the number one producer of NdFeB-based sintered magnets (Yang, 2008): of the 40,000 tonnes of NdFeB produced in 2005, Chinese production accounted for 78.6% of the global aggregate with the production rising by another 30% to 39,000 tonnes in 2006 (China Electronic Components Association, 2006*).*

China exported 28% of its total NdFeB production in 2006 (valued at more than $300 million) and export levels are set to remain at current levels. It is not surprising then, that China is thought to be responsible for 97.5% of all rare-earth production (Hatch, 2010) Figure 2- 5 demonstrates that, as well as controlling 72.6% of the total NdFeB market in 2005, China also held 51% and 56% of the total global hard ferrite and Alnico magnet markets, respectively.

The United States, Japan, Singapore and South Korea are the top export destinations for sintered NdFeB magnets from mainland China, although Chinese magnet suppliers expect their shipments to increase further during 2010. However, they will continue to allot a large share of their monthly output for their local market, including Hong Kong (Hatch, 2010)

Country/Area	Alnico[3]	Hard Ferrite[4–6]	NdFeB.[6–8]
China	3,500t (56%)	(S) 390,000t (54.3%)	(S) 30,160t (77.1%)
		(B) 65,000t (37.5%)	(B) 1700t (35.7%)
		(T) 455,000t (51%)	(T) 31,860t (72.6%)
Japan	300t (5%)	(S) 180,000t (25%)	(S) 85,00t (21.7%)
		(B) 13,000t (7.5%)	(B) 560t (11.8%)
		(T) 193,000t (21.6%)	(T) 9060t (20.7%)
USA	700t (11%)	(S) 40,000t (5.6%)	(S) -
		(B) 41,000t (23.6%)	(B) 200t (4.2%)
		(T) 81,000t (9.1%)	(T) 200t (0.5%)
Europe	750t (12%)	(S) 49,000t (6.8%)	(S) 450t (1.2%)
		(B) 44,000t (25.4%)	(B) 350t (7.3%)
		(T) 93,000t (10.4%)	(T) 800t (1.8%)
Others	1,000t (16%)	(S) 60,000t (8.3%)	(S) -
		(B) 10,500t (6%)	(B) 1,950t (41%)
		(T) 70,500t (7.9%)	(T) 1,950t (4.4%)
Global total	6,250t	(S) 719,000t	(S) 39,110t
		(B) 173,500t	(B) 4,760t
		(T) 892,500t	(T) 43,870t

Note: S—Sintered magnet; B—Bonded magnet; T—Global total.

Figure 2- 5: Global output of Alnico, Hard-Ferrite and NdFeB magnets for the top producers in 2005 (in tonnes). ***(Adapted from L. Yang, 2006)***

In addition to experiencing lower production costs, there is a fundamental difference in attitude toward production in China compared to that in the West. In China, investment is kept to a minimum in order to maximise returns and it is this approach which has had a major impact on resources and the environment and has allowed the Chinese to market to produce NdFeB-type magnets at a relatively low cost. This is illustrated in Figure 2- 6 which plots the average and individual prices offered by the top 4 NdFeB producers (in $US per kg) between 1996 and 2005. It can be seen that China has consistently marketed their sintered NdFeB-type magnets at a price below

the average and at prices significantly lower than those of products from the USA, Japan or Europe.

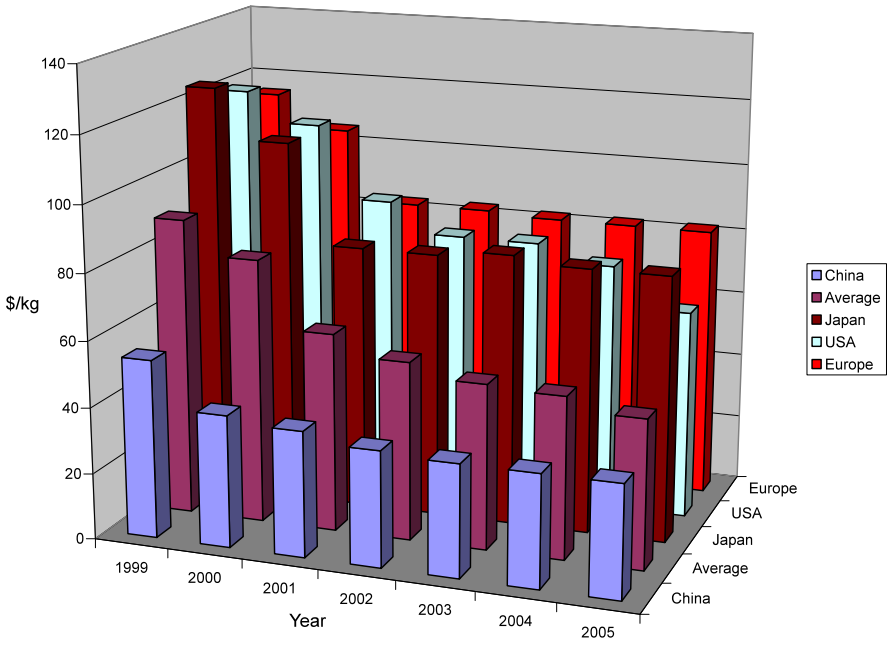

Figure 2- 6 Price changes of sintered NdFeB magnets in the top 4 producers, 1999-2005 ($US/kg) ***(adapted from: L. Yang (2006)***

Low cost has obviously made the Chinese products more attractive to buy and consequently the demand for some products such as NEOMAX and MQI has started to decrease. However, Chinese products did not initially, have penetration in the production of specialist components such as VCM (Voice Coil Motors), MRI (Magnetic Resonance Imaging) and automotive motor parts. As manufacturers could typically only produce low-end products. However, enhanced manufacturing processes and production technologies, about two-thirds of all NdFeB magnet suppliers on the mainland of China are now able to produce midrange products and, in recent years, midrange NdFeB sintered magnets (with BH_{max} of 302 to 358 kJ/m^3) have became mainstream, (Yang, 2008). These types of magnets are designed for motors and are used mostly in electric bicycles, acoustic components and toys.

The price of magnet grades has risen exponentially and the higher the grade, the higher the price. The end-user application determines the magnets individual qualities which in turn determine the price. In the case of the automotive industry, for example, the reliability of magnets should be able to withstand temperatures of 180-220 ^{o}C (Yang, 2006).

There has been a change in the production of sintered NdFeB magnets since 1983 as shown in figure 2-2. In the Chinese magnet market in 2008, there were 1096 magnetic producers of which 359 focus on the ferrites, 226 on the rare-earth and other metallic magnets with the rest producing associated equipment and auxiliary raw materials. Of the ferrite producers, 197 produce permanent ferrite with an annual output of 410,000 tonnes (of which sintered magnets account for 360,000 tonnes and bonded magnets 50,000 tonnes) 162 produce soft magnetic ferrite (269,000 tonnes), nickel-zinc ferrite and magnesium-zinc ferrite (together 40,000 tonnes) whilst NdFeB magnets was 40,000 tonnes and Alnico magnets 3500 tonnes.

2.4 Applications

In addition to its dominance in the NdFeB export market, China has a considerable domestic requirement. This is demonstrated in Figure 2- 7 which details the Chinese market value and NdFeB price, as well as their considerable domestic use and export tonnage of NdFeB between 1998 and 2007.

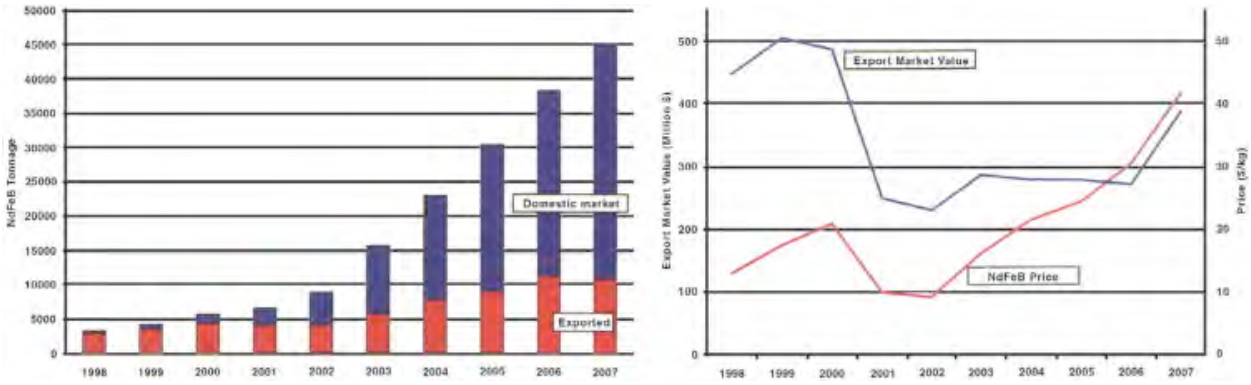

Figure 2- 7 Export and domestic NdFeB tonnage, export market value and NdFeB price in China, 1998 to 2007 (Adapted from L. Yang, 2009).

In view of their considerable domestic usage, it is useful to use the Chinese market in order to demonstrate typical applications for NdFeB magnets. Figure 2- 8 shows the % distribution of application for sintered NdFeB in China in 2005. It is important to note that the author has seemingly ignored wind generators and electric motors although it is possible that these applications may fall under other categories.

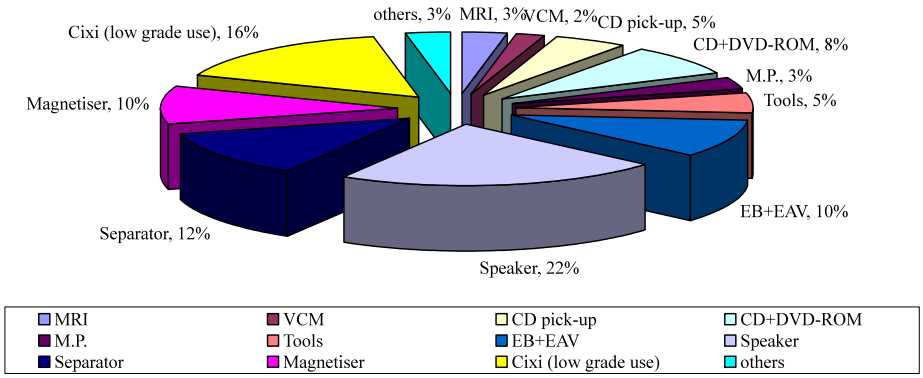

Figure 2- 8 % Distribution of applications of sintered NdFeB in China 2005. *(Adapted from L. Yang 2006).*

By analysing the applications in Figure 2- 8, it is possible to categorise the Chinese application of sintered NdFeB magnets into three distinct groups;

High-tech applications such as MRI, VCM, CD pick-up, CD-ROM/DVD-ROM, mobile phones, cordless tools, electrical bicycles and vehicles.

Traditional applications such as speakers, magnetic separator, magnetiser and de-waxer used in the oil industry.

Low grade application such as magnetic buttons for box, cases, chests and cloths.

The change in the application of the Chinese market is shown in Figure 2- 9. This graph shows how the tonnage of NdFeB produced is allocated to different applications between 1998 and 2007.

Note: Cixi are low-grade magnets products made at Cixi city and are mostly used in magnetic buttons in cases, clothing European adaptor manufacturing and furniture.

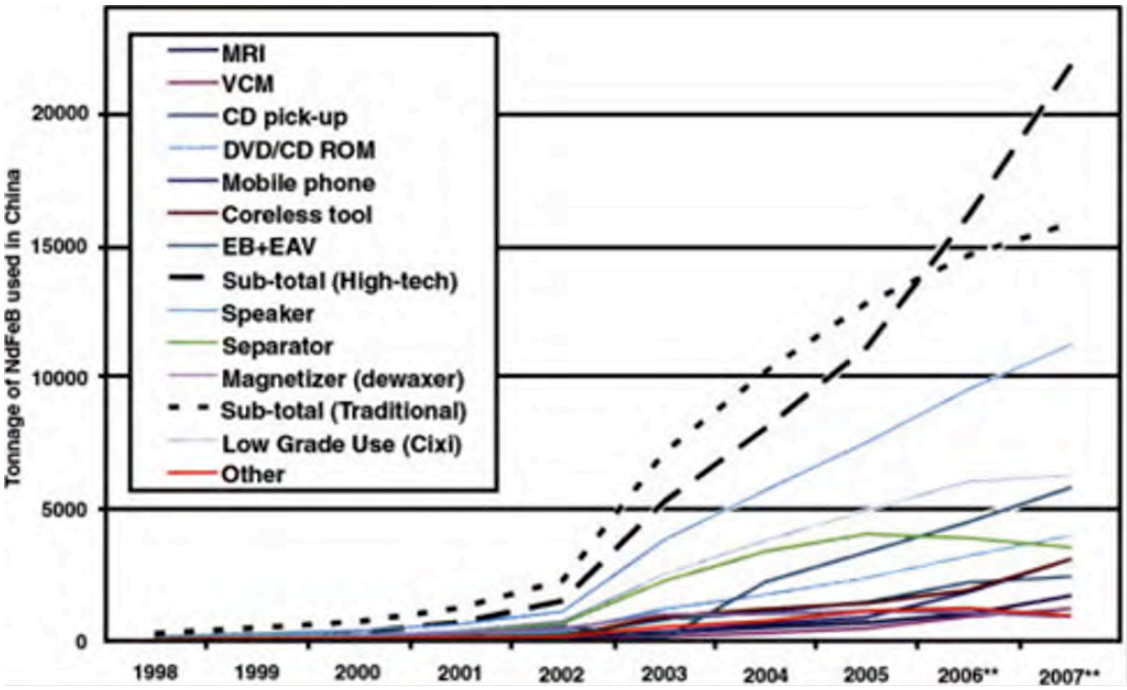

Figure 2- 9 Distribution of sintered NdFeB in applications in China 1998 to 2007 (adapted from L. Yang, 2009)

2.5 Factors affecting NdFeB supply and demand

2.5.1 IT sector

The NdFeB market relies heavily on the IT sector, where a significant proportion of more than 50% of the magnets production goes into the manufacture of voice coil motors (VCM) which are used in the production of hard disc drive (HDD) (Yang, 2006). In the past, the development within IT and NdFeB sintered magnets have developed in proportion, although this is not true anymore due to the cost. The sharp

increase in prices diverted all the attention to the Chinese magnets producers where they have managed to acquire sophisticated equipment to allow them entry into the VCM market. This is due to the zero defect production rate and the good quality of magnets now being produced by Chinese manufacturers.

Recycling of magnets in IT applications can be justified on financial grounds as well as for environmental reasons due to the sheer volume of magnets in circulation. Seagate produces hard discs for the computer manufacturers all around the world and uses approximately 20g of NdFeB magnets on each hard drive. With an estimated 600 million computers worldwide (see Figure 2- 10) this means that around 15k tonnes of NdFeB are contained in the HDD of computers alone, all of which is potentially available for recycling.

Annual Computer Shipments

	US	EU	Japan	Brazil / Mexico	China / India	
Population	300 M	250 M	125 M	300 M	2.5 Bn	
Computer ownership %	75	70	70	15	1.2	
No of computers	220 M	175 M	88 M	50 M	25 M	Total 600 M

- Total computers sold in 2008 ≈ 600 M
- Amount of sintered NdFeB per HDD = 10-20g
- At around $60-70/kg for sintered NdFeB = annual world market of - $400- $800 million

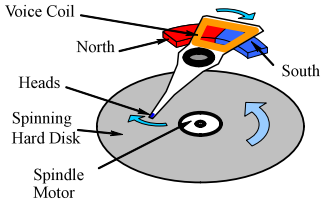

Figure 2- 10 Summary of computer ownership worldwide. ***(Speight, J.D, 2010)***

Even in the UK, the 45 million PCs equate to 900 tonnes of NdFeB available for recycling. If re-sold at an average price of, for example, half of the price of virgin metal ($42 per kg as of 2006-2008) this could generate ($22 per kg) which could provide a good income as well as conserving the plant's resources.

2.5.2 Global price of Dy and Nd

An important factor in the global output of rare-earths is the supply of dysprosium and neodymium. An ever-increasing demand for these metals has recently led to a significant increase in the price of both Dy and Nd, with the former reaching $US3500/kg and the latter 450$US by July 2011 (Metal Pages, 2011). The price increase in Chinese Dy and Nd is shown for February and July 2011 in figure 2-10. (The price of Dy in the year 2006, February was ¥800/kg (£5.45/kg)). The graphs indicate the dramatic price rise of Dy and Nd, suggesting that a peak in demand will be reached in the coming years. This will facilitate the need to implement a remedial strategy, including widespread product recycling.

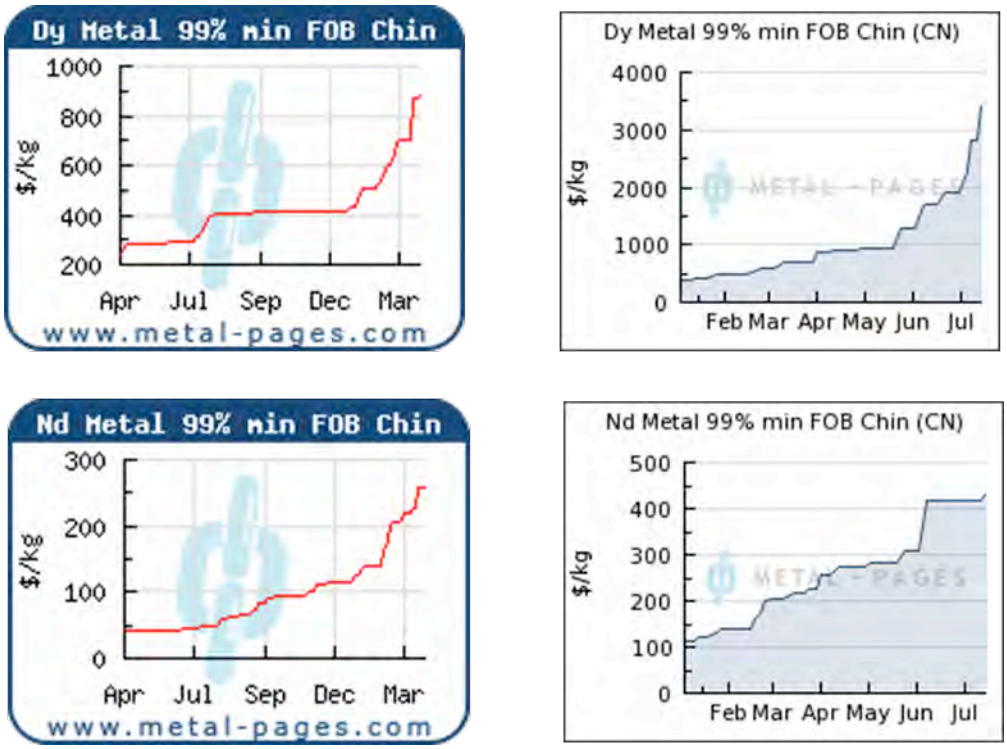

Figure 2- 11 Nd and Dy prices on 02/08/2011 from China. ***(Adapted from www.metal-pages.com)***

After June 7, 2012, according to the Metal-Pages quotations, there was a sudden fall in prices: from the highest levels of July 2011, the price of neodymium lost 52% (now 154 US$/kg); dysprosium, 40% (now 1500 US$/kg) and terbium, 23% (now 3400

US$/kg) (Metalpages Inc., 2011–2012). These changes were most likely due to different reasons: the economic crisis in industrialised countries; the contraction of hi-tech consumption; the placing on the market of large stocks of REOs by some Chinese private operators fearful of possible inspections and confiscations by the Chinese Government. (Massari et al., 2012)

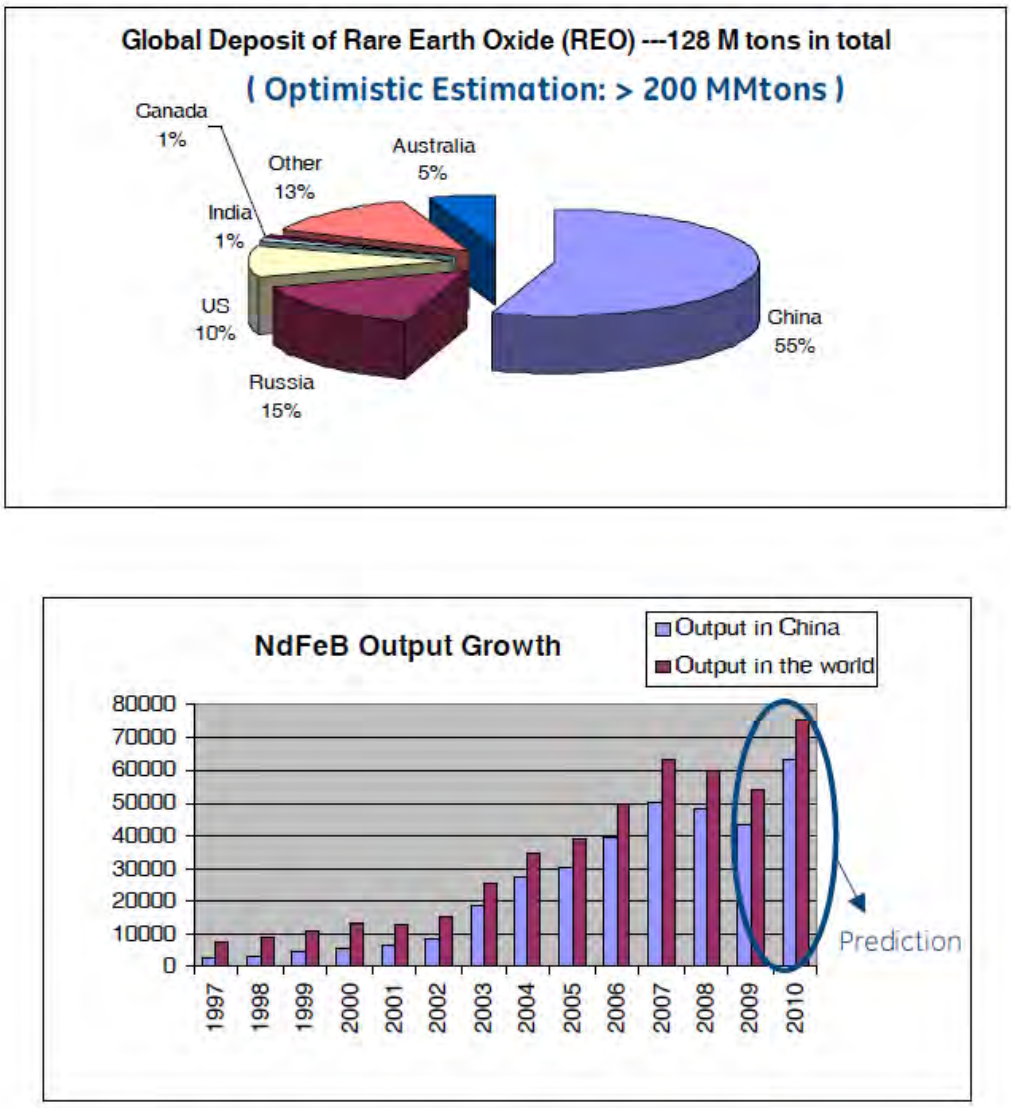

Figure 2- 12 Ronghai Qu (Rensselaer Polytechnic Institute- May 2010) - GE Global Research Centre

As shown in the pie chart, rare–earth (RE) resources are unevenly distributed around the world. In 2003, world mine production was concentrated in countries in the Far

East: China, India, Malaysia and Sri Lanka. Other potentially productive countries are USA, Australia, Canada, South Africa, and Brazil (Hedrick, 2004). However, it is evident from the data in figure 2-12 that China has become the largest player in the field of magnets in the 21st century not only through its reserves of manpower and expertise but also through its 55% share of global rare earth oxide deposits. China has rightly earned its title of "Global Centre" for RE minerals (L. Yang, 2009).

Kennedy, D. (2010), stated that China had imposed a tax on rare-earth exports – then 15%-25% on oxides, compounds and metals and 20% on alloys. Kennedy showed that there had been a rise in the demand since 2008 and forecast that the demand for Nd, Pr, Tb, Dy and Sm would almost be doubled. Dr Stan Trout (MolyCrop, USA), in his talk at the same venue, mentioned that the production of rare-earth magnets and all intermediate products outside China had languished over the last two decades. The recent confluences of strong international demand, coupled with environmental, production and export constraints in China, have all led to increased prices in RE and raised concerns about their availability in the future. Trout predicted that this crisis would eventually create a once in a lifetime opportunity for every RE deposit owner to re-examine their business model and plan for the future.

2.5.3 Environmental Considerations

1 Green Applications

Hatch, G. (2010), stated in his paper that the magnets industry is inextricably linked to the ups and downs of the wider rare-earth supply chain. These magnets present the majority of overall rare-earth usage and the key to green technologies drivers such as wind turbines and electric cars. However, rare earths are increasingly subjected to the vagaries of geopolitics.

He stated that the growth of "green" technologies is the key driver in the long term forecasted demand for rare-earth-based components and permanent magnets are no exception. In particular, their projected usages for the next generation direct drive wind turbines, as well as hybrid and plug-in electric vehicles.

Jacobson et al., (2010) in their energy policy paper have agreed that climate change, pollution and energy insecurity are among the greatest problems of our time. They have suggested an alternative energy produced using green sources such as wind turbines (using NdFeB-type magnets), solar energy captured in the form of CSP (concentrated solar power). Jacobson and co-workers have analysed the feasibility of providing worldwide energy for all purposes (electric power, transportation, heating/cooling etc.). The authors have given detailed analysis of how the energy can be used to save the natural resources.

Ronghai Qu (2010), emphasised the need for permanent magnets wind generators and indicated that the demand will rise significantly over the coming years. He also indicated that the usage of rare earth oxides will reach ≈ 0.16 M tonnes (160,000 tonnes).

2 Potential for Recycling

Figure 2-12 shows a projected annual production of NdFeB of 75,000 tonnes in 2010 and 15k tonnes in HDD in the 660 m computers worldwide alone (section 2.5.1) and the need for an efficient recycling process is evident. In addition to the considerable amounts of NdFeB already in circulation, 20-30% of raw magnets are wasted during manufacture due to the necessity to cut to a desired shape (Harikawa et al., 2006). This amounts to the substantial figure of 1500-2500 tonnes per year. Therefore, there are three possible main sources of NdFeB available for recycling;

1. “Swarf” or “internal waste” from machining of magnets.

2. Magnets damaged during production e.g. chipped units.

3. ‘End of life’ magnets.

These issues prompted research into strategies to effectively recycle NdFeB-based magnets.

The Öko-Institut conducted a study in January 2011 which included the development of a European strategy for a sustainable rare earth economy. It particularly addresses recycling, substitution and the efficient use of rare earths and develops a strategy towards a green rare earth economy. According to this study published in 2011, it

clearly states “Only a few industrial recycling activities are currently implemented for rare earths. Until now, there has been no large scale recycling of rare earths from magnets, batteries, lighting and catalysts” (Schüler et al., 2011).

The treatment of many relevant wastes is already regulated by the Waste Electrical and Electronic Equipment Directive (hereafter WEEE), the EU End of Life Vehicles Directive (ELV) and the EU Battery Directive. Thus, the collection of rare earths containing wastes has to be integrated into existing collection schemes. The development of pilot plants is accompanied by large-scale R&D projects which aim to gain more insight into the complex chemical processes and the required sophisticated equipment.

The WEEE Directive and the ELV Directive, mainly support the recycling of the basic materials but not the recycling of scarce and precious metals which have a high ecological relevance but only contribute a low share in terms of volume. Rare earth recycling should be addressed by specific requirements, e.g. the obligation to dismantle selected rare earth containing components.

Recycling plants bear high financial risks due to the required high investment and the high uncertainty of the future price development of rare earths. Therefore, it should be analysed whether the European Investment Bank (EIB) could reduce financial risks for investments in rare earth recycling. The only pilot plant (scheme) known to the author is the one that was set up in the School of Metallurgy and Materials, University of Birmingham supported by other partners (DTI) and Shiu-Etsu and Hitachi have recycling plants.

Japanese companies/researches have developed many patents that tackle these issues such as “Regeneration of method of permanent material: JP58136728, JP2002348632” its purpose is to regenerate and recover scrap such as working chips of rate earth magnets as raw materials of rare earth magnets by adding metallic Ca or hydrogenated Ca to said scraps and heating the same in an inert gaseous atmosphere then submerging the scraps in water. (JP62187112, JP58193331) is patented in Japan

and addressing the separation and recovery of rare earth metals; JP2001143916, JP200111615 addresses the recovery of magnetic powder from bonded magnets.

A recycling scheme of rare earths not only requires adequate logistic and technical preconditions but also an appropriate legal framework. Hence, an important step will be the adaptation of the legal EU framework in order to optimise post-consumer rare earth recycling. Potential relevant directives which should be verified in terms of modification for the support of a rare earth recycling scheme are the Ecodesign Directive, the WEEE Directive, the ELV Directive and the Battery Directive.

3 Detailed aspects of NdFeB-type magnets recycling

3.1 Introduction

To produce the desired NdFeB composition from raw material (Bastnasite or Monazite) is quite costly particularly with regard to energy. The process of production takes the following format:

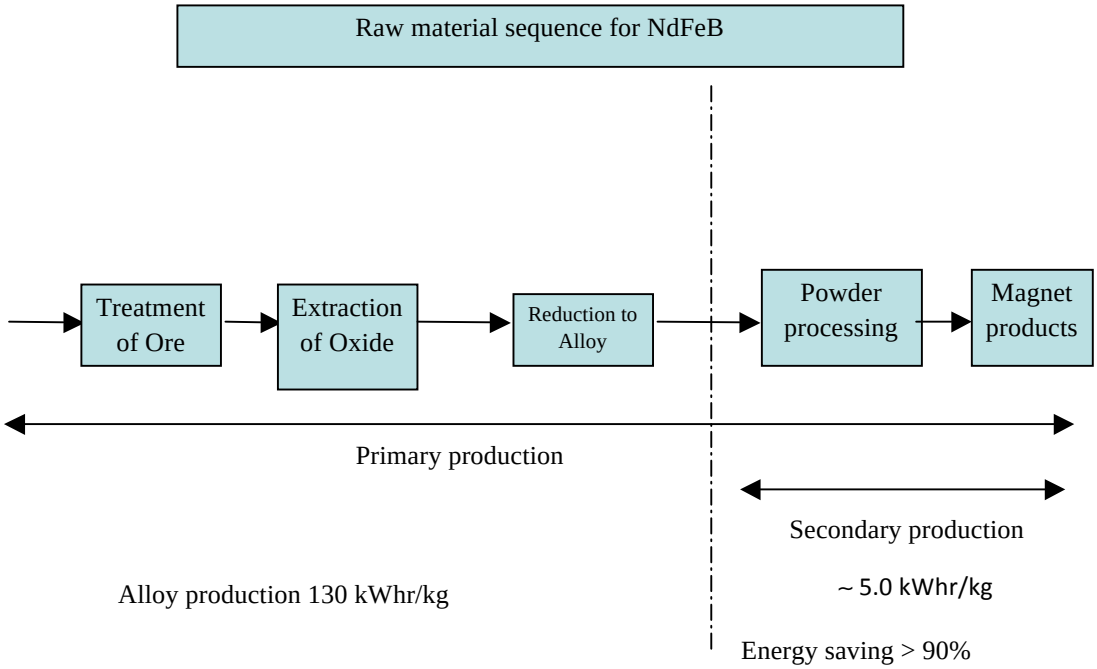

Figure 3-1 Raw material sequence for the production of NdFeB.

3.2 Introduction:

The process of production of a virgin material is always high and recycling can save on the natural resources and energy consumption of up to 90%. This saving can have a tremendous effect on the long term environmental factors. Although, to this date, there is no analysis as to the actual cost of recycling of permanent magnets. Researches and review papers has been produced (Gutfleisch, 2011, and Nemoto et al., 2011) but with no real evidence as to the actual or near cost of recycling permanent magnets.

From the CEAM (1995) it was suggested that a saving of 50% in energy (based on 50kg of powder recycled) is possible though the recycling route as the energy input is much lower than that of producing virgin material.

CEAM (1995) suggested that a saving of 50% in energy (based on 50 kg of powder recycled) is possible though the recycling route as the energy input is much lower than that of producing virgin material.

As illustrated in the previous chapter, China in the 21st century has become by far the largest player in the magnets field due to its abundance of natural resources, huge manpower and expertise, which had earned China the title “Global Centre” for RE minerals.

Recycling of permanent magnets can be justified by the financial gains as well as for environmental reasons. Seagate produces hard discs for computer manufacturers around the world, and, typically, they use ~20 g of NdFeB magnets on each hard drive. This presents an annual turnover of $2.66 billion. Using the global population as a reference, this represents a total amount of NdFeB in HDD of ~ 15 k tonnes. This amounts to around 600 million computers worldwide (see figure 2-10).

This should be an encouraging factor with regard to recycling, as the demand for NdFeB in HDD is increasing every year. However, rare earth (RE) resources are unevenly distributed around the world. In 2003, production was concentrated in China, India, Malaysia and Sri Lanka. The other potentially productive countries are USA, Australia, Canada, South Africa, and Brazil, as reported by Hedrick (2004).

From various talks and research publications it should be emphasised that the rare earth permanent magnet business scene is changing rapidly. The key current factors that are playing a vital role, as mentioned before are the taxes and export restrictions currently being imposed by China.

Routes for recycling permanent magnets can be classified into 2 main routes: chemical and powder metallurgy. The chemical route covers the hydro process that are used by Takeda and others, the powder metallurgy process was used by Ishigaki, Zakotnik and others (see figure 3-2 for summary)

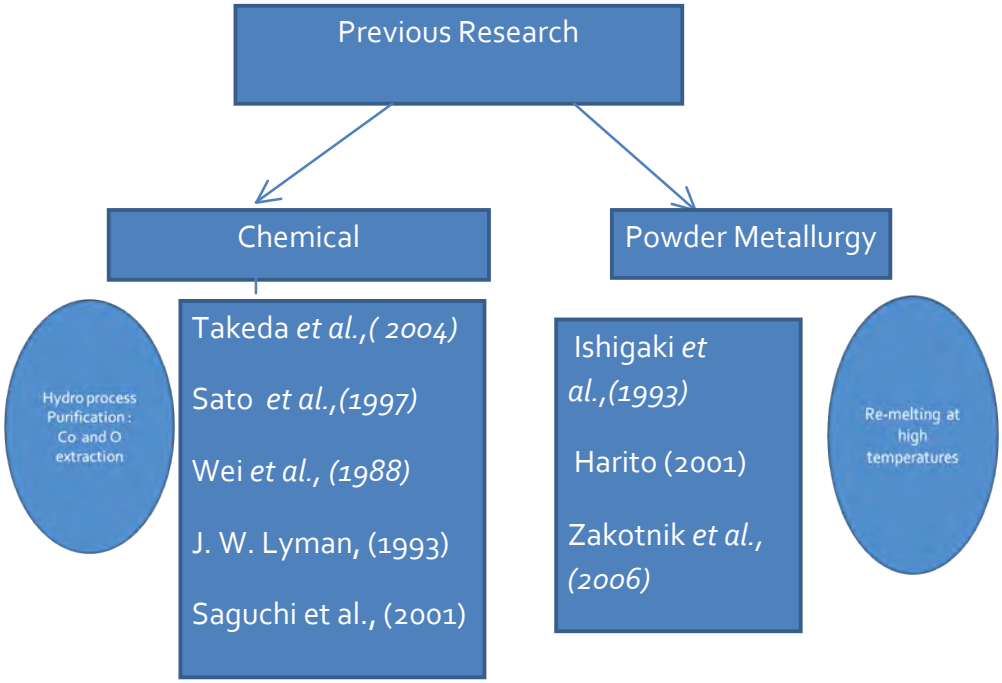

Figure 3-2 Recycling routes followed by some researchers.

The routes employed within this work are illustrated in the following diagram:

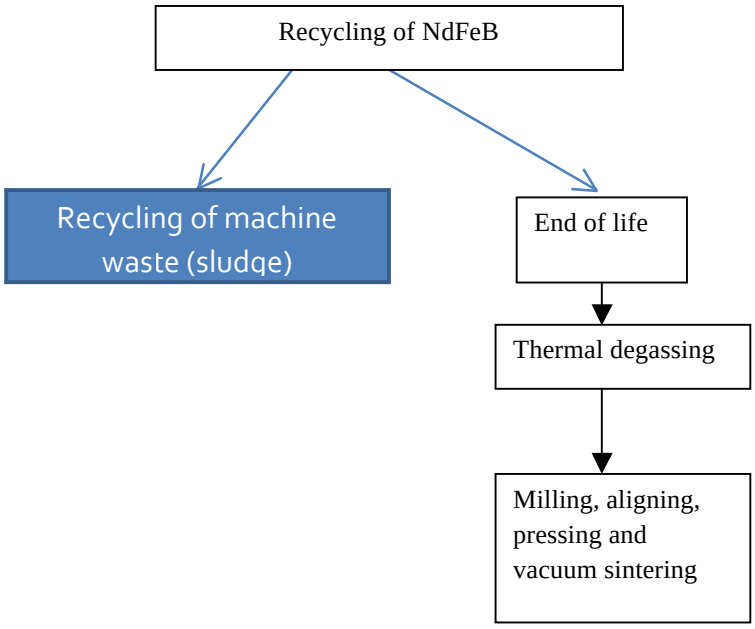

Figure 3-3 Routes of Recycling NdFeB.

3.3 Processing of Recycled NdFeB over the years:

As described previously, since their discovery in 1984, NdFeB-type magnets have been used widely for various applications due to their excellent magnetic properties. As electronic appliances are replaced, it is inevitable that some of these devices are discarded and replaced with new ones, particularly PCs. According to Horikawa et al., 2006, during manufacture, 20-30% of raw magnets are lost mainly due to the requirement to machine to a desired shape. This amounts to the substantial figure of 1500-2500 tonne/yr. These issues had prompted many researchers to devise an effective way of recycling NdFeB-based magnets.

Therefore, there are two types of scrap NdFeB-type magnet that need to be considered for recycling:

1. “Swarf” or internal waste from the machining/designing of magnets.

2. Defected magnets during production e.g. chipped units.

3. Magnets at the end of life of a particular device.

Hydrometallurgical process

According to Uda et al., (2003), (Uda referenced the following: Yamamura et al.(2001); Kuzuya et al., (1999); and Bertuol et al.,(2003)] the hydrometallurgical process was developed initially for the recovery of cobalt, nickel and rare earth elements from the electrode materials of spent NiMH batteries. The mischmetal (mixed-metals) nickel-cobalt intermetallic compound was separated from the electrode materials mixture by sedimentation (56 wt% nickel, 13.4 wt% cerium, 10.6 wt% lanthanum and 7.9 wt% cobalt). Rare earths leached quickly in sulphuric acid, nickel less so. Sulphuric acid dissolved the rare earths followed by precipitation at pH 1.2 using sodium hydroxide (NaOH). At pH 5-7 iron, zinc and manganese were precipitated. Nickel and cobalt can be obtained by electro-winning from the remaining solution. Hydrochloric acid was used to dissolve 98% nickel, 100% cobalt and 99% rare earth elements can be precipitated from aqueous solutions by the addition of oxalic acid or hydrogen fluoride to form the oxide or fluoride. As Rare Earth elements are produced by the calciothermic reduction of the fluoride, it is advantageous to precipitate it in this form. However, although high quality material can be produced by aqueous processing, removal of other dissolved species can cause problems.

3.3.1 Recycling of NdFeB magnets:

Various processes have been proposed in the past (Takeda et al., (2004, 2005, and 2006) for recycling magnet scrap. The majority addressed wet processing using aqueous solutions (Osamu Takeda referenced the following investigators: Sato et al., (1997), Wei et al., (1988), Lyman et al (1993)) and other methods are based on re-melting of alloys at high temperatures (referencing: Ishigaki et al., (1983), Hirato et al., (2001)).

The hydro process is complicated, time consuming, and generates a significant amount of waste. This is a hindrance to commercial applications. The melting process is far simpler and faster but it does not prevent Nd from oxidising during the melting processes as well as the difficulty of the separation process of the metal from the slag. Suzuki and co-workers (Suzuki et al., 2001) have investigated a process to recycle NdFeB magnets using calcium metal and $CaCl_2$ (see figure 3-2 and 3-3). The table below shows the variations between re-melting and the hydro processes:

Table 3-1: Variation between re-melting and the hydro processes.

Hydro		Re-melting	
Advantages	Limits	Advantages	Limits
Cheap	Complicated	Fast	Does not prevent Nd oxidation
Low temperatures	Time consuming	Simpler	Separation of metal is difficult
	Generates even more waste		High temperatures

This section will be divided into two parts: (1) Recycling of machined waste (sludge) and (2) End of life cycle (reprocessing of scrap). The following diagram shows the routes that will be discussed:

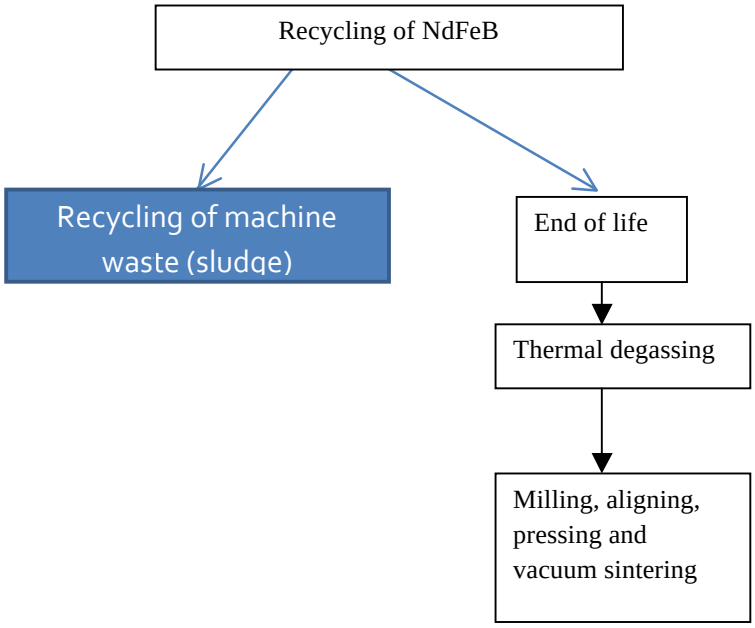

Figure 3-4 Routes of Recycling NdFeB

3.3.2 Recycling of machine (internal) waste (sludge)

Horikawa and co-workers (Horikawa et al., 2006; Takeda et al., 2006) developed a process of recycling the sludge powders in order to recover raw materials for isotropic bonded magnets and for microwave absorption materials for the GHz range. Horikawa's case study found that rare earth sintered magnet scrap powders can be used as a source of Fe and a variety of Fe- based intermetallic compounds of Fe-Si and Fe-Ti. They concluded that an effective way of preparation of Fe-Si compounds of 5 g of sludge-Fe cubes and Si (3-25 at% for Fe) was to place in a quartz nozzle and melt in Ar followed by rapid quenching on a melt-spinning device with a roll surface velocity of 25 m/s. By this means a thin ribbon of Fe-Si was produced and the rare earth component remained inside the nozzle as RE oxide pellets. This was then ground to a fine powder by using ball milling at 400 rpm for 2 h. The samples were then nitrogenated at 500 ^{o}C for 2hrs and then the process repeated at 400 ^{o}C for 2 h, before milling and then hydrogenated at 450 ^{o}C for 2 h after ball-milling. The Fe-Si materials and Ti were arc-melted in Ar in each process. The ingots were then re-melted five times in order to melt them homogenously. The ingots were separated by a mechanical process into the main alloy ingot portions of Fe-Ti intermetallic compounds and co-products of RE oxides slugs.

The ingot alloy was then ground to fine particles of <38 μm size. Some powder was reheated at 100 -250 ºC for 1-12 h. An epoxy resin was used to combine the powders which were then pressed into disc shapes to a thickness of about 2 mm, and heated to 130 ^{o}C for 30 min followed by heating to 170 ^{o}C for the same time. The material was cut to a toroidal shaped sample of 3.04 mm inner diameter and 7 mm outer diameter to be used for microwave absorbing property measurements using Agilent technology 8720ES at 0-18 GHz equipment. The crystal structure, magnetic properties, composition of elements and then oxygen content of the powder were all measured. The amounts of RE oxide-pellets were in the range of 12.3 to 17.5 % of the total weight. Using XRD the diffraction peaks indicated the presence of Nd_2O_3 and FeO.

The oxygen content was 3.88, 10.72 and 10.53 wt% of the raw material. EDX measurements of atomic compositions showed a Nd: Fe ratio of 25.6: 69.5 (wt%) which matches very approximately the $Nd_2Fe_{14}B$ phase. It was found that the wt% of Nd and Fe was almost the same between 2 samples (73.5 -73.7 wt% for Nd and 15.0 - 15.3 wt% for Fe) which is consistent with XRD results. 62.1 and 64.3 wt% Nd in the powder was collected efficiently as RE oxide slugs during the melting and solidification processes of Fe-Si and Fe_2Ti.

In three different papers, Saguchi reported on how to remove carbon and oxygen (2001, 2002, & 2006) from Nd magnet scraps. It was reported that Co and O could damage the magnetic properties. He developed a 2-stage removal process by deoxidation and removal of oxygen by heating in air and iron oxides are reduced through heating in hydrogen as well as the removal of the rare earth oxides by Ca reduction and leaching. The Ca leaching condition can have an effect on the oxygen contents of the recycled material. He reported that free carbon and carbides due to grain boundary segregation in the magnet scrap, are harmful to the magnet's performance.

3.3.3 End of life cycle

Two methods have been employed in order to reprocess the magnets successfully using the well established hydrogen decrepitation (HD)-process (developed prior to Zakotnik) (Zakotnik et al., (2006, 2008)):

1) Thermal degassing of HD powder to produce anisotropic coercive powder suitable for bonded or hot-pressed magnets.

2) Milling, aligning, pressing and vacuum sintering to produce fully or almost fully dense magnets. The role of sintering temperature is shown in figure 3-5.

The best magnetic properties for powder were found by performing a thermal degassing treatment at 700 ^{o}C. Lower degassing temperatures resulted in low coercivity values due to the presence of soft magnetic iron, which recombines with Nd after the Nd hydride degasses to form Nd metal at about 700 ^{o}C. This is in agreement with the Mössbauer measurements of the Fe content. A reduction in the coercivity relative to that of the initial bulk magnets was attributed to surface demagnetisation and oxidation.

Sintering Temperature (^{o}C)
1030
1080
1130

Milling Time (hour)
0
0.5
1
20

Energy Product (kJm^{-3})		
1030°C	1080°C	1130°C
50	130	150
190	260	180
210	270	280
230	260	260

Bad
Satisfactory
Good

Figure 3-5 Recycling routes and BHmax values (Zakotnik et al., (2008))

Zakotnik and co-workers (Zakotnik et al. 2006) reported in their paper on the recycling of sintered magnets using an adaptation of the HD-process. The study was conducted using magnets weighing about 10 g with a typical composition of Nd 13.98 at%, Pr 0.06 at%, Dy 0.63 at%, Nb 0.36 at%, Al 0.69 at%, Fe 77.81 at% and B 6.44 at% (± 0.02%) recovered from a hard disc drive. The procedure for de-coating the nickel was manual, and the magnet was then broken into little pieces to expose a fresh

surface to aid the HD-process conducted at room temperature and at a pressure of around 1 bar.

The HD powder was milled for different times from ½, 1 or 20 h under cyclohexane. The powder was then dried in a vacuum chamber (within a glove box) and pressed into a cylindrical tube and placed into a coil where it was pulse magnetised in a field of 6 T that was applied 3 times in order to align the powder which was then isostatically pressed.

It was found that the best-sintered magnets were produced by milling decrepitated powder for ½ hour followed by pressing, alignment and vacuum sintering at 1080 ^{o}C for 1 hour. To achieve a fully dense magnet using this sintering temperature and time a milling time of 20 hours was found to be required. The max energy product (BH_{max}) of the recycled product was around 15% less than the starting material, possibly due to grain growth and reduced density.

Another recycling technique to recycle Ni-coated Nd-Fe-B sintered magnets is to process them into isotropic bonded magnets using the melt-spinning method. This has been reported (Itoh et al., 2004) and the oxygen contents were reduced greatly in the recycled material compared with that in the waste sintered magnets, due to the production of an oxide slug which was separated from the molten alloy during the sample preparation. The powder with the best magnetic properties (Br~0.73 T, H_{cj} = 0.72 MA/m and (BH_{max}) = 87.8 kJ/m^3) was achieved when the speed of the roll surface was 16m/s. The magnetic properties of the bonded magnet of the above powder were very similar, namely Br~0.69 T, H_{cj} = 0.70 MA/m and (BH_{max}) = 71.0 kJ/m^3. According to these authors (Itoh et al., (2004), these results were similar to the commercial properties of MQPB powder which, typically, exhibited Br~0.73 T, Hcj = 0.79 MA/m and (BH) max = 86.0 kJ/m^3.

3.3.4 Recycling after end of life

Magnets supplied by various companies have a variety of different shapes and sizes. The majority of magnets have been coated with zinc, nickel Cu/Ni or epoxy. The regular shapes that are available in the present work are of crescent shapes which were employed in disk drives. Their weights range for each magnet is 5-10 g.

To date, three methods have been used to reprocess these magnets successfully using the HD-process, these are:

1) Thermal degassing to produce anisotropic coercive powder suitable for bonded or hot-pressed magnets. (Rivoirard et al, 2000. Zakotnik et al, 2006).

2) HDDR to produce isotropic, highly coercive powder suitable for bonded or hot pressed magnets. This powder has lower magnetic properties but better corrosion resistance.

3) Milling, aligning, pressing and vacuum sintering to produce fully densed magnets.

Zakotnik et al., (2008) reported in their paper on multiple recycling of sintered magnets using the HD process. The study was conducted using a magnet recovered from a HDD and weighing about 10 g in weight which had a typical composition as mentioned before**.** The magnets were cleaned in order to expose a fresher surface to aid the progress of the HD-process at room temperature and at a pressure of ~1 bar. The composition of all the magnets both before and after recycling was established by inductively coupled plasma (ICP) analysis and this was carried out at Less Common Metals. The HD process was carried out by placing the magnet pieces in a stainless steel container which was evacuated before introducing hydrogen at a pressure of 1 bar. It was found that the magnet pieces absorbed hydrogen at room temperature with a subsequent small rise in temperature because of the exothermic nature of the reaction.

The changes in composition arising from multiple recycling procedures on the same magnet are summarised in table 3-2. It can be seen that the rare earth elements have been reduced in content over the period of recycling and the oxygen and carbon content has increased, suggesting that the material increasingly oxidises with the number of recycling cycles.

Table 3-2: Analysis (there are other minor additions not being included) of the typical composition of the magnets, [±0.008–0.073] (adapted from M. Zakotnik 2008).

(at %)	Nd	Dy	B	Al	Fe	C	O
Starting material	13.78	0.66	6.30	0.76	75.51	0.32	1.84
1st cycle	13.69	0.66	6.20	0.74	75.11	0.36	2.44
2nd cycle	13.27	0.66	6.10	0.72	73.66	1.09	3.71
3rd cycle	13.02	0.64	6.05	0.72	73.06	1.52	4.12

The scrap magnets have been analysed. A typical composition is given in Table 3-2 and it can be seen that the majority rare earth component is Nd with minor additions of Dy in order to improve the coercivity. Second quadrant demagnetising curves of the magnets recycled up to four times are shown in figure 3-6 and summarised in table 3-3. There are also small additions of Al to improve the wettability of the grain boundary material and small amounts of the impurities carbon and oxygen.

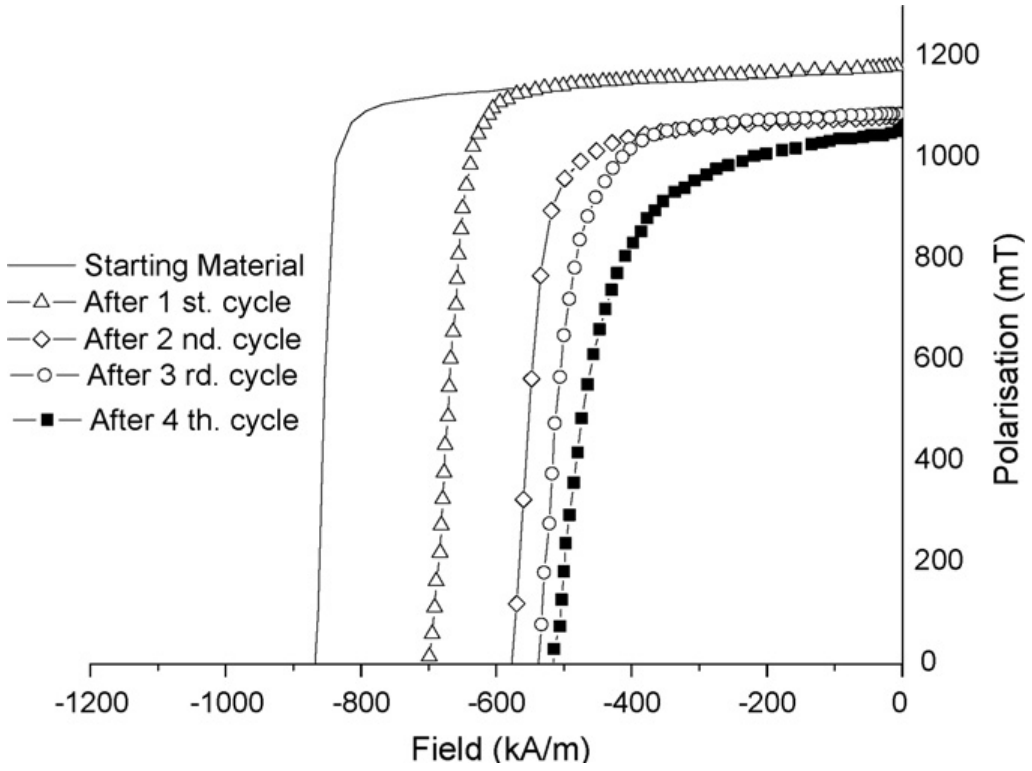

Figure 3-6 Demagnetisation curve of magnets recycled up to 4 times (Zakotnik, et al., 2008)

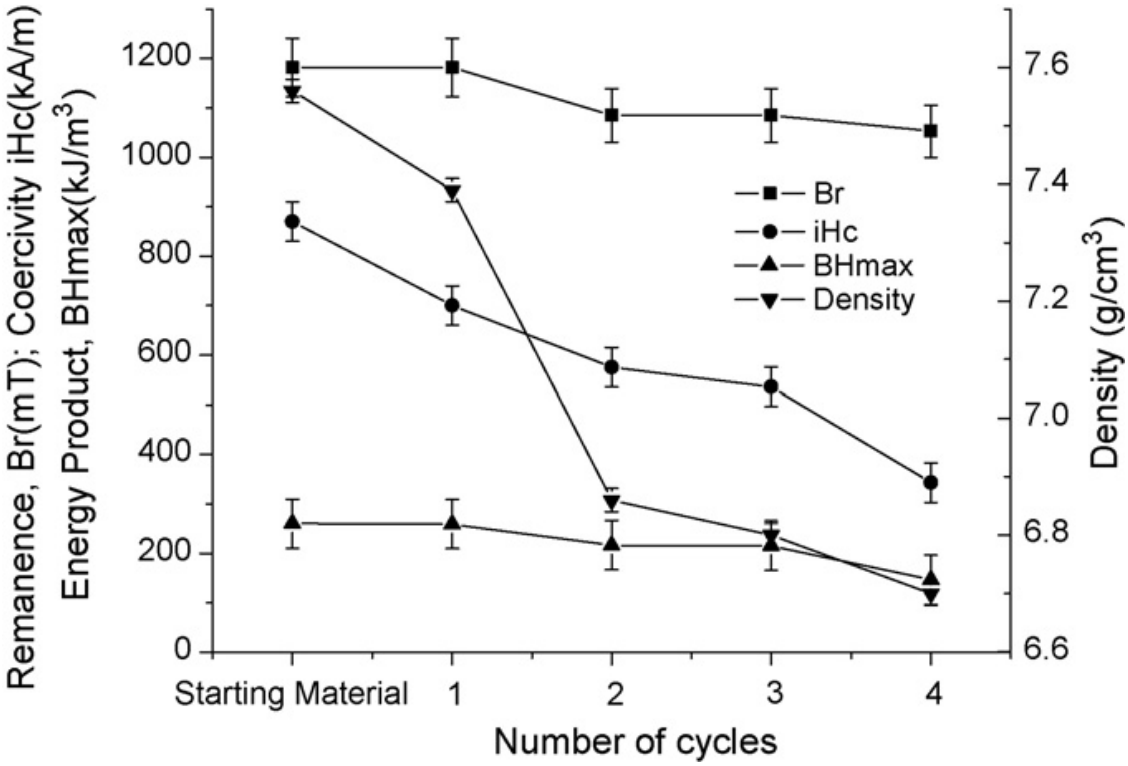

Figure 3-7 Summary of the magnetic properties of recycled magnets against sintering cycles without blending additions (Zakotnik, et al., 2008).

Table 3-3 summarising the magnetic properties after recycling of magnets without blending (Zakotnik, 2008):

	Br (mT) ± 60	$_jH_c$ (kA/m) ± 40	BHmax (kJ/m^3)	Squareness factor	Density (g/cm^3) ± 0.02
Starting material	1180	870	260	0.94	7.56
1st cycle	1180	695	260	0.90	7.39
2nd cycle	1082	575	216	0.86	6.86
3rd cycle	1087	536	215	0.79	6.80
4th cycle	1053	343	146	0.61	6.70

It can be seen from the demagnetisation measurements (figure 3-6) that recycling results in a reduction in the loop squareness as well as in the coercivity and the remanence. This is accompanied by a fall in the density (figure 3-7) indicating incomplete sintering.

To improve the density and magnetic properties during recycling, blending additions were made to the recovered material. The key blending addition was neodymium and generally blended magnets exhibited lower overall grain growth than the unblended material. The maintenance of the Nd-rich grain boundary material in the former would be expected to encourage grain growth as this material is liquid at the sintering temperature. The results presented are shown in figure 3-8. (The use of a powder blending technique using metal hydrides provides an effective and convenient way of varying the composition and properties of the NdFeB-type magnets. This technique is relatively simple and provides an effective way of adding a wide range of elements to NdFeB-type magnets. One of the first papers to report the use of blending mixed alloys of composition $Nd_{12}Fe_{82}B_6$ with $Nd_{30}Fe_{64}B_6$ (Otsuki et. al., 1990). The two alloys were combined after rough milling, but before fine milling; blending therefore occurred during the pulverisation stage.

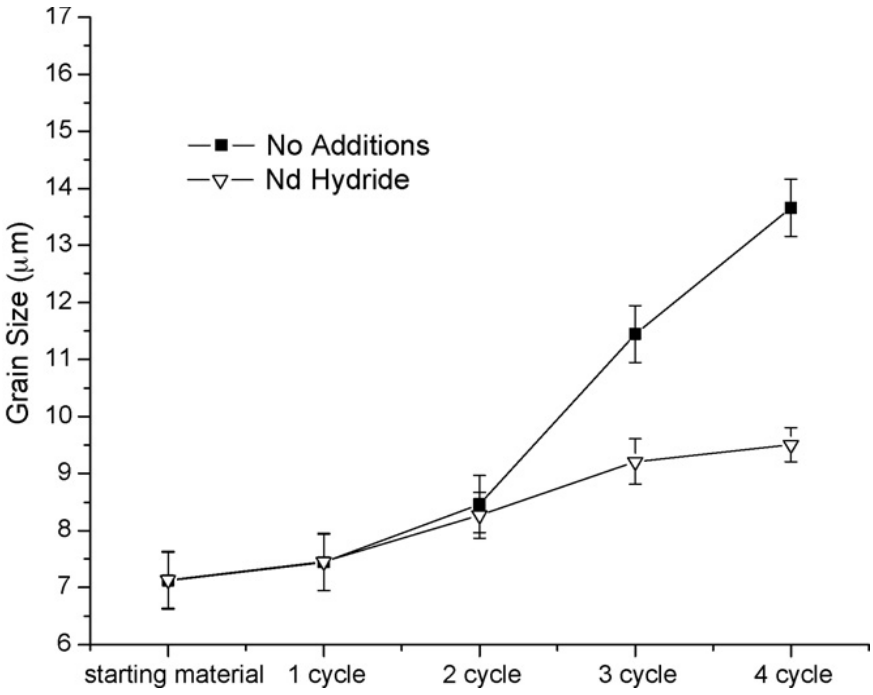

Figure 3-8 Variation in grain sizes for multiple recycling of sintered magnets (Zakotnik, 2008).

One possibility is that, because of the slightly increased oxygen content there is a suitable blend of Nd-rich phase and Nd_2O_3 at the grain boundaries and this inhibits the extent of grain growth in these magnets. Blending lean rare alloys with neodymium allowed densification to occur at lower sintering temperatures (Mottram et. al., 2001)

Zakotnik and co-workers (2008) envisaged that with this and many other processes, the next stage in the development of the recycling progress was to see if the process could be applied on an industrial scale operation and during the course of this programme; a large scale pilot plant was constructed, shown in figure 3-9. Another possible use of hydrogen during recycling is the use of hydrogen in the extraction of the NdFeB magnet material from actual devices such as HDDs and larger items, by placing them in a suitably designed hydrogenation system and removing the NdFeB powder as it decrepitated. The author is aware that Zakotnik and co-workers had successfully accomplished the construction and operation of a plant prototype at Birmingham in conjunction with industrial partners, where large numbers of voice coil motors and other assemblies could be accommodated.

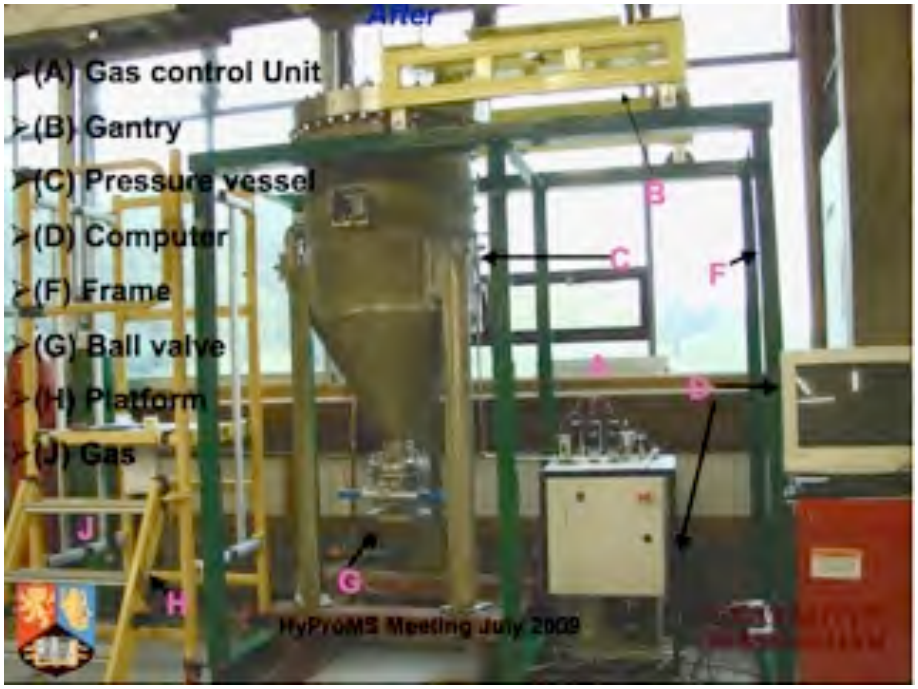

Figure 3-9 Recycling rig at the School of Metallurgy and Materials, University of Birmingham. Capacity ≈50 kg tested at lab scale.

3.3.5 Recovery process on NdFeB-type magnet scrap by selective chlorination using NH_4Cl

As stated previously, the NdFeB-type sintered magnets production has reached more than 100,000 tonne p.a. worldwide. About 30% of the NdFeB-type sintered magnets become either bulk or powder scrap during the manufacturing processes, e.g. pressing, sintering, cutting and polishing. A large proportion of the scrap being powder sludge, which is mainly generated during the cutting and polishing processes to fit the tight tolerances required for the finished products. In recent NdFeB-type sintered magnets, Dy and/or Tb can be substituted for Nd to improve the magnetic coercivity for high temperature applications. Rare earth resources, particularly Dy and Tb, are only located in certain countries and their availability has been influenced by political and economic considerations. Therefore, efficient recycling processes for NdFeB sintered magnets are needed to ensure resource security.

Itoh and co-workers (Itoh et al., 2009) stated that, on an industrial scale, the rare earth components in the powder scrap are currently recovered by solution processes such as ion exchange and solvent extraction methods (Itoh referred to Lyman and Palmer, 1993 for his process), although these processes involved the generation of much industrial drainage. Several dry processes for the powder scrap have been proposed by Xu et al., (2000)), Okabe et al., (2003), Murase et al., (1992) and Uda et al., (2002). The rare earth components can be extracted by forming a liquid alloy with a metallic reagent such as Mg or Ag at the relatively moderate temperature of 700 ^{o}C in the case of the powder scrap having a low oxygen contamination (Xu, et al., 2000; Okabe et al., 2003).

The chemical vapour transport method based on metal chlorination also allows the recovery of the rare earth elements from the NdFeB-type sintered magnet scrap, and furthermore they are mutually separated from one another by the stability difference of such metal chloride vapour complexes. However, all components of the rare earth and transition metal such as Nd, Fe, B, and the other additives (Dy, Tb, Co, Cu, and so on) are fully chlorinated, so that unwanted chlorides are also produced. This chemical vapour transport method has been further improved by Uda et al., (2002), in which $FeCl_2$ can be used for selective chlorination of the rare earth elements in the

powder scrap. Although these dry processes hardly generate any industrial wastewater, they have not yet met all the industrial requirements.

The selective chlorination method using NH_4Cl was applied to the powder scrap of NdFeB-type sintered magnets to separate the rare earth elements as their chlorides from Fe-based solid residue. The feasibility as a recovery process for the magnet scrap was evaluated and the reuse of the resultant Fe-based solid residue as an electromagnetic wave absorber was also evaluated. (Uda et al., 2002),

Commercially available NdFeB-type sintered magnets were ground in air into fine powders below several micrometers in diameter, by a planetary ball mill apparatus and these served as test specimens of powder scrap. Their average oxygen content was ca. 1 wt%. A mixture of 1.0 g of NH_4Cl (three times in excess of the chemical equivalent) and 1.0 g of the powder scrap was charged in a Pyrex reactor tube (internal diameter: 10 mm) and heated at 250–350 ^oC for 3–12 hours in a N_2 gas flow (50 ml/min). After these reactions, the resultant powders were soaked in distilled water to leach the rare earth chlorides. The damp substances and solid residues were then analysed by EDX. The recovery rate of the rare earth elements was evaluated on the basis of the rare earth (neodymium and dysprosium)/Fe metal ratio of the solid residue before and after the chlorination process. The solid residue was identified by XRD using Cu Kα radiation.

The specific surface area of the raw powder scrap and residual powders was measured by conventional nitrogen adsorption using the BET (Brunauer, Emmett, and Teller's) equation. The surface morphology of the products was observed by a scanning electron microscope (SEM). The magnetic properties were characterised by a VSM. To evaluate the electromagnetic properties, the resin compacts were prepared by mixing thermosetting epoxy resin with 60–70 wt% of the solid residues and pressed into a toroidal shape using a metal mould. Then the compacts were cured at 120 ^oC for 1 h.

The following table shows the amount of rare earth recovered from scrap powder at various reaction conditions:

Table 3-4: rare earth recovery rate from $Nd_2Fe_{14}B$ based magnet scrap

Chlorination conditions	Element ratio/ at%[a] (Nd+Dy) :Fe	Rare earth recovery rate/%
300 ^oC for 3 h	1.2 : 98.8	87
300 ^oC for 12 h	1.3 : 98.7	86
350 ^oC for 3 h	3.2 : 96.8	66
350 ^oC for 3 h[b]	1.0 : 99.0	90
300 ^oC for 3 h	2.6 : 97.4	73

[a] before chlorination, the element ratio of (Nd + Dy) : Fe was 9.5 : 90.5 in the as milled sample. The rare earth recovery rate was calculated from the elemental ratio changes before and after the chlorination. [b] Twice the amount of NH_4Cl has been used (Itoh et al., 2009).

Itoh et al., (2009) concluded that the chlorination process recovered about 90% of the rare earth elements from scrap NdFeB sintered magnets with a low oxygen contents, using NH_4Cl as the agent. This selective chlorination is due to the difference of standard formation enthalpy between RCl_3 and $FeCl_2$. Although part of the iron component is also chlorinated together with the rare earth component, $FeCl_2$ works as a chlorination reagent and reacts with rare earth components in the inner parts of the scrap particles to form more RCl_3. The resultant RCl_3 is consequently recovered by soaking the reacted solids.

The Fe-based solid residue powder obtained as the by-product possesses a relatively high coercivity of around 0.04 T with a saturation magnetisation value of 140 mT. The resin compacts prepared from the above α-Fe powders provide good electromagnetic wave absorption ability in the SHF band (super high frequency). These results indicated that it was possible to construct an efficient rare earth recovery process for NdFeB sintered magnet scraps by using NH_4Cl, in which all the elements can be reused as a starting source or as a possible functional material.

Takeda and co-worker (2006) reported that the Nd extraction process they had established was an environmentally friendly process where the combined scrap

contained valuable metals. 98% pure Nd could be recovered from the magnet scrap under set conditions.

Other chemical process studied the extraction of cobalt from magnetic scrap (Xu et al., 2010) using chemicals to separate the RE and cobalt from magnets. Cobalt-iron residue was soaked by hydrochloric acid, the $Fe(OH)_3$ was preferential solution, pH was adjusted using hydrochloric acid, $Co(OH)_3$ did not dissolve, cobalt and iron were separated, after heating of $Co(OH)_3$, the resultant was cobalt oxide. The total recovery of cobalt was found to be 97% and rare earths was 96%. (Xu et al., 2010)

Multiple processes are required for the separation of Nd from other rare earth elements. Since the feed material is thermodynamically extremely stable, a large amount of energy is necessary in order to obtain the metal or alloy by reduction of the feed material. Although Nd is a relatively abundant rare earth element, it is important to develop an effective recycling process for this element, in order to conserve the environment. This is because a large quantity of solid waste and waste solution is generated during the initial Nd refining process.

4.0 Different classes of magnetism and their properties

Materials can interact with magnetic fields in five ways.

Diamagnetism: In the presence of zero applied field atoms within a material have no magnetic moment

Paramagnetism: In the presence of zero applied field atoms within a material have randomly oriented magnetic moments

Ferromagnetism: Atoms within a material have parallel-aligned magnetic moments with and without an externally applied field.

Ferrimagnetism: Atoms within a material have anti-parallel aligned magnetic moments with net moment in one direction.

Antiferromagnetism: Atoms have mixed parallel and anti-parallel aligned magnetic moments which exactly cancel each other.

All materials can be classified in terms of their magnetic behaviour falling into one of these five categories, depending on their bulk magnetic susceptibility. The two most common types of magnetism are diamagnetism and paramagnetism, which account for the magnetic properties of most of the elements of the periodic table (at room temperature).

These elements are usually referred to as non-magnetic, whereas those which are referred to as magnetic are usually classified as ferromagnetic. The only other type of magnetism observed in pure elements at room temperature is antiferromagnetism. some magnetic materials can also be classified as ferrimagnetic and although this is not observed in any pure element it can be found in certain compounds, such as the mixed oxides known as ferrites, from which ferrimagnetism derives its name. The value of magnetic susceptibility falls into a particular range for each type of material and this is shown in table 4-2 with examples.

1. **Ferromagnetism:** this type has a permanent magnetic moment when there is no external field. This causes the moment to align parallel to the external field. At the saturation point, there will be an increase in the external field which has little or no effect on the magnetisation.

4.1 Magnetism terms and units

There are two sets of unit systems used to quantify magnetic parameters: The Gaussian or C.G.S (centimetre-grams-second) system and System International (SI) or M.K.S. (meter-kilogram-second) system. The C.G.S. units system has been generally accepted over many years. Today, the use of the SI system is widespread and used in engineering and other technical fields. Units throughout this thesis will be expressed in the S.I. system whenever possible. However, as a comparison, the conversions and relationships between the two systems are given in table 4-1.

Table 4-1: The relationship between some magnetic parameters in cgs and S.I. unites. (Where: G = Gauss, Oe = Oersted, T = Tesla)

Quantity	Gaussian (cgs units)	S.I. Units	Conversion factor (cgs to S.I.)
Magnetic Induction *(B)*	G	T	10^{-4}
Applied Field *(H)*	Oe	Am^{-1}	$10^3/ 4\pi$
Magnetisation *(M)*	emu cm^{-3}	Am^{-1}	10^3
Magnetisation *($4\pi M$)*	G	-	-
Magnetic Polarisation *(J)*	-	T	-
Specific Magnetisation *(s)*	emu g^{-1}	$JT^{-1}kg^{-1}$	1
Permeability *(μ)*	Dimensionless	H m^{-1}	$4\pi.10^{-7}$
Relative Permeability *(μ_r)*	-	Dimensionless	-
Susceptibility *(X)*	emu cm^{-3} Oe^{-1}	Dimensionless	4π
Maximum Energy Product *(BH_{max})*	M G Oe	k J m^{-3}	$10^2 / 4\pi$

4.2 Magnetic Quantities

The measurement of the magnetic flux per unit area is referred to as the magnetic induction B and in vacuum is defined as:

$B = \mu_o . H$ Equ. 1.0

H = the magnetic field

μ_0 = the permeability of free space. A magnetic induction B of 1 Tesla can generate a force of 1 N/m on a conductor carrying a current of 1 A at a right angle to the direction of the induction.

When a material is placed in a magnetic field H, the overall atomic moment within the material is affected by the external magnetic field. The effect of such an external field is excited magnetic moments within the exposed material. The magnetic moment per unit volume is defined as the magnetisation M. This magnetic moment creates a field of induction of its own which will affect the applied field H. Therefore, the overall behaviour of the system can be described as:

$B = \mu_o . (H + M)$ Equ. 1.1

B, H and M = vectors.

The magnetic susceptibility χ, alias bulk or volumetric susceptibility is dimensionless and represents the degree of material magnetisation in response to a magnetic field and can be expressed as:

$$x = \frac{M}{H}$$ Equ. 1.2

The value of the susceptibility is an important characterising mark which can be used to distinguish several kinds of magnetism in a material as well as characterising their magnetic behaviour.

Another factor that illustrates the magnetic response of a material and its strength is the permeability μ. Absolute permeability μ which can be defined:

$$\mu = \frac{B}{H}$$ Equ. 1.3

Combining equations 1.1 and 1.2 gives:

$B = \mu_o \cdot H \cdot (1 + \chi) = \mu_o \cdot \mu_r \cdot H$ Equ. 1.4

(1.4)

Where μr is the relative permeability of the material.

Combining equations 1.3 and 1.4 gives:

$\mu = \mu_o \cdot \mu_r$ Equ. 1.5

μ, μ_r or χ , these can be used to characterise the magnetic response of a material within a magnetic field.

The magnetic polarisation J [Tesla] is an important factor. This value is the magnetisation of a material and can be expressed as follows:

$J = \mu_o \cdot M$ Equ. 1.6

There is a parallel alignment to the atomic moments. Ferromagnetism exhibits a positive and large values of the susceptibility ($\chi = \frac{M}{H}$) with the onset of ferromagnetism on cooling through the Curie temperature (Tc) (Table 4-2). The inverse of the susceptibility varies linearly with T and extrapolates to the Curie temperature at $\frac{1}{\chi} = 0$.

This is described by the Curie-Weiss equation:

$\chi = \frac{C}{(T - \theta)}$ or Equ. 1.7

$\frac{1}{\chi} = \frac{T}{C} = \frac{\theta}{C}$ i.e. T= θ when $\frac{1}{\chi} = 0$ Equ. 1.8

θ = Curie constant (-ve/+ve) units (K), where θ originated from the Weiss theory and defines the interactions between the neighbouring magnetic moments which are local to atomic or ionic sites. Positive (+ve) for ferromagnets and negative (–ve) for antiferromagnets.

2 **Antiferromagnetism:** The susceptibility is small and positive as it is a form of paramagnetism; typical values are giving in table 4-2. The moments align in a pattern which is regular to the neighbouring moments pointing in the opposite direction. In antiferromagnetism the moments are aligned below the ordering temperature (Néel point). Below this temperature, the atomic moment are magnetised as in ferromagnetism materials but with antiparallel alignment. Above

the Néel temperature, the material behaves like a paramagnetic with random magnetic moments.

3 **Ferrimagnetism:** these exhibit self-acting magnetism and the atomic moment is unequal. This is due to the ions in the sub-lattice being different such as Fe^{2+} and Fe^{3+} in ferrites. The magnetic behaviour is close to that of ferromagnetism except the susceptibility does not follow the Curie-Weiss Law. The value of its susceptibility is shown in table 4-2.

4.3 Weiss Molecular Field Theory

In 1907, Weiss introduced the concept of an internal molecular field but did not present an adequate explanation of its origin until Heisenberg in 1927 explained the molecular field in terms of exchange forces, which is different from the electrostatic attraction between electrons and protons as well as the repelling forces between electrons and between protons. The exchange force is dependant on the orientation of the spin on the electrons. This may result in the magnetic moment of neighbouring atoms being either parallel of anti-parallel. As the distance increases, the exchange forces reduces rapidly and figure 4-1 below, shows the Bethe-Slater Curve. This describes the variation of the exchange integral J_{ex} with the r_{ab}/r_d ratio. r_{ab} = atom radius, r_d = 3d electron shell radius (Chen, C.W. 1986). The exchange energy has a small positive value at high r_{ab}/r_d ratio, and reduces to zero with the r_{ab}/r_d ratio as the 3d electrons approach each other closely. A large magnetic moment results from the alignment of spins. This corresponds to the ferromagnetic materials where there are partly filled 3d-shells. However, if the shells are completely filled this corresponds as in $3d^{10}$, this results in the inert gas configuration and thus diamagnetism.

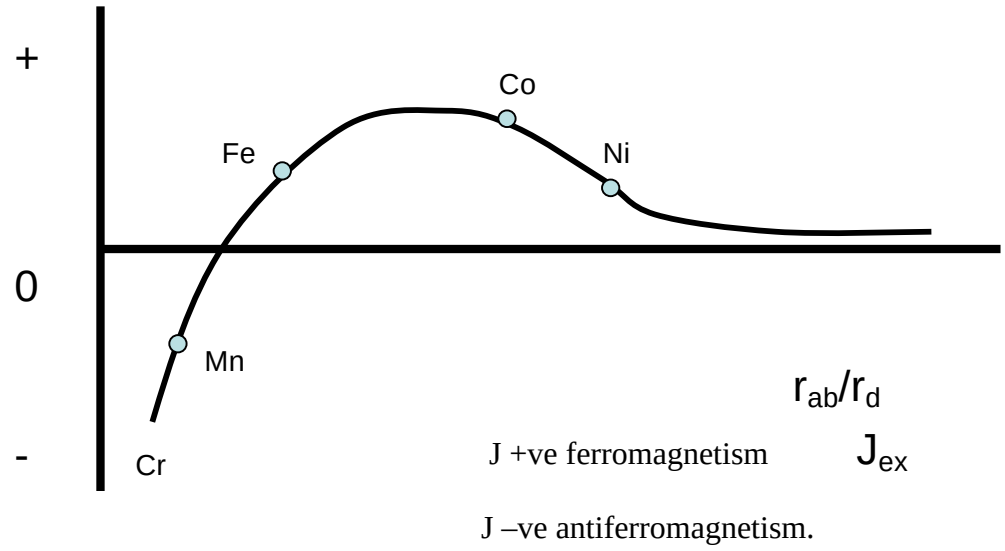

Figure 4-1 Bethe –Slater curve. Exchange integral Jex vs r_{ab}/r_d

In the figure shown above, the x-axis gives the ratio of radius of atom (r_{ab}) to the radius of 3d shell of electron (r_d). The elements with a positive J value show a ferromagnetic nature such as Fe, Co and Ni and elements with a negative J show an antiferromagnetic nature, such as Mn and Cr.

4.4 Magnetic materials properties of the elements

The elements in the periodic table are shown in figure 4-2 along with their magnetic behaviour. All the elements of the periodic table falls into the previously mentioned types of magnetism. There is an approximately 50/50% split of the table into either paramagnetic or diamagnetic elements.

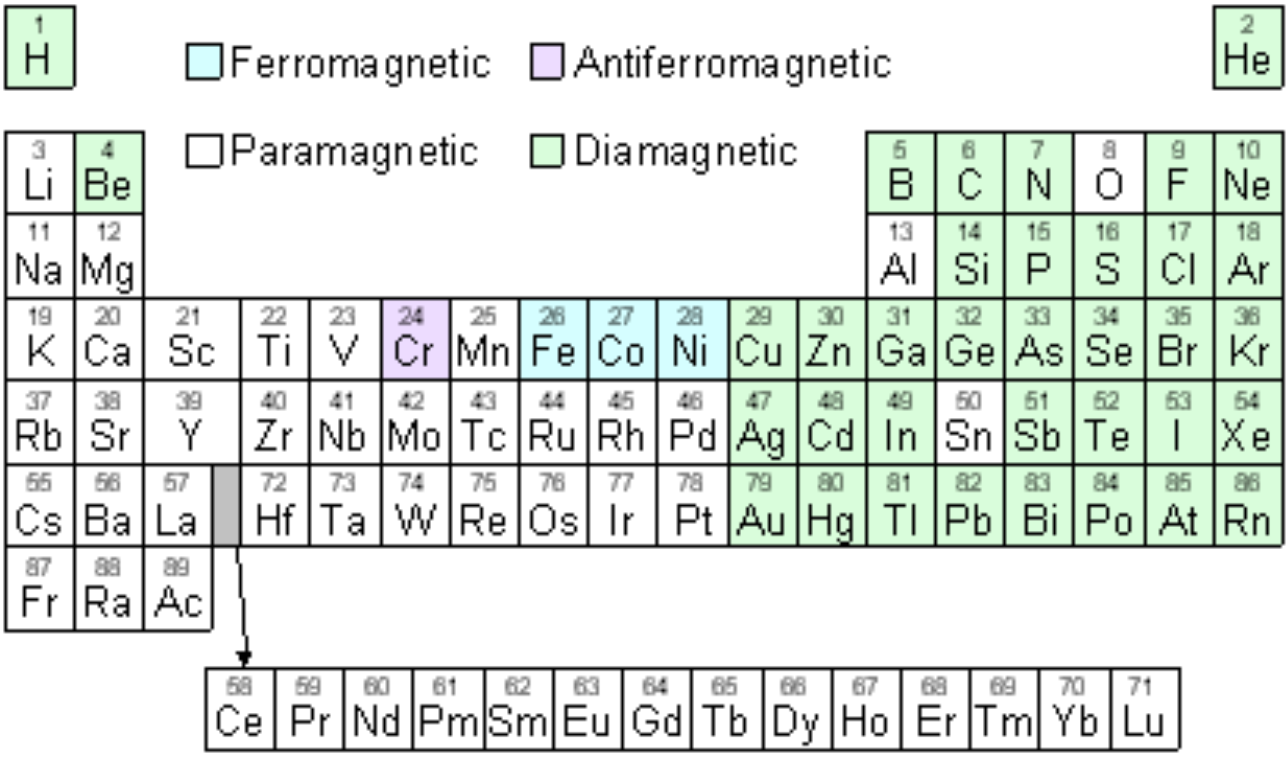

Figure 4-2 Periodic table showing magnetism types. Note Mn is antiferromagnetic at room temperature.

The interaction of the different classes of magnetism is also summarised in table 8.

Table 4-2: magnetic behaviour of different types

Type of Magnetism	Susceptibility	Atomic / Magnetic Behaviour	Example/ Susceptibility
Diamagnetism	Small & negative.	Atoms have no magnetic moment 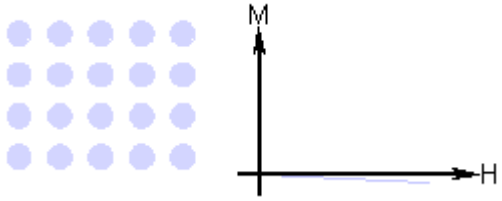	Au $-2.74x10^{-6}$ Cu $-0.77x^{10-6}$
Paramagnetism	Small & positive.	Atoms have randomly oriented magnetic 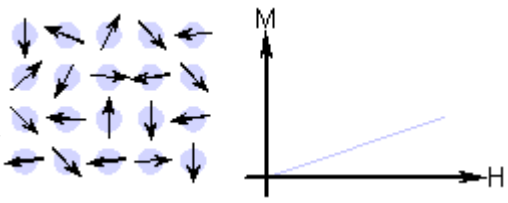	β-Sn $0.19x^{10-6}$ Pt $21.04x^{10-6}$ Mn $66.10x^{10-6}$

		moments	
Ferromagnetism	Large & positive, function of applied field, microstructure dependent.	Atoms have parallel aligned magnetic moments 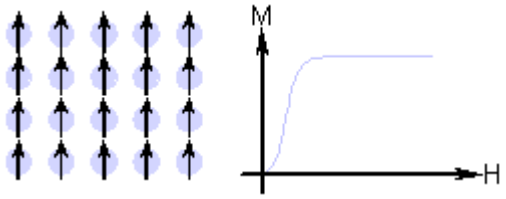	Fe ~100,000
Antiferromagnetism	Small & positive.	Atoms have mixed parallel and anti-parallel aligned magnetic moments 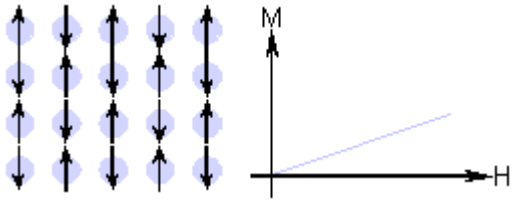	Cr $3.6x^{10-6}$
Ferrimagnetism	Large & positive, function of applied field, microstructure dependent	Atoms have anti-parallel aligned magnetic moments 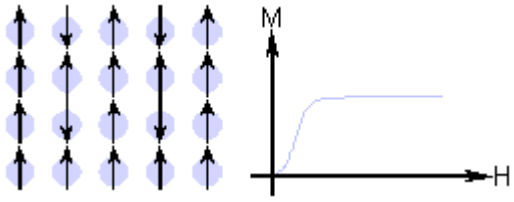	Ba ferrite ~3

4.5 Magnetic Anisotropy

The magnetic properties within crystals are often anisotropic and vary with crystallographic direction according to the alignment of the magnetic dipoles. Figure 4-3 shows magnetic anisotropy in a single crystal of cobalt. In its hexagonal structure, cobalt can be easily magnetised in the [0001] direction (c-axis) but has a hard

magnetisation in the [1010] direction which lies in the plane 90^{o} from the easy direction (basal plane).

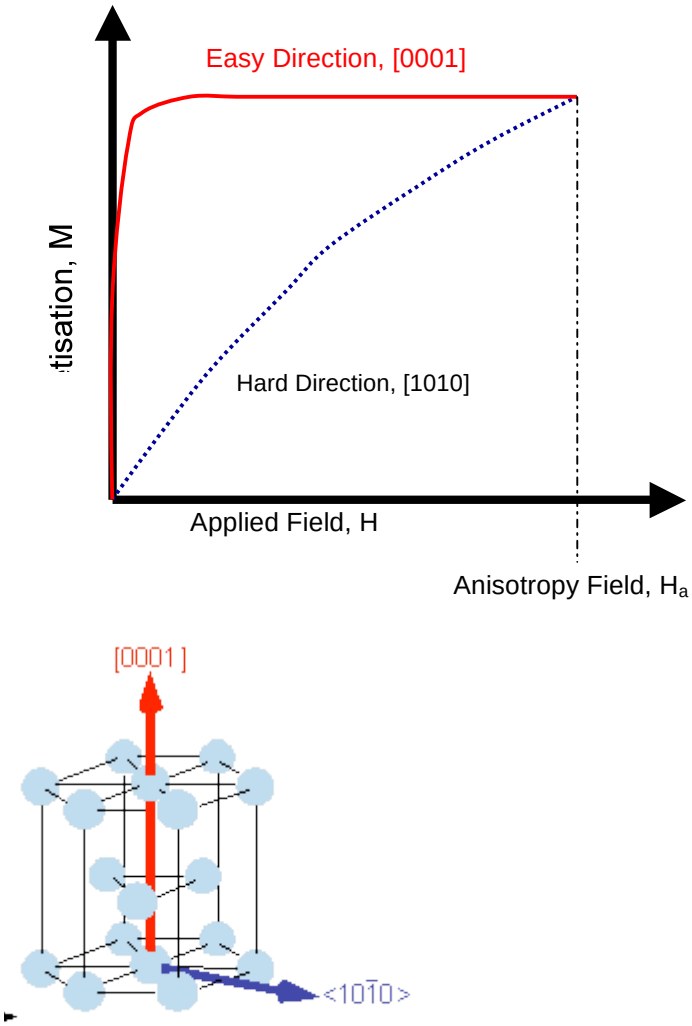

Figure 4-3 The cobalt magnetocrystalline anisotropy.

The anisotropy field in figure 4-3 is designated H_a which is defined as follows:

$H_a = 2K/M_s$ Equ. 1.9

M_s = saturation magnetisation

K = anisotropy constant.

The temperature dependence of H_a is a result of the thermal disorder and the change in the influence in the sub-lattice anisotropies. The energy required (E_a) to magnetise

a material with anisotropy in a simple cubic system such as iron by can be described the following:

$E_a = K_1 (\cos^2\theta_1 \cos^2\theta_2 + \cos^2\theta_2 \cos^2\theta_3 + \cos^2\theta_1 \cos^2\theta_3)$ Equ 1.10

K_1= anisotropic constant.

θ_1, θ_2, and θ_3 = angles between the magnetisation and the three crystal axes.

The anisotropy field is what is needed to rotate all the moments by 90^o as one unit in a uni-axial saturated single crystal. The anisotropy takes place due to the coupling of electron orbiting around the lattice with their spin-component. These then have a low energy state in the easy direction of magnetisation.

The magnetisation in the easy direction for a permanent magnet, based on ferrite or rare earth alloys, must be uniaxial, but there is the possibility of having materials with many easy axes or where the easy direction can lie anywhere on a certain plane or on the surface of a cone. In this case it is not possible to produce clear alignment and hence a high coercivity.

Uniaxial anisotropy of a permanent magnet is desirable and indicates its difficulty to undergo the demagnetisation process due to the resistance to rotation of the magnetisation through a hard direction.

4.5.1 Shape Anisotropy

The shape anisotropy has a reaction with energy called magnetostatic energy E_{as} and is defined as follows:

$E_{as} = K_1 \sin^2\theta$ Equ 1.11

K_1 = shape anisotropy constant

θ = angle between magnetisation and the easy direction.

4.6 Magnetic Domains

Magnetic domains exist to reduce the overall system energy. A simple illustration is shown in figure 4-4 where a material element is uniformly magnetised and the role of magnetic domains is shown in reducing the overall system energy. This is due to

presence of magnetic free poles at the surface where the demagnetisation field H_d is generated. The demagnetising field opposes the magnetisation of the material. The H_d magnitude is dependant on the sample geometry and magnetisation. If the sample's length/ diameter ratio is high, then the demagnetising field and magnetostatic energy will be low. By splitting magnetisation into 2 domains (figure 4-4(b)) this will halve the magnetostatic energy. If the magnet breaks down to N domains, then the magnetostatic energy will be 1/N (figure 4-4(c)) which shows a quarter of the energy in figure 4-4(a). Figure 4-4(d) shows a closure domain structure where the magnetostatic energy is zero. This only happens when the material does not have a strong uniaxial anisotropy and the neighbouring domains are not placed 180^o to each other. Domain introduction increases the system overall energy. Therefore, whilst the division into domains continues, the size of the reduction is eventually greater than the energy needed to make domain wall.

A schematic of domain walls shown in figure 4-5 were the atoms dipole moment within the domain wall are not all pointing in the magnetisation easy direction and therefore a higher energy state exists. In addition, as the atomic dipoles are not situated in 180^o formation to each other, this raises the exchange energy within the wall. Hence, domain wall energy is an intrinsic property of a material and depends on a combination of magnetocrystalline anisotropy and on the exchange interaction between the atoms. Strong magnetocrystalline anisotropy prefers a thin wall whilst a strong exchange interaction favours a thicker wall.

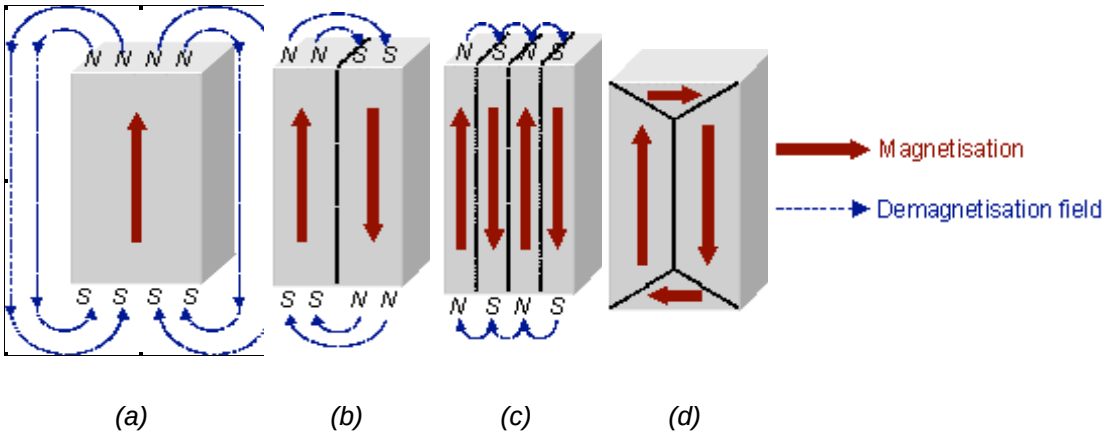

Figure 4-4 Schematic illustration of the break up of magnetisation into domains *(a)* single domain, *(b)* two domains, *(c)* four domains and *(d)* closure domains.

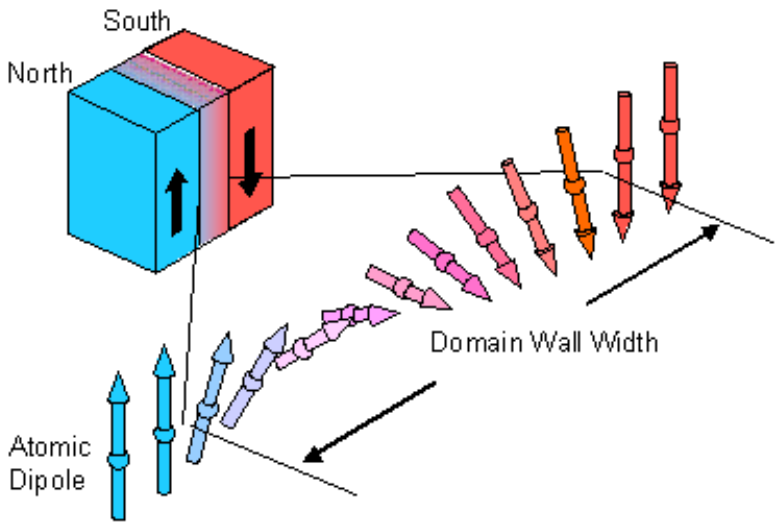

Figure 4-5 Schematic representation of a 180^{o} domain wall

4.6.1 Magnetisation in multi Domain particles.

A domain wall can move as the field is increased. The figure below illustrates what happens when the magnetisation is increased. The magnetic domains grow continuously in the parallel direction of the applied magnetic field. When the field is sufficiently high, there will effectively be one single domain with the magnetisation being in the easy direction. This will occur only if the material is aligned in the same direction. When a much higher field is applied then the magnetisation direction will rotate away from the easy axis until magnetisation saturation is achieved. This will result in the formation of only one domain with a strong resultant magnetisation in the direction parallel to the applied field.

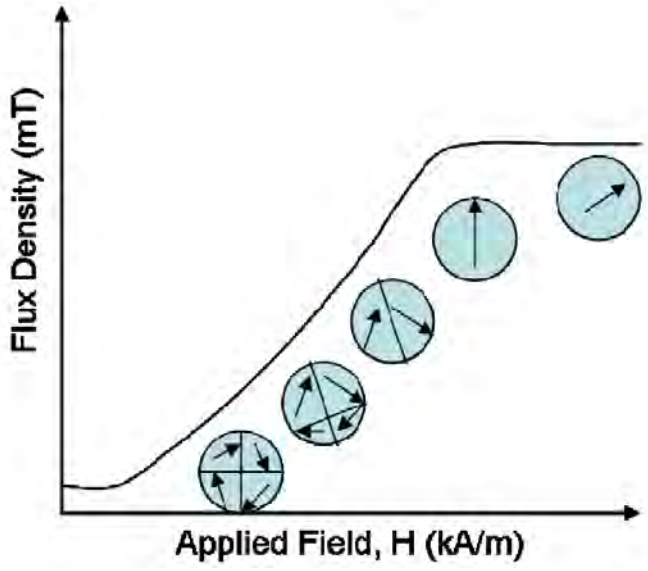

Figure 4-6 Domain movement with applied field in a polycrystalline material.

4.6.2. Domain Wall Pinning

The characterisation of any permanent magnet is determined by the coercive field. If the magnet requires a low coercive field to reverse magnetisation domains this material is known as a soft magnet. If however, the nucleation proves to be difficult and the domain wall is difficult to mobilise, then this will lead to the need for a large coercive field to be employed and hence will result in permanent magnet behaviour. This process defines the action of domain wall pinning. Strnat, K.J. (1988) and Durst K.D. et al (1988) are well known scholars in the development of pinning controlled magnets. The above authors have carried out substantial work in the 2/17 SmCo-type magnets, where pinning was determined by the presence of the $SmCo_5$ phase which has a lower domain wall energy than that of the 2-17 phase. The 2/17 type has its domain wall pinned within the material and consequently, the reverse process of magnetisation proved to be difficult.

4.6.2.1 Domain Nucleation

As mentioned before, the difficulty in reversing the domain nucleation, results in the generation of a large coercive field resulting in permanent magnet behaviour. The microstructure can be developed further by having a specific sintering processing technique as well as using annealing for the further development of smooth and fine grains. When the grains structure is in a distorted state, this can facilitate the

nucleation of reverse domains. In order to increase the field needed for domain nucleation, any damage to the grains should be reduced and this should require further smoothness to the grain boundaries, with this, the coercivity would increase as well. This would take place when a reverse field is applied after the material has reached saturation. This will induce a high resistance to demagnetisation because of the difficulty in the nucleation of the reverse domains.

Figure 4-7 shows the magnetic behaviour of 2 types of coercivity mechanism; namely, nucleation and pinning type. In the nucleation type, the domain walls move freely when there is an external magnetic field and a steep magnetisation curve takes place. For pinning on the other hand, there will be low initial magnetisation which is caused by the pinning of the domains. Once the pinning field (H_p), is exceeded there is a rapid magnetisation of the sample.

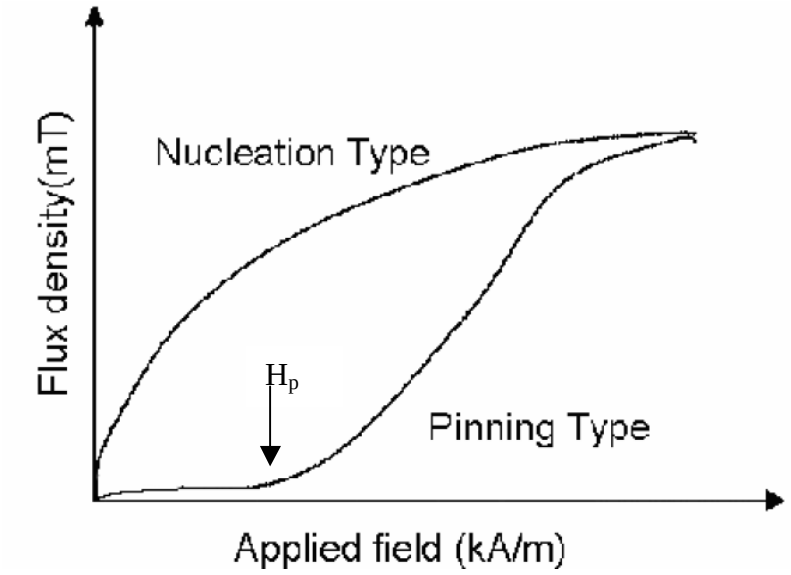

Figure 4-7 Nucleation & pinning type of coercivity mechanism magnetisation curves.

4.7 Summary of Coercivity Mechanisms

There are many methods of increasing or decreasing coercivity. These involve controlling the magnetic domains within the material. (Bollero et al., 2001). For a hard magnetic material, it is desirable that the domains cannot easily rotate their

direction of magnetisation and that the domain walls do not move easily and/or nucleation of domains is difficult. (Givord et al., 2003)

To prevent easy rotation of domains, the material needs strong uniaxial magnetocrystalline anisotropy. Alternatively, shape anisotropy can occur in needle-like particles / grains, where the magnetostatic energy is less when the magnetisation is in the long axis of the needle compared to that in the short axis.

If the size of a magnetic domain is within a single grain then the material possesses 'single domain particles', and if they have sufficient high anisotropy to prevent the easy rotation of the direction of magnetisation then the particles will be permanently magnetic and very difficult to demagnetise. This type of coercivity mechanism can be observed in melt-spun NdFeB magnets where the crystal size is ~50 nm, compared to the critical size for single domain particles of ~300 nm. (www.magnets.bham.ac.uk)

As discussed previously, permanent magnets can also achieve their resistance to demagnetisation by pinning domain walls. In $Sm_2(Co,Fe,Cu,Zr)_{17}$ type magnets this is achieved by the presence of a $SmCo_5$ based phase in which the domain wall energy is significantly lower than that of the majority Sm_2Co_{17} based phase. The domain walls are therefore pinned within the $SmCo_5$ phase and both magnetisation and demagnetisation processes are difficult.

Permanent magnets can also achieve coercivity by making the nucleation of new domains difficult. This mechanism can be found in sintered NdFeB permanent magnets where a non-magnetic grain boundary phase acts to smooth the grain boundaries, removing domain nucleation sites. Nucleation controlled permanent magnets are easily magnetised as the initial state has several domains in each crystal, but are difficult to demagnetise because this would require the nucleation of new reverse domains.(Vial et al., 2002)

4.8 Hysteresis Loop

The hysteresis loop, shown in figure 4-8 is used to characterise a magnetic material. From the 1st quadrant, saturation polarisation, J_S and magnetisation, M_S can be determined. The field produced by the magnet after the magnetising field has been removed is called the Remanence, Br or Jr. The reverse field required to bring the

induction to zero is called the Inductive Coercivity, ${}_bH_c$, whereas the reverse field required to bring the magnetisation to zero is called the Intrinsic Coercivity, ${}_jH_c$. The maximum value of the product of B x H in the second quadrant is called the Maximum Energy Product, (BH_{max}) and is a measure of the maximum amount of useful work that can be performed by the magnet. (BH_{max}) is used as a figure of merit for permanent magnet materials.

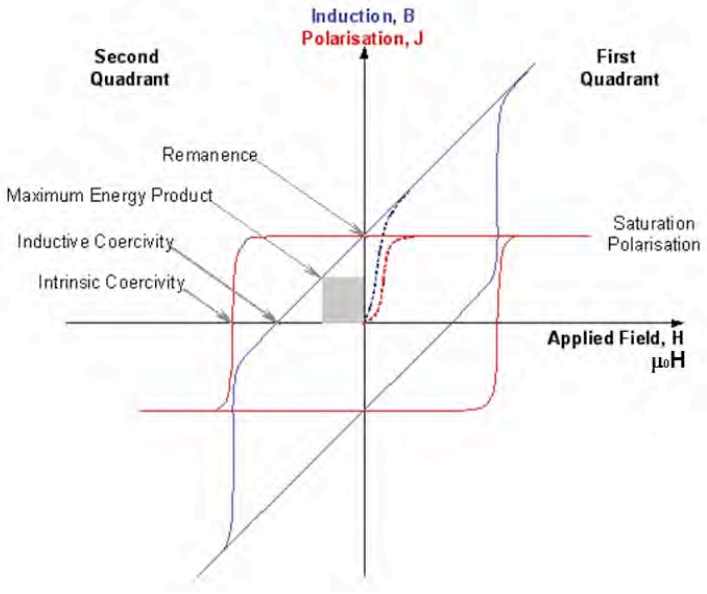

Figure 4-8 A typical hysteresis loop for a ferro- or ferri- magnetic material. (www.magnet.bham.ac.uk)

The maximum possible energy product for a given composition is $\frac{(Js)^2}{4}$ (for a perfectly square demagnetisation curve).

$(BH)_{MAX}$ is used as a figure of merit for permanent magnet materials.

The polarisation will only decrease after a sufficiently high field applied to:

1. Nucleate and grow domains favourably oriented with respect to the applied field

Or

2. Rotation of the direction of magnetisation of the domains towards the applied field.

After applying a high enough field, saturation polarisation will be achieved in the negative direction. If the applied field is then decreased and again applied in the positive direction then the full hysteresis loop is obtained.

If the field is repeatedly switched from the positive to the negative directions and is of sufficient magnitude, then the polarisation and induction will cycle around the hysteresis loop in an anti-clockwise direction. The area contained within the loop indicates the amount of energy absorbed by the material during each cycle of the hysteresis loop. The shape of the loop can give an indication of the magnetic domain behaviour within a specific material. In order to determine the squareness of the second quadrant, a J vs. $\mu_o H$ should be plotted against $\mu_o H$, and H_k represents 90% of the remanence of the applied field. This squareness factor is dimensionless and has a value between 0 and 1.

$$\text{Squareness factor} = \frac{H_k}{{}_jH_c} \qquad \text{Equ. 1.12}$$

Throughout this thesis, the reported magnetic properties consist of: remanence, coercivity and maximum energy product (BHmax). These are used to compare and study the behaviour of the magnetic materials under investigation. Figure 2-1 (Chapter 2), shows the improvement in $(BH)_{max}$ of the permanent magnet materials, which is used as a figure of merit, and is a measure of the ability of magnets to do work per unit volume of material. The sizes of magnets have been reduced dramatically over the years through the technological advancement of magnet materials and their processing.

5.0 Sintering

5.1 Introduction

German defined Sintering in his books (1985 & 1996) as:

"*Forming a coherent bonded mass by heating metal powders without melting; used mostly in powder metallurgy* (this excludes liquid phase sintering). He adds further on that*:*

"The sintering lowers the surface energy by reducing the surface area with concomitant formation of inter-particle bonds".

The bonds grow by various mechanisms that occur at the atom level. For many metals and ceramics, bonding is by solid-state diffusion. Alternatively, particle melting occurs during liquid-phase sintering, resulting in a solid-liquid mixture during thermal cycle.

By the 1940's, sintering was used in the fabrication of tungsten alloys, uranium dioxide nuclear fuel elements, electrical contacts, ferrous structural alloys, and many refractories. Towards the end of the 20^{th} century, there was an enormous increase in materials made by sintering, especially in the creation of technical ceramics. Special attention was paid to materials with high temperature properties. Nowadays, sintering is employed in a huge range of products such as dental implants, rocket nozzles, magnetic materials; aircraft wing weights, ultrasonic transducers, turbochargers, semiconductors substrates and golf clubs. Modern applications in today's world reflect the need to include the economy of manufacturing, improved properties and novel compositions.

5.2 The Sintering Theory

Sintering models started emerging from fundamental studies in the 1930's and 1940's. One of the first quantitative models by Frenkel and Kuczynski was published in the late 1940's and subsequent work by Lenel, Coble, Kingery, Berg and others succeeded in providing a theoretical work (German, 1996). Sintering theory is based on previous models and provides a good guide to sintering of single-phase powders

sintered by solid state diffusion (Davies, 2004). Most sintering systems consisting of multi-phases which may incorporate a liquid at the sintering temperature as is the case of the RE-FeB type systems examined in the present work. The ranges of sintering techniques that can be applied are shown in Figure 5-1.

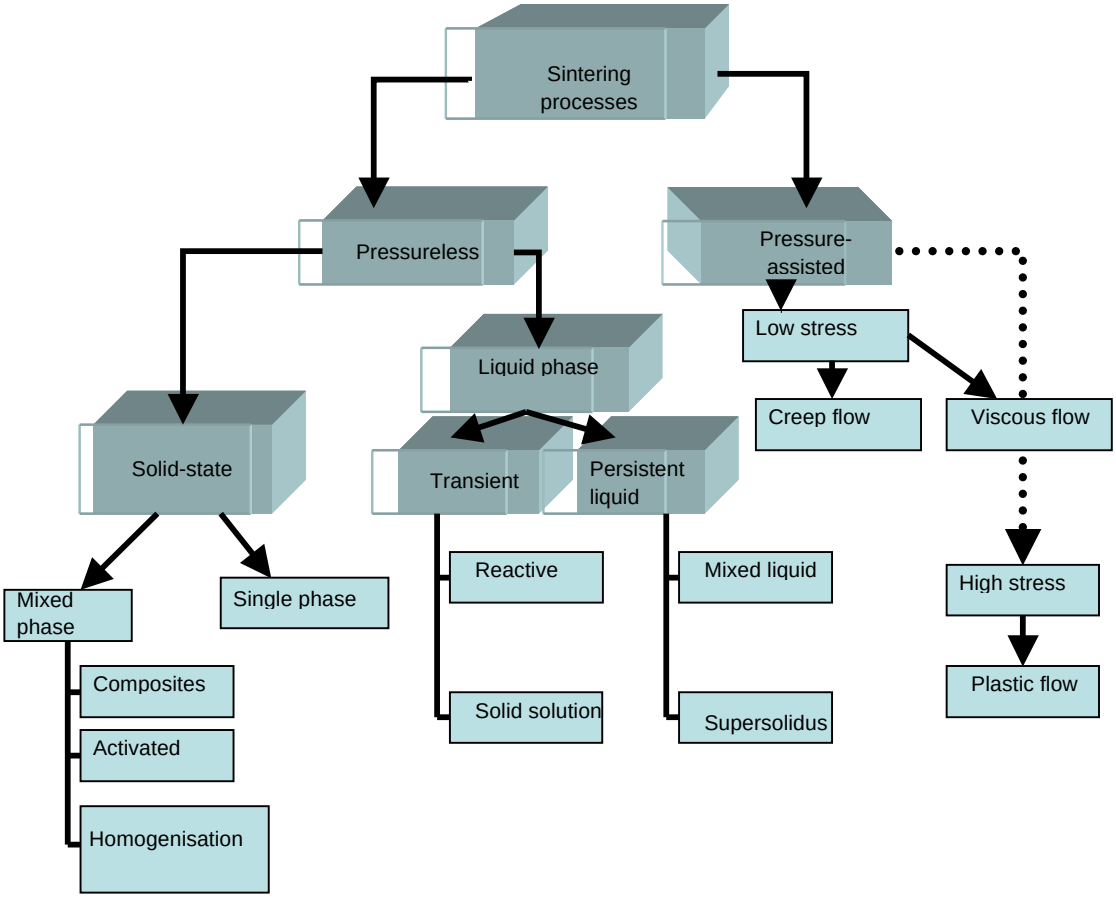

Figure 5-1: Sintering Processes (adapted from German, 1996)

In the majority of sintering categories, the first element always to be considered is the pressure. In some cases, most of the sintering techniques are performed without an external pressure (Pressureless sintering). As the sintering evolution becomes more progressive (more difficult to desnsify), the pressure-assisted method is becoming a favoured approach and an example is hot isostatic pressing (HIP). Materials that often require pressure-assisted sintering include intermetallics or materials with high melting points with no liquid phase present.

As far as the NdFeB-type magnets are concerned, sintering generally occurs with the presence of a liquid phase. Hence pressure-less sintering is used; however, during sintering the liquid phase can be consumed (transient liquid phase) and solid state

sintering also plays an important role in the final stages. To improve control of grain size and the densification of high $(BH)_{max}$ (low Nd-rich phase) NdFeB-type magnets, pressure assisted techniques could be advantageous for the production of these materials as well.

5.3 Liquid Phase Sintering (LPS)

LPS for metals was first used over 400 years ago by the Incas who converted platinum grains into a consolidated form by use of the gold bonds. The idea was that the gold melted during the sintering process. Nearer the present day (1900-1930), LPS was used in the production of cemented carbides. This type of material proved to be an invaluable product in the enhancement of tool and machining materials. Carbide products were patented during the 1920's and these were mixed with metallic binder alloys. During the 1920's, bronze bearing materials were also developed, based on sintering mixtures of copper and tin powders. The classic oil-less bronze bearings have inter-connected pore networks created by the transient liquid phase when tin melts (German, 1996: referencing Morgan, 1978). These pores are subsequently filled with oil to provide self-lubrication during operation. Some examples of materials sintered using LPS are shown in table 5-1.

Table 5-1: shows some of the examples of liquid phase sintering systems and its uses.

Liquid Phase Sintering and its uses	
System	Use
WC + Co	Cutting & machining tools
Cu + Sn	Oil-less bearings
Al + Pb	Wear & bearing surfaces
W + Ni + Fe	Radiation shields, weights
Al_2O_3 + SiO_2	Refractories for steel making
W + Ag	Electrical contact
Fe + Cu + C	Structural components & gears
Ag + Hg	Dental amalgam for fillings
Pb + Sn	Soldering pastes

Fe + P	Soft magnetic components
Al + Si + Cu	Light-weight structural components
$BaTiO_3$ + LiF	Electrical capacitors
Si_3N_4 +Y_2O_3	High temperature turbines.
	NdFeB-type magnet production

Table 5-1: examples of LPS and its application (adapted from German (1996)

Densification by typical liquid phase sintering occurs in 3 overlapping stages as illustrated in figure 5-2: (1) initially, when the mixed powders are heated to a specific temperature where the liquid forms.

(2) With this liquid formation there will be a rapid initial densification if good capillary force exists by the liquid metal wetting the solid particles. As the system reduces its energy, porosity elimination takes place. The elimination of porosity increases compact viscosity, consequently the rate of densification can slow down. The amount of densification determined by rearrangement is dependant upon the particle size, amount of liquid and the solubility of the solid in the liquid. Finer particles usually result in better rearrangement. With rearrangement, and with enough liquid being formed, this may constitute zero porosity (full density).

(3) Concurrently, with the rearrangement stage, there are other stages: solution-reprecipitation and solid state phase. All these stages overlap with the initial stage being the shortest. As mentioned previously, the rearrangement is part of the initial stage where the liquid formation takes place, there being significant densification, which is a direct result of the particle repacking.

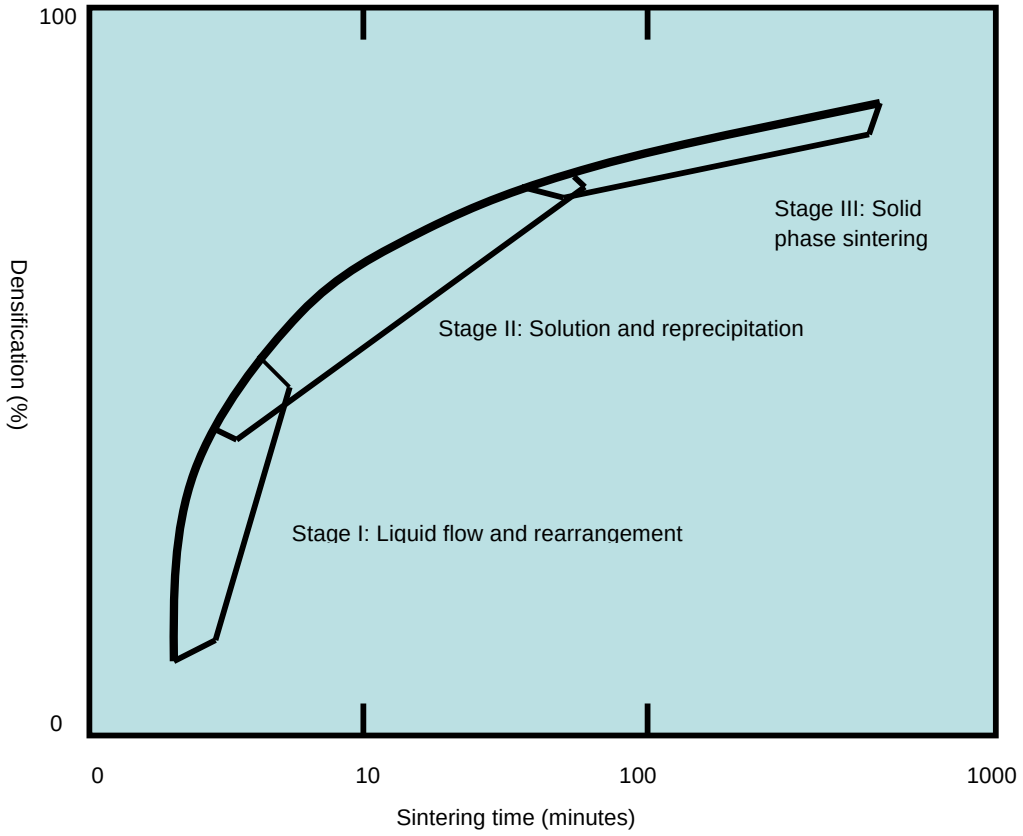

Figure 5-2: diagram shows the stages of liquid phase sintering (adapted from German, 1996)

6 NdFeB magnets

6.1 Rare-earth Iron Boron Magnets

Since their discovery in the mid-sixties (Strnat et al (1967)) rare earth magnets dominated the market throughout the seventies, but civil wars in the African country of Zaire resulted in a substantial increase in the price of cobalt. This prompted the search for an alternative within the much cheaper and potentially stronger iron-based rare earth magnets. Many rare earth binary and ternary systems with iron were investigated (Croat et al, 1980–1982). The discovery of neodymium–iron-boron magnets (based on $Nd_2Fe_{14}B$) resulted eventually in an acceptable new magnetic material. This type of new material had an energy product which was the highest in 1984 (Sagawa, Fujimura et al. 1984) and was based on the atmospheric and complex $Nd_2Fe_{14}B$ tetragonal compound.

6.2 The NdFeB system

Chaban (Chaban et al., 1979) reported the first phase diagram of the Nd-Fe-B system, five years before the importance of the magnetic system was realised. At the beginning of 1980, Stadelmaier and co-workers (Stadelmaier, Elmasry et al., 1983) pointed out the importance of earlier Russian studies of several RE-T- B -based systems (Chaban et al., 1979) because the Russian scientists did not report any structural or magnetic information. Stadelmaier and co-workers suggested that there are possible permanent magnet materials in this system. During 1983, there were a number of researchers working in collaboration with the Office of Naval Research and, they announced their latest findings at the 29th Conference on Magnetism and Magnetic Materials in Pittsburgh, USA. (Koon et al., 1985), Becker (1984) and Hadjipanayis et al., (1984) presented their results on melt-spun RFeB alloys which showed that the microstructure responsible for the optimum magnetic properties consisted of a fine-grained, hard magnetic tetragonal compound with a composition similar to that reported by Chaban and co-workers (Chaban et al., 1979). This phase was stable and was also capable of being produced by conventional melting and casting methods rather than by melt spinning and this was confirmed by Stadelmaier and co-workers, (Stadelmeier et al., 1983) and (Sagawa, Fujimura et al., 1984) who prepared a ternary of RE_2-Fe_{14}-B systems with RE=Nd, Pr or La, produced by arc

melting. Within the cast alloys they discovered the ternary magnetic phase with the tetragonal crystal structure and high uniaxial magnetocrystalline anisotropy. Independently, workers at General Motors in the USA had similar results to those of the Office of Naval Researchers. Sagawa et al., (1984) were the first to produce sintered bulk material based on this alloy and patented the discovery.

During 1980, Sumimoto Special Metals of Japan announced their intent to produce using powder metallurgical processing, based on Nd-Fe-B. At the 29th Magnetism and Magnetic Materials conference, Sagawa and co-workers (Sagawa et al., 1984)) reported their results of studies of the light rare earths, Fe and B ternary systems. In particular, a ternary compound in the Nd-Fe-B – based system with a composition in the range 12 at% Nd, 6 at% B and 82 at% Fe which was similar to that of the Russian scientists. The compound had a tetragonal structure, with a high uniaxial anisotropy and Curie temperature of 312 ^{o}C. Permanent magnets were produced by standard powder metallurgical processing (very similar to that employed previously for $SmCo_5$), from a Nd-rich alloy composition of 15 at% Nd, 8 at% B and 77 at% Fe, with BHmax values in excess of 279 kJ/m^3.

Croat announced, at the 29th Magnetism and Magnetic Materials Conference (Croat et al., 1984), that, a room temperature BHmax value of up to 110 kJ/m^3 was obtainable through the use of melt spun Nd-Fe-B and Pr-Fe-B alloys. The optimum microstructure contained spherical grains of the equilibrium tetragonal compound with a stoichiometry close to that of the Russian findings.

The pre-cursor cast alloy constitution comprised mainly of 3 regions: a $Nd_2Fe_{14}B$ matrix phase, a secondary phase of $Nd_{1+\varepsilon}Fe_4B_4$ and a ternary eutectic at the grain boundaries consisting in part of a Nd-rich phase. Figure 6-1(a) shows the liquidus surfaces and Figure 6-1(b) the isothermal section at 850 ^{o}C of the Nd-Fe-B ternary phase diagram.

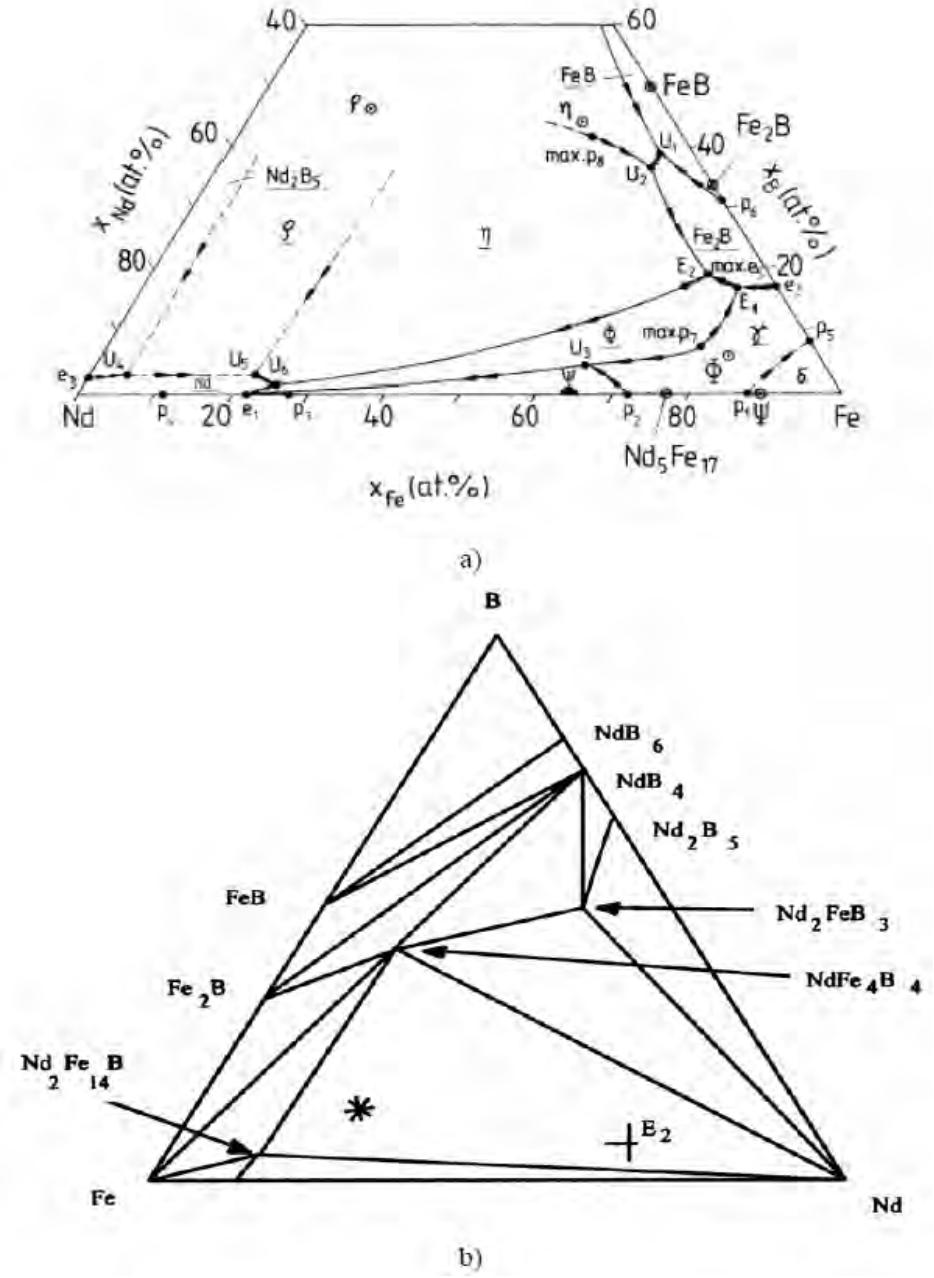

Figure 6-1 (a). Liquidus surfaces of Nd-Fe-B ternary phase diagram (Matsuura et al (1985)) and (b) Isothermal section at 850 ^{o}C. Where E = eutectic, P = peritetectic and U = liquidus temperature.

Sagawa et. al., (1984) developed the Neomax composition which is shown in figure 6-1(b) and marked with an asterix. Figure 6-1(b), shows three equilibrium phases which are present when the alloy solidifies. These are $Nd_2Fe_{14}B$, $Nd_{1+\varepsilon}Fe_4B_4$ and Nd-rich phases, shown as pure Nd on the diagram. The primary phase is the $Nd_2Fe_{14}B$ (ϕ

phase) formed from the melt. The vertical section shown in Figure 6-2 demonstrates that Fe is the primary phase, as long as B = <7 at% (Nd/B = 2), with the $Nd_2Fe_{14}B$ phase being formed through a peritectic reaction: L + Fe →$Nd_2Fe_{14}B$. Excess B and Nd are needed to prevent the formation of magnetically soft α-Fe phase, as it has a very deleterious effect on magnetic properties.

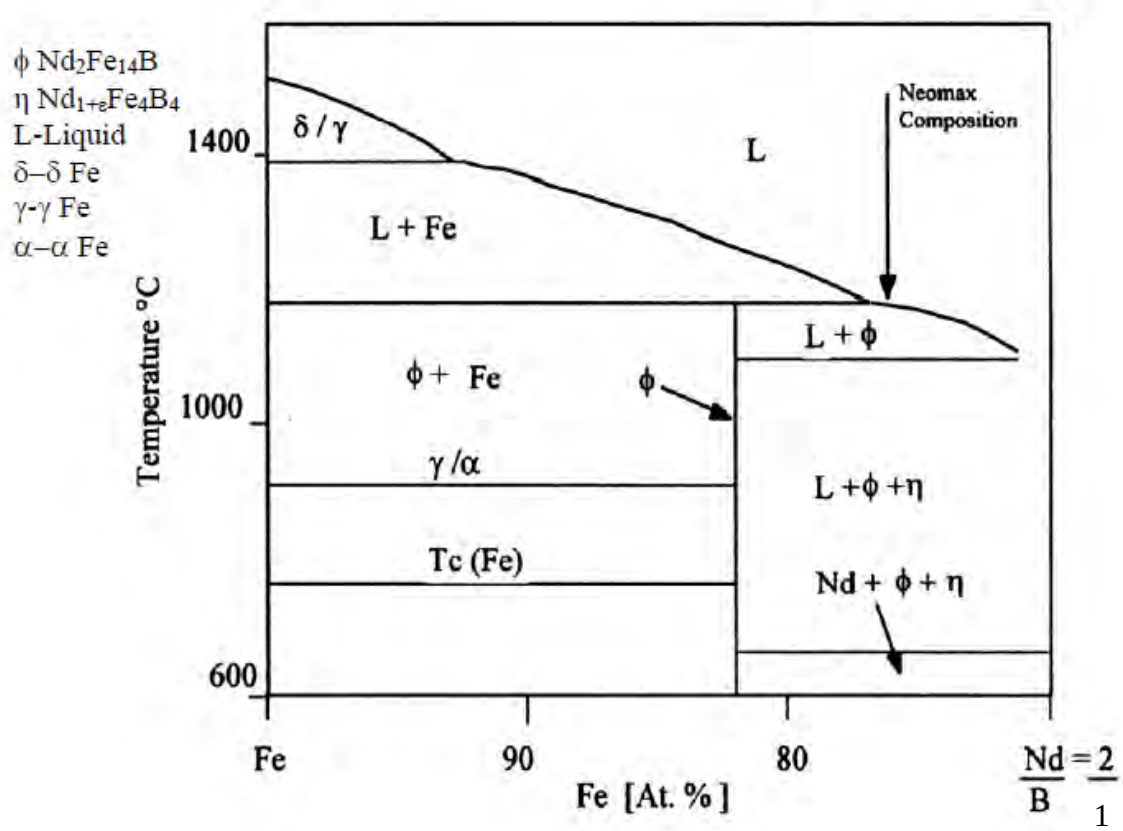

Figure 6-2 Isopleths Fe-$Nd_2Fe_{14}B$ (adapted from Schnieder et al., 1987 and Ozawa et al., 2006).

When the alloy that has the $Nd_2Fe_{14}B$ (ϕ) composition solidifies as the temperature decreases, the composition of the liquid phase changes from liquid to liquid + Fe which then changes to the $Nd_2Fe_{14}B$ (ϕ) phase region according to the peritectic reactions.

The incomplete peritectic reaction will have a cast structure of αFe + $Nd_2Fe_{14}B$ + Nd-rich eutectic phase. The formation of the αFe is avoided by employing the Neomax composition which is Nd-rich with respect to $Nd_2Fe_{14}B$ (see figure 6-2) When the

liquidus valley between the $Nd_2Fe_{14}B$ and $Nd_{1+\varepsilon}Fe_4B_4$ phases is reached then secondary $Nd_2Fe_{14}B$ and $Nd_{1+\varepsilon}Fe_4B_4$ phases are formed without any α Fe. The $Nd_{1+\varepsilon}Fe_4B_4$ forms small grains within the liquid phase, between the primary $Nd_2Fe_{14}B$ grains.

On further cooling, the composition of the liquid moves down the liquidus valley to the ternary eutectic at the Nd-rich corner of the phase diagram (marked as E2 in figure 6-3 (b)). The last phase to solidify is the Nd-rich eutectic phase, formed via a eutectic reaction at 655 °C. The remaining liquid solidifies forming the Nd-rich grain boundary phases together with the phases, Φ $Nd_2Fe_{14}B$ and $Nd_{1+\varepsilon}Fe_4B_4$ which form on the surface of the existing phases. The resultant as-cast microstructure (Figure 6-3) is comprised of:

(a) primary grains of $Nd_2Fe_{14}B$

(b) smaller secondary grains $Nd_{1-\varepsilon}Fe_4B_4$, surrounded by the

(c) Nd-rich regions. Due to non-homogeneity within the liquid and non equilibrium cooling there will also be:

(d) Some iron dendrites present in the $Nd_2Fe_{14}B$ grains.

(e) Cast structure of $Nd_2Fe_{14}B$ consists of α-Fe dendrites, Nd-rich regions and $Nd_2Fe_{14}B$.

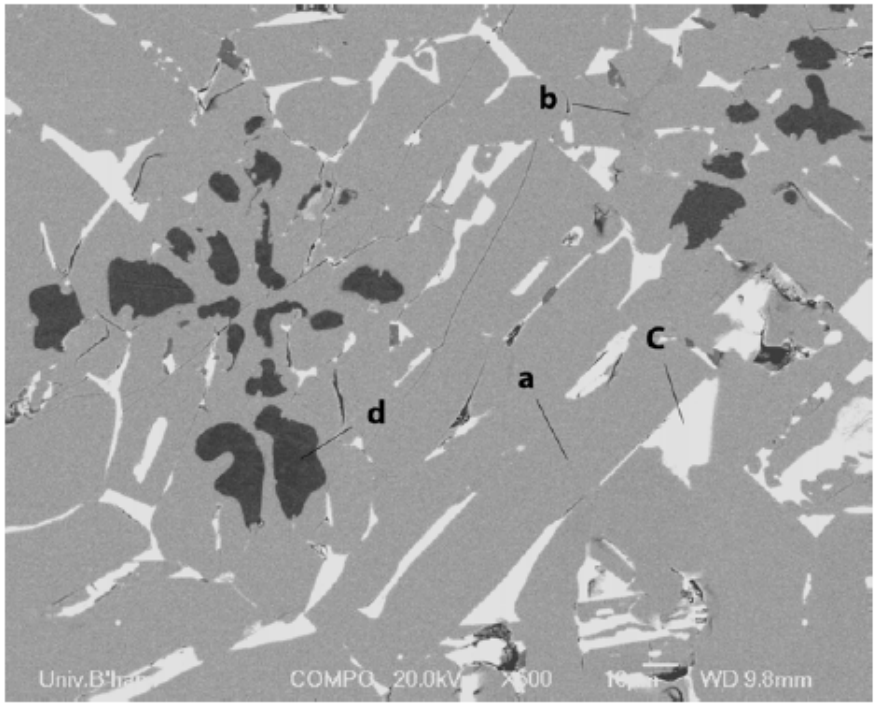

Figure 6-3 as-cast Nd-Fe-B type: (a) $Nd_2Fe_{14}B$, (b) $Nd_{1-x}Fe_4B_4$ (c) Nd-rich (d) iron dendrites (10 µm magnification).

The hard magnetic phase is $Nd_2Fe_{14}B$ which is responsible for the high saturation magnetisation and remanence of the alloy. This structure of this phase determined by Herbst (Herbst, Croat et al. 1984), using neutron diffraction and by Givord et al, (1984), Shoemaker et. al., (1984), Boller and Oesterreicher (1984) using XRD and their results agreed with those of Herbest et al, (1984). These studies indicated that the $Nd_2Fe_{14}B$ phase has a tetragonal structure of space group $P4_2/nm$, as shown in figure 6-4. The unit cell is complicated, containing four formula units (68 atoms). Buschow et al, (1985 and 1986) and Buschow (1986) indicated that $Nd_2Fe_{14}B$ is virtually a line compound (i.e. it has a very narrow homogeneity range). Within the structure there are:

6-non-equivalent iron sites,

2-rare-earth sites and

1- boron site.

These have been named using various nomenclatures by different authors; figure 7-4 uses the system that was developed by Herbst et al, (1985). The line – compound nature of $Nd_2Fe_{14}B$ means that it has, so far proved impossible to produce a precipitation hardened magnetic alloy based on the (φ) – phase.

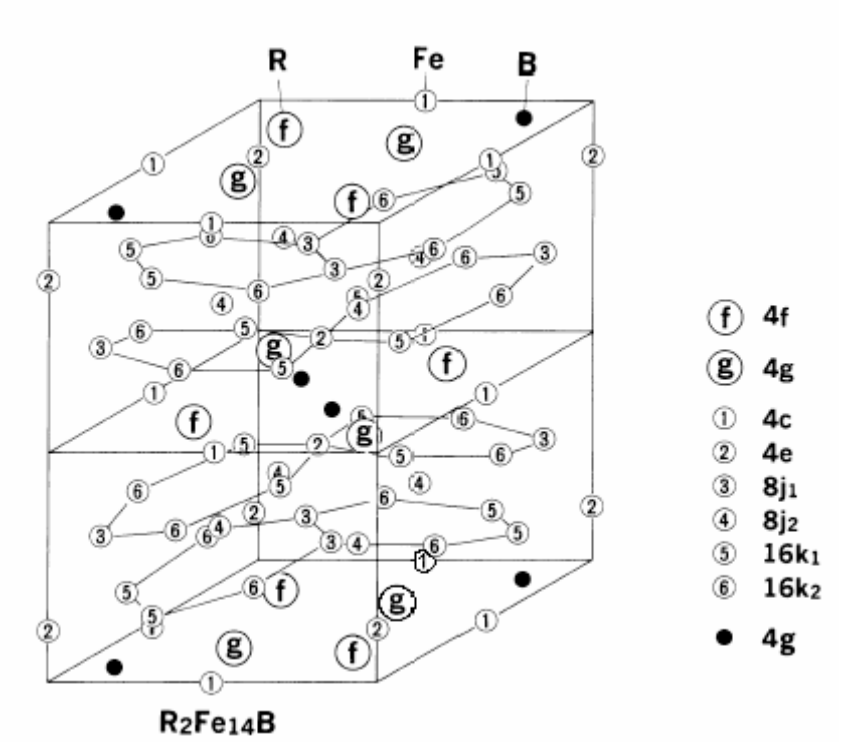

Figure 6-4 Crystal structure of $Nd_2Fe_{14}B$ (Herbst et al.,(1984 & 1985).

In this system, there are 16 Fe atoms, $16K_1$ indicates that there are 16 equivalent sites of its kind present in the unit cell**.** The top half of figure 6-4 symmetrical to the bottom half of the unit cell**,** with mirror planes at z = 0 and z = 1/2. All of the Nd and B atoms and only 4 of the iron atoms in the unit cell are found on these mirror planes, the rest of the iron atoms form networks of atoms between the mirror planes. The Fe(k_1), Fe(k_2), Fe(j_1) and Fe(e) sites make up two slightly distorted hexagonal arrays, one of which is rotated by ~30^o relative to the other. Sandwiched between these two layers are the Fe(j_2), atoms which are located above or below the centres of the hexagons.

$Nd_{1+\varepsilon}Fe_4B_4$ is a non-ferromagnetic boride phase with an FeB primitive tetragonal structure superimposed on a rare-earth, body centred tetragonal system (Givord et. al., (1985)), such that the composition of this phase can be varied; it was first reported

to be $Nd_{1.1}Fe_4B_4$ (using single crystal X-ray data) (Braun et. al., (1982)) and later Matsuura et. al., (1985) proposed the formula to be $Nd_2Fe_7B_6$. However, further work by Bushow et. al., (1986) indicated that the phase has a slight composition range and so the formula $Nd_{1+\varepsilon}Fe_4B_4$ is generally accepted as a description of this phase, where ε ~0.1**.**

The Nd-rich Phase (s)

The paramagnetic, Nd-rich phase is important in determining the Nd-Fe-B magnetic properties (see for example Otsuki et. al., (1990) or Vial et. al., (2002)). Its main function is thought to be to smooth the grain boundaries, thus reducing the number and degree of reverse domain nucleation sites (see earlier discussion on the Domain Nucleation model)**.** In addition, it also isolates the $Nd_2Fe_{14}B$ grains, thus preventing the exchange coupling between adjacent grains**.** The phases at the grain boundaries, as reported by Sagawa et al., (1984b), contained 85-95 at% Nd, 5-15 at% Fe and traces of boron. By using X-ray analysis, this phase was reported to have a Double-Hexagonal-Close-Packed (DHCP) structure in the as-cast, ingot material (Matsuura et. al., 1985). However, in sintered magnets the phase was reported as having a Face-Centred-Cubic (FCC.) structure (Sagawa et. al., (1984)a; (1984)b; Ramesh et. al., (1986))**.** This was attributed to the higher oxygen content in the grain boundaries of the sintered magnet (0.017 wt% in the ingots compared to up to 0.63 wt% in the sintered magnets) (Weizhog et. al., 1988). From the literature, it appears that the Nd-rich regions are rather complex. Four types of structure were reported as shown in table 6-1. Most rare earth metals contain oxygen introduced inevitably when they are processed. The additional oxygen means that the alloy system has to be considered as a quaternary system (Nd-Fe-B-O) and additional phases may well be present.

Schneider et al., (1987) showed by DTA studies that oxygen causes two types of eutectic in the system, one forming at 685 ^oC and the other at 655 ^oC. The formation of an FCC phase is the result of the higher oxygen content compared with that of the DHCP phase**,** and this also leads to an increase in the amount of $Nd_{1+\varepsilon}Fe_4B_4$ phase present. This was found to have an important influence on the sintering behaviour of the alloy (see for example Kim and Camp (1995) or Vial et. al., (1985))**.** If this phase

was not formed then the sintering process would not have produced fully dense magnets (Fidler et al., (1995)). This presents a real problem for those magnets with compositions close to that of stoichiometry and, in the case of recycled magnets, the addition of Nd (in the form of NdH_2) is required (see later)

Table 6-1: The crystal structure and lattice parameters of all reported Nd-rich phases (adopted from Wang and Li 2005 and Zakotnik, 2008).

Phase	Prototype	Space group	Lattice parameters, nm	References
DHCP-Nd_2O_3	Unknown	HPC	A=0.365-0.37, c=1.18	Fidler (1985), Tang (1988)
FCC-NdO	NaCl	$Fm\bar{3}m$	A= 0.507-0.524	Tang (1988), Lemarchand (1990)
Complex-Nd_2O_3	Unknown	FCC+BCC	a_{FCC}=0.52 and a_{BCC}=1.04	Lemarchand (1990), Jin (1993)
hNd_2O_3	La_2O_3	$P\bar{3}m1$	A = 0.383, c = 0.6	Grier (1991)

6.3 Development of NdFeB-type magnets:

The developments in Nd-Fe-B permanent magnet production came with the development of $Nd_{15}Fe_{77}B_8$ (trade name “Neomax”) in 1984 by the Sumimoto Company of Japan. Magnets of this type offered good coercivity and very high remanence values, and possessed the highest energy product then available. Recent developments (Kaneko et al., 2006) have resulted in magnets with an energy product of 460 kJ/m^3 and a Br value of 1.533 T corresponding to almost 96% of the theoretical value of the $Nd_2Fe_{14}B$ system. However, the world record for energy product was

established in 2006 at 474 kJ/m^3 by NEOMAX Co. Ltd. (Matsuura et al., 2006). See figure 2-1 for the trend in $(BH)_{max}$ values.

6.4 Neodymium Iron Boron Magnetic System:

As mentioned previously, melt-spun NdFeB magnets were produced in 1984 by Croat and co-workers through the use of melt-spinning (Croat, Herbst et al. 1984) and simultaneously by Sumitomo-Sagawa by the sintered route. The starting ingots were arc or induction melted and these ingots were then melt spun (see figure 6-5) in an argon atmosphere. This involved forcing the melted ingot through a nozzle onto a rotating disk which is water cooled. The cooling rate depends on the speed of the rotating disk. The bonded magnet exhibited a maximum energy product $(BH)_{max}$ of ~112 kJ/m^3 (14 MGOe), the largest value ever reported for a light rare-earth-iron magnet during that year. Croat concluded that the addition of boron improved the coercivity and the BHmax of melt-spun NdFeB and PrFe alloys.

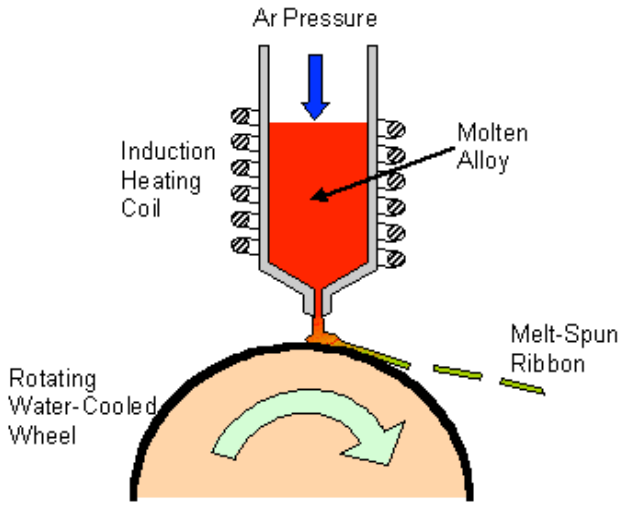

Figure 6-5 Schematic representation of the melt-spinning process.

At around the same time, Sagawa et al., ((Sagawa, Fujimura et al. 1984) developed similar type magnets using the processing of sintering. They milled the powder to a specific size, then aligned and pressed the powder in the direction of alignment. The powder was subject to a high sintering temperature of 1310-1430 K (1037-1157 ^{o}C) for 1 hour in an argon atmosphere and then cooled rapidly in a cooling chamber. The samples were post-heat-treated at a temperature of 400-1400 K (127-1127 ^{o}C) for 1

hour and cooled rapidly again. These cheaper and stronger magnets became a possible alternative to $SmCo_5$ and $Sm(Co,Fe,Cu,Zr)_{17}$ magnets.

The NdFeB type magnets combine a high saturation magnetisation with a good resistance to demagnetisation. The then high cost of samarium and the instability in the price of cobalt led to these magnets becoming the material of choice for applications requiring high-energy magnets. Despite the high room temperature $(BH)_{max}$ values, these magnets have a relatively low Curie temperature (~ 312 °C) which limits their use in high temperature applications: an addition of Co and Dy (see later) improves the temperature characteristics but also increases the costs.

6.5 Processing of magnets

The primary improvement in the production of these magnets is the use of the Hydrogen Decrepitation process (HD).

6.5.1 Hydrogen Decrepitation

Given the right conditions, materials such as $Nd_2Fe_{14}B$, $SmCo_5$ and $Sm(Co,Fe,Cu,Zr)_{17}$ all have the capability of absorbing significant amounts of hydrogen. This hydrogen absorption process can result in the decrepitation of the brittle alloy into a relatively coarse powder. In order for the decrepitation to take place, the material has to be exposed to hydrogen within specific conditions such as pressure, exposure time and the initial condition of the alloy, such as microstructure and temperature.

Harris in 1979 was the first to introduce this process and it was patented (Harris (1979)) and was given the title HD-process (Hydrogen Decrepitation, (Evans, J. P. S. Wyholm, UK Patent 1554384 (1979))). Subsequently, it has become an essential part of the manufacturing the magnetic powder to be used for the production of sintered NdFeB-based magnets. In 1987, Harris disclosed the characteristics of the HD process and the HD process was applied to the production of $SmCo_5$, NdFeB and 2/17 phase in $Sm(Co, Cu, Fe, Zr)_{8.92}$.

Summary of the HD process:

The particles produced are easily crumbled and the size can be reduced further by additional milling (e.g. jet mill).

If the HD were controlled to give finer grains, this might eliminate the need for further milling.

The particles produced are of a clean nature, i.e. their surfaces are ideal for the production of sintered or bonded magnets.

Using hydrogen can overcome the obstacles to the crushing of the ingot using conventional/mechanical methods due to the presence of free iron.

The preponderance of intergranular failure can increase the proportion of single crystal particles.

The decrepitation in hydrogen can reduce significantly the oxygen uptake during milling.

When the green compact is aligned it possesses zero remanent magnetism making handling much easier.

When hydrogen is desorbed during vacuum sintering it produces a clean reducing atmosphere for the sintering process.

The sintering temperature is reduced greatly due to the particles' clean surfaces compared with powder produced by conventional means.

The sintered magnets' grain sizes are much smaller.

The HD process gives a greater control over the size, particle shape and distribution of the microstructure of the alloy.

With the use of alloys such as Neomax, this process is relatively quick and easy as the size of the grain is quite large and hydrogen can penetrate easily through the Nd-rich material at the grain boundaries. Initially, Sagawa (Sagawa, Fujimura et al. 1984) used mechanical jaw crusher in order to prepare for a coarse powder for milling.

Alternatively, the HD process can be used to break up the alloy as first proposed by Harris et al., 1985.

Figure 6-6 shows schematically that when the hydrogen is absorbed initially by the Nd-rich grain boundary material which causes the expansion of the material and hence decrepitation which means the “separation of parts with a crying sound”. The process has 2 stages, firstly hydrogen being absorbed by the Nd-rich phase and then by the $Nd_2Fe_{14}B$ matrix phase.

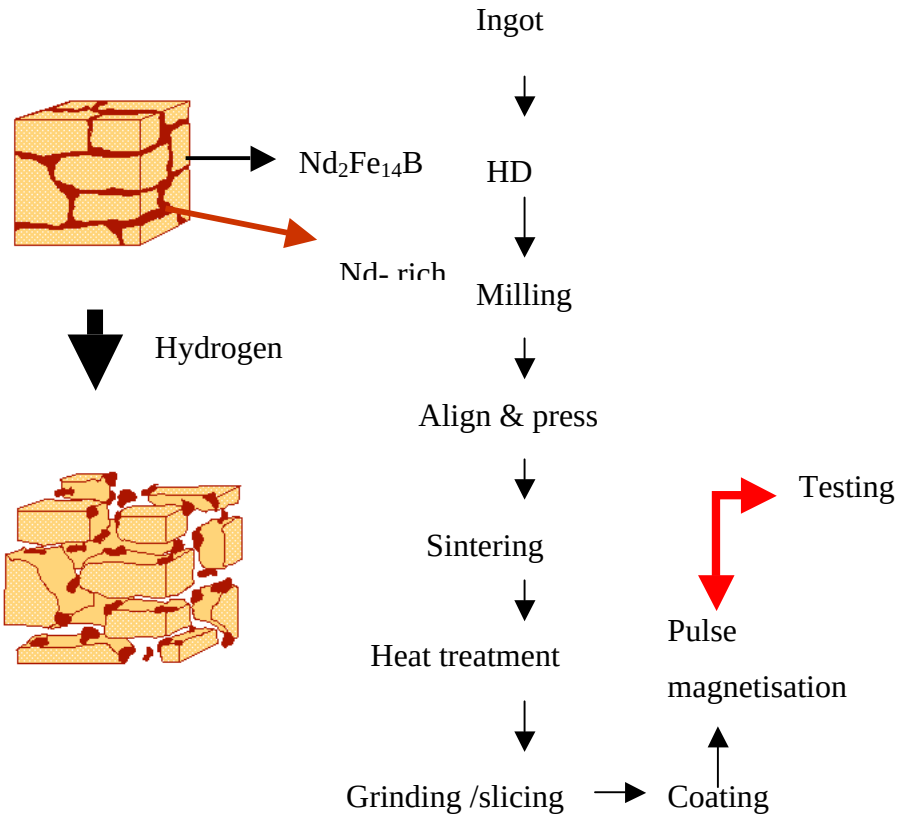

Figure 6-6: The processing route for sintered NdFeB permanent magnets using HD

These processes are accompanied by the lattice expansion in the respective phases which leads initially to inter-granular then trans-granular fracture. The main advantages of using the HD process have been summarised previously.

Perhaps the most important advantage is that the powder is much more friable in the hydrided from and hence there is a spectacular reduction in the jet milling time. It has been estimated that, overall, there is a reduction in production costs of around 25% using the HD-process as opposed to mechanical comminution.

6.5.2 Behaviour during decrepitation

Harris et al., (1985) reported, along with Pollard and Oesterrecher, (1986) that Neomax alloys (Nd-Fe-B-type) and related compositions can produce powder by the use of the Hydrogen Decrepitation process.

The experience gained working with this type of rare earth alloy indicated that the NdFeB material was extremely active in absorbing hydrogen and thus made it a prime candidate for future HD processing. When hydrides are formed in RE materials, it is accompanied by an expansion of the lattice. Westlake (1983a & b) claimed that the metal lattice expansion is directly proportional to the number of hydrogen atoms within the alloy or compound. Each hydrogen atom results in a volume increase of 0.29 nm^3. For a large hydrogen uptake, the expansion is in the region of 25% as in $LaNi_5$, $SmCo_5$ exhibits around 10% and $Nd_2Fe_{14}B$ around 5% (L'Heriter et. al., (1984); Pourarian et. al., (1986)).

Harris et al., (1985) reported that the existence of the Nd-rich phase in the grain boundaries makes the NdFeB-type alloys very reactive with respect to hydrogen. This was followed by the absorption into the matrix ($Nd_2Fe_{14}B$) phase which created an inter and then trans-granular fracture. The temperature at the interface increases (due to the exothermic nature of hydrogen absorption) and thus results in the subsequent absorption of hydrogen by the matrix $Nd_2Fe_{14}B$ (ϕ) phase. This can be shown schematically (see figure 6-8). The ϕ phase forms a hydrogen solution rather than a specific hydride. Combination of intergranular failure and surface decrepitation due to layered failure causes the formation of flakes like particles.

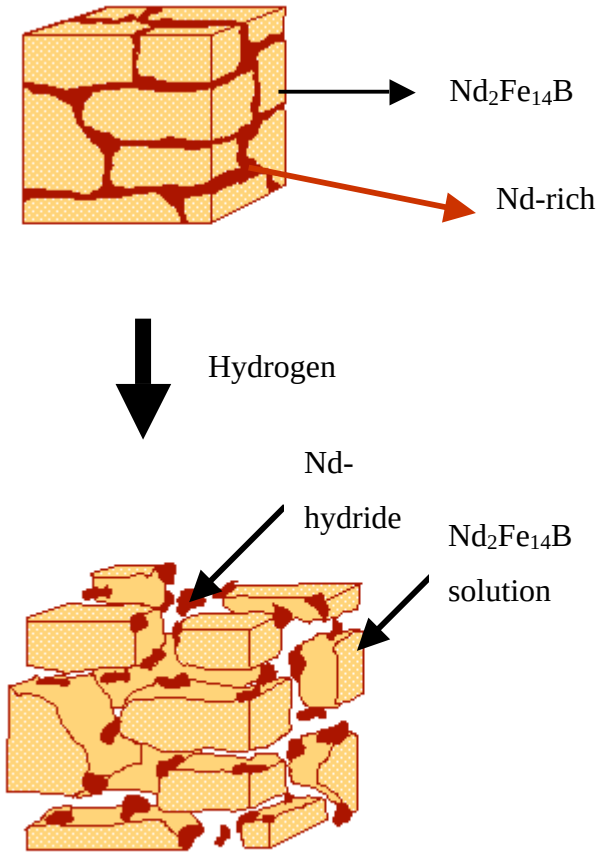

Figure 6-7 Hydrogen Decrepitation of NdFeB-type alloys.

This strain causes fracture at the interface and thus the material breaks into flakes (McGuiness et al., 1990a). A DTA study showed that the absorption consisted of 2 stages, as shown in Figure 6-8 (McGuiness et al., 1986 & 1989).

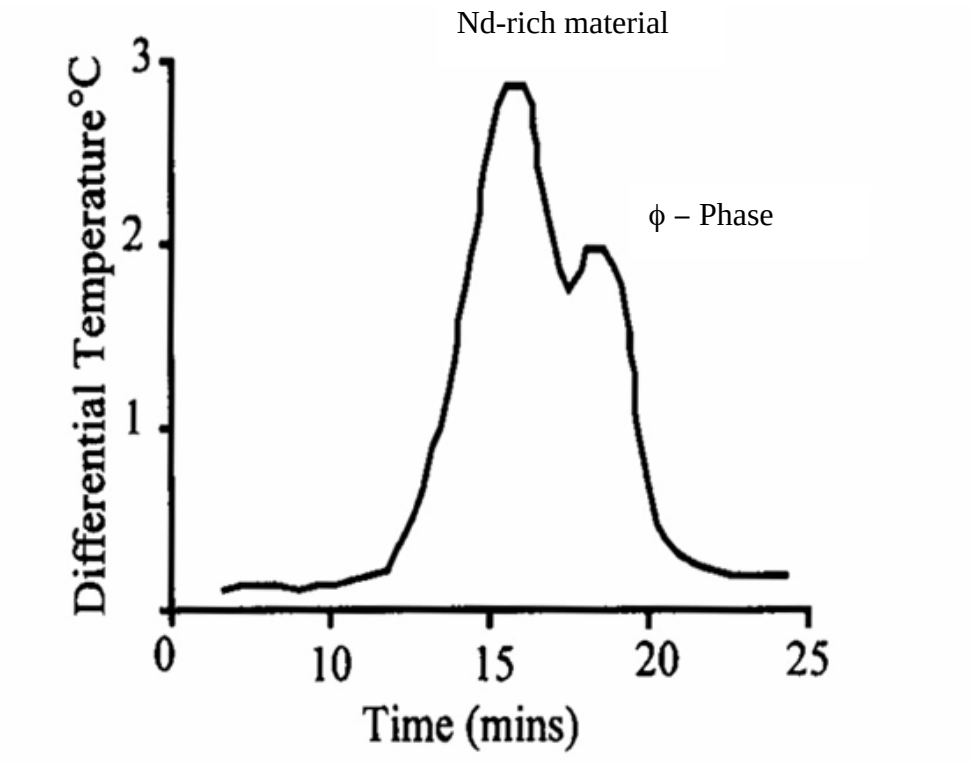

Figure 6-8 Hydrogen absorption in $Nd_{15}Fe_{77}B_8$ using DTA (McGuiness, (1989)).

The H_2-absorption process is a reversible process, where the hydride powder can be converted back to hydrogen free material. Desorption of hydrogen can be performed if the temperature is increased and the pressure decreased. Within the Nd-Fe-B system, the complete desorption of hydrogen can take place during vacuum sintering. Oesterreicher and Oesterreicher (1989), reported that desorption from the $Nd_2Fe_{14}B$-solution occurs at ≈180 ^oC. In addition, Harris et al., (1989) stated that the desorption cycle from $Nd_{15}Fe_{77}B_8$ takes place in 2 stages and most of the hydrogen is desorbed in a temperature range of 150-260 ^oC with further desorption at temperatures of 350-650 ^oC. The 2 stage desorption cycle is due to the initial hydrogen loss from the matrix ϕ-phase ($Nd_2Fe_{14}B$), at low temperature and from the Nd-rich grain boundary phase at the higher temperatures.

Rupp et al., (1987) postulated that single stage desorption and two stage desorption occurs in $Nd_2Fe_{14}B$ and $Nd_{15}Fe_{77}B_8$ respectively. They reported that the same effect takes place for the $Nd_{14}Fe_{79.5}B_{6.5}$ alloy hydrided and degassed at 600 ^oC for 1 hour;

the high temperature peak was not observed after the powder had been exposed to air for 120 hours. (Nakagawa and Onitsuka, 1990). Williams et al., (1993) confirmed that hydrogen desorption from $Nd_{15.5}Fe_{77.5}B_7$ was primarily from the majority matrix phase ($Nd_2Fe_{14}B$) and during hydrogen desorption, the Nd-rich grain boundary phase gives up and hydrogen will move from "trihydride to dihydride". The trace in figure 6-9 (Williams et al., 1993) shows the desorption trace for $Nd_{15}Fe_{77.5}B_7$ hydride**.** At low temperatures there will be desorption from ϕ-phase**,** whilst partial desorption from grain boundary material will have the following reaction:

$NdH_{2.8}$ → NdH_2 and a complete desorption will have NdH_2 → Nd at ≈ 600 ^oC. Magnets with high (BHmax) are partially degassed before alignment.

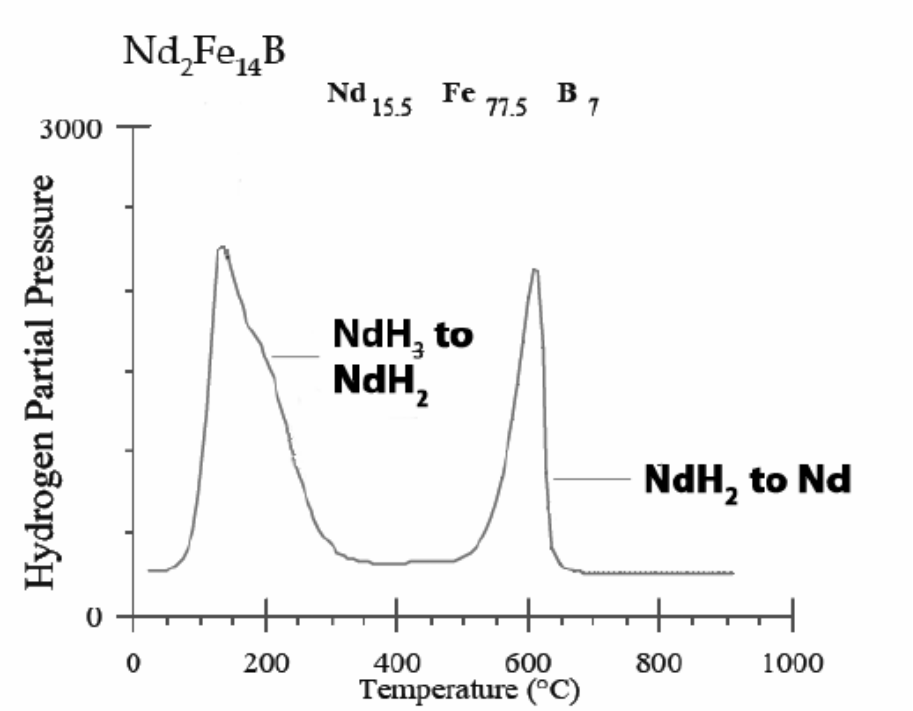

Figure 6-9 The $Nd_{15.5}Fe_{77.5}B_7$ hydrogen desorption trace (Williams et al., (1993)).

6.6 Magnet Production

There are many ways of producing permanent magnets. This can be in many forms whether chemical or mechanical. All processing of magnetic powder normally takes the route of powder metallurgy. The coercivity of RE-based magnets is critical to the magnetic properties and depends on the chemical composition which, in turn, depends on limited oxidation at any stage of the processing. (Harris et al., 1985; Omerod et al.,

1985; and McGuiness et al., 1989). Before the magnets are produced, they will have to undergo many processing steps in order to arrive at the final product. This will have to include: alloys preparation, milling, the control of the alloy composition (possibly by blending), alignment, pressing, sintering/heat treatment and finally machining the product to the required dimensions before being pulse magnetised. Before all this, Hydrogen Decrepitation can be employed as an effective tool in the production of permanent magnets. The HD process proved to be a vital tool in the manufacture of permanent magnets and figure 6-10 gives an outline to the process:

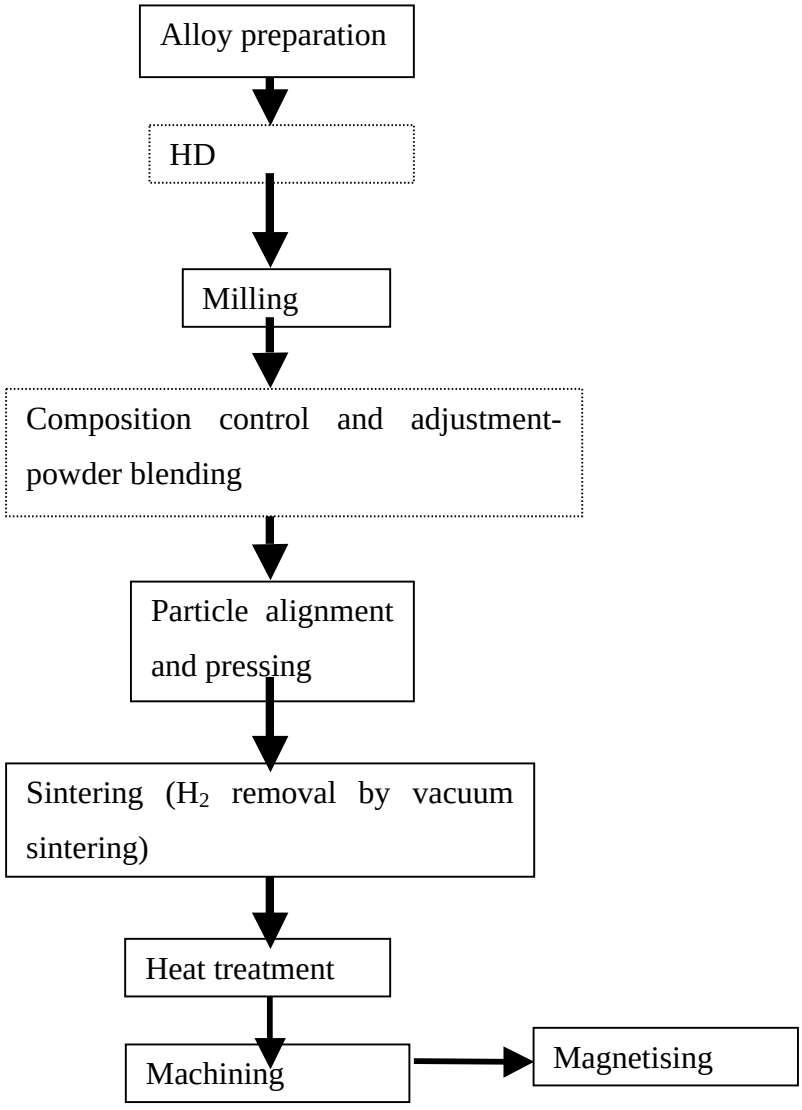

Figure 6-10 The process of rare earth magnet production

The alignment of the individual particles in the green compact controls the level of the remanence and hence contributes to the particular value of (BHmax). All particles

have to align in the same magnetic direction (orientation). This necessitates that the powder's grain size has to be of a very fine microstructure, and this will have a marked effect on the magnet's coercivity (Nothnagel et al.,1991). The alloy has to be milled to a particle size of 3-7 μm in order to achieve a high energy product (BHmax) (Kaneko et al., 1994). The HD-process had a very positive impact upon the production of coercive and anisotropic powder and was critical in achieving good magnetic properties for the sintered NdFeB-type magnets.

6.7 Bonded magnets

The magnetic properties of bonded NdFeB-magnets depend greatly on the loading factors of magnetic powder to resin and moulding characteristics to achieve a high energy product (BH_{max}) value for the end-product. The ease of magnet magnetisation is another factor in the magnet efficiency for many applications. Additionally, the magnets' flux aging loss and their thermal stability are important to their applications where magnets may be subjected to elevated temperatures. As there are many types of magnetic powders and polymer binders available for bonded magnet production, there is a need to determine the precise thermal properties for the polymer and the powder in order to achieve the best BHmax bonded magnets.

The remanence can be affected by the following factors: the proportion of the magnetic phase, degree of the crystal alignment for anisotropic magnets, magnetisation saturation and the density of the bonded compact. All these factors have an effect on the remanence and ultimately will have an effect on the value of BHmax which is approximately proportional to the squareness of the remanence.

As stated above, the magnet remanence is proportional to the volume fraction of the magnetic phase which can be improved by increasing the overall magnet density and/or a decrease in the proportion of the non-magnetic secondary phases of the binder. For maximum alignment; for each particle, the c-axis needs to be orientated in the easy direction of magnetisation. The saturation magnetisation of the magnetic phase is an intrinsic property and can only be affected by changes in the composition.

In the middle of the 80s, Philips (Buschow et al, 1986) developed a new composition which contained an excess of iron and boron. This lean rare earth material exhibited exchange-coupling behaviour whereby the permanent magnetic phase couples with the soft magnetic phase. This latter phase has high magnetic saturation (Fe-rich) resulting in an enhanced remanence. Later, Magnequench made a series of rapidly quenched MQP-Q compositions available which have a similar effect. One advantage of having lean rare earth materials is the excellent corrosion resistance in comparison to that of the standard alloys. The highest remanence (Br) possible from melt spun single phase $RE_2Fe_{14}B$ powder is currently around 900 mT, higher values are possible when the iron content is increased and a $RE_2Fe_{14}B/\alpha$-Fe type nano-composite microstructure has been developed (Brown et. al., 2006). See figure 6-11.

Figure 6-11 illustrates the range of commercially available MQ-powders relative to their magnetic properties (B_r, $_iH_c$).

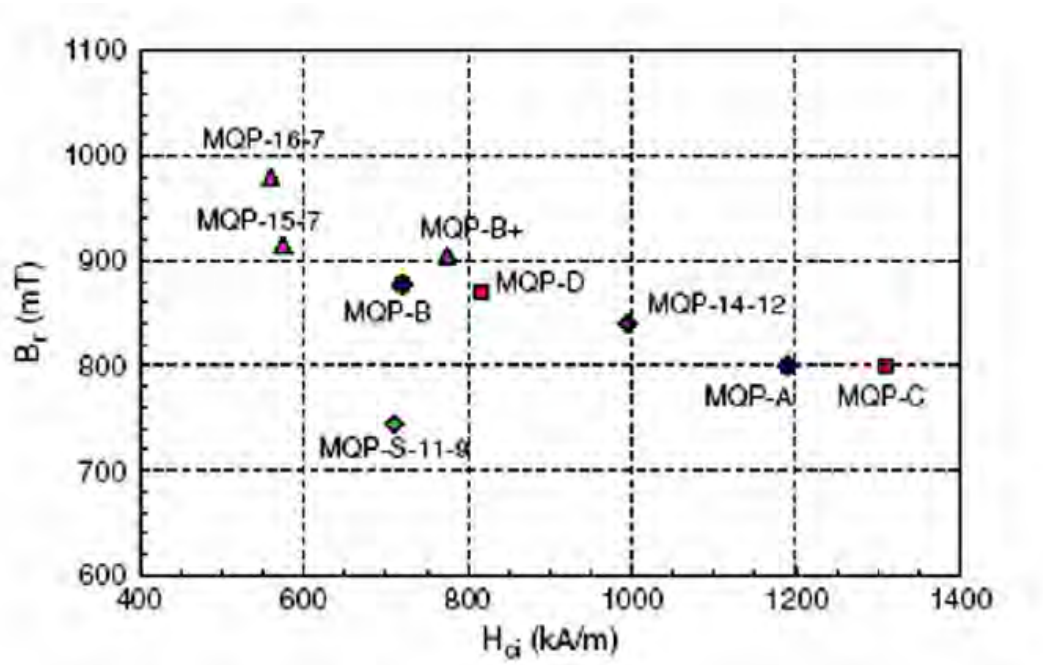

Figure 6-11: shows the magnetic properties range achieved from commercially available MQ-isotropic melt spun powder, (Brown et. al., 2006).

When the magnetic powders are mixed with hard ferrite then there can be combined inter-actions between the coercivities of the two materials. These magnets have generated interest in the market place. Other hybrids using conventional neo-compositions and ferrite, mixtures of neo grades and even Sm–Co with other

materials are being actively marketed today (see for example Schneider and Schmidt, 1996).

After the development of anisotropic bonded magnets through the Hydrogenation, Disproportionation, Desorption and Recombination (HDDR) method by Takeshita and Nakayama (1991), extensive efforts have resulted in a progressive increase of the energy product of bonded magnets in the NdFeB system. In 1999, the Aichi Steel Corporation started commercial production of a family of magnets called *MAGFINE* using an anisotropic powder with a $(BH)_{max}$ of 158 kJ/m^3 produced by the d-HDDR method, (Honkura et. al., 2002). The d-HDDR method is prepared in 4 different steps, while the conventional HDDR has 2 steps in its process (Mishima et. al., 2000). In d-HDDR, each step has a distinctive hydrogen pressure in order to control the reaction rate at a slow value in the disproportionation and recombination stages (Mishima et. al., 2001).

6.8 Sintering of NdFeB

There is still research being performed to investigate the factors that which control the sintering of NdFeB powders. These variables include: time, temperature, particle size and chemical composition. These variables have a direct effect on the outcome of the microstructure and the final magnetic properties in the sintered NdFeB magnets. Sintering is normally carried out in an inert atmosphere (for example argon) or under vacuum. At approximately 630 ^oC the grain boundary eutectic phase melts (Sagawa et al., 1984a), at this low melting, the liquid acts as a sintering aid to enable liquid phase sintering and associated mechanisms of mass transport and densification. Sintering is normally performed for one hour at temperatures between 1040 – 1100 ^oC; (the particular temperature depends on the exact composition), before cooling to room temperature. Having the correct parameters can lead to the achievement of a value of the density of more than 95% of the fully dense value (Ormerod, 1985). This will lead to the reduction of porosity (Davies et al., 2001), which can result in an improvement in the oxidation resistance and decrease in aging during use.

A great advantage would be to try and produce precipitation hardened NdFeB magnet similar to the 2/17s magnets. This would exhibit much greater high temperature stability. The major problem is that the 2-14-1 phase has a very limited range of

stability (see, Buschow 1986) and it is challenging to find the appropriate system to give precipitation hardening

The rare earth content for NdFeB based magnets is important to a factor of 10 greater of that in the $SmCo_5$ type magnets (Ormerod, 1985). Many of the factors that affect the sintering system of NdFeB need to be considered. One critical consideration is the proportion of the liquid phase present at the sintering temperature and this will depend on the excess of the Nd content over that characteristic of the stoichiometric $Nd_2Fe_{14}B$ composition.

Ma and Krause (1987) have studied the effect of varying the amount of Nd on the physical and magnetic properties of NdFeB sintered magnets. It was found that a composition containing less than 33 wt% Nd resulted in incomplete densification and hence poor magnetic properties. Increasing the Nd proportion to more than 33 wt% gave a much better densification. However, the microstructure remained unfavourable for magnetic properties where, in particular, the coercivity had a substantial low value. It was also found that, when the Nd content increased to 34.5-36 wt%, the magnets exhibited an optimum microstructure and magnetic properties. However, this led to a decrease in the remanence which was due to the excessive amount of non-ferromagnetic material at the grain boundary. As this also causes an abnormal grain growth during sintering, there was also a reduction in the coercivity. The Nd–rich material is also susceptible to oxidation (Omerod, 1984 and 1985) and if this can be prevented then it can lead to much better sintering densities (approximately 99% of the theoretical value). Ma and Krause (1987) have indicated that the powder size also plays a vital role, fine particles resulting in more effective alignment, finer sintered grain size and hence higher coercivities (Ma and Krause,1987).

McGuiness et al., (1989) had investigated the effects of varying the processing factors on the magnetic and physical properties of the alloy $Nd_{16}Fe_{76}B_8$. In order to produce compacts, isostatic pressing and jet milling were used and sintering at various temperatures. It was noted that the density of the sintered samples fell significantly when sintered below 1000 ^oC. The density diminished from 7.45 g/cm^3 by sintering at 1000 ^oC to 7 g/cm^3 when sintered at 970 ^oC.

A gradual increase in the remanence was observed for sintering temperatures above 1000 ^{o}C, even though there was a small reduction in the density. This effect was attributed to the preferential grain growth of the larger, well-oriented grains at the expense of smaller, more misaligned grains. Figure 6-12 shows the effect of sintering temperature on density (a) and on remanence (b) (McGuiness, 1989).

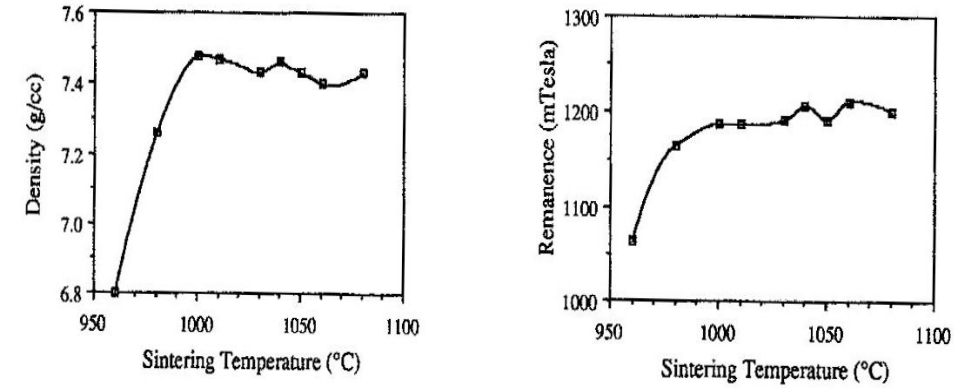

(a) (b)

Figure 6-12 Effect of sintering temperatures on density and remanence (McGuiness et al., 1989).

McGuiness and Harris, (1989) also noted the effect of sintering temperature on the intrinsic coercivity of magnets based on $Nd_{16}Fe_{76}B_8$ (see figure 6-13).

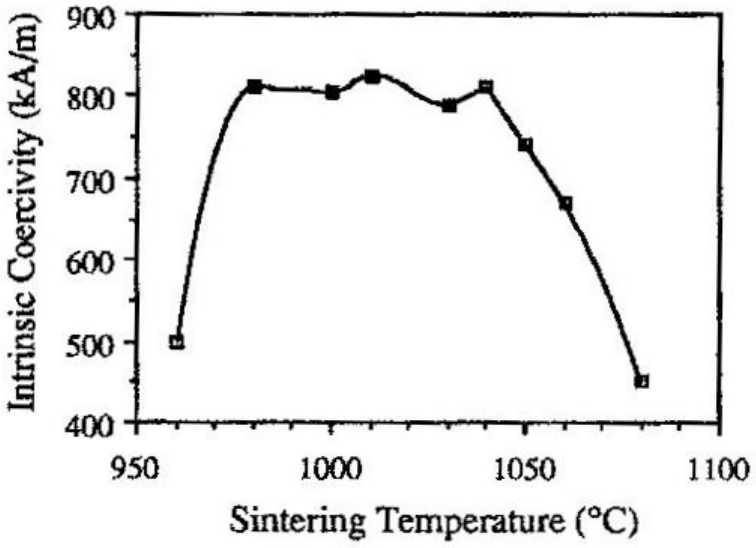

Figure 6-13: Effects of sintering temperature on the intrinsic coercivity (McGuiness et al., 1989)

According to this study, the value of the intrinsic coercivity was reduced by 50% (of its optimum value) after a sintering temperature of 1080 ^{o}C. This was attributed to grain growth during sintering which is in agreement with similar work by Rozendaal et al., (1987). Lowering the temperature (1040-980 ^{o}C) resulted in a remarkable increase in coercivity of up to 800 kA/m. If the sintering temperature was below 980 ^{o}C there was also a reduction in the coercivity and this was attributed to the porosity because of incomplete densification.

Ramesh and Srikrishna (1988) have confirmed statistically and experimentally using the demagnetisation loop, that there is an inversely proportional relationship between coercivity and the grain size. Possible sources of this effect are surface defects, responsible for the low coercivity of large grained magnets and these were listed as steps on the grains surfaces, vacancies, and impurities such as oxides, interface dislocations or lattice distortions. Thus, it is very important to use an optimum sintering temperature in order to avoid inhomogeneous grain growth.

McGuiness concluded that there was a near linear relationship between the spread of the grain size and the sintering temperature (Figure 6-14) for magnets based on the composition of $Nd_{16}Fe_{76}B_8$. Thus small, disoriented gains start to shrink as the favourably oriented grains get larger. These facts were confirmed by Kaneko (1996)

when he studied the effect of process variables on the composition of $Nd_{14.5}Fe_{79}B_{6.5}$ type magnets. He observed that, sintering below 1040 ^{o}C, produced magnets with 7% porosity. To achieve 95% density of the theoretical value, the sintering temperature needed to be 150 ^{o}C lower for the hydrided material (McGuiness et al (1989b).

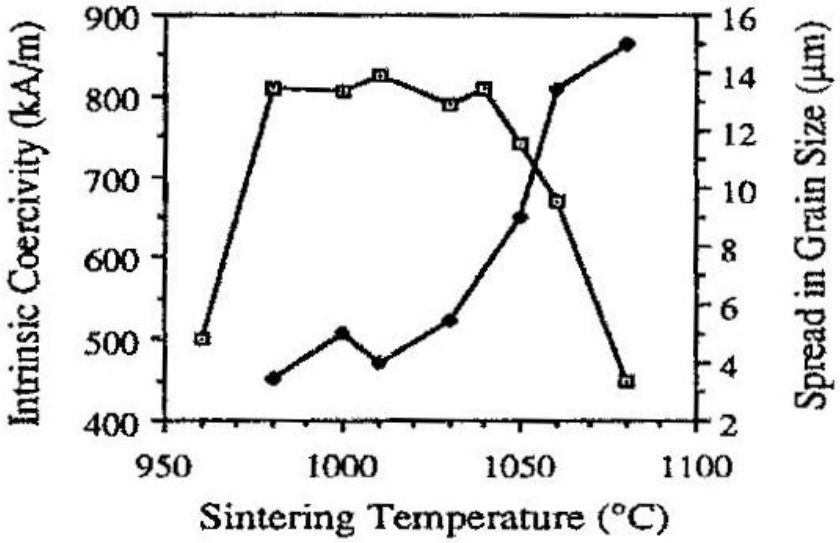

Figure 6-14: effect of sintering on the spread grain size and the intrinsic coercivity (McGuiness et al., 1989).

Similarly, when another sample was sintered at a slightly higher sintering temperature (1069 ^{o}C) the magnets exhibited 4% porosity and a higher coercivity. However, increasing the sintering temperature to above 1070 ^{o}C resulted in a severe reduction in the coercivity. Weizhong et al., (1991) established the relationship between the grain size and coercivity and again deduced that there is an inverse relationship. Weizhong et al., (1991) also ascertained that increasing the Nd content can increase the decoupling of the grains and hence increase the coercivity.

Thus, researchers have reached similar conclusions on the factors governing the exact or desired magnetic properties which are controlled by tight factors. Thus, sintering at low temperatures produces porous magnets with a low density and coercivity. However, as mentioned before, increasing the sintering temperature reduces the porosity, but it may also cause grain growth which may lead to the curtailment of the

coercivity. An increase or decrease in the rare earth content will also have an effect on the production of large grains during sintering.

McGuinness et al., (1989a) made a comparison between the hydrogen decrepitated powders and conventional powders. Dilatometry studies indicated that the HD compacts exhibited shrinkage at low temperatures because of the two hydrogen desorption stages. Sintering of the HD powder is rapid and can result in grain growth unless the temperature and times were tightly controlled. Image analysis indicted that the grain growth was more apparent in the a-axis than c-axis direction. McGuiness (McGuinness et al., (1989a)) had attributed the grain growth of the HD magnets to clean debris free powder. McGuiness and co-workers observed that, for the HD powder, the optimum sintering temperature was lower than that of the non-hydrided compacts.

There have been other comparisons between the sintering behaviour of jet milled magnets produced using hydrided powder and other magnets produced by conventional jet milled of standard powder (Liu and Kim, 1990; Kim, 1991). Compacts with the composition $Nd_{15.3}Fe_{75.55}B_{9.15}$ were vacuum sintered at 860 – 1080 ^{o}C for 1.5 hours and slowly cooled to room temperature. This work indicated that acceptable magnetic properties were achieved in the hydride compacts when sintered at temperature of 900 – 1000 ^{o}C, but, again it was found that grain growth could hinder the optimum value of the coercivity. Conversely, the magnets produced from conventional powder did not exhibit abnormal grain growth and this can be attributed to the grain being pinned by the increased oxide content.

6.8.1 The effect of oxygen content

As stated previously, the NdFeB system must be considered as a quaternary system with oxygen as an additional element. Oxygen plays a critical role in affecting the sintering behaviour of NdFeB based magnets. A high oxygen content results in the oxidation of the Nd-rich phase, with a consequent loss of the liquid phase for the sintering process. Conversely, a small oxygen content can lead to rapid mass transport diffusion (Wecker et al., 1994) and hence to a large amount of grain growth. Typically, the oxygen content of magnets has a value of around 4000 ppm with the assumption that the microstructure contains Nd_2O_3 oxide which equates to 2.4 wt% of Nd being used to form the oxide (Hirosawa and Kaneko, 1989). Hence, if the oxygen

level is increased, then this will require an effective level of Nd to compensate for this. This is an important factor in the sintering of the recycled material discussed in this thesis.

Therefore the oxygen level needs to be closely controlled in order to assist the use of alloys with compositions close to that of stoichiometry, therefore maximising the proportion of the ferromagnetic phase. The aim of most researches concerned with sintering of NdFeB is the minimisation of the oxygen level in magnets with an optimum value of BHmax.

The composition $Nd_{15}Fe_{77}B_8$ (at%) was one of the earliest selected for the sintered magnets. This composition contained ≈ 85 vol. % $Nd_2Fe_{14}B$ and yielded BHmax values of ≈ 379 kJ/m^3 compared to the 100 vol.% of $Nd_2Fe_{14}B$ which would yield ≈ 510 kJ/m^3. However, when moving towards a much higher proportion of $Nd_2Fe_{14}B$ phase can cause significant processing problems:

(1) The $Nd_2Fe_{14}B$ phase is a formed by a peritectic reaction and therefore the cast microstructure will contain free iron which will affect the sintering and ultimately the magnetic properties. (See Fig 6-13)

(2) The sintering conditions require precision control due to the reduced fraction of the liquid phase formed from the Nd-rich phase.

(3) The oxygen reacts with the more limited proportion of Nd-rich phase, hence reducing the extent of the LPS (liquid phase solution). (Kaneko and Ishigaki, 1994).

These effects are illustrated in the variations shown in Fig 6-15.

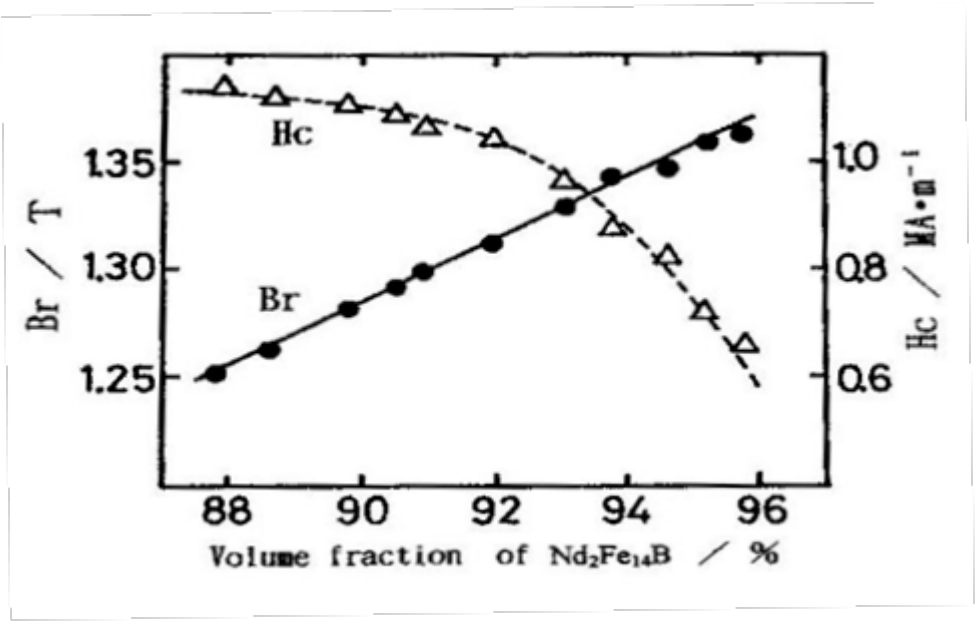

Figure 6-15: Magnetic properties dependence on volume fraction of $Nd_2Fe_{14}B$ phase (Kaneko and Ishigaki, 1994).

Magnets made from hydrided material with 0.94 wt% oxygen content have shown good coercivity and fine microstructure at a sintering temperature of 1060 ^{o}C which is a normal sintering temperate for excessive grain growth (Liu and Kim, 1990). They have suggested that an increase in the oxygen content will create a fine Nd oxide layer at the grain boundaries thus pinning the boundary movement and hence, slowing the progress of grain growth at higher temperatures. Kim et al., (1991) stated that, having an optimum oxygen level can improve the BHmax by producing a squarer hysteresis loops.

Nothnagel et al., (1991) indicated that there is a reduction in the mean grain size, whilst the coercivity and oxygen content increased to a maximum at a critical oxygen content. The coercivity then decreased rapidly due to powder oxidation, and therefore poor sintering. For fixed milling conditions, the oxygen content is critical and increased with the RE content because of an increase in the Nd-rich phase.

Verdier et al., 1994) agreed with these outcomes and attributed the coercivity improvement to the grain growth inhibition by partly oxidised grain boundaries. Corfield et al., (2000) observed a similar effect where the NdFeB based magnets had been annealed at 1000 ^{o}C for an extended time and showed excessive grain growth at

the magnet centre but much finer grains were observed in the outer region where there was a higher oxygen content.

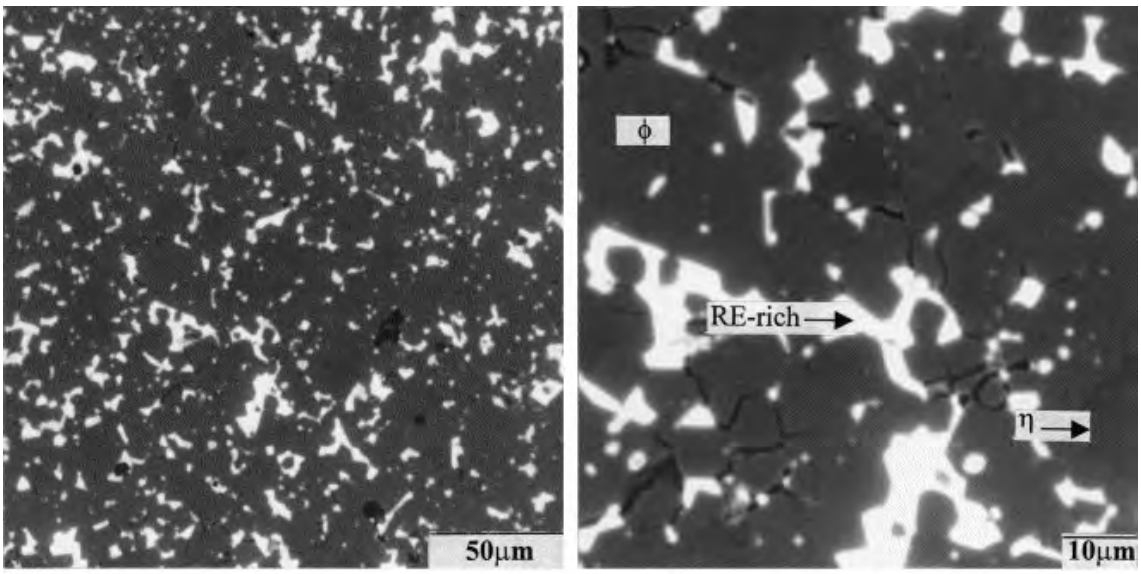

Figure 6-16: Back-scattered electron micrographs of $Pr_{16}Fe_{76}B_8$ sintered magnet (φ, $Pr_2Fe_{14}B$ phase; η, $PrFe_4B_4$ phase; RE-rich, Pr-rich phase (Corfield et al., 2000).

6.9 The effect of additives

The magnetic characteristics of the NdFeB-type magnets can be improved by adding elements which will affect its properties and change the matrix behaviour and produce microstructural improvements. These alloy additions can be categorised into three groups:

1) Some elements can have a total substitution in the matrix for example cobalt (in this case replacing the Fe) and Dy (in this case replacing Nd).

2) Type 1 dopant such as aluminium can have an influence on the liquid phase during sintering and form new grain boundary phases.

3) Elements that have low solubility in the matrix phase e.g. type II dopants which form as precipitates in the matrix and at the grain boundary, e.g. niobium (Fidler, 1992).

Some of the effects of additions on the NdFeB-type based magnets will be reviewed in this section. Many authors have reviewed the effect of blending techniques of two compositions together. The blending technique is normally used to investigate the production of high energy product magnets. This blending technique is based on laboratory level experiments. One of the aims of this project is to see how the behaviour of the additives change the original powder's sintering process and subsequent magnetic properties on recycling.

The effect of bulk alloying or powder blending on the magnetic properties should be the same; however, the effect on the microstructure can differ and this offers the possibility of targeting certain elements to particular areas in the microstructure e.g. grain boundaries. A summary of the effect of additions made by blending only is shown in the following table.

Table 6-2: Summary of the additives element reviewed by other authors using blending technique of NdFeB type magnets (Mottram et al., 1998).

Author/year	Starting Alloy	Additive Alloy	Blending technique	Main findings
Otsuki/1990	$Nd_2Fe_{14}B$ annealed	Melt quenched $Nd_{30}Fe_{64}B_6$	Co-pulverisation	Enhanced alignment, homogenised microstructure, low oxygen content, excellent magnetic properties.
Alander/1994	$Nd_2Fe_{14}B$ Co-reduced	Hydrogen decrepitated $Nd_{30}Fe_{64}B_6$ and Dy_2O_3	Co-milling	Good magnetic properties, excellent corrosion resistance.
Hong/1995	$Nd_{2.09}Fe_{14}B$ annealed	Hydrogen decrepitated $Nd_{29.5}Fe_{64.6}B_{5.9}$	Co-milling	Hydrogen reactions of additive phase in agreement with Williams 1991, excellent magnetic properties, low O_2 content.
Jang/1995	$Nd_{16}Fe_{78}B_6$ melt	Al-Cu and Ag-Zn	Co-milled and	Al diffuses into matrix, Cu, Zn and Ag distributed at

	quenched		hot pressed	grain boundaries, improved coercivity possible.
Velicescu/1995	$Nd_2Fe_{14}B$ annealed	$(Nd/Dy)_3Co$ $(Nd/Dy)_3Co_2$	Powder blending	Needed high temperature and long sinter to get full density. Uneven distribution of Dy found in large grains. Good magnetic properties.
Ferengel/1995	$(Nd/Dy)_2Fe_{14}B$ annealed	$Nd_{28}DyCo_8Cu_3Fe_{60}$ hydrogen decrepitated	Powder milling	Comprehensive investigation of combined copper and cobalt additions, excellent magnetic properties obtained.
Velicescu/1998	$Nd_2Fe_{14}B$ annealed	$RE_5(Co,Ga)_3$ $RE_6(Fe,Co)_{13}Ga$ Dy_2Co_3	Co-jet milling?	Excellent magnetic properties, process of blending powders used by Vacuumschelze GmbH to produce commercial 416 kJ/m^3(52 MGOe) magnets
Mottram/1998 (a, b)	$Nd_{13}Fe_{80.5}B_{6.5}$ $Nd_{13}Fe_{78}B_7CoNb$ $Nd_{13}Fe_{79}B_7$ $Nd_{16}Fe_{76}B_8$	Nd-hydride Dy-hydride Nb-hydride V-hydride Co, Al, Cu	Powder milling	Al and Co evenly distributed in grains, Cu limited to grain boundaries, V and Nb form new borides at grain boundaries, Nd hydride promotes densification, Dy unevenly distributed at edge of grains. Good magnetic properties.

Type 1 Substitution of Fe by other elements

6.9.1 The effect of cobalt addition

Sagawa et al., (1985) determined the main effect of cobalt on the NdFeB magnets is the improvement in the remanence temperature coefficient. This improvement is due to the increase in the Curie point which occurred as Co substitutes for the Fe in the matrix. The tetragonal phase $Nd_2(Fe_{1-x}Co_x)_{14}B$ can exist for the entire compositional range of $0 \leq x \geq 1.0$.

The Co contained within the NdFeB alloys indicated additional grain boundary, Co containing phases (Fidler, 1985). These Co phases are: $Nd(Fe,Co)_2$, Nd_7Co_3, $NdCo_3$, and $Nd_3(Fe,Co)$. The relatively poor coercivity of the Co containing NdFeB magnets could be attributed to the presence of the first three phases consistent with their soft ferromagnetic properties, with Curie points just above room temperature. The results of the EDX Spectroscopy (Arai et al., 1987) showed that the Co had modified the Nd-rich and $NdFe_4B_4$ compositions. The addition of cobalt results in a significant improvement in the corrosion resistance (Ohashi et al., 1987; Szymura et al., 1991) took the investigation further and deduced that improvement could be attributed to low activity cobalt-containing grain boundary phases when compared with that of Nd-rich material. Magnets with small addition of Co and Al were found to exhibit excellent corrosion resistance when placed in an autoclave which had a steam temperature of 115 ^{o}C (Camp and Kim, 1991). This improvement was attributed to the presence of Nd_3Co at the grain boundary.

El-Moneim et al., 2001) employed isotropic nanocrystalline $Nd_{14}Fe_{80}B_6$ and $Nd_{12}Dy_2Fe_{73.2}Co_{6.6}Ga_{0.6}B_{5.6}$ magnets with different grain sizes in the range of 60–600 nm which has been produced from melt-spun materials using hot pressing at 700 ^{o}C and subsequent annealing at 800 ^{o}C for 0.5–6 h. They concluded that a partial substitution of Fe with Co and Ga leads to an improvement in the corrosion resistance and reduces the affinity and binding energy for hydrogen in these materials. The microstructure coarsening also results in a better corrosion performance of these materials.

Al, Co, Cr, Cu, Mo ,Nb, Ga, Ti ,Zr and W [Fidler, 1992]. Dy, Pr and Tb additions exert no obvious beneficial effect on the corrosion behaviour, whereas, Al, Co, Cu and Ga additions are found to improve the corrosion resistance of NdFeB magnets in many corrosive environments (Steyaert et al., 1998; and El-Aziz et al., 2000). The improvement in the corrosion resistance was attributed to the change in the microstructure and phase composition, by segregation of these kinds of additions into intergranular phase regions (Szymura et al., 1991); and El-Aziz et al., 2000). This process seems to reduce the electrochemical potential difference between ferromagnetic and intergranular phases and hence, lowers the driving force for galvanic corrosion. El-Moneim et al., (2001) did not consider the influence of Al, Co, Cu and Ga additions on other properties, which could seriously affect the overall corrosion process such as grain size, phase distribution and sensitivity to surface hydrogenation.

Velicescu et al., (1996) produced blending alloys such that the Co and Cu was added simultaneously to sintered Nd-Dy-Fe-B magnets and this resulted in a refined microstructure and an improvement in the (BH)max values. This was attributed to the replacement of the conventional Nd-rich constituents by RE-(Co, Cu) phases with low melting points, such as RE Cu or RE_3Co. They achieved a remanence of 1.41 T and an energy product of 383 kJ/m^3. (Here, RE denotes a mixture of Nd and Dy).

Bras et al., (1991) reported that when Co and other elements such as vanadium, when added to NdFeB based sintered magnets, good thermal stability and better corrosion resistance were achieved (Tenaud, et al., 1994; Kim, A.S. and Camp, F. E. 1995; Ma, B. M. et al., 1994; Zhang et al., 2007; Mottram et al., 2001; Ali et al., 2009).

6.9.2 Dysprosium addition

According to Sagawa et al., (1984a), adding Dy as a substitute for the Nd in the NdFeB system improves the coercivity. They reported that the $(Nd, Dy)_2Fe_{14}B$ magnetocrystalline anisotropic phase can result in a coercivity increase at a rate of 640 kA/m per at% Dy in a $(Nd_{1-x}Dy_x)_{15}Fe_{77}B_8$ magnet. The coercivity exhibited a further improvement by the addition of Dy which was found to inhibit the grain growth during sintering (Ma and Bounds, 1991). However, the Dy additions decrease the saturation magnetisation due to the magnetic moments of the Nd (Fe) and Dy in the $(Nd_{1-x}Dy_x)_{15}Fe_{77}B_8$ crystal being aligned antiparallel. However, the remanence

temperature coefficient is improved by the Dy addition (Gong et al., 1991). There is also a reduction in the coercivity with temperature irreversible losses (Ma and Bounds, 1991). This, combined with the increase in coercivity makes the additions of Dy in magnets suitable for applications where elevated temperatures are experienced.

The Nd to Dy ratio in the matrix phase is similar to that of the overall addition (Fritz et al., 1992). However, a small amount of Dy was also found in the rare earth-rich phase, but the ratio is less than the total added.

Ghandehari (1986) have added Dy_2O_3 to $Nd_{15}Fe_{77}B_8$ using hand mixing and this process increased the coercivity but at a lower rate than that expected when the Dy alone is added. The Dy_2O_3 is reduced partially to Dy during the sintering process. The reason for this was thought to be the oxygen combining with Nd to form the more stable Nd_2O_3. The addition of Dy_2O_3 was adopted as a cheaper option than pure Dy powder. The Dy has a high melting point of 1412 ^oC and the Dy_2O_3 addition presented an uneven distribution of Dy using the blending technique (Velicescu et al., 1995). This work produced good magnetic properties despite requiring high sintering temperatures because there was an inhibition of the grain growth.

Mottram et al., 1998) investigated the Dy-hydride (DyH_2) effect when it is added to $Nd_{14}Fe_{79}B_7$. Again, the increase in coercivity was confirmed at a low rate. The microstructure was observed using SEM-EDX analysis to see the distribution of Dy in the matrix grain and this was found to be non-uniform, as can be seen from figure 6-17.

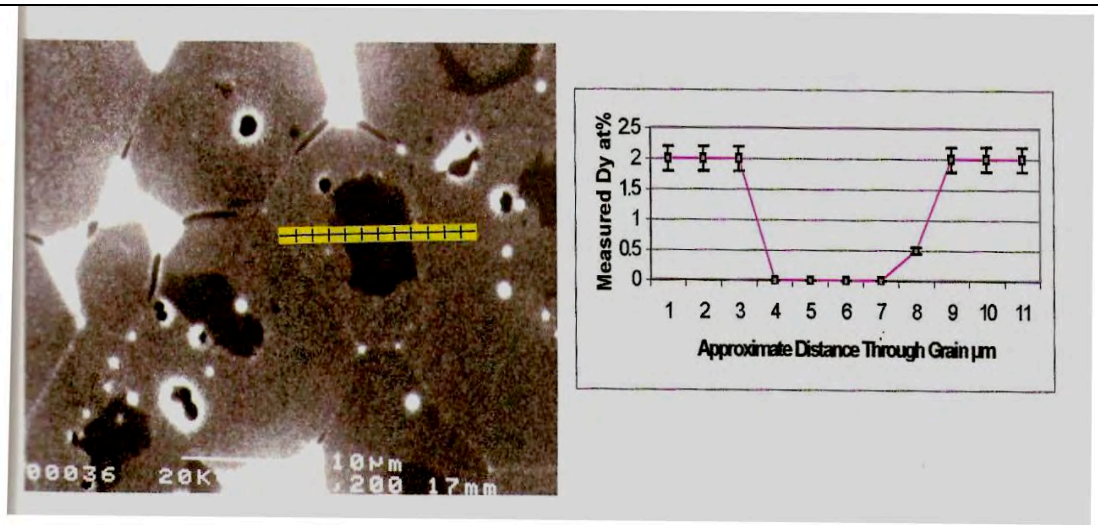

(a) (b)

Figure 6-17: (a) $Nd_{14}Fe_{79}B_7$ microstructure made by blending with 2 at% Dy hydride. (b) EDX analysis of grain in figure (a) (Mottram and Harris, 1998).

Li et al., 2007) reported that the addition of just 2 wt% Dy_2O_3 or/and 0.3 wt% tin (Sn) proved to be very effective in improving the permanent magnetic properties of Nd-Fe-Nb-B–type based magnets. Moreover, the Dy_2O_3 additions resulted in the increase of coercivity ($_iH_c$) and hence improved temperature dependence due to the increase of Tc, formation of (Nd Dy)-rich phase and the grain refinement of the Φ phase. This improvement of the coercivity stability of the magnets from the addition of tin (Sn) was attributed to the smoothing effect of the tin addition at the grain boundaries.

Kianvash et al., (1999) stated that, as a result of the additions of Nd, Dy or (Nd+Dy) hydrided powder, and using a powder blending technique, with set conditions, it proved to be impossible to achieve a full density in the sintered magnets, processed from the Nd_{13} Fe_{78} $NbCoB_7$-type alloy. Increasing the sintering temperature and the duration of the sintering did not result in any significant improvements in the density values and the highest possible density achieved in the sintered magnets was only 7.05± 0.05 g/cm^3. By using the same processing conditions, it was found that, by an addition of only 2 at% Nd or Dy, practically full densification could be achieved and magnets with densities of more than 7.40 ± 0.05g/cm^3 could be produced consistently. The total addition of (Nd+Dy), with varying proportions of Nd and Dy, was limited to

2 at% and at each addition, a full density in the sintered state was attained. Using 1 at% Nd and 1 at% Dy, an intrinsic coercivity (iHc) of 780 kA/m with a corresponding energy product (BH_{max}) value of 324 kJ/m^3 were obtained. The coercivity and BH_{max} values were improved to 950 kA/m and 331 kJ/m^3, respectively, by applying a standard annealing treatment of 600 ^oC for 1 h, followed by air-cooling to room temperature. The studies of Kianvash's (and co-workers) confirmed that powder blending using Nd and Dy hydrides as an addition is a very effective means of promoting liquid phase sintering and of optimising magnetic properties in Nd–Fe–B-type magnets (Zhang et al., 2007; Mottram et al., 200; Davies et al., 2001).

6.9.3 Nb Additions

Hu et al., (2008) reported that, when Nb is added to NdFeB-based magnets, there was an improvement in the magnet's impact toughness and coercivity. This improvement was achieved by adding 1.5 at% Nb to the alloy. The Nb addition resulted in the grain size of the main phase becoming more regular, and the grain boundaries become clear and smooth, so that the intrinsic coercivity of the sintered magnets was increased. The addition of Nb formed the compound of NbFe within the grains, which may contribute to the improvement of the impact toughness. The grain boundaries where the two grains contact directly make intergranular fracture more difficult. Furthermore, the Nb addition widens the grain boundaries of sintered magnets and changes their shape. All of these effects may contribute to the improvement in the impact toughness of the sintered magnets.

The Nb addition also plays an important role in improving the magnetic properties and according to Ahmed et al., (1994) who investigated the effect of niobium addition on the microstructure and phase compositions of an $Nd_2(Fe_{0.98}Nb_{0.02})_{14}B$ alloy and an $Nd_{16}Fe_{76.3}$ $Nb_{0.3}B_{7.4}$ magnet. The microstructure of the as-cast alloy contains four phases, the $Nd_2Fe_{14}B$ matrix phase, a Nb-Fe-B ternary phase, Nd-rich regions and free iron. After homogenisation, the alloy contained only the first two phases and very small amounts of the Nd-rich phase. Quantitative electron probe microanalysis of the Nb-Fe-B phase revealed a composition of approximately $Nb_{26}Fe_{32}B_{42}$. This ternary phase was found in the as-cast alloy, the homogenised alloy and also, to a lesser extent, in the magnet. The shape of this phase in the as-cast and the sintered magnet was hexagonal whereas, in the homogenised alloy, it was also observed in an acicular

form. In the as-cast alloy, the ternary phase was found to nucleate within the free iron phase and then grows at the expense of the surrounding free iron. This provides strong evidence for the role of Nb in the removal of free iron from the microstructure. The results indicate that, by controlling the solidification behaviour of the alloy, free iron may be prevented from nucleating or at least reduced to a very thin film near the surface of the ingot which can be removed by machining to produce Nd-Fe-B material without free iron.

Bala et al., (1992) reported that the replacement of Nd by terbium in Nd-(Fe,Co)-B sintered magnet, increases the coercivity and reduces the remanence. The increase of the coercivity also lowers the irreversible losses at elevated temperature. The temperature coefficients of the magnetic properties have also been improved through Tb substitution. Partial substitution of Dy by Tb does not influence the corrosion behaviour of the magnets. As reported earlier, the corrosion tests confirm that addition of Co exhibits an advantageous effect on the corrosion behaviour of the sintered RE-Fe-B magnets.

6.9.4 Nd additions

On a different material, Wang et al., (2006; 2008) investigated the effect of Nd and B addition on the microstructure and thermal stability of nano-composite (Nd, Zr)$_2$Fe$_{14}$B/α-Fe magnets. It was shown that, for the Nd$_x$Fe$_{93-x}$Zr$_1$B$_6$ (x = 9–11) alloys, the volume fraction of Nd$_2$Fe$_{14}$B increases with increasing Nd content, and the sample with x = 10 exhibits the optimal microstructure and thermal stability. Though the room-temperature $_iH_c$ of Nd$_{11}$Fe$_{82}$Zr$_1$B$_6$ sample is the highest, it decreases more rapidly than that of Nd$_{10}$Fe$_{83}$ZrB$_6$ as the temperature increases, indicating the deterioration of the temperature coefficient coercivity. For Nd$_{10}$Fe$_{89-y}$ZrB$_y$ (y = 5–8) alloys, the remanence and the temperature coefficient of remanence deteriorate with increasing B content. The coercivity and the temperature coefficient of coercivity first improve with increasing B content, reaching the optimal values at y = 7, then deteriorate with further increasing in B. Coarse grains and the Fe$_3$B phase are observed in the Nd$_{10}$Fe$_{81}$ZrB$_8$ alloy.

Kianvash et al., (1999) as mentioned before, reported that the addition of Nd can improve the density and hence the magnetic properties. Liu et al., (2009) reported

adding NdF_3 to both Dy-free and Dy-containing Nd–Fe–B sintered magnets with little decrease in the remanence. NdF_3 reacts with the Nd-rich grain boundary phase and a new rare-earth oxyfluoride (ROF) phase with an ordered face-centred cubic structure is formed. Dy was detected in the ROF phase in the Dy-containing magnet. This suggested that the increase in coercivity can be related to the uniform grain boundary phase as well as to Dy segregation.

Takezawa et al., (2007) showed that the effect of an adequate addition of Nd-rich phase had an effect on the c-axis orientation of the Nd–Fe–B melt-spun ribbon. The effect of the Nd-rich phase promotes the c-axis orientation of the Nd–Fe–B ribbon. The $(Nd_2Fe_{14}B)_{95}$(Nd-rich phase)$_5$ ribbon exhibited a c-axis orientation in the entire body from bottom to top when melt-spun at a wheel speed of 10.0 m/s.

According to Chen et al., (2012), the intrinsic coercivity and thermal stability of the magnets, could be improved by substituting Nd with Pr. When Pr replaces all Nd in the magnets, magnetic properties did improve with Br = 1.365 T (13.65 kG), cHj = 1760 kA/m, (22.13 kOe) (BH)max = 367 kJ/m^3 (46.1 MGOe) are obtained with a low Dy content (1.3 wt%).

7 Corrosion of NdFeB magnets

Many authors have investigated the effect of various elements that may affect the performance and the magnetic properties of NdFeB based magnets in various corrosive environments. The testing/ experiments may be based on a salt bath (see aims of the project), environmental degradation in moist air or just water-based. The author investigated the corrosion resistance of the recycled magnets and compared them with the initial magnets. In particular, this work was carried out to determine the corrosion resistance of all magnets both in the initial and recycled states.

7.1 Environmental degradation of NdFeB magnets

Yan et al., (2009) reported in their paper about the degradation of NdFeB magnets and how they exhibit general corrosion along the grain boundaries when etched in Viella's reagent. However, localised corrosion of these magnets resulted in a crater-like feature when corrosion was produced in an environmental chamber, e.g. when $Nd_{16}Fe_{76}B_8$ magnets were corroded using an environmental chamber at 85 ^{o}C, relative humidity (RH): 80%. This was attributed to the condensation of water droplets on the surface of samples and the concentration gradient of oxygen dissolved in the droplets which then influenced the corrosion process. It is thought that, during this process of pitting, the high concentration of H+ ions in the centre of the pit accelerated the pit development; meanwhile, the cathodic $Nd_2Fe_{14}B$ matrix phase absorbs the emerging hydrogen atoms. It is believed that pits start at the Nd-rich phase (probably triple-points) and then propagate along the grain boundaries.

The magnetic field distributions of magnetised NdFeB magnets were also measured by a MagScan (a computer software and instrument for analysing the magnetic fields of permanent magnets). The polished $Nd_{16}Fe_{76}B_8$ sintered magnets were sealed in a plastic bottle and then placed in the environmental chamber at 85 ^{o}C, RH: 80% for 1 hour to preheat the sample, the sealed bottle was uncovered to expose the magnets to the hot, humid environment chamber for 1.5 hours, and then examined using an optical microscopy.

The Kerr effect images of magnetised NdFeB magnets after corrosion were also examined by optical microscopy.

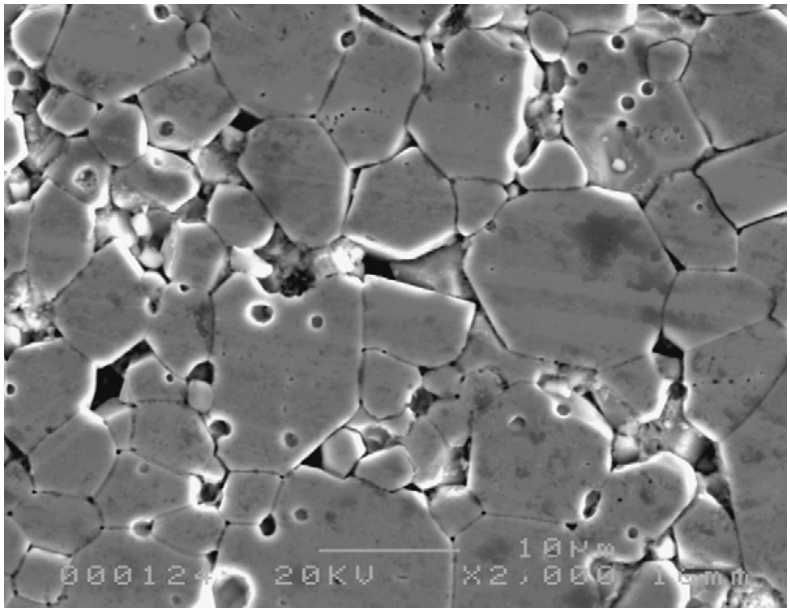

Figure 7-1 Micrograph of $Nd_{16}Fe_{76}B_8$ magnet etched in Viella's reagent for 5 s. The sample was made by sintering at 1060 ^{o}C and the density was 7.52 g cm^{-3} SEM (JEOL 6300). (Gaolin Yan, 2009).

$Nd_{16}Fe_{76}B_8$ sintered magnets were etched in Viella's reagent for 5 seconds rinsed quickly and dried. The microstructure was then examined using a JEOL 6300. The microstructure of the corroded $Nd_{16}Fe_{76}B_8$ is shown in Figure 7-1. From the micrograph it is clear that the etching process proceeded along the grain boundaries. This is in agreement with previously conducted research on the corrosion of NdFeB magnets. [Sugimoto and Matijevic, 1980; and Sugimoto et al., 1987].

$Nd_{16}Fe_{76}B_8$ magnets were exposed to a humid environment (temperature: 85 ^{o}C, relative humidity: 80%) for 5 and 16 hours respectively. The morphology was examined using a JEOL 5410 and it was found that areas of localised corrosion spots appeared with crater-like shapes on the surface see Figure 7-2 (a) and (b).

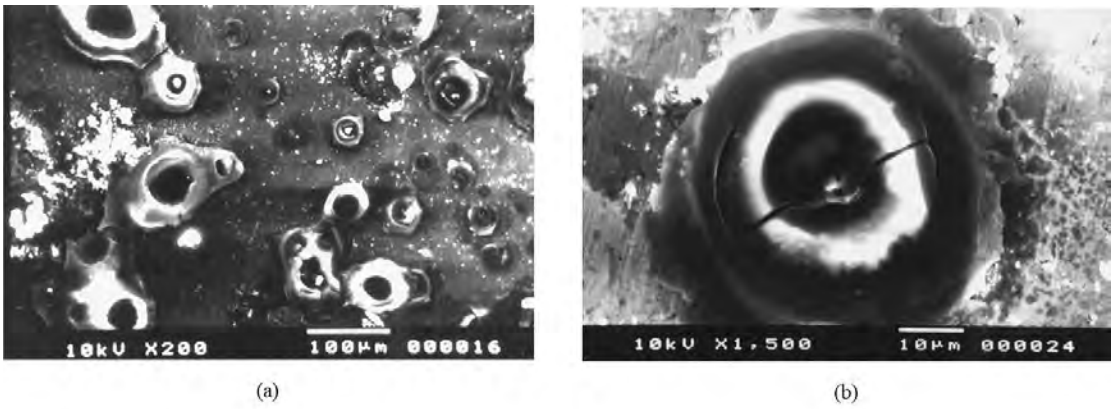

Figure 7-2 (a) Craters of localised corrosion on a $Nd_{16}Fe_{76}B_8$ magnet corroded in the environmental chamber for 5 hrs, temperature: 85 ◦C, RH: 80%, examined by an SEM (JEOL5410). (b) A crater of localised corrosion on $Nd_{16}Fe_{76}B_8$ magnet corroded in the environmental chamber for 5 h, temperature: 85 ^{o}C, RH: 80%. Examined by an SEM (JEOL5410). (Gaolin Yan, 2009).

7.1.1 Pitting corrosion of NdFeB magnets.

The corrosion sites developed a crater-like morphology. This was due to the condensation of water droplets on the Nd-rich grain boundaries at the surface of NdFeB magnets with pitting corrosion occurring under the water droplet. It is proposed that differential-aeration occurs under the water droplet. The initiation of a pit involves corrosion over the whole area under the condensed water droplet. The consumption of oxygen by the cathodic reaction in a neutral solution causes an oxygen concentration gradient within the water droplet or electrolyte. The edge of the droplet, i.e. the air–electrolyte interface, receives more oxygen by diffusion than the area at the centre of the drop.

7.1.2 Additional features associated with corrosion behaviour

Shimizu et al. (1995); and Shimotomai (1994) stated that a magnet is composed of an Nd-rich area (grain boundary), $Nd_{1+\varepsilon}Fe_4B_4$ (boron rich phase) and $Nd_2Fe_{14}B$ (matrix phase). The electrical potential of the Nd-rich phase is much more negative than those of the $Nd_{1+\varepsilon}Fe_4B_4$ and $Nd_2Fe_{14}B$ phases. When a water droplet condenses on the surface of the magnet, micro-corrosion cells form under the droplet. Thus, the Nd-rich phase becomes the anode against both $Nd_{1+\varepsilon}Fe_4B_4$ and $Nd_2Fe_{14}B$. The Nd-rich phase is then oxidized anodically to Nd_{3+} dissolving in the droplet, these positive Nd_3+ ions

combining with cathodically produced OH^- or with water, giving a precipitate of $Nd(OH)_3$. This insoluble corrosion product, forms a ring of precipitate at the edge of the droplet. Meanwhile, hydrogen ions produced by the dissociation of water were reduced cathodically on both the $Nd_{1+\varepsilon}Fe_4B_4$ (boron rich phase) and $Nd_2Fe_{14}B$ (matrix phase). Part of the resulting hydrogen is released as H_2, which causes the occasional breaking of the crust of the corrosion product.

Some of the emerging hydrogen atoms reduced cathodically from H_2O were absorbed by the $Nd_2Fe_{14}B$ (matrix phase) resulting in a lattice expansion (see table 8-1 below for lattice expansion during corrosion) and decrepitation of this hard magnetic $Nd_2Fe_{14}B$ phase (Yan, et al., 1999). A sintered $Nd_{16}Fe_{76}B_8$ magnet was corroded in an environmental chamber for 16 h at a temperature of 85 ^oC and a relative humidity of 80%. The morphology was examined by HRSEM. The corrosion products were observed to spread out of the Nd-rich phase i.e. the observations by HRSEM support the proposed corrosion mechanism. The composition distributions for Nd, Fe and O of an isotropic $Nd_{16}Fe_{76}B_8$ magnet corroded in the environmental chamber for 16 hours and were examined by EDX (JXA-840A) and WDX (JXA-840A).

Interestingly, it was found that Nd, Fe and O had a symmetrically localised distribution across the centre of the crater. The Nd and O composition distribution satisfied the proposed corrosion mechanism and represented the distribution of the corrosion product $Nd(OH)_3$. The Fe composition distribution was just opposite to that of the Nd, i.e. where the Nd content was higher than the Fe content would be lower, and vice versa. The Nd content was found to be higher in the centre and along the edge of the crater. This corresponds to the distribution of the remains of the Nd-rich phase in the centre and the insoluble $Nd(OH)_3$ precipitated along the periphery of the drop.

Table 0-1 values for *a* and *c* spacings for the material before and after the corrosion test. McGuiness et al., 1994)

	a-(nm) ±0.0002	c-(nm) ±0.0002	$Nd_2Fe_{14}BH_x$
$Nd_{16}Fe_{76}B_8$ magnet	0.8798	1.2171	$x = 0$
$Nd_{16}Fe_{76}B_8$ magnet hydride (H_2 gas)	0.8886	1.2296	$x = 2.7$
$Nd_{16}Fe_{76}B_8$ corrosion product	0.8931	1.2343	$x = 5$
$Nd_2Fe_{14}B$ alloy [1]	0.879	1.218	$x = 0$
$Nd_2Fe_{14}B_{-5}$ [1]	0.893	1.232	$x = 5$
[1] value are almost identical to Ram & Joubert (1992)			

7.1.3 Localised corrosion of magnetised NdFeB magnet

The rotation of the direction of polarisation of a polarised light beam reflected from the surface of magnetic materials is known as the Kerr effect. The Kerr effect images of an unmagnetised $Nd_{16}Fe_{76}B_8$ magnet before and after corrosion and a magnetised $Nd_{16}Fe_{76}B_8$ corroded at 85 ^oC, RH: 80% in the environmental chamber for 16 hours were examined by optical microscopy. The domains with different directions distribute randomly since this was an isotropic magnet. Generally speaking, a complete domain stops at the grain boundary. A crater-like corrosion spot of an unmagnetised $Nd_{16}Fe_{76}B_8$ magnet was recorded. The corrosion products seem loose compared to those appearing on a magnetised sample. It is thought that, for the magnetised magnet, although the Nd-rich phase in the grain boundary dissolves anodically, the grains still hold to each other because of the magnetic attractive force (Yan et al. 1999).

The magnetisation may slow the corrosion process by reducing the contact with the reaction area. The observed white phase was the corrosion product, $Nd(OH)_3$. It is evident that the pit starts at the junction of the grain boundaries and develops along the grain boundaries. (Yan et al., 1999)

Therefore, it was deduced that the corrosion of Nd–Fe–B magnets was a combination of both grain-boundary failure and pitting. In fact the initiation of the pitting was due to grain-boundary failure. The magnetic field decreases rapidly after the corrosion process and this was attributed to the pitting leading to the degradation of the grain boundaries shown in figure 7-3 and to absorption of hydrogen by the matrix phase during the corrosion process (Yan et al., 1999; and Yan et al., 2009)

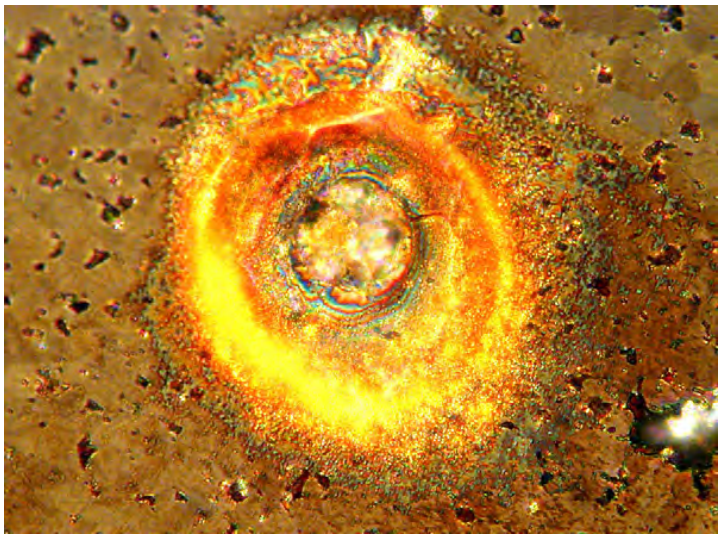

Figure 7-3: Kerr-effect image of an unmagnetised $Nd_{16}Fe_{76}B_8$ magnet after corrosion at 85 ^{o}C, RH: 80% in the environmental chamber for 1 h, examined by optical microscopy.

As mentioned previously, when a polished $Nd_{16}Fe_{76}B_8$ sintered magnet was exposed to 85 ^{o}C, RH: 80% for several seconds and then removed, it was observed that water droplets condensed on the surface of the sintered magnet. This was due to vapour condensation having contact with a solid wall (cooling surface) with a temperature lower than the saturation temperature of the vapour. The sub-cooling temperature was the driving force for the condensation of the vapour. When a similar magnet was preheated before exposure to the atmosphere in the environmental chamber, it was found that no corrosion spots occurred on the surface. Hence, if there were no condensed water droplets, the crater-like corrosion did not occur. This is because a complete galvanic corrosion cell cannot form on the surface of the NdFeB magnets; therefore the corrosion process cannot proceed. During their application, damage to

NdFeB magnets was most severe in moderate climates during the autumn and spring periods where cold dry air alternates with air of high moisture content. It is severe during the entire year in tropical climates. In cool periods, the magnet is cooled, and the lag in temperature when the warmer moist air appears results in high relative humidity or actual condensation on the surface of the magnet. In a moist atmosphere with temperature fluctuations, condensation often appears on the surface of NdFeB magnets. (Yan et al. 1999)

7.1.4 Conclusions

Pitting corrosion occurs when Nd–Fe–B magnets were corroded in the environmental chamber at 85 ^{o}C, RH: 80% and this resulted in the rapid decrease of the magnetic field strength of magnetised NdFeB magnets. During the process of pitting, the high concentration of H+ in the centre of the pit accelerates the pit propagation; meanwhile, the cathodic $Nd_2Fe_{14}B$ matrix phase can absorb the hydrogen ions. It is believed that pits start at the Nd-rich phase and propagate along the grain boundaries. The combination of grain-boundary failure, pitting and hydrogenation leads to a marked degradation of the Nd–Fe–B magnets. (Yan et al., 1999).

7.2 Anisotropy Hydrogen decrepitation and corrosion behaviour in NdFeB magnets

McGuiness et al., (1994) reported that when samples of NdFeB are subjected to hydriding (by flow of H_2/Ar mixture) and corrosion (by suspending samples above boiling distilled water surface using polymer wire). It was deduced that hydrogen has an effect on the NdFeB materials (Harris, 1987). Figure 7-4 and Figure 7-5 show the schematic diagram of the apparatus used for hydriding and corrosion.

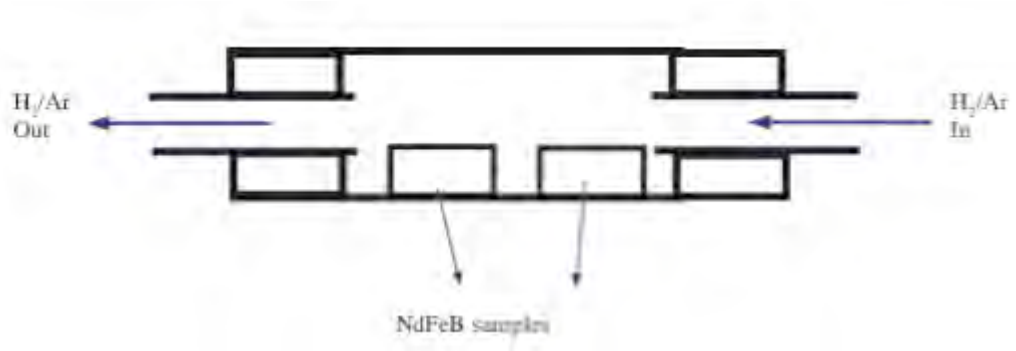

Figure 7-4 Schematic diagram showing apparatus used for hydriding experiment. (Adapted from McGuiness et al., 1994).

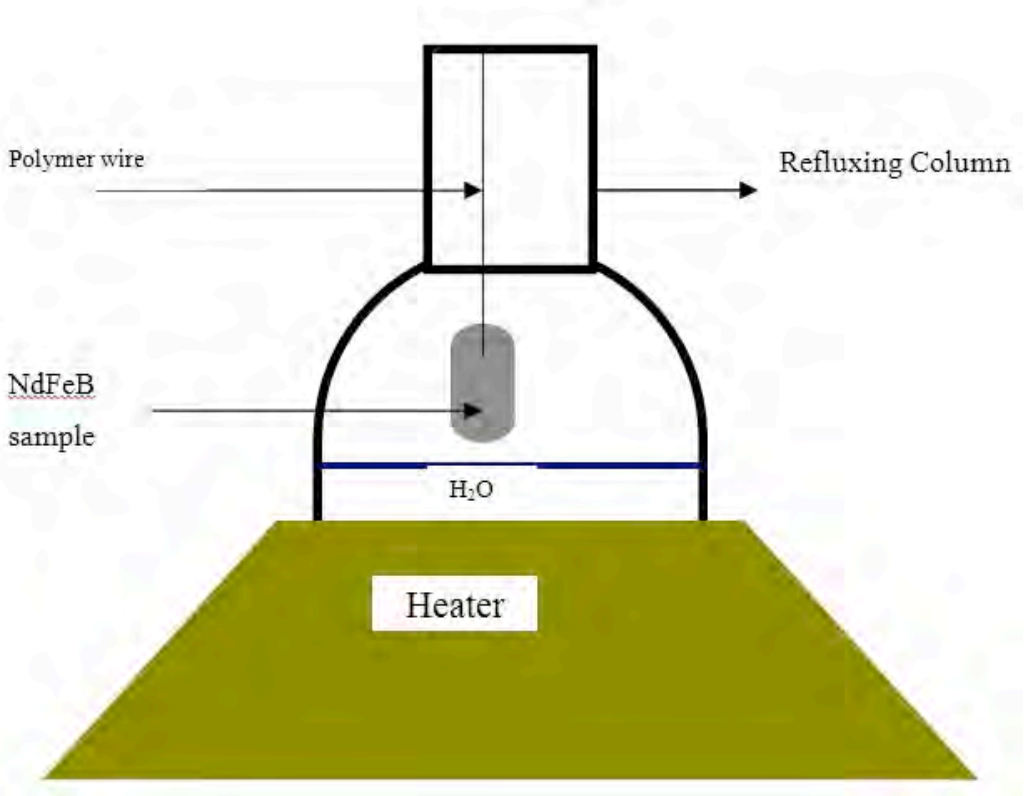

Figure 7-5: Schematic diagram showing apparatus used for corrosion experiment. (Adapted from McGuiness et al., 1994).

Hydrogen usually attacks the $Nd_{16}Fe_{76}B_8$ type magnets alloys at room temperature due to presence of the Nd-rich material. Without this phase i.e. in the case of $Nd_2Fe_{14}B$ single phase alloy and the MQI type melt spun material with its amorphous grain boundaries. The HD-reaction is only initiated when hydrogen was combined with reasonable pressure coupled with a temperature of around 160 ^oC.

It was found that sintered magnets with a composition of near $Nd_{16}Fe_{76}B_8$ were shown to be very susceptible to hydrogen attack and decrepitation. However, with these magnets it took some time for the activation to take place (this was possibly due to the indirect contact with the H_2/Ar and the ratio of H_2:Ar was 1: 9 and this reaction would be much quicker had the ratio been reversed and the magnets were totally immersed in the distilled water). As the hydrogen decrepitated the magnets, this invalidated this type of magnet for employment in a hydrogen based environment.

These authors have also reported on whether $Nd_2Fe_{14}B$ phase had an effect on the HD-process and corrosion properties, investigating the effect of hydrogen on anisotropic and isotropic magnets. The $Nd_{16}Fe_{76}B_8$ type isotropic sintered magnets where left exposed to a flow of H_2/Ar (ratio 1:9) and it took 1-3 hours before any reaction could be seen (decrepitation). In order to activate the corrosion part, the magnets were suspended above boiling distilled water. This test was referred to as Bulk Corrosion (BC). The corrosion behaviour was found to be comparable to the hydriding reaction. The dimensional changes took place during 12 days of the corrosion test. In the case of those magnets, the length and diameter were found to have a linear relationship with time. For the anisotropic magnets, it was found that there was almost no change in the diameter over the period of the experiment, but the length was reduced. This indicated that corrosion was only taking place at the poles of the magnet. The weight loss for both types of magnets was almost the same. When the magnets were characterised using XRD, the $Nd_2Fe_{14}B$ structure was found to be preserved although there was an expansion of the lattice (Table 0-1 for lattice spacing values) consistent with the absorption of hydrogen.

McGuiness acknowledged that corrosion of the magnets at their poles was a particular problem as; the magnet had the highest flux density and was often close to the moving part of the machine or storage disc, so then any fragmentation could cause major damage.

The anisotropic behaviour of the hydrogen decrepitation process and a similar behaviour on corrosion provided strong evidence that there was a link between the corrosion type that happens during the BC test and the one where magnets are left exposed to a hydrogen atmosphere. This is supported by the XRD results which

proved that the corrosion in the $Nd_{16}Fe_{76}B_8$ type magnets takes place as a result of the material reacting with hydrogen.

In the corrosion process, the hydrogen is produced by reaction (see below equation) of the water vapour with the Nd-rich material and is then subsequently absorbed by the matrix ϕ-phase ($Nd_2Fe_{14}B$), :

$Nd + 3H_2O \rightarrow Nd(OH)_3 + 2H_2 \leftarrow$ absorbed by ϕ-phase

7.3 The effect of density on the corrosion of NdFeB magnets

Yan et al., (1999) reported that, during the normal vacuum sintering process used in producing the magnets, the hydrogen produced from the hydrogen decrepitation process is desorbed completely. However, as we have seen, the Nd–Fe–B magnets are capable of absorbing hydrogen from moisture in the atmosphere. They found that the higher the density of the magnets, the less hydrogen was absorbed. The combined effects of the lattice expansion due to the formation of $Nd_2Fe_{14}B$–H solutions and the NdH_{2+x} phases as a result of the hydrogen absorption, and the volume expansion on formation of $Nd(OH)_3$, resulted in the eventual decrepitation of the magnets. Thus it has been clearly established that hydrogen plays a vital role in the corrosion of Nd–Fe–B type magnets when they are exposed to humid conditions.

Several studies (Claude et al., 199; McGuiness et al. 1994; Arenas & Warren, 1997; Kim et al., 1996; Henning, 1996), of the corrosion of NdFeB-type magnets in humid environments, have demonstrated that hydrogen can be absorbed during corrosion, as a result of the dissociation of water by the Nd-rich phase. These papers demonstrated that the ϕ phase present in the corrosion product had an expanded lattice which was attributed to the presence of hydrogen with a stoichiometry of $Nd_2Fe_{14}BH_{\sim 5}$. Yan et al., (1999) and Henning (1996) showed that corrosion of NdFeB-type magnets was enhanced by a low density and the presence of hydrogen, which Henning suggested could be introduced during the plating process. Yan stated that, Henning referred to this enhanced corrosion as ‘the Negative Harris Effect’ (NHE), while referring to HD as ‘the Positive Harris Effect’. The aim of their study was to investigate the factors influencing the NHE by producing magnets with the $Nd_{16}Fe_{76}B_8$ (atomic %) composition and with a range of densities.

Yan et al., (1999) revealed the variation of sintering temperature proved to be an effective means of producing magnets with a range of densities, as can be seen in Table 7-2.

Table 7-2 Density of Nd_{16} Fe_{76} B_8 magnets produced using a range of sintering temperatures for one hour duration (Yan et al., 1999).

Sintering Temperature (^oC)									
724	756	822	856	892	924	958	987	1026	1060
Density (g/cm^3)									
5.38	5.49	5.71	5.83	5.97	6.38	6.85	7	7.41	7.51

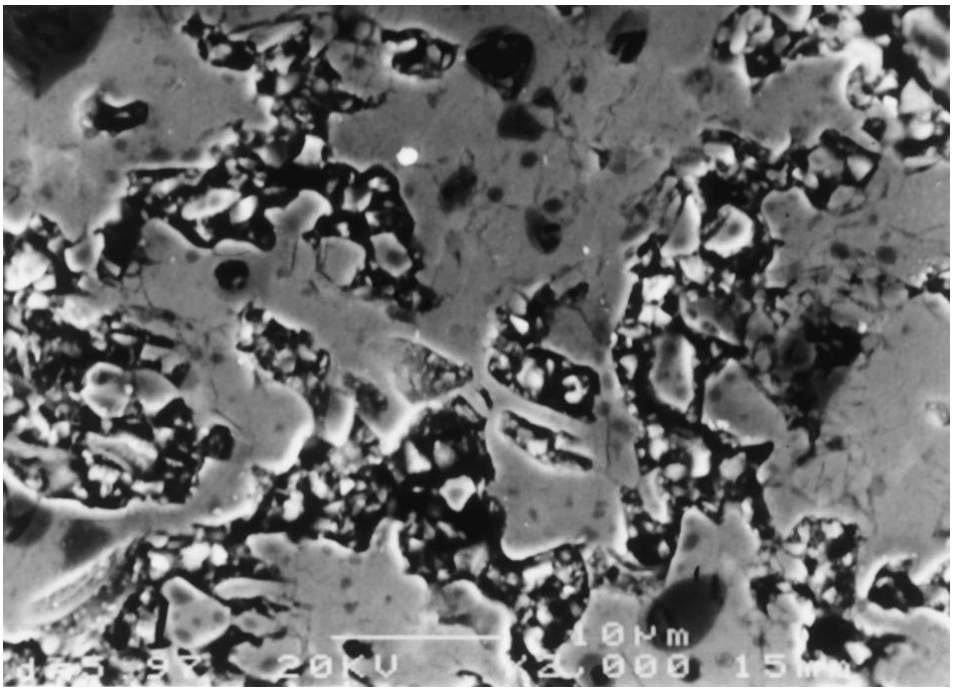

Figure 7-6: $Nd_{16}Fe_{76}B_8$ magnet sintered at 892 ^oC, Density: 5.97 gcm^{-3}, SEM, JEOL 6300. (G. Yan et al., 1999)

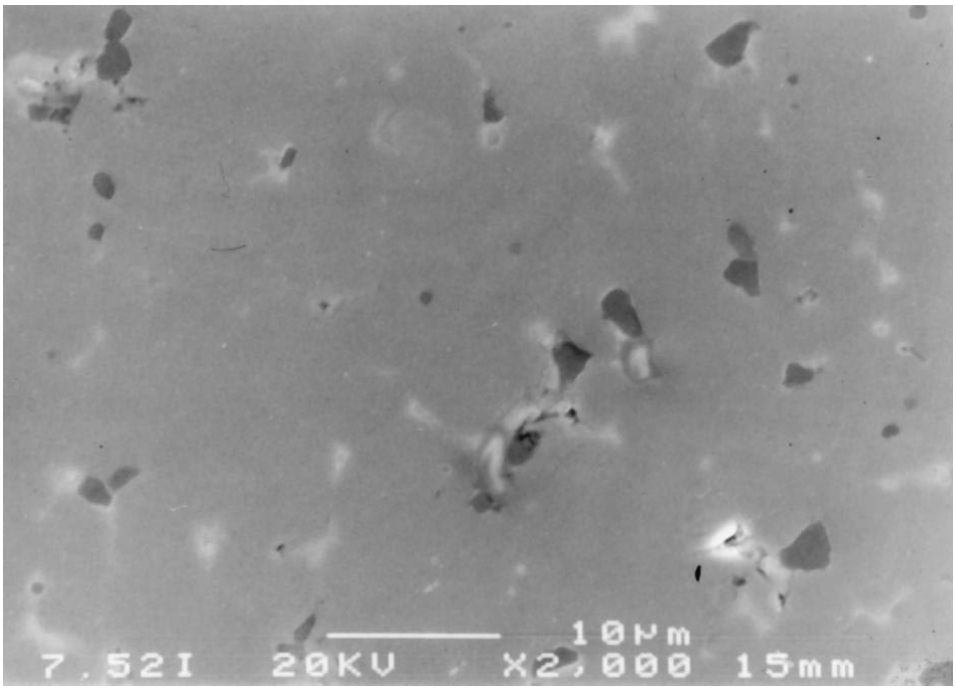

Figure 7-7: NdFeB magnet sintered at 1060 ^{o}C, Density 7.52 gcm^{-3} , SEM, JEOL 6300. (G. Yan et al., 1999)

Figure 7-6 and Figure 7-7 show the microstructures of a lower and higher density magnet, sintered at 892 ^{o}C and 1060 ^{o}C with corresponding densities of 5.97 gcm^{-3} and 7.52 gcm^{-3}, (Gaolin Yan et al., 1999)

From the micrographs, it is obvious that the magnet with a low density had more porosity than the magnet with much higher density and contained a greater surface area. The vacuum desorption from the jet milled HD powder as shown in Figure 7-8 indicated consistency with previous authors (McGuiness et al., 1989; Rupp et al., 1988; Williams et al., 1991).

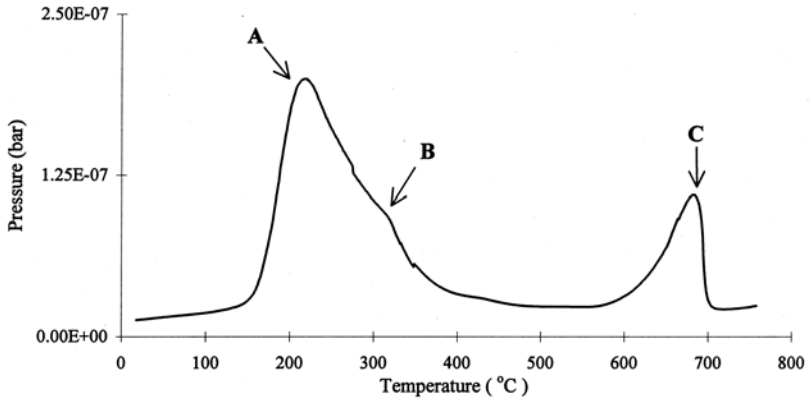

Figure 7-8 Vacuum desorption from $Nd_{18}Fe_{76}$ B_8 jet milled HD powder. Desorption events labelled A, B and C refer to those (described in Equ. (1) – (3) in appendix A1), respectively. (G. Yan et al., 1999)

From their results, the authors assumed that samples were sintered at temperatures above 700 ^{o}C, which meant that the hydrogen had been desorbed totally from the powder. In order to make sure, another freshly sintered magnet was heated in the system and changes in pressure (Figure 7-9) were measured.

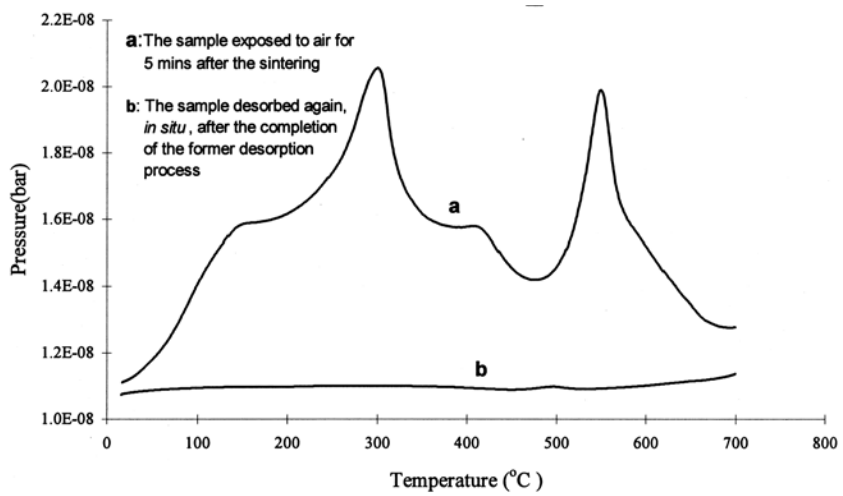

Figure 7-9 Vacuum desorption from a sintered $Nd_{16}Fe_{76}B_8$ magnet sintered at 892^{o}C. Note the much lower pressure scale compared with that of figure 7-8 (G. Yan et al., 1999)

The amount of gas desorbed is negligible compared to that of the sintered powder (figure 7-8) and the hydrogen may have been re-absorbed due to corrosion whilst the sample was transferred from the furnace to the vacuum desorption system.

The gaseous desorption curves shown in figure 7-9 agree with desorption behaviour shown in figure 7-8 for desorption from $Nd_{16}Fe_{76}B_8$ jet milled HD powder. The lower desorption temperature between 30 and 350 ^oC was related to partly to the hydrogen desorption from the $Nd_2Fe_{14}BH_x$ matrix phase and to the change from Nd 'trihydride' to 'dihydride'.

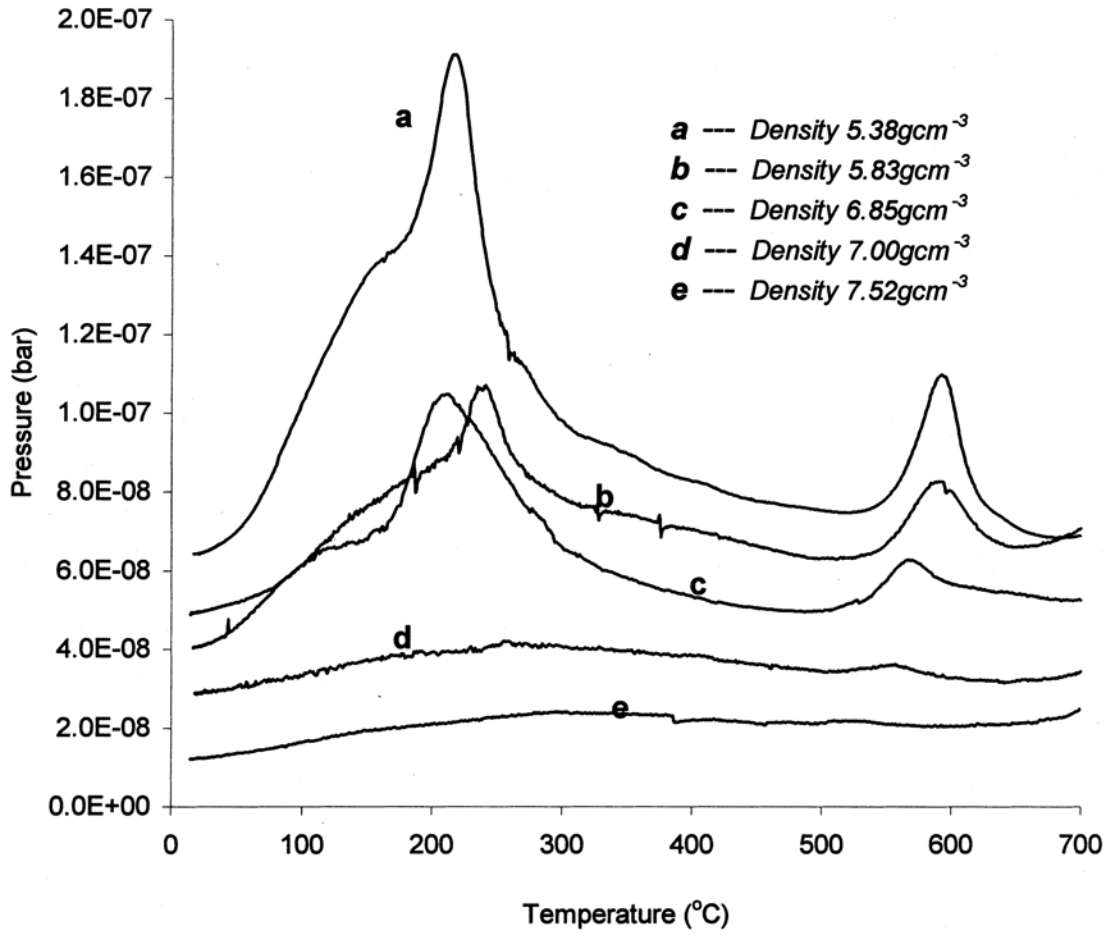

Figure 7-10 Vacuum desorption from sintered $Nd_{16}Fe_{76}$ B_8 magnets after exposure to laboratory air for 60 days. (Gaolin Yan et al., 1999)

The higher temperature peak between 500 and 650 ^oC completed the desorption from Nd 'dihydride' (Williams, McGuiness et al. 1991). Another desorption event seen by [(Rupp and Wiesinger 1988) & (Williams, McGuiness et al. 1991)] is evident in these traces and was attributed to the breakdown of Nd hydroxide, between 200 and 250 ^oC resulting in water which then reacts with Nd hydride resulting in production of hydrogen, as show in equations 1.23 and 1.24:

$2Nd(OH)_3 \rightarrow Nd_2O_3 + 3H_2O$ Equ. 1.13

$2NdH_x + 3H_2O \rightarrow Nd_2O_3 + (3+x)H_2$ Equ. 1.14

Hence, the highest peak (200-250 ^oC) corresponded to the overlap of the desorption of hydrogen from the ϕ phase, the conversion of Nd 'trihydride' to 'dihydride' and from the reaction of Nd hydride with H_2O, from the breakdown of Nd hydroxide (and possibly from hydrated iron oxides). The vacuum system only measures the total pressure and the increase in pressure could also be due to the evaporation of water. To test this possibility, the desorbed gases were analysed using a mass spectrometer and were found to be mainly H_2 with some H_2O at low temperature. It was assumed that the water is from the breakdown of $Nd(OH)_3$ and the reaction between the hydrogen and residual oxygen in the vacuum system. Figure 7-10 also indicated that the lower the density of the sintered magnet, the higher the amount of hydrogen being desorbed.

The magnets that were corroded in the environmental chamber had shown a percentage increase in weight as a function of density. The less dense the magnets, the greater the weight gains during corrosion. This was attributed to the large surface area being exposed to moisture. The less dense magnets were corroded heavily and largely turned to powder. This product had a similar resemblance to the HD process used in the production of the magnets. The opposite to this behaviour was that the higher the density of the magnet, the less corrosion occurred, although there was some evidence of decrepitation at the edges. (See figures 7-10 and 7-11)

Figure 7-11: NdFeB-type magnet sintered at 856 ^{o}C and corroded in the environmental chamber for 158 days, temperature: 858 ^{o}C, RH: 80%, density: 5.83 gcm^{-3}. (Gaolin Yan et al., 1999)

Figure 7-12: NdFeB magnet sintered at 1026 ^{o}C and corroded in the environmental chamber for 158 days, temperature: 858 ^{o}C, RH: 80%, density: 7.41 gcm^{-3}. (Gaolin Yan et al., 1999)

7.4 Corrosion protection of NdFeB

7.4.1 Zinc coating using LPPS

Walton et al., (2000) examined the stability of the magnetic properties in humid atmospheres and the effect of providing LPPS coated Nd–Fe–B magnets are compared to those of other protective coatings for the finished Nd–Fe–B magnets. Problems with corrosion inhibited have wider applications (Jones, 1995 and Sagawa, 1995). The addition of alloying elements to Nd–Fe–B has also been explored widely (Walton et al., 2000) in order to provide better inherent corrosion resistance. The use of metallic and polymeric coatings on finished magnets has also been reported (Walton et al., 2000).

In recent years, nickel has been the most widely used coating material for Nd–Fe–B magnets. The nickel plating procedure is a multistage process which may account for as much as 8% of the total production cost of a magnet (for volume applications, a plating process should represent no more than 2% of the total cost) (Walton et al., 2000). A further disadvantage is the possibility of hydrogen absorption by NdFeB during the plating process leading to subsequent embrittlement (Walton et al (2000). The protection of Nd–Fe–B by zinc layers created using a recently developed Low Pressure Pack Sublimation (LPPS) process (Speight and Harris, 1994; Walton et al 2000) has been investigated. The essentials of the zinc deposition process are described together with the magnetic properties and corrosion performance in humid environments. The performance of the LPPS coated NdFeB magnets are compared to those of identical magnets either uncoated or coated with electroplated nickel or zinc.

Walton et al., (2000) stated that the LPPS-process was first applied first to mild steel samples before moving onto the NdFeB magnets. The cylindrical NdFeB magnets used in this study were fully dense and sintered with similar dimensions and with atomic percentage of $Nd_{14}Dy_{1.4}Nb_{0.5}Fe_{76.5}Al_{0.6}B_{7.0}$. Walton conducted his study in several stages:

(1) The magnets surfaces were prepared using SiC paper and IMS.

(2) The zinc powder particle size was 6-8 μm and silica sand were combined into a mixture, approximately 20:25, weight ratio of Zn to sand.

(3) The mixture was then poured into a stainless steel envelope.

(4) The magnets were placed in the middle of the mixture and sealed and placed in a vacuum furnace.

(5) The samples were coated at a temperature just below the melting point of zinc (390 ^{o}C), the same temperature as that used for sherardizing.

(6) Zinc coated magnets were then placed in an autoclave and left for up to 70 h where they were subjected to severe humid condition (100 ^{o}C and 1 bar pressure).

Walton et al., (2000) also subjected commercial magnets to similar conditions as a comparison, and reported that the growth rates of the zinc layers are higher on the mild steel sample than on the NdFeB. For substrates, the variation of growth rate versus temperature is almost linear which indicate a thermally activated formation process.

7.4.2 The characterisation of Zn-coated layer:

Lower coating rates previously indicated errors due to coating thickness calculations. Sherardizing produced thickness of 15-20 μm. The LPPS process produced 20 μm for mild steel samples and NdFeB magnets after 1 and 1.5 h respectively at 390 ^{o}C. A thickness of up to 30 μm has been achieved on both substrates. For mild steel, the zinc layer closely followed the morphology of the underlying surface and the Zn-Fe interface was sharply defined. Etch contrast within the zinc layer showed a thin area adjacent to the mild steel. The NdFeB magnets metallography showed intergranular diffusion of the zinc, up to a depth of 10 μm at 390 ^{o}C. Using EDX; the Zn/Nd-Fe-B interface showed the intergranular phase to be Zn-rich. This can cause a reduction in coercivity probably due to the greater number of reverse domain nucleation sites. After heat treatment in air at 390 ^{o}C for 5 hours, metallography showed that there is an extensive disruption of the interface due to inter-diffusion of zinc up to a depth of 70 μm. EDX studies revealed that in-diffusion of the zinc along the NdFeB grain boundaries was the dominant mechanism. Figure 7-13 below shows EDX images of zinc mechanism during corrosion:

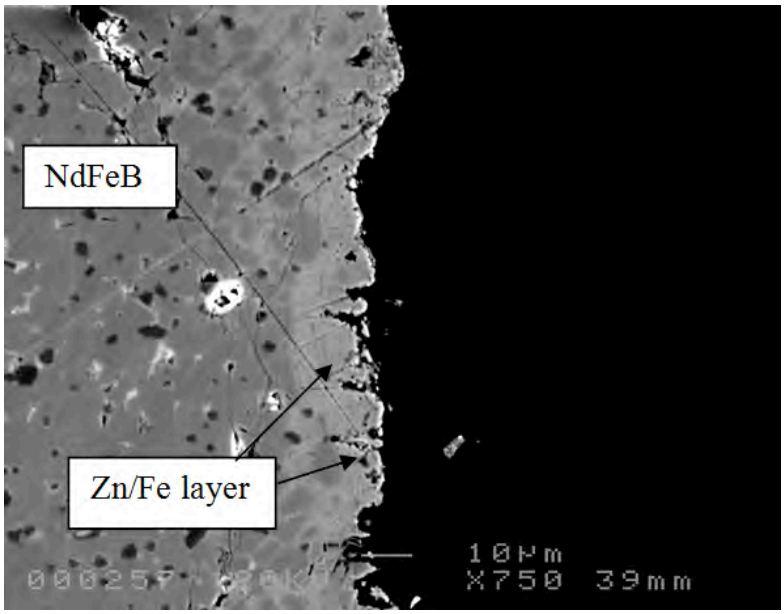

Figure 7-13: SEM micrograph of a cross section through an LPPS coating after 70 h of autoclave exposure. (Walton et al., 2000)

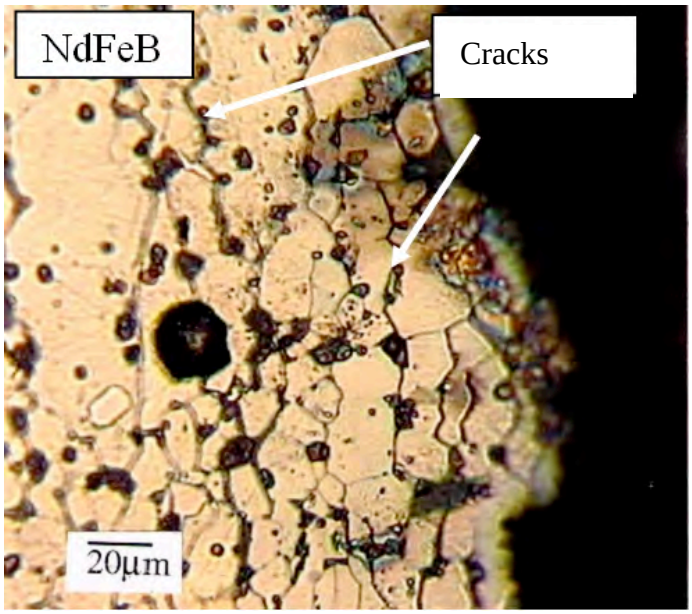

Figure 7-14: Optical micrograph of an uncoated NdFeB sintered magnet cross section after 70 h in an autoclave

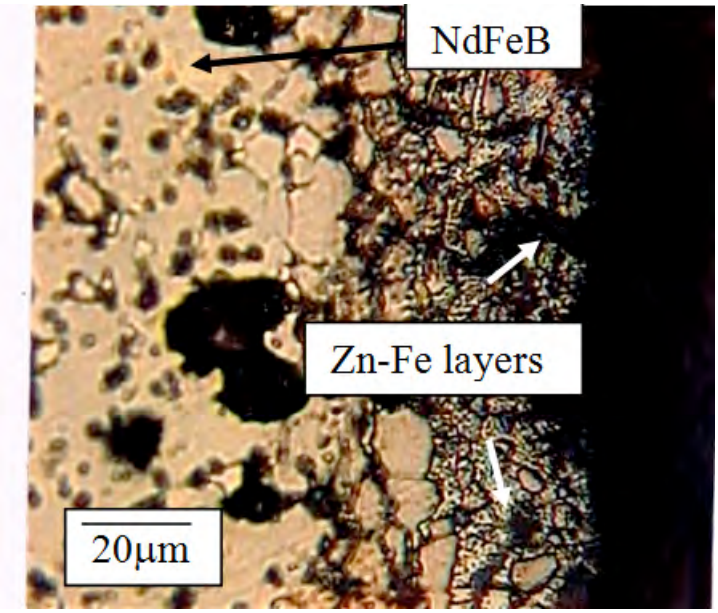

Figure 7-15 Optical micrograph of an LPPS zinc coated NdFeB magnet cross section after 70 h in an autoclave. (Walton et al., 2000)

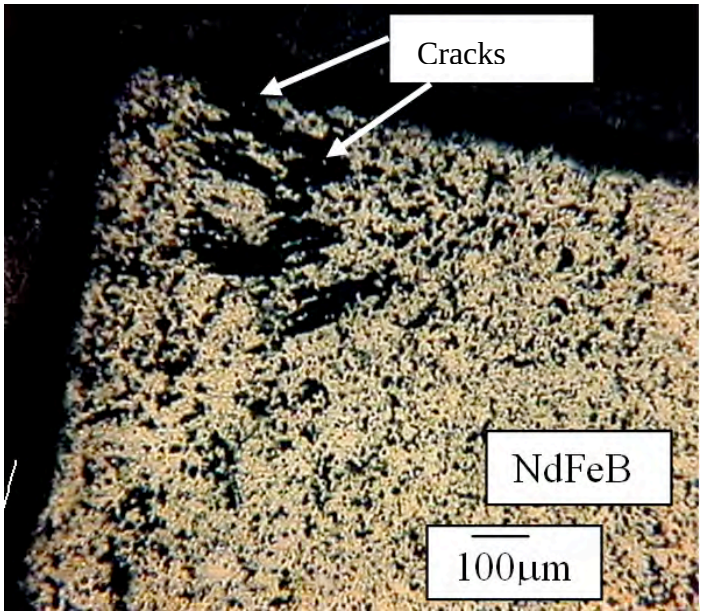

Figure 7-16 Optical micrograph of a zinc electroplated NdFeB cross section after 70 h autoclave exposure where extensive peeling of the zinc had occurred. (Walton et al., 2000)

In the autoclave, uncoated and coated magnets developed brown and orange surface products and showed a rapid weight gain up to 40 h of exposure. After longer times, the corrosion products became detached from the magnets together with grains of $Nd_2Fe_{14}B$ thus reducing the weight considerably. XRD revealed that the corrosion

products to be predominantly $Nd(OH)_3$ and Fe_2O_3. In contrast, the Zn coated magnets developed a white product which was found to be ZnO and showed little change in mass during the 70 h in the autoclave. The thickness of the zinc layer appeared to influence the degree of corrosion protection. Corrosion was more pronounced in the case of the samples with a coating of less than 12 μm compared those with 20μm. This indicated that a zinc coating of 20 μm and more was most suitable for the NdFeB magnets in a humid atmosphere.

The remanence and coercivity of the uncoated NdFeB magnets decreased as the magnets corroded in the autoclave atmosphere; this was due to the loss of magnetic material from the surface of the magnet, the grain boundaries nucleating reverse domains throughout the structure and absorption of hydrogen by the ϕ-phase. However, Walton et al., noted that the B_r and $_jH_c$ values seemed unchanged with time as the sample accumulated significant amounts of corrosion products on the surface. This was attributed to the fact that the corrosion products protect the magnet to a certain degree until they lose their attachment to the surface. It was assumed that the corrosion process may be re-initiated at longer times and the remanence and coercivity would again decrease.

The workers performed XRD analysis on the surface of the uncoated (Philips) and on the LPPS coated NdFeB sintered magnets where they were exposed to an autoclave environment for 70 h (Figure 7-6 & Figure 7-7). These analyses were performed in order to identify any NdFeB corrosion products which might be pushing through the LPPS coating and could not be observed visually. No phases other than ZnO or the FeZn (ζ-phase) could be identified on the LPPS coated sample (Figure 7-17).

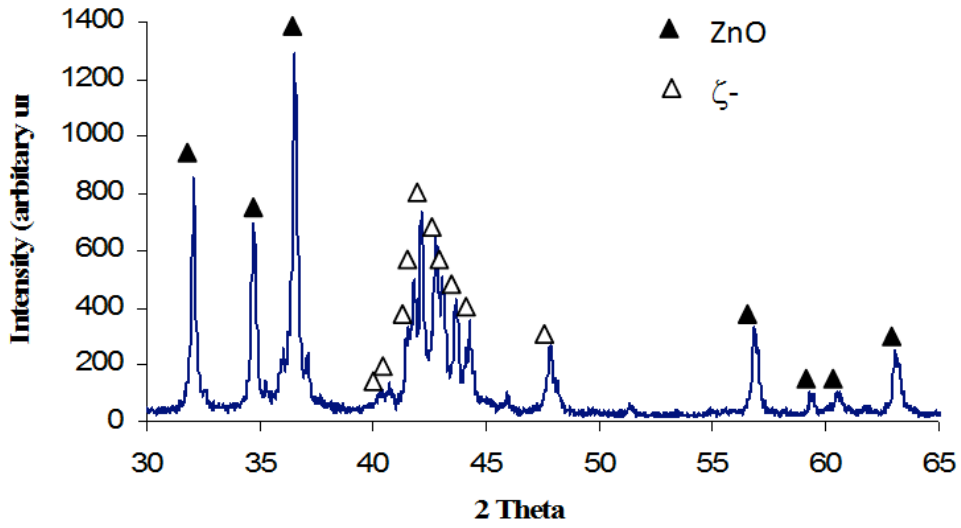

Figure 7-17: XRD trace on the surface of an LPPS magnet after 70 hours of autoclave exposure. (Walton et al., 2000)

Using XRD analysis showed that for the uncoated magnets the brown corrosion products containing predominantly Fe_3O_4, with some $Nd(OH)_3$ (Figures 7-17 and 7-18). The brown corrosion products which formed on all the commercially coated magnets were shown to contain these compounds, indicating corrosion of the underlying substrate. This was confirmed by metallography.

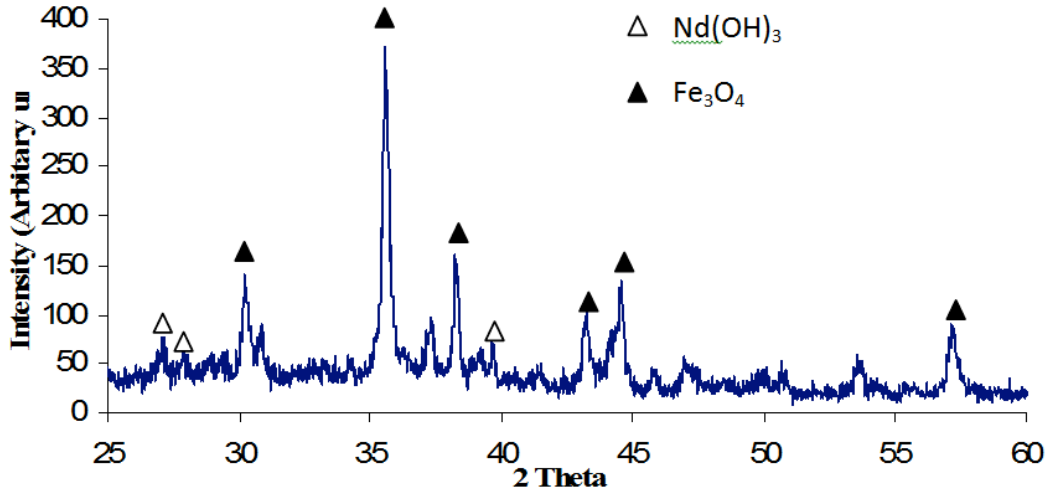

Figure 7-18: XRD trace produced on the surface of an uncoated NdFeB magnet after 70 h of autoclave exposure. (Walton et al., 2000)

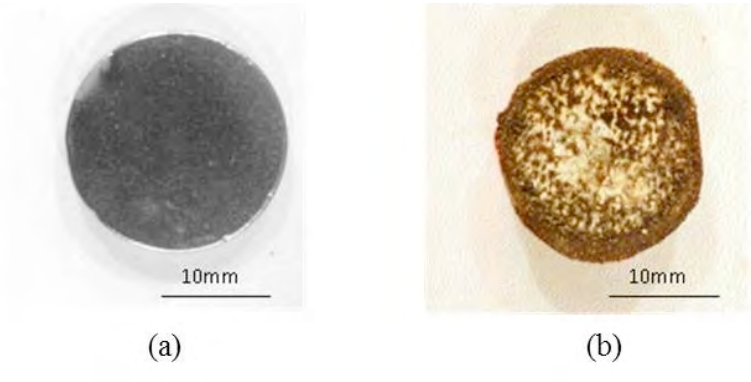

Figure 7-19: A Zn plated magnet before (a) and after (b) 70 hours in an autoclave. (Walton et al., 2000)

It was observed that, in the case of the LPPS magnets, their coercivity and remanence values were more stable than those of the uncoated ones. During the autoclave exposure, the ${}_jH_c$ varied by less than ±2% which was within the experimental error. However, the remanence had fallen with time of up to 40 h and this was probably due to the surface loss of material (the poles tips of the permeameter tended to remove corrosion products during the measurements).

Walton et al., concluded that, under the autoclave conditions, uncoated NdFeB were found to corrode through the reactions with the Nd-rich grain boundaries giving $Nd(OH)_3$, Fe_2O_3 and $Nd_2Fe_{14}B$ corrosion products. Corrosion resistance of the zinc coated magnets were significantly better than that of the electroplated nickel and zinc samples thus proving that LPPS can be used as an alternative corrosion protection process due to its lower costs and its zinc coating effectiveness of NdFeB magnets and provide corrosion prevention in humid atmosphere.

The LPPS process has been applied to some of the magnets investigated in the present work and the results of these studies will be reported later in this thesis.

8 Experimental Techniques and Apparatus

8.1 Introduction

This section discusses the range of experimental techniques used throughout this project to investigate the starting materials and the re-sintering behaviour of the recycled powder.

8.2 De-coating (magnet preparation)

Some of the starting magnets were initially nickel coated (for corrosion protection). To provide a consistent batch of starting materials the nickel coating was removed manually. This process was carried out using SiC paper within a grinding machine using 120 grit. This treatment resulted in a clean surface on the starting material, suitable for the subsequent HD treatment. Prior to HD, the magnets are broken into small pieces, and then placed in a chamber where they are exposed to hydrogen.

8.3 Hydrogen Decrepitation (HD)

A schematic of the HD-unit is shown in Figure 8-1. The procedure was to load the clean stating material into the chamber, which initially is evacuated by a rotary pump before back filling to around 2 bar with hydrogen. As the hydrogen is absorbed by the magnet, causing expansion which, in turn, results in the magnet breaking apart into a coarse powder. This is processed at a constant pressure of 2 bars until the process is complete. The powder is then transferred into an argon atmosphere glovebox (see Figure 8-2).

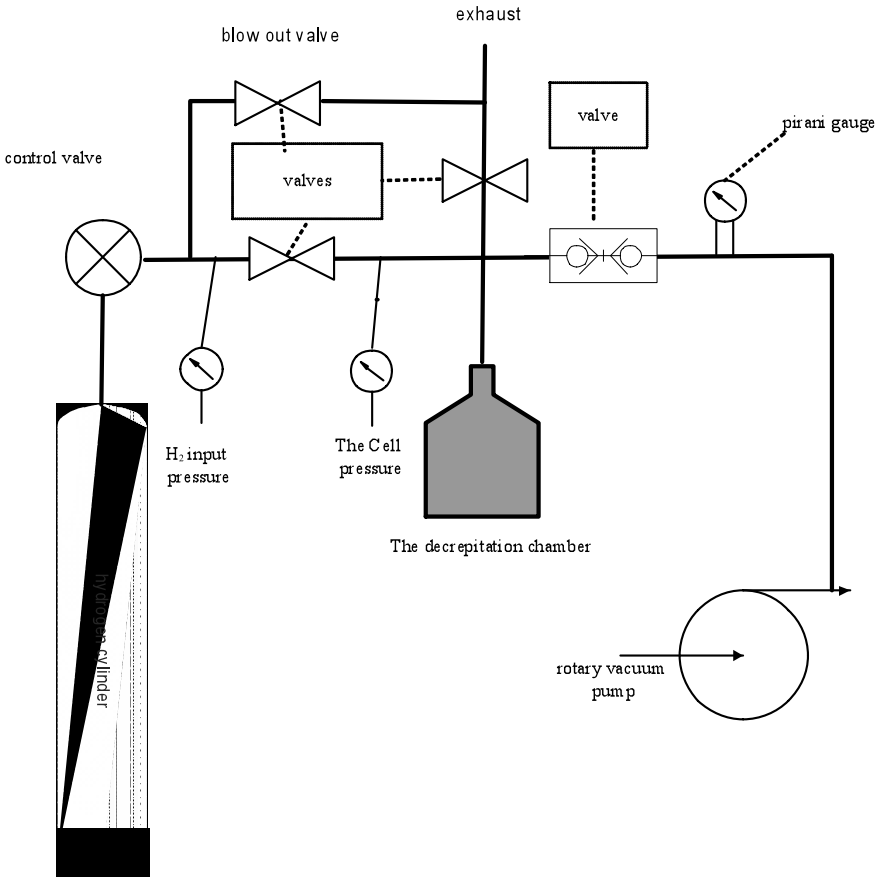

Figure 8-1 The Hydrogen Rig.

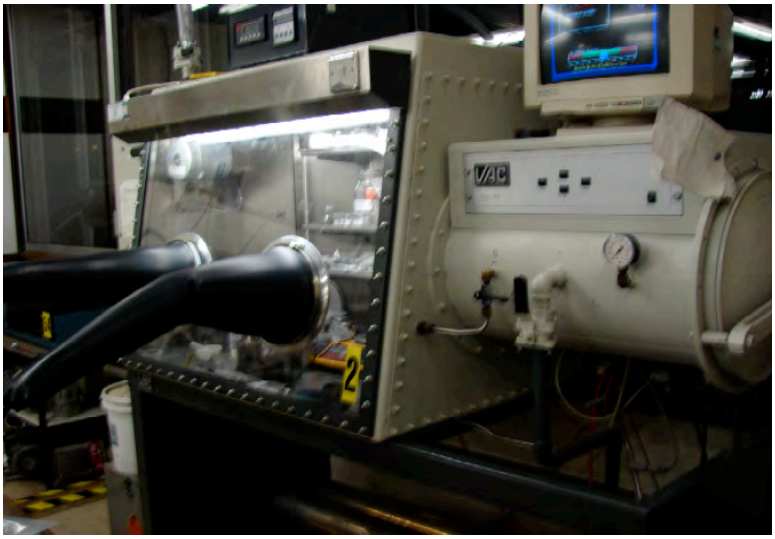

Figure 8-2 glove box where the powder is transferred after the HD treatment.

8.4 Powder production

8.4.1 Roller Milling

To produce a fine powder, suitable for sintering, the relatively coarse powder generated by the HD-process is placed in a milling pot together with tungsten-carbide milling balls (Figure 8-3) and cyclohexane as the milling medium. To ensure consistency, the same amount of powder is used every time, i.e. 35 g of powder against 250 g of milling balls. The pot is sealed inside the glove-box and place on a Pascall roller (see Figure 8-4) rotating at 100 rpm. The milling is achieved according to a set time in hours. After the milling is complete, the pot is removed and opened in the glove-box (containing less than 20 ppm O_2). The cyclohexane is removed and the powder dried using the vacuum port where cyclohexane is completely evaporated, before transferring the milling pot back inside the glove box.

The ball milling process is the best available source for the author to conduct experiments using this method to produce the desirable powder size. This method is used widely and still in existence but high energy milling machine are used to produce powder with 3-7 μμ particle sizes. (Gaolin Yan et al., 2010)

Figure 8-3 Milling pot with ball bearings

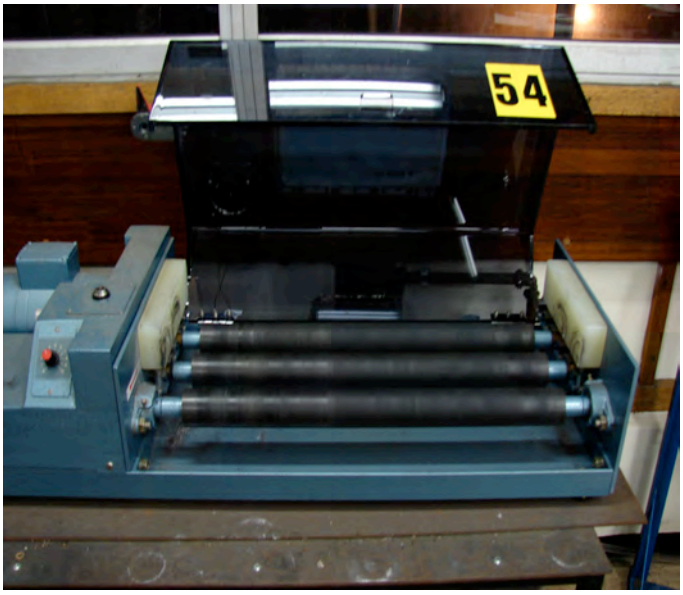

Figure 8-4 Pascall roller

8.4.2 Aligning and Isostatic press

8.4.2.1 Isostatic Tubes

The milled powder (with an average weight of 35 g) is then placed into Neoprene tubes, Figure 8-5 where it is isostatically pressed (50-60 bars) into a cylindrical shape. The tube is loaded with powder within the glove and sealed with insulation tape prior to removal.

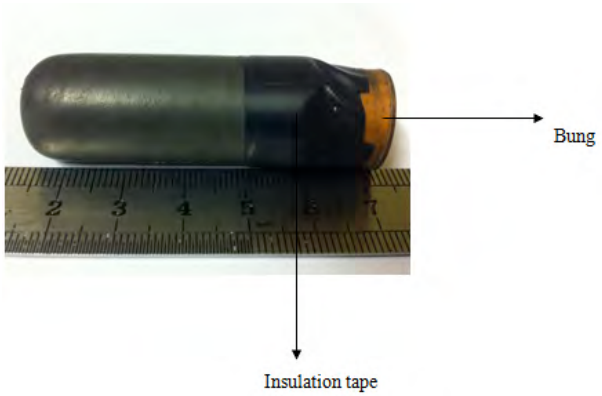

Figure 8-5 Isostatic Tube

8.4.2.2 Pulse Magnetise

To align the powder along the c-axis, the powder is then subjected to a pulsed magnetic field (~ 4 T) (Figure 8-6) where the particles are aligned with the c-axes pointing parallel to the direction of the applied field.

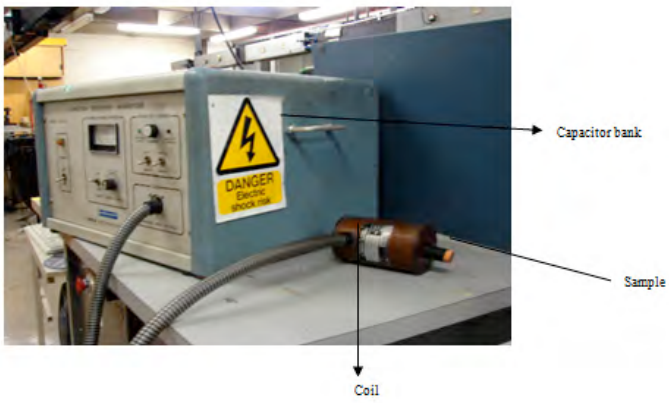

Figure 8-6 Pulse Magnetiser

8.4.2.3 Hydrostatic Press

After magnetic alignment the powder in the tubes was subjected to a high hydrostatic pressure (see Figure 8-7) of 60 bars for about 3 minutes. The press used is a modified bench press, Clarke model which has a loading of up to 10 ton and has the features shown in Figure 8-7 where the ram is manually pushed to enable the press to reach the desire load (pressure) and then is left at this pressure for the time stated earlier and then released.

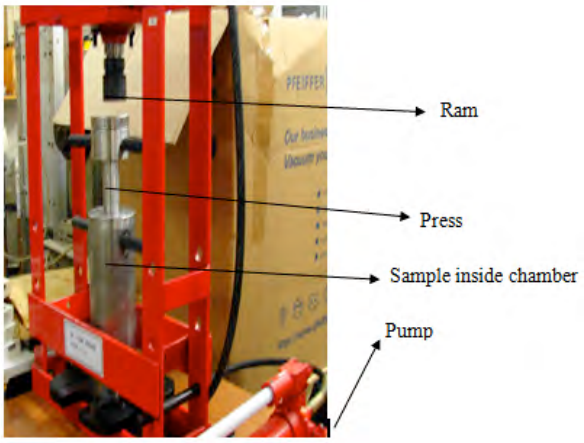

Figure 8-7 Hydrostatic Press for pressing powder

8.4.2.4 Compact Sintering

The HD powder (NdFeB powder green compacts) is then densified by means of liquid phase sintering. The sintering temperature profile used is shown in Figure 8-8. The profile uses a heating rate of 10 ºC/min to 1090 ºC with a hold time of 1 hour at 1090 ºC before furnace cooling. Other sintering conditions have also been applied in these investigations. The sintering system used is a vacuum furnace tube evacuated (better than $4x10^{-1}$ bar). The furnace is controlled by a Eurotherm multi ramp temperature controller (shown in Figure 8-9). Other thermocouples can be attached to the temperature controller which gives a second temperature reading from the hot zone of the furnace and this can be checked regularly using a voltmeter linked to a K-type thermocouple.

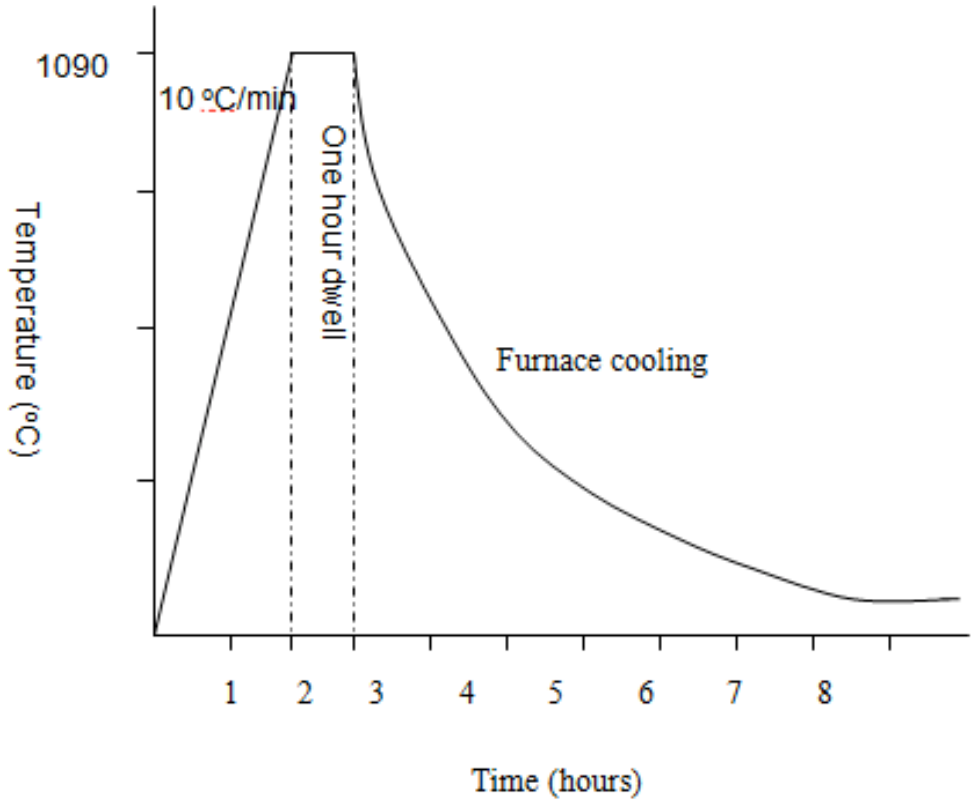

Figure 8-8 The general sintering program but others also have investigated.

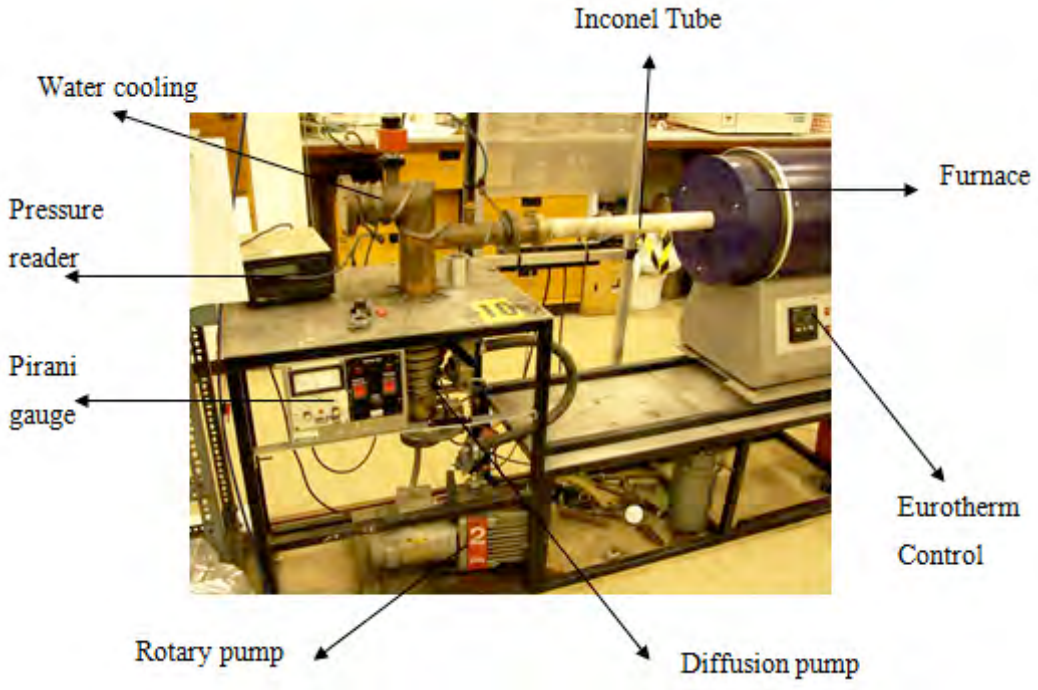

Figure 8-9 Sintering Furnace.

8.5 Slurry Solution using Dy and Tb hydride

To investigate the effect of treating sintered magnets based on NdFeB with dimensions of approx 14x15x2 mm with a slurry of Dy and Tb. The TbH_3 or DyH_3 powder was mixed with cyclohexane to form a suspension. This mixture was in the ratio of 2:1 in weight, with a mean particle size of 3-5 μm. The sintered magnets were coated and dried in a glove box, housed in a stainless steel envelope and placed in a furnace. The magnets were then heated at 800 ^{o}C for 0.5 h, 1h, 3 h and 10 h under vacuum conditions of $6x10^{-2}$ Pa. The magnetic properties were measured using a permeameter after applying a pulse of ~4 T. The microstructural analyses of these magnets were performed using a SEM JEOL 7000.

8.6 Low Pressure Pack Sublimation (LPPS) Technique

Low pressure pack sublimation (LPPS) technique has been developed as an alternative technique to the more conventional sherardizing method for coating metallic parts with a protective zinc coating. In LPPS the coating vessel is not rotated and the process is carried out in a low vacuum (~10^{-2} Torr). Figure 8-10 shows a schematic diagram of the LPPS process and Figure 8-11 is a photograph of similar rig used in the zinc coating work.

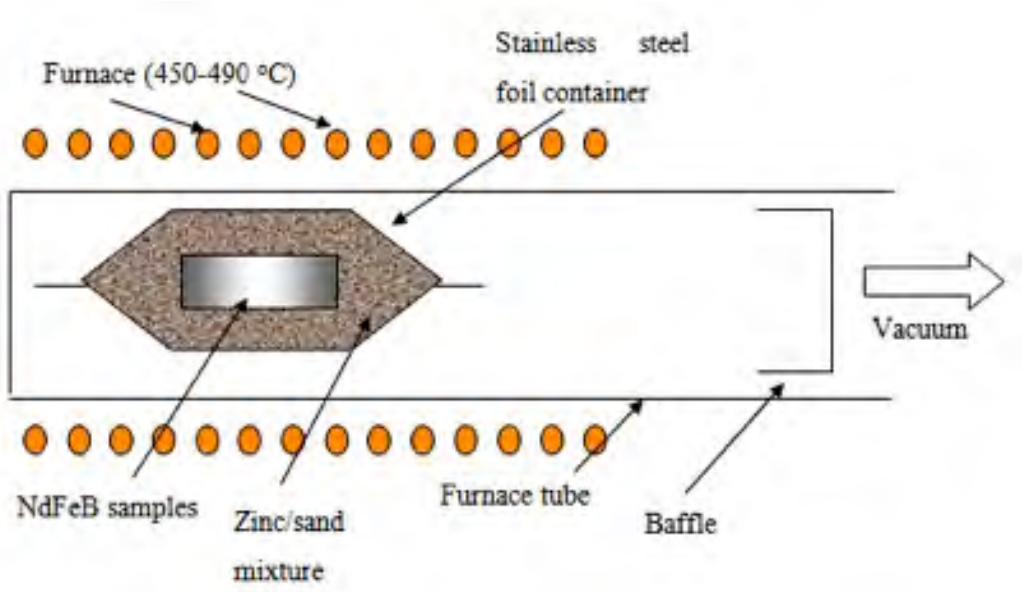

Figure 8-10 Schematic diagram of the LPPS process (adapted from Walton, 2002).

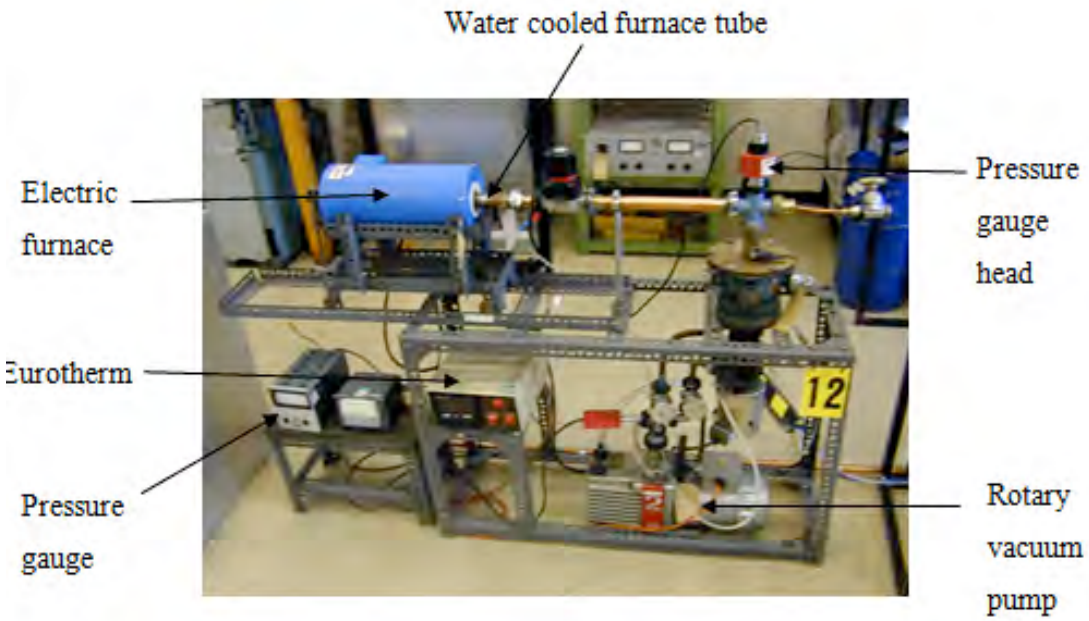

Figure 8-11 Photograph of the LPPS coating rig. (Walton, 2002).

The procedure followed prior to coating the samples with the LPPS process was to clean the magnetic material to be coated by washing in industrial methylated spirit and drying. The LPPS process was carried out on a laboratory scale rig shown in Figure 8-11. A stainless steel foil container was formed around a wooden mandril and closed at one end. This container was then filled to a 1/3 full of a blend of zinc dust (6 – 8 μm) and silica sand (300 μm) in a weight ratio of 20:25 (g) respectively and the clean NdFeB magnets placed in the mix. The capsule was subsequently filled to the top with the zinc dust / sand mix and sealed. Then placed into a vacuum chamber and evacuated to 10^{-2} Torr. A K-type thermocouple, positioned adjacent to the sample and linked to a Eurotherm is used to control and monitor temperature. A range of coating the temperatures between 450 - 490 ^{o}C were investigated. After coating the samples were shaken to remove excess zinc/sand.

It is subsequently found that the magnets placed in the 'hot zone' along the furnace tube have thicker coatings deposited within the hottest part of the furnace. To provide consistency a ceramic spacer is formed and slid into the furnace tube so that each sample is placed in exactly the same place within the hot zone of the furnace on every coating run.

The sample weight is measured before and after LPPS coating and the weight change also used as a guide to the coating thickness. It is known that 150×10^{-4} g/cm^2 of zinc produces a coating of 20 μm, so by calculating the mass change per unit area of each sample, a coating thickness could be derived (Walton, 2002).

8.7 Characterisation Techniques

8.7.1 SEM Specimen Preparation

Prior to SEM analysis samples were prepared by taking a cross section of the sintered samples and mounting in conductive bakelite using a hot mounting press. The mounted samples are then ground on four grades of silicon carbide papers (240, 400, 800, and 1200 grit). In order to prevent oxidation of the sample, methanol is used as a lubricant. Finally, the samples are then polished on a polishing-wheel impregnated with 0.25 μm of diamond paste and a non-water-based lubricant. The samples are then cleaned using acetone or methanol and dried.

If the grain structure (particularly the grain boundaries) needs to be seen clearly, then the polished samples are subjected to etching in 2% (Viella's reagent) for approximately 20 seconds. (Villela's reagent consisting of 1g of picric acid, 5 ml hydrochloric acid and 100 ml of ethanol is used for etching).

8.7.2 Densitometer

The densities of samples (ρ_s) are measured using an Archimedes' principle. This takes place by measuring the weight of each sample (W_a) in air and in a fluid (W_l) of a known density ρ_l.

A standard pure copper sample is used to calibrate the system

The density of the samples was calculated using the Archimedes principle, whereby a body submerged in a fluid experiences a buoyant force equal to the weight of fluid

displaced. The samples were weighed in air (W_{air}) and then in a standing liquid, (diethyl phthalate), (W_{liq}) of known density (ρ_{liq}) on a Ohaus balance (see Figure 8-12). Using the equation given below, the density of each sample was calculated. The overall accuracy of the density measurements is estimated to be ± 0.05 g/cm^3.

To find the density of a sample is accomplished using the following equation:

$$\rho_S = \frac{(w_{sair})(\rho_{liq})}{(w_{sair} - w_{sliq})} \qquad \text{Equ. 1.15}$$

ρ s = density of sample

w_{sair} = weight of sample in air

ρ_{liq} = density of liquid

w_{sliq} = weight of sample in liquid

To mitigate the effect of thermal expansion the sample's temperature should be the same as the temperature of the liquid when measuring the weight in liquid.

The density of the liquid is determined through the following equation:

$$\rho_{liq} = \frac{(\rho_{cu})(w_{cuair}) - (\rho_{cu})(w_{liq})}{w_{cuair}} \qquad \text{Equ. 1.16}$$

Density of Cu =8.93 g/cc, and the weight of the copper rod in air should be 15.56 g, thus, measurements were made by using a sensitive Ohaus balance with an accuracy of ± 0.0001 g.

Figure 8-12 Densitometer

8.7.3 Permeameter

Figure 8-13 shows the permeameter which is used to measure the magnetic properties with values of B_r (remanence), intrinsic ${}_jH_c$, inductive ${}_bH_c$ coercivity and (BH_{max}). The permeameter consists of an electromagnet that has 2 movable poles, a set of measuring coils, 2 flux integrators, power supply and a computer interface. The poles lie parallel to each other.

The errors in the readings have been determined from the standard deviations of many results in the present and other authors' work (Zakotnik et al., 2008) to be Br ± 10 mT, ${}_iH_c$ and ${}_bH_c$ ± 10 kA/m, (BH)max ± 5 kA/m^3 respectively (at a temperature of 20 ^oC ± 3 ^oC).

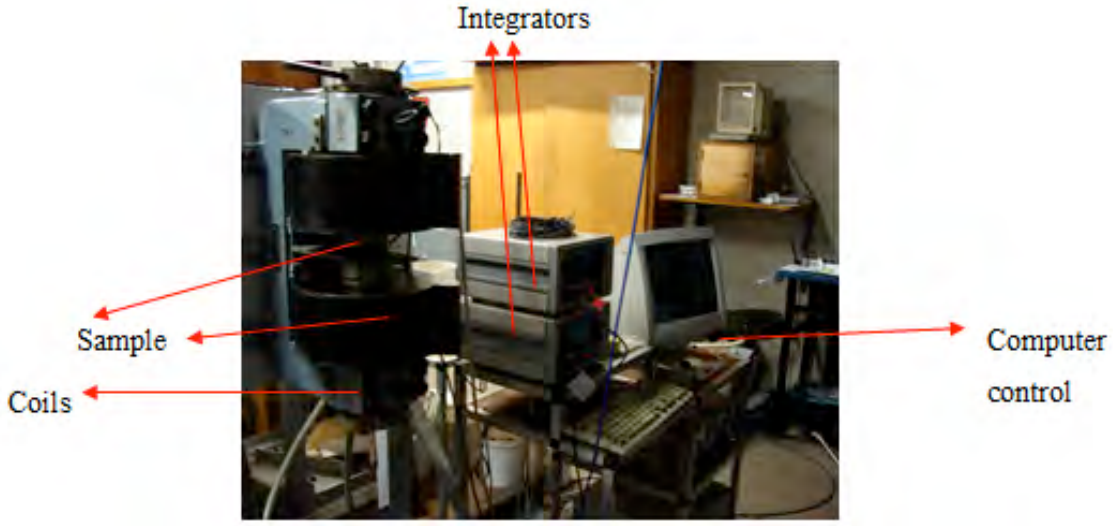

Figure 8-13 Permeameter

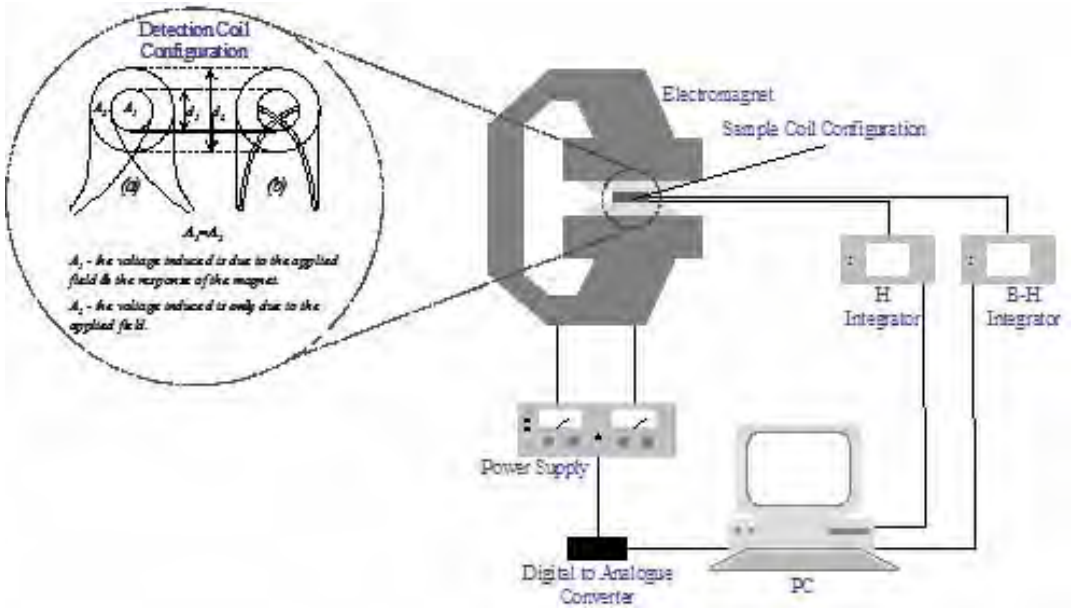

Figure 8-14 Schematic diagram of the permeameter showing closed loop permeameter and detection coil configuration; (a) measures the applied field and (b) measures the polarisation.

8.8 Differential Scanning Calorimetry

Useful information can be obtained from a study of phase transformations using Differential Scanning Calorimetry (DSC). Information given from the DSC includes phase transformation temperatures, for example, melting of a eutectic phase on heating, shown by an endothermic reaction where heat is taken in. The procedure used in this work is to initially perform a benchmark run of blank sample crucibles using the same heating and gas flow conditions which will be used during the sample run. This measurement (run) is deducted from the sample run to account for variations in sample and reference crucibles (Al_2O_3) and any non-linear heating within the DSC.

The (DSC) measurements are performed by heating pieces of sintered magnets (or just magnetic powder) up to a maximum temperature of 1350 ^oC at a rate of 10 ^oC/min in a flowing argon atmosphere at 100 ml/min to study phase transitions or kinetics of the reactions. The device used is a DSC 404 C (Netzsch) with a maximum operating temperature of 1600 ^oC. Alumina and aluminium pans were used in the measurements, where the latter one presents the advantage of a much higher thermal conductivity but a much more limited temperature range due to the low melting point of aluminium (Figure 8-15).

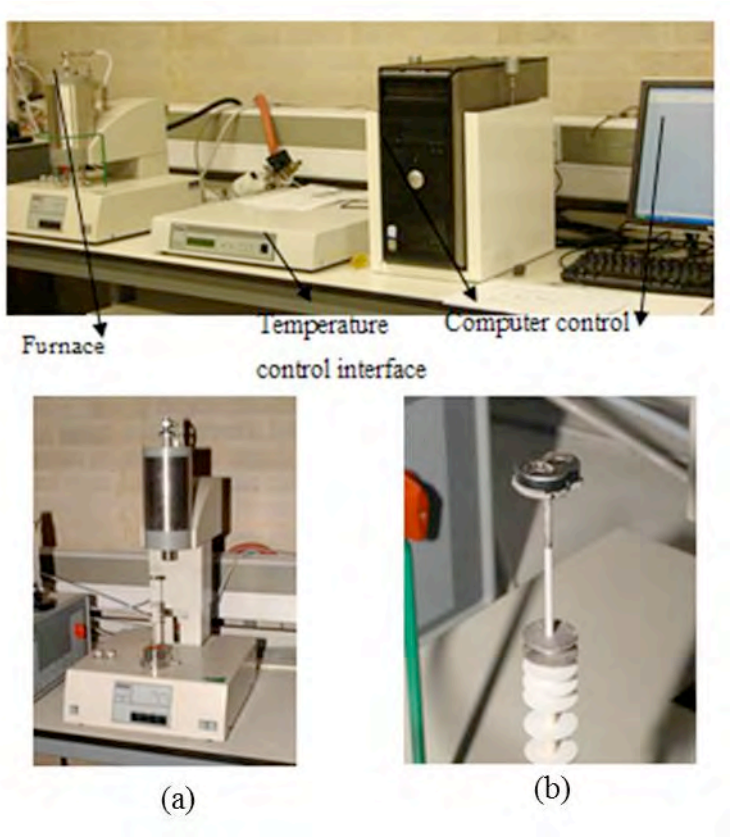

Figure 8-15 Differential Scanning Calorimetry (DSC): (a) furnace open (b) the sensor with 2 crucibles

Microstructure analysis:

This will analyse the microstructure compositions, shape and proportions of secondary phases. This is determined mainly through the use of SEM and EDX techniques.

8.9 Scanning Electron Microscopy

The polished samples were investigated largely using a SEM (Joel 6060). The operating conditions were a working distance of 10 mm with an acceleration beam voltage of 5-25 kV, (see Figure 0-16).

The SEM is used to examine the microstructure, morphology and grain size. This produces images by using secondary or backscattering electron signals. During secondary electron signals, the images produced from the electrons that are ejected

from the atoms occupying the top surface of the sample. The sample's surface morphology will have an effect on the contrast of the sample topography. When using backscattered signals, electrons are reflected from the surface in an elastic collision. The information gathered from this can help to identify phases with chemical information. In backscattered imaging a light contrast is generated from elements which have a high average atomic number, element with darker features indicate a lower average atomic number.

It is possible within an SEM to perform simultaneously, EDX (Energy Dispersive X-ray) analyses which will provide information on the sample's chemical composition. EDX analysis depends on the characterising of the energy of X-rays given off from the sample. These X-rays are generated by the electron beam displacing electrons within the sample. Electrons from higher energy shells fall down to replace the electrons from the lower energy shells whereby an X-ray is emitted, characteristic to the element. The difficultly, however, is to differentiate between certain elements as the characteristic X-ray energies overlap, for example terbium and dysprosium.

It is possible to differentiate between elements which overlap in energy using a technique called WDX (Wavelength Dispersive X-ray) analyses which rely on the diffraction of the X-rays being generated by using a crystal to filter out the unwanted X-rays. This technique is slow and requires calibrating for each element during use. However, the energy resolution of WDX is much better than that of EDX. Since this improvement in resolution results in a better peak/background ratio, the detectors resolution is better: 0.01 % for normal elements and 0.1 % for light elements (Hall, M.G. 1990).

Figure 0-16 Joel 6060 (Oxford INCA) SEM.

8.10 Inductively Coupled Plasma (ICP) Analyses

A section of the magnets (this can be performed both before and after processing) have been analysed by ICP to give an overall composition.

The composition of the starting material was determined using ICP (Inductive Coupled Plasma). Inductively Coupled Plasma (ICP) is an analytical technique used particularly for the detection of trace metals in samples. The primary goal of ICP is to get elements to emit characteristic wavelength specific light which can then be measured. The technology for the ICP method was first employed in the early 1960's with the intention of improving upon crystal growth techniques.

An ICP typically includes the following components:

- Sample introduction system (nebulizer)
- ICP torch
- High frequency generator
- Transfer optics and spectrometer
- Computer interface

Its effectiveness depends largely on good standards and regular calibration.

9.0 Results and Discussions

9.1 Introduction

This chapter presents the results obtained during this project, including the measurements conducted on (1) the starting material, (2) the recycled material (Philips, USA, China and IPM). (3) Complete section dedicated to the IPM magnets (lean rare earth). Studies on the effect of milling on the grain size and on the magnetic properties. The effects of adding heavy rare earth hydrides on the magnetic properties have also been studied. Thermal characterisation, the effect of additions and the heat treatment of recycled lean rare earth magnets, the effect of corrosion on NdFeB-type sintered magnets have also been investigated.

The materials investigated in this project were supplied by the following companies:

China Magnets were imported by Precision Magnetics LTD, Rotherham, USA Magnets imported by Precision Magnetics from Val Pareiso in Indiana, USA. Philips Magnets: Southport, Lancashire (now closed) was made in the UK and Less Common Metals, Liverpool, supplied as-cast Neomax alloys. IPM magnets were imported from Shin-Etsu Chemicals Ltd, Japan.

In addition a sintered magnet was prepared from a Neomax cast alloy (starting composition $Nd_{16}Fe_{77}B_8$). This was carried out in order to check the validity of the processes employed in the present work and to provide a comparison with commercial magnets described above.

9.2 Characterisation of Initial magnets: carried out at LCM laboratories

9.2.1 ICP analysis (at%)

Table 9-1: ICP measurements of composition of magnets (± 0.008-0.073)

	Nd+Pr	Dy	Fe	Co	B	Al	O (ppm)
USA	13.55	0.889	78.27	0.056	6.37	0.859	4068
China	12.56	1.8	77.51	1.17	6.14	0.812	3883
Philips	14.04	0.63	77.81	-	6.44	0.69	4670
IPM*ni*	12.8	0.79	77.09	2.57	6.19	0.56	2565

From the above table, the RE content shows that the Philips magnet has the most Nd and contains the lowest amount of Dy. China magnets has the most Dy and least Nd+Pr but a low value of Fe but not lower than that of IPM*ni*. Unfortunately, the ICP measurements were not able to measure the amount of Co in the Philips magnets as it was very low. The oxygen content in the USA and Philips magnets is higher than that of the China magnets. The IPMni had the lowest oxygen contents than the other compositions. No measurements were available for the Neomax alloy to make appropriate comparison, but 300-400ppm oxygen is typical of the cast alloys. The Japanese magnets (IPM*ni*) have the lowest oxygen contents and low Nd+Pr percentage, high cobalt and high B content.

9.2.2 Magnetic properties

All the magnets have been subjected to the same test conditions for the purpose of consistency. First to be discussed will be the starting magnets along with a combined analysis using metallography and the permeameter. The magnetic properties characterised are summarised in table 9-2.

Table 9-2: magnetic properties of starting magnets

Magnet	BHmax (kJ/m^3) ±2%	Inductive Coercivity (kA/m) $_bH_c$ ±1%	Br (mT) ±1%	Intrinsic Coercivity (kA/m) $_jH_c$ ±1%	Squareness factor	Density g/cm^3 ±0.05 g/cm^3
China	298	940	1236	1250	0.82	7.64
USA	290	893	1275	970	0.87	7.66
Philips	275	889	1187	1050	0.82	7.66
IPM*ni*	359	845	1370	849	0.99	7.65

From the magnetic measurements it can be seen that the magnet with by far the highest Dy-content (China) exhibits the highest value of the coercivity ($_jH_c$). in addition, the remanence increases with lower RE contents, i.e. increasing the proportion of the 2-14-1 magnetic phase.

The second quadrant demagnetisation curve for each magnet, along with a typical microstructure is now examined.

Philips:

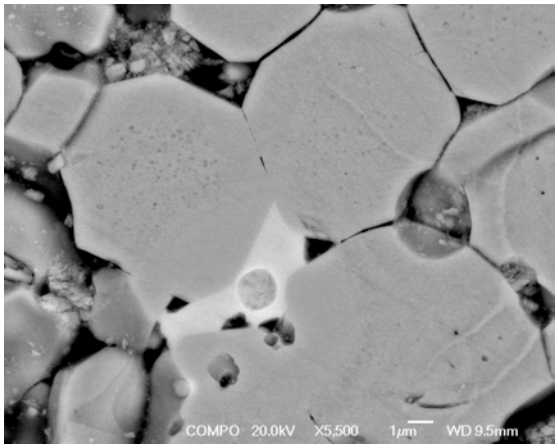

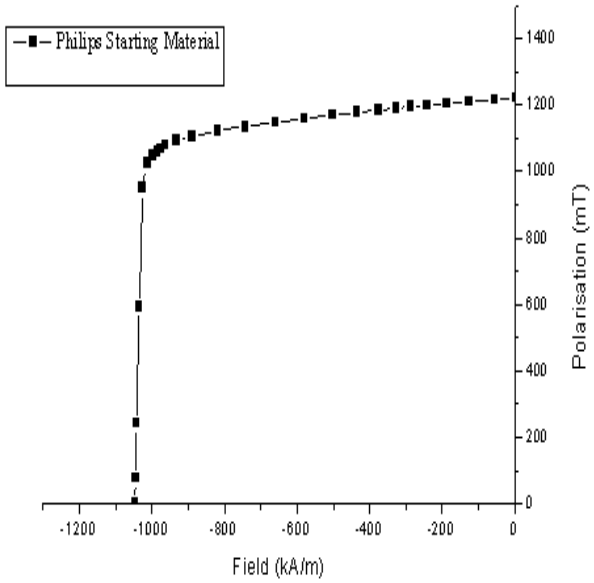

Figure 9-1 Shows the 2nd quadrant demag curve and a SEM image of the Philips alloy. Bright features in the SEM image indicate the Nd-rich phase. Density = 7.66 g/cm^3

China:

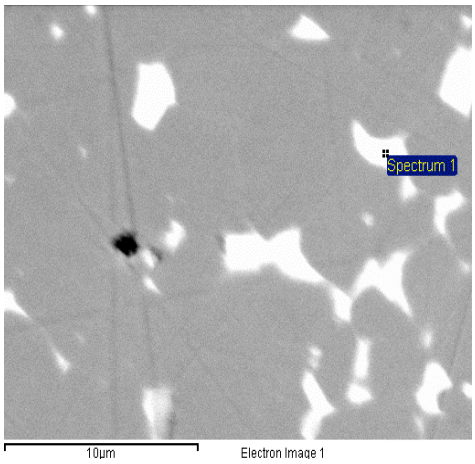

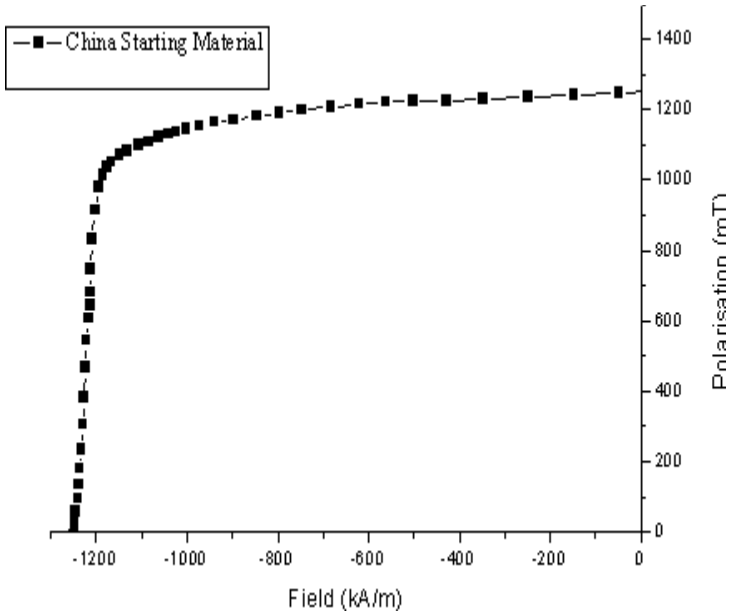

Figure 9-2 Shows microstructure of China magnet (alloy). It indicates that this magnet exhibits the best coercivity. density = 7.64 g/cm^3

USA

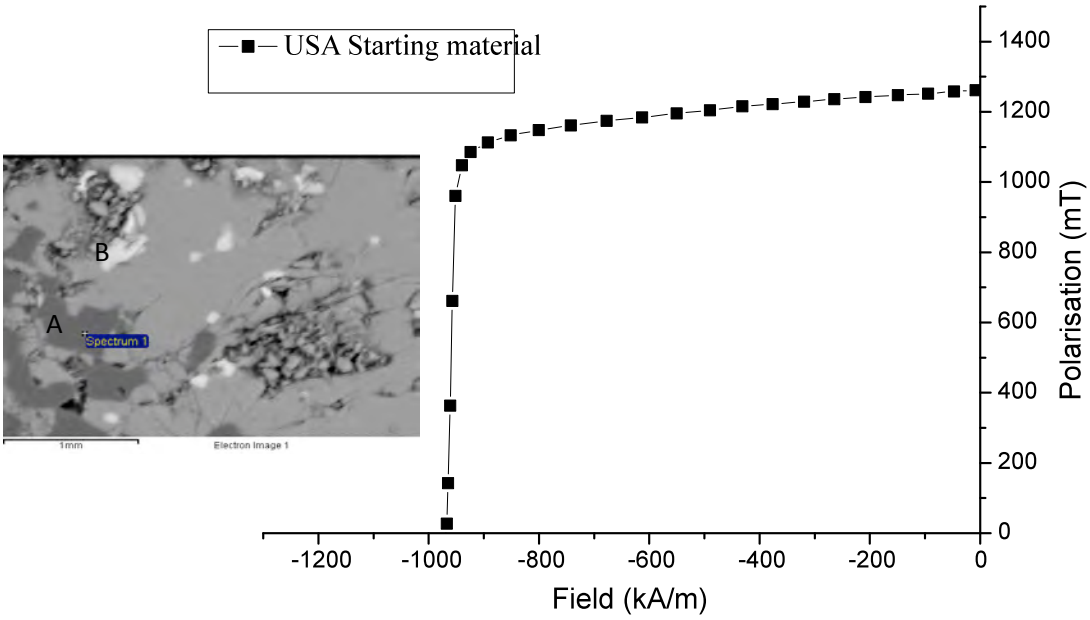

Figure 9-3 Shows H- Loop for USA starting magnet. Inset SEM image of microstructure of USA starting magnet. Density = 7.66 g/cm^3

The presence of free iron within the USA magnet did not appear to degrade the shape of the demagnetisation curve. There is also evidence of incomplete sintering which is surprising in view of the excellent density and hence cannot be typical of the whole structure.

IPM*ni*
magnet:

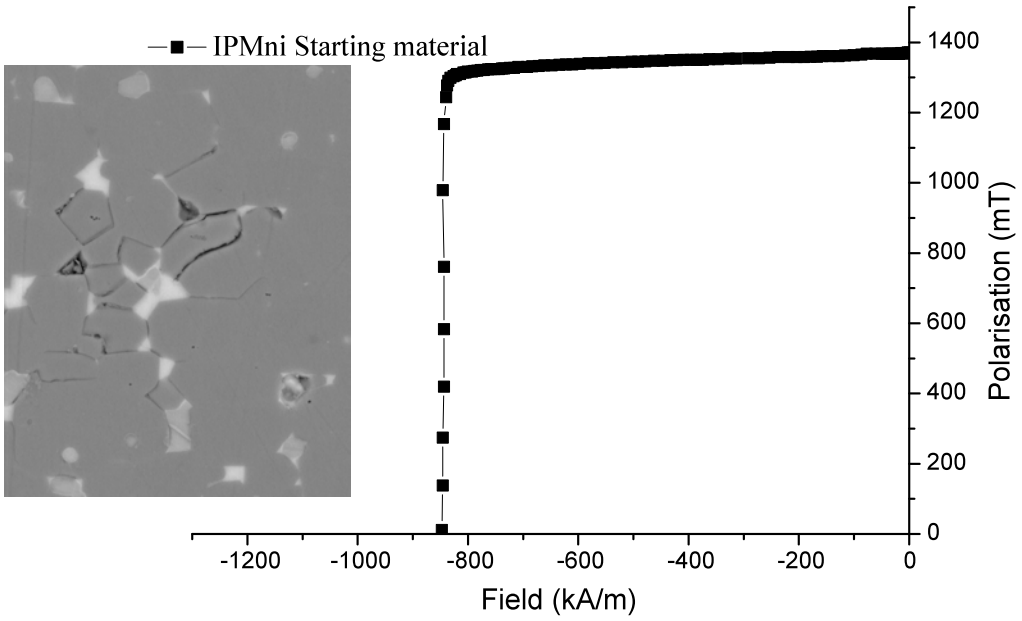

Figure 9-4 IPMni Alloy shows the H-Loop and the excellent squareness factor of this magnet should be noted. Density = 7.64 g/cm^3

This magnet exhibits the best characteristic with regard to Br, (BH)max and squareness factor.

Summary:

As illustrated in the demagnetisation loops, each magnet behaves somewhat differently. China magnets have produced a better coercivity than the others. This may be attributed to the high level of Dy and the smaller grain sizes. The USA magnet has a higher value of Br possibly due to the presence of a greater proportion of the $Nd_2Fe_{14}B$ phase, good alignment and density.

A summary of the magnetic properties of the starting magnets is shown in figure 9-5.

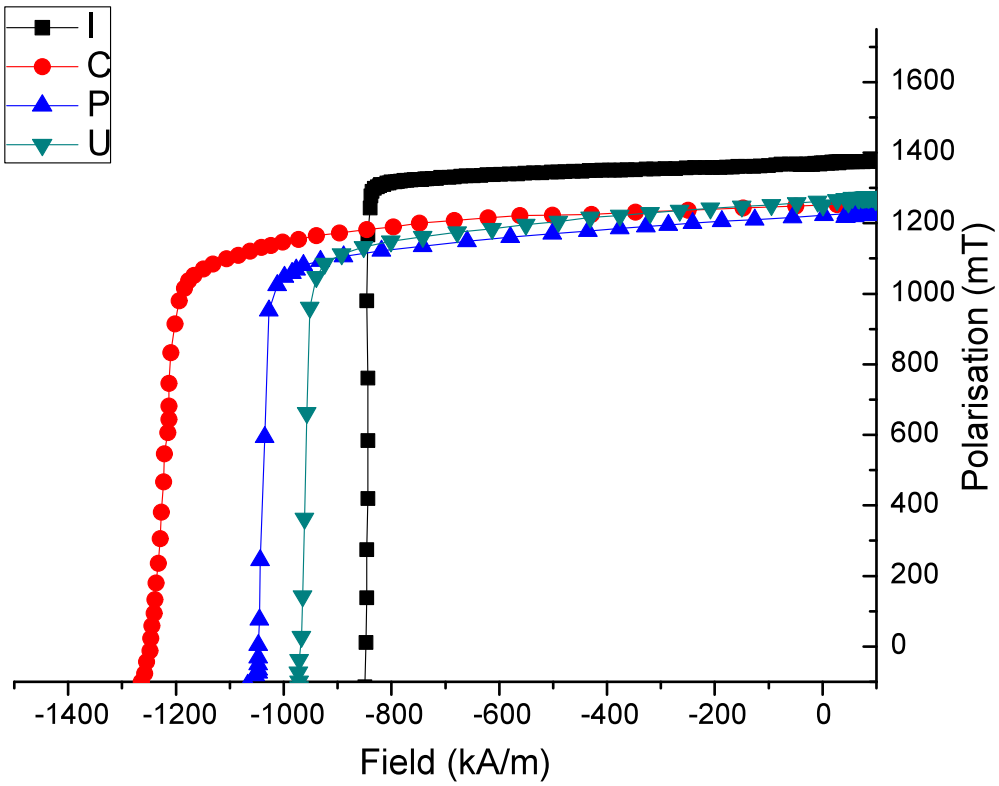

Figure 9-5 Summary of all magnets' magnetic properties.

9.3 Recycling of commercial (and Neomax) magnets:

The magnets described previously have now been subject to recycling process by exposing them to hydrogen and then subjecting the HD-powder to a milling procedure (as described in the experimental section) for varying times.

A standard sintering procedure was applied to all the magnets and this consisted of sintering at 1090 ^{o}C for 1 hr and then quickly cooling to room temperature.

9.4 The effects of milling after the HD process:

The following images are to show the effect of milling time on the final powders size

1) China

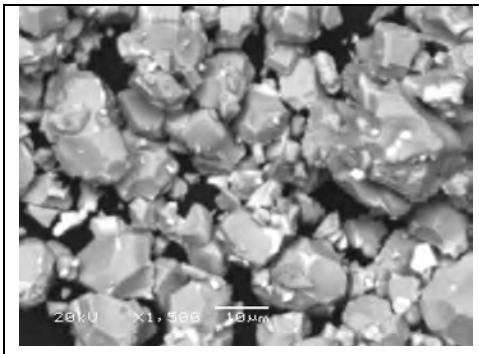	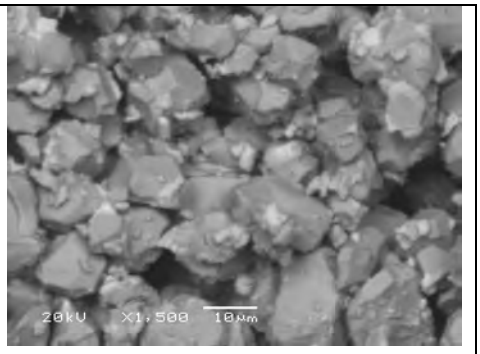
Half hour milling X 1500	1 hour milling

Figure 9-6 SEM images of China magnetic powder with milling times

2) IPMni

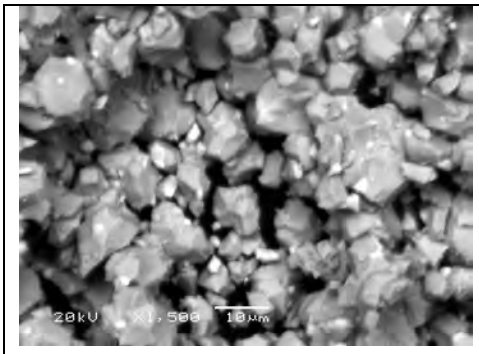	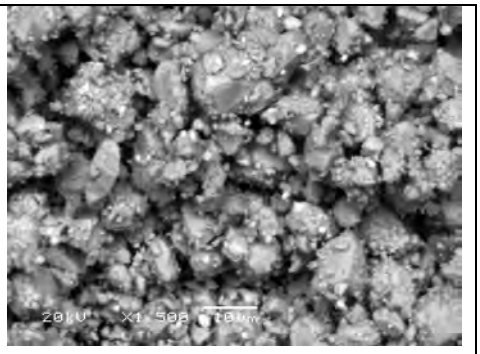
Half hour milling	1 hour milling

Figure 9-7 SEM images of IPMni magnetic powder with different milling times

3) Philips

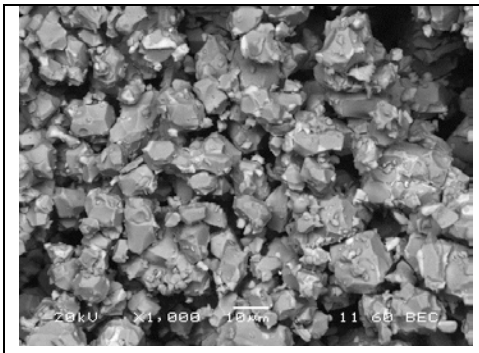	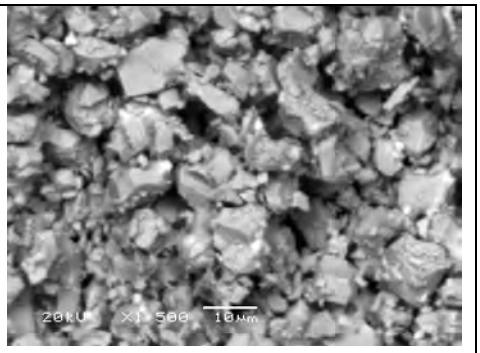
Half hour milling	1 hour milling

Figure 9-8 SEM images of Philips magnetic powder with milling times

4) USA

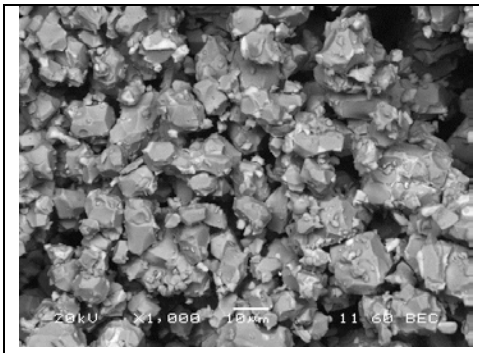	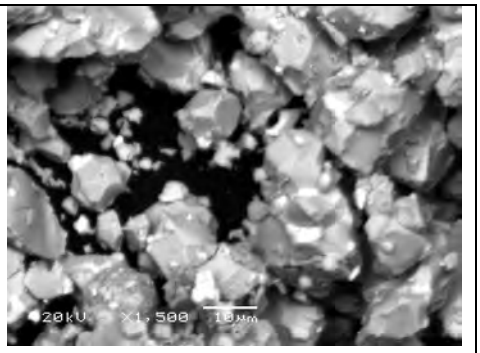
Half hour milling	1 hour milling

Figure 9-9 SEM images of USA magnetic powder with milling times

The powders morphology, as a function of milling time is shown in the above figures. From figures 9-6→9-9, after 30 minutes of milling, the larger (>100 μm) particles, that were most likely extensively cracked after the HD process, have now been significantly reduced in size. There is little difference after 1 hour milling (figures 9-6 →9-9) although the particles may have been further broken up.

9.5 The effect of milling time on the subsequently sintered magnetic properties:

Batches from each of the various starting materials were milled for different durations and sintered under previously described, identical conditions. The magnetic properties were measured from each compact and are now summarised below.

9.5.1 Neomax:

The results from the Neomax material are summarised in table 9-3 and figure 9-11and 9-12.

Table 9-3: Neomax magnetic properties

Magnet Milling time	Remanence Br (mT) ±1%	Intrinsic Coercivity (kA/m $_jH_c$) ±1%	Inductive Coercivity (kA/m $_bH_c$) ±1%	BHmax kJ/m^3 ±2%
6hrs Neomax	1180	372	354	196
12hrs Neomax	1318	427	405	252
24hrs Neomax	1215	402	386	192

It can be seen; the values of $_jH_c$ and $_bH_C$ fluctuate around the 400 kA/m. This may suggest that the powder of the Neomax alloy was not stable or clean enough (oxidised) during the recycling process.

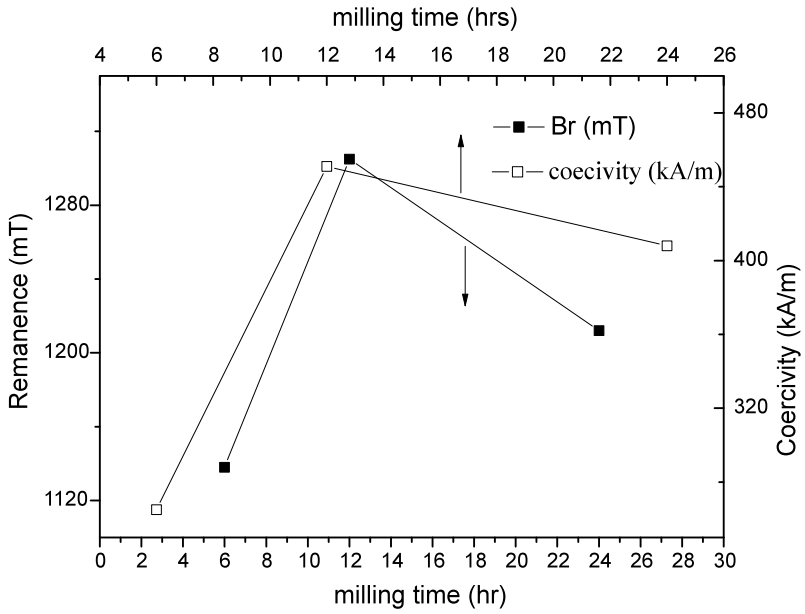

Figure 9-11 Neomax magnets: comparing milling time against B_r and $_jH_c$ properties.

The following graph will show the comparison between the BHmax against the milling time:

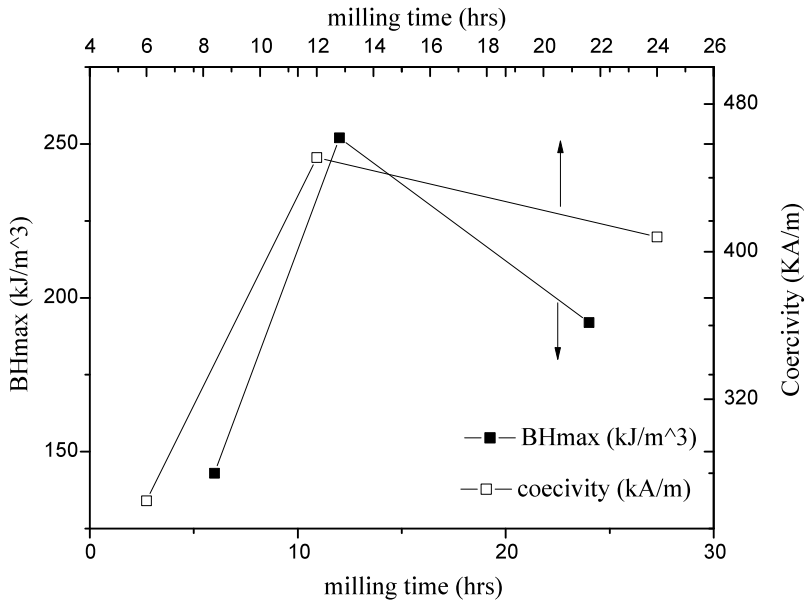

Figure 9-12 Neomax magnets: comparing milling time against BHmax and jHc.

The Neomax alloy, milled for 24 h showed an improvement in coercivity compared with that obtained after 6 h milling, however, the highest coercivity was obtained with 12 h milling. This suggests that longer milling times are detrimental to the overall magnetic properties, probably due to oxygen pick up.

9.5.2 Philips:

The recovered magnetic properties measured on sintered magnets obtained by recycling of the Philips magnet are shown in table 9-4.

Table 9-4: Philips magnetic properties

Magnet Milling time	BHmax (kJ/m^3)	Br mT	Intrinsic Coercivity (kA/m) $_jH_c$	Inductive Coercivity (kA/m) $_bH_c$
6 h sintered Philips	229	1257	370	356
12 h sintered Philips	20	792	170	129

The results in table 9-4 indicate that the 6 hrs mill achieved much better magnetic properties than the 12 h milling. A further 24 h milling was impossible on this alloy due to time and equipment constraints.

The Philips magnets exhibit a similar trend to that of Neomax. The more milling, probably the more oxygen contamination and hence the magnetic properties decrease as the milling time increases.

The other starting materials were also milled for specific (1/2 hrs) duration. A comparison between the different starting materials is shown in table 9-5 and figures 9-13 and 9-14.

The best overall magnetic properties from the recycled magnets with a ½ h milling time were found from the China magnets. This may be attributed to the higher content of Dy (see table 9-1) and finer initial grain size (<10 μm) within the starting material.

Table 9-5: Magnetic properties after ½ h milling time of the various magnets:

Magnet All milled for ½ hour	Br (mT) ±1%	Intrinsic Coercivity (kA/m $_jH_c$) ±1%	Inductive Coercivity (kA/m $_bH_c$) ±1%	BHmax (kJ/m^3) ±2%	Squareness factor	Density (g/cm^3) ±0.05 g
USA	1221	506	476	236	0.73	7.51
China	1144	930	828	246	0.86	7.57
Neomax	1182	378	368	197	0.6	7.54
Philips	832	221	209	68	0.42	7.42

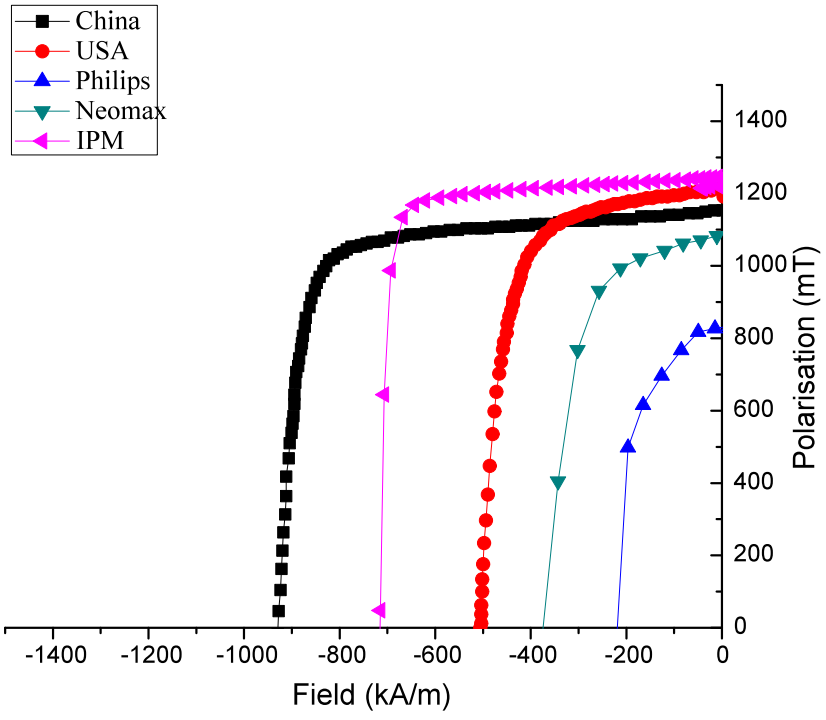

Figure 9-13 Summary of the demag curves for half hour milled magnets.

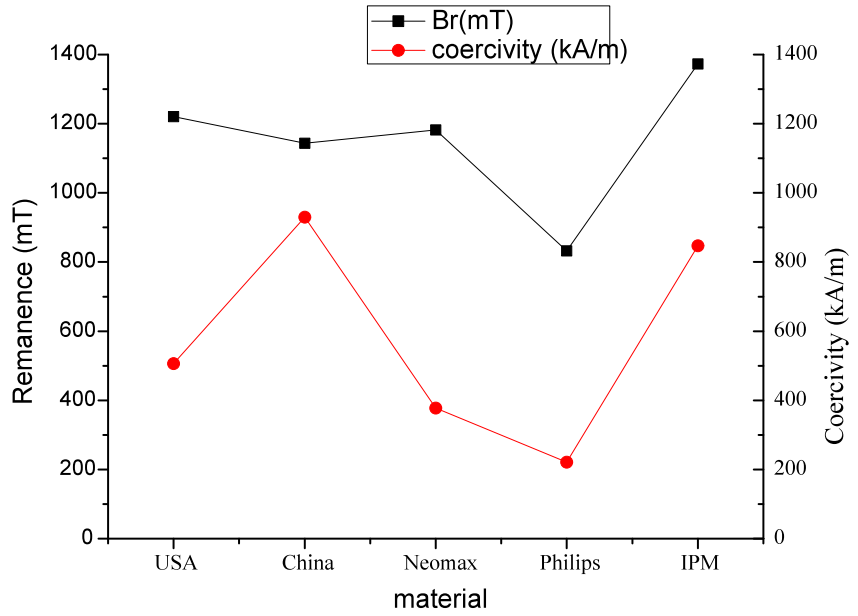

Figure 9-14 USA, China, Neomax and Philips and IPM ½ h milled magnets: their $_jH_c$ and B_r values.

The above graph shows a comparison between the remanence and coercivity values. The following graph illustrates the BHmax values of the four magnets.

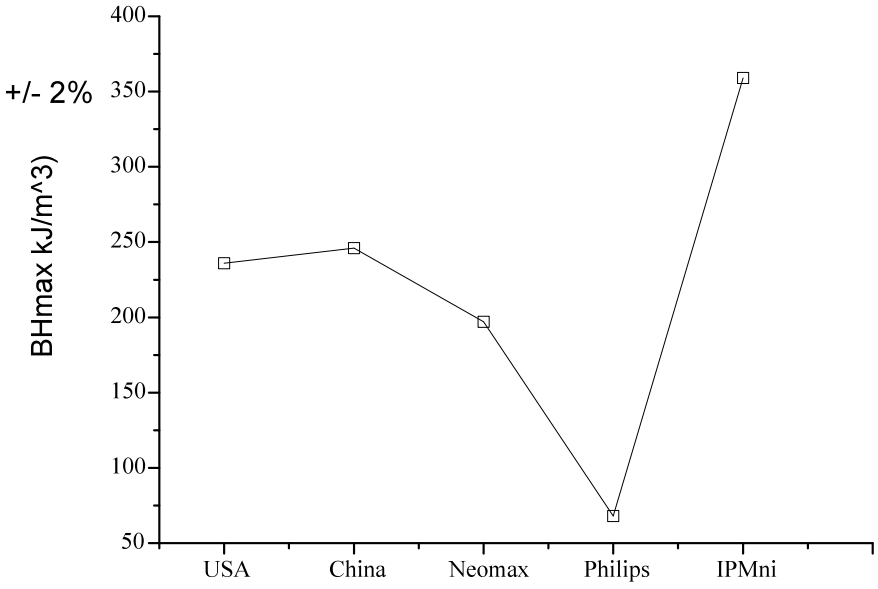

Figure 9-15 Shows BHmax values of the four different magnets.

The second quadrant demagnetisation curves, for the magnets before and after recycling of the different starting materials in figures 9-16 to 9-18:

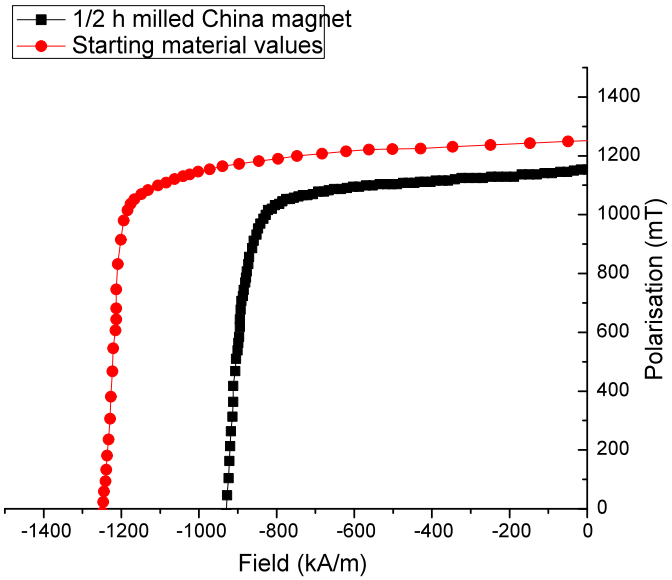

Figure 9-16 ½ h milled China magnet, (density = 7.57 g/cm^3).

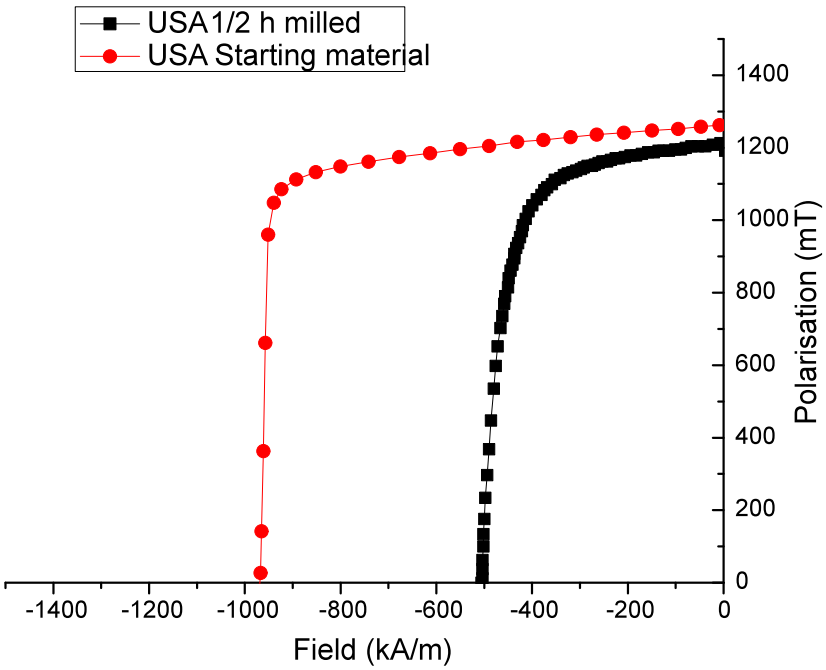

Figure 9-17 ½ h milled USA magnet with (density = 7.51 g/cm^3)

This magnet has lower magnetic properties but still maintains a reasonable BHmax, Br and Hcj and its density was 7.51 g/cm^3. However, the magnetic properties were less than that of the ½ h China magnet's magnetic properties.

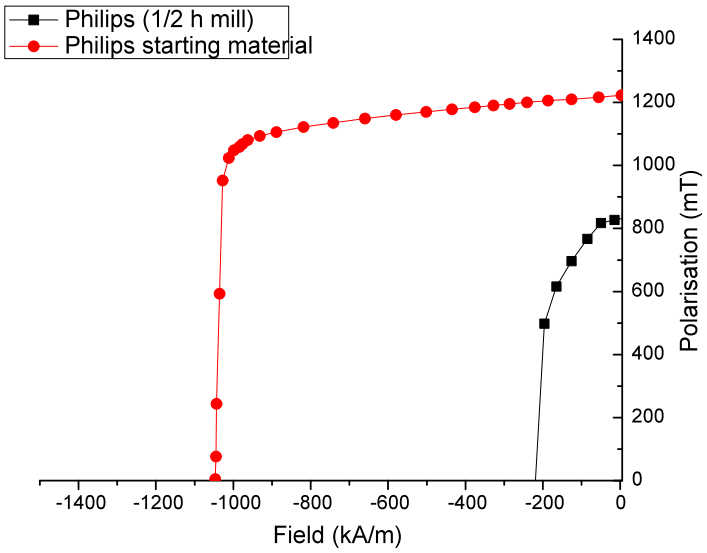

Figure 9-18 Shows demag-curve for ½ h mill Philips magnet compared with its starting material. The SEM analysis indicates the NdFeB phase and very little of the Nd rich phase. Density = 7.42 g/cm^3.

In figure 9-19, the results of recycling the Neomax alloy are shown (1/2 h mill).

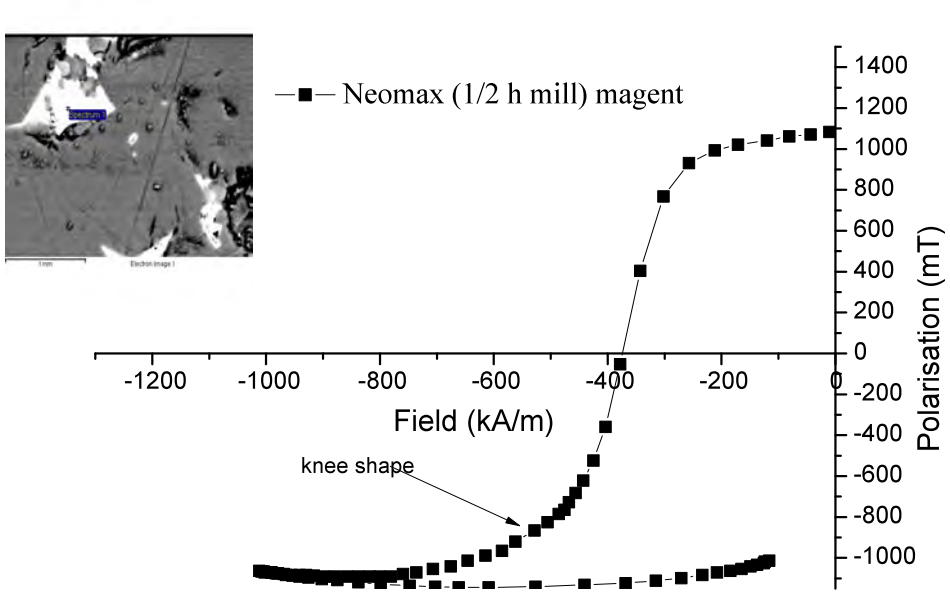

Figure 9-19 Shows demag loop and SEM image of ½ h milled Neomax sample along with the sintered microstructure, shown in backscattered SEM mode. (Density = 7.54 g/cm^3)

The figure above indicates a reasonable 2nd quadrant loop shape with much more significant properties than for the other milling times of the same magnet. This loop shows similarity with previous ½ Neomax loop where a small knee is indicated by an arrow in the 3rd quadrant.

The second quadrant demagnetisation curves for sintering milled powder from different times for the Neomax alloy is shown in figure 9-21.

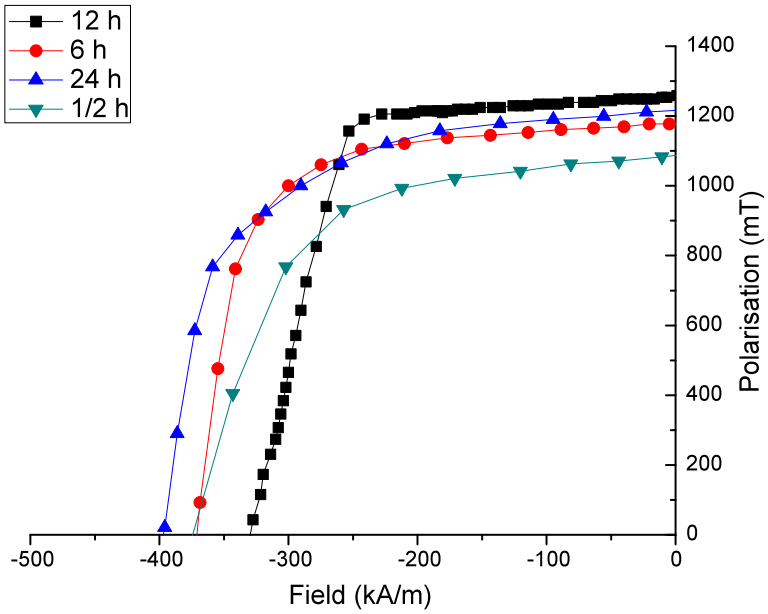

Figure 9-20 The results of different milling times for Neomax Magnets

It is shown clearly from the above loops that the 12 h milling exhibits lower coercivity but higher Br than those of the other milling times; this could be due to the effect of over sintering.

However, from a 6 h milling time, the Neomax magnet had performed much better and yielded better magnetic properties. This may be attributed to increased oxygen uptake when milling for longer periods.

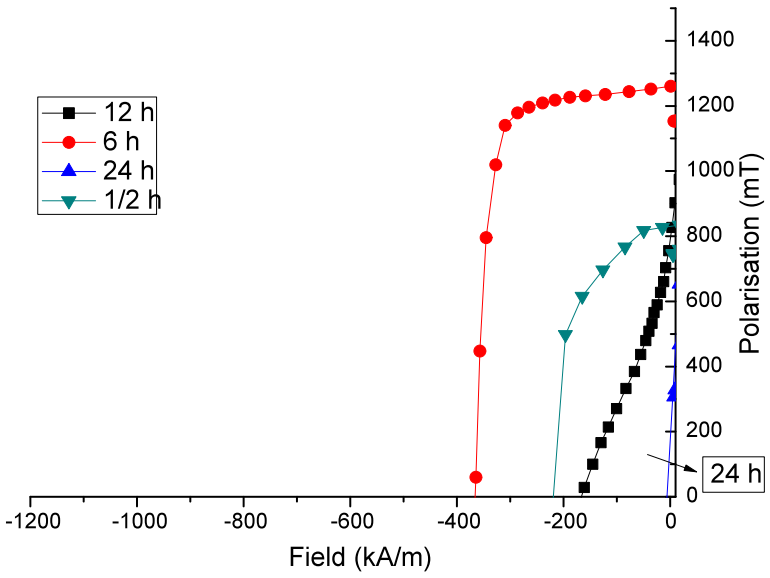

Figure 9-21 Shows the three Philips magnets milled at different times

Table 9-6: 6 and 12 hour milling times for Philips magnets and their corresponding magnetic properties:

Magnet milling time	Density ($g/cm^{3)}$ ***±0.05g***	Br (mT)	Intrinsic Coercivity (kA/m) $_jH_c$	Inductive Coercivity (kA/m) $_bH_c$	BH*max* *(*kJ/m^3)
6 h Philips	7.47	1257	370	356	229
12 h Philips	7.11	792	170	129	20

Note: The 24 h milled Philips magnet exhibited virtually no useful magnetic properties (see figure 9-21).

These measurements show that the 6 h milling time possessed better Br than that of the 12 h Philips. However, it does not have better magnetic properties than that obtained after ½ h milling treatment of the same magnet. This magnet in some respect had some improvement over the same material. It sintered better than the other magnets of the same material. There is still some evidence of over sintering.

At this stage, the Neomax alloy has been replaced by IPMni (from Japan) due to the fact that the alloy was not performing as published data as well as being oxidised.

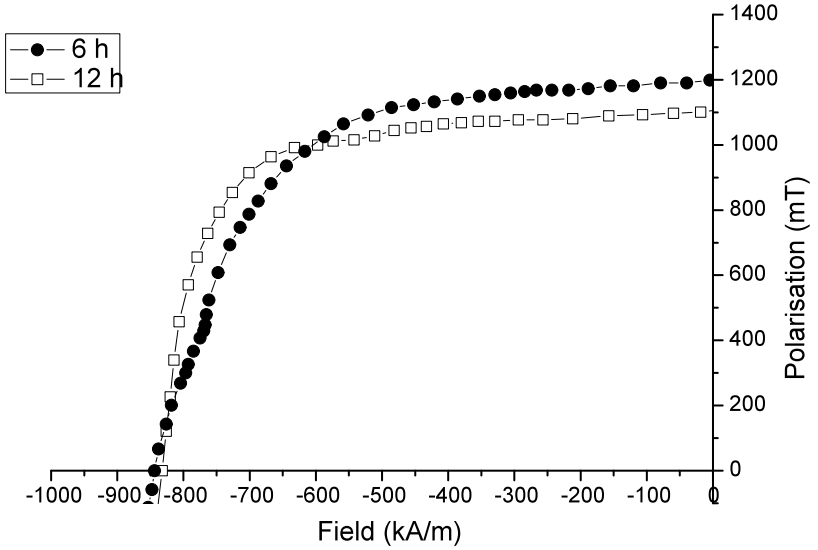

.

Figure 9-22 The effect of milling time on the recycled properties from the China magnets.

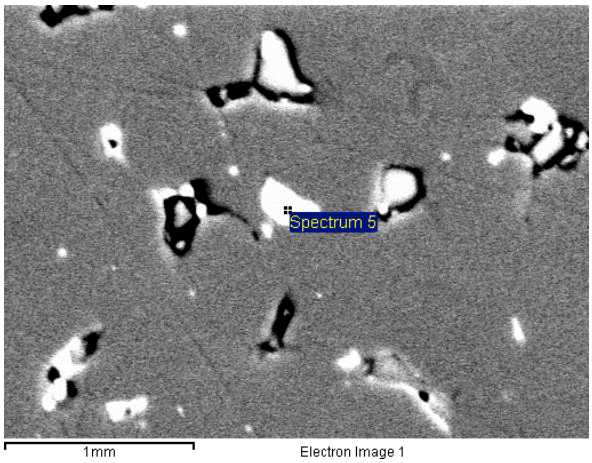

6 h milled China magnet. Spectrum 6 analysis consist of Fe = 12.05 (at%) and Nd = 87.95 (at%) –Nd-rich phase (ϕ-phase). Density = 7.65 g/cm^3.

Figure 9-23 SEM image of 6 h milled China magnet.

The apparent lack of grain growth could be due to increased oxygen content which would inhibit grain growth.

9.6 Summary of the Density Measurements of recycled magnets

The following table shows the measured density values of the sintered recycled magnets compared with their original counterpart.

Table 9-7: density of magnets after various milling times:

Magnet	Milling time	ρ ±0.05 g	% porosity(compared with staring magnet)	ρ Philips starting magnet
Chinese	30 minutes	7.3	4.45	7.66
Philips	12 hours	7.42	3.13	
Philips	30 minutes (oxidised)	5.9	22.98	
Philips	6 hours	7.52	1.83	
Philips	6 hours	7.42	3.13	
Philips	12 hours (oxidised)	7.11	7.2	
Philips	24 hours	7.6	0.8	
Neomax	30 minutes	7.54	1.42	ρ Neomax alloy
Neomax	6 hours	7.52	1.7	7.65
Neomax	12 hours	7.54	1.44	
Neomax	24 hours	7.54	1.44	
Chinese	30 minutes	7.57	0.92	ρ China starting magnet
Chinese	6 hours	7.65	0	7.64
Chinese	12 hours	7.4	3.14	
Chinese	24 hours	6.8	10.99	
USA	30 minutes	7.4	3.4	ρ USA starting magnet
USA	30 minutes	7.51	1.96	7.66
USA	6 hours	7.45	2.74	
USA	12 hours	7.4	3.39	
USA	24 hours	6.2	19.1	

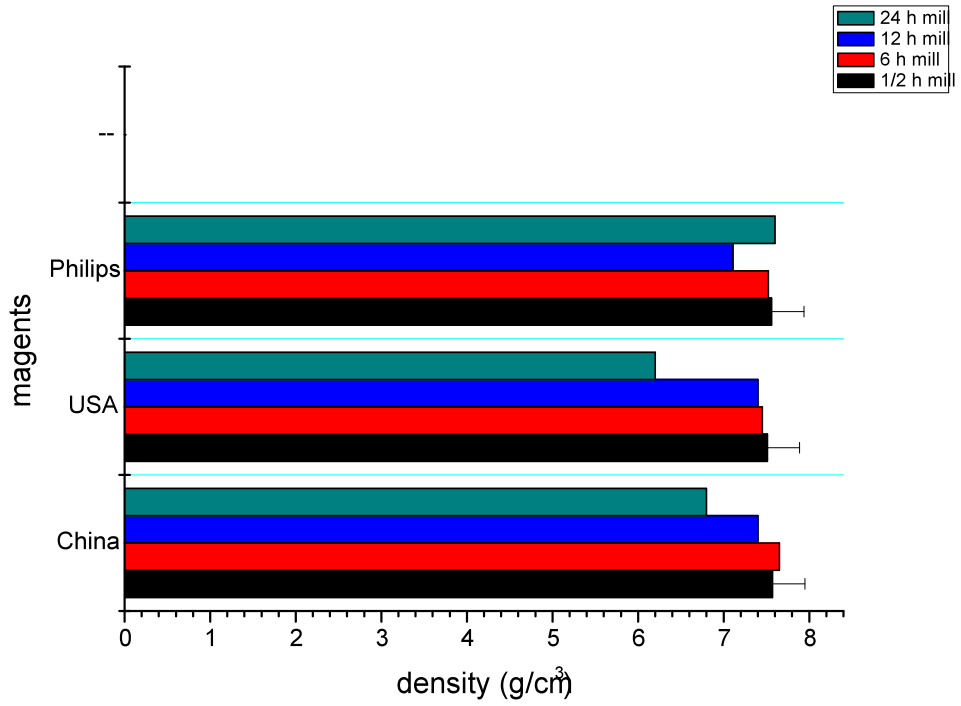

Figure 9-24 Density of all magnets with various milling times.

The figure above shows that the optimum milling time for a consistent density is ½ hour milling. As the milling times increases the sintered density is seen to fluctuate resulting in porous microstructure and therefore poorer magnetic properties. This may be attributed to the increased oxygen uptake from prolonged milling and the generation of particles with higher surface areas being more susceptible to corrosion and partial oxidation.

Summary:

The summary of the main findings in this section are:

1) Milling times can influence the density and magnetic properties attributed to oxygen uptake.

2) All the magnets behave differently when subjected to different milling times.

3) Neomax alloy milled and sintered for long periods indicated over processing.

4) Philips exhibited similar trend as of that Neomax, the more milling, the more oxygen contamination.

5) The ½ h mill time China magnet exhibited acceptable properties. This was attributed to the high Dy content.

6) The USA magnet had better Br than the other magnets (1/2 h mill time) and become denser.

7) Consistent and acceptable magnetic and density results were obtained after ½ h milling treatment.

9.7 The effect of Dy addition to the recycled magnets

The next stage of the investigation was to study the effects of blending the HD powder with additions such as Dy in an attempt to improve the final properties of the sintered magnets. The previous work in this section has shown that it is not possible to match the original properties in the recycled magnets and this has been attributed to the oxidation of the rare earth component (mainly Nd) during the powder processing. With this in mind, the following experiments have been carried out where blending agents (such as Dy and Nd) have been added to the milled powder and the blended mixture then sintered in an attempt to produce fully dense sintered magnets. This should provide a means of restoring or even improving the initiated properties. (Tang et. al., (2012)

A comparison between all the recycled magnets and how they behave when an addition of set Dy atomic percentage (at%) is also included.

9.7.1 ½ at% Dy addition:

The Dy powder added was in the form of fine DyH_2 powder (processed using HD process). The magnetic properties obtained from blending DyH_2 with the Philips and China magnets is shown in figure 9-25 to 9-26. the magnet HD powder was subject to ½ h mill treatment.

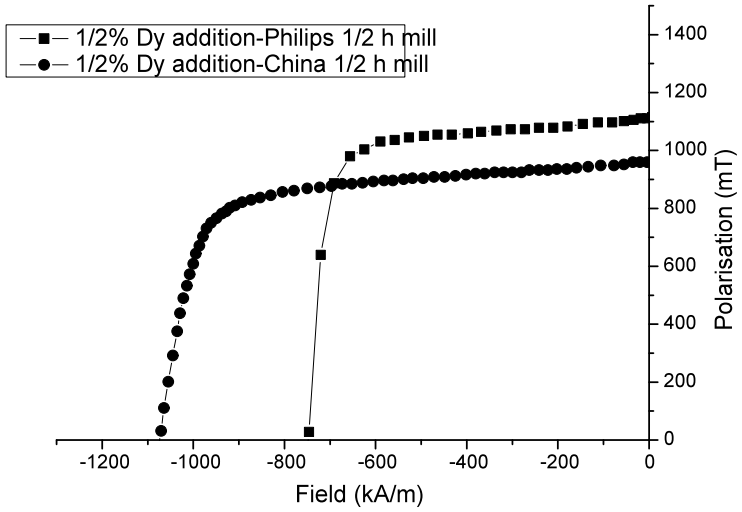

Figure 9-25 Shows demag-Loop obtained from an addition of DyH_2 on material milled for the same duration (1/2 h).

These magnets (shown in figure 9-25) exhibited different magnetic properties. The Philips magnet has a much higher remanence than that of the China magnet. As expected, the Dy addition reduces the remanence and increases the coercivity (Zakotnik et al., 2008; and Fidler and Knoch, 1989).

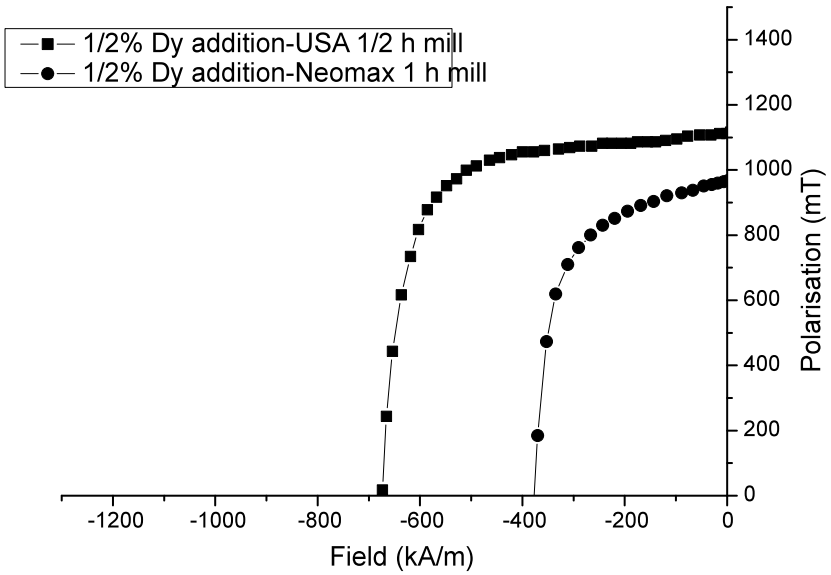

Figure 9-26 Demag-Loop of 2 different magnets with the same at% Dy addition

Table 9-8: Summary of the change in magnetic properties by the addition of 0.5at% DyHx

magnet	B_r (mT) [initial value of ½ h mill] ± 1%	jHc (kA/m) [½ h mill value] ± 1%	BHmax (kJ/m^3) [½ h mill value] ± 2%
Philips	1115 [832]	758 [221]	223 [68]
China	960 [1144]	1075 [930]	169 [246]
Neomax	965 [1182]	374[380]	132 [197]
USA	1160 [1221]	765 [506]	244 [236]

The values in the square brackets are the values without Dy addition (see Table 9-5)

From table 9-8 it is evident that the addition of Dy has benefited the Philips and USA magnets by enhancing their magnetic properties, especially BHmax. However, the China magnet did not follow the same pattern as the remanence and $(BH)_{max}$ were decreased and only jHc increased.

9.7.2 1at% Dy addition:

The proportion of the DyH_2 addition was doubled to 1 a% and the recycled magnetic properties are shown in figure 9-27 and summarised in table 9-9.

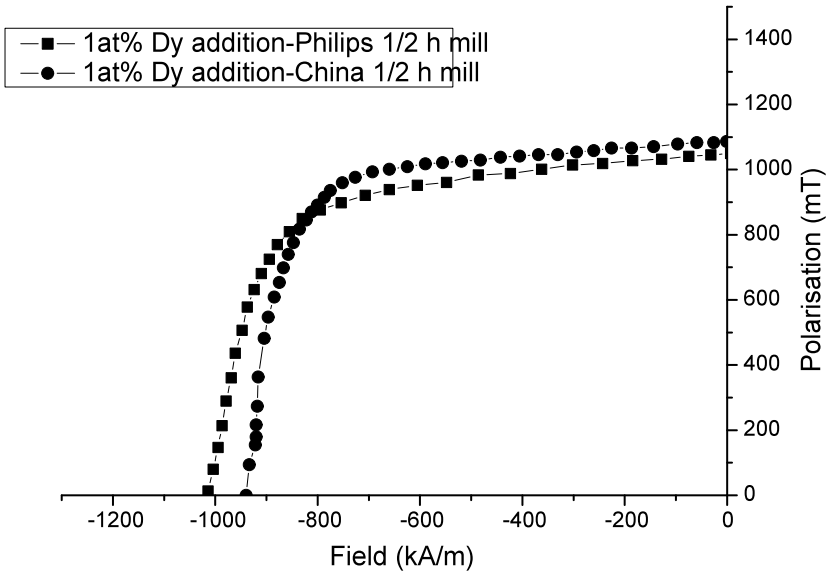

Figure 9-27 Demag-Loop of 2 different magnets with the same 1at% Dy addition

The table below summarises the magnetic properties of the Philips magnet compared with the China magnet even though they had similar at% Dy addition.

Table 9-9: magnetic properties of 1at% Dy addition to Philips and China magnets

Magnet	B_r (mT)	$_jH_c$ (kA/m)	BH_{max} (kJ/m^3)
Philips	1048 [832]	1018 [221]	198 [68]
China	1087 [1144]	940 [930]	216 [246]

The values in the square brackets are the values without Dy additions (See table 9-5)

9.7.3 2 at% Dy addition:

To further study the effect of a DyH_2 addition to the Philips magnets, a further increase to 2at% was investigated and it was found that the resulting magnet was difficult to demagnetise within the existing permeameter as its coercivity was too large, as shown in figure 9-28.

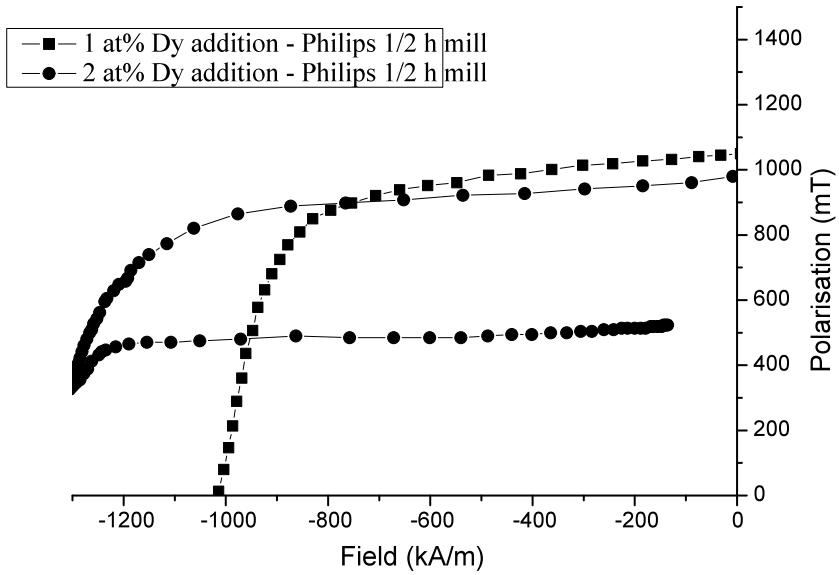

Figure 9-28 Demag-Loop of Philips magnets with the different at% Dy addition.

Summary of Dy addition to recycled magnets:

The results are summarised in table 9-10 for the DyH_2 addition.

Table 9-1-: Magnetic properties of recycled magnets with DyH_2 addition

Magnet	Br (mT) ±1%	Intrinsic Coercivity (kA/m) $_jH_c$ ±1%	BH*max* (kJ/m^3) ±2%	Density (ρ) g/cm^3 ±0.05 g
½ *at*% Dy added to Philips	1154	834	246	7.2
1 *at*% Dy added to Philips	1048	1018	198	6.97
2 *at*% Dy added to Philips	980	Not demagnetised	189	7.05
½ *at*% Dy added to China	1040	1073	195	7.13
1 *at*% Dy added to China	979	1211* *difficult to demagnetise	173	7.1
2 *at*% Dy added to China	872	1024	140	7.01
½ *at*% Dy added to USA	1160	765	244	7.42
1*at*% Dy added to USA	969	501	118	6.92
2 *at*% Dy added to USA	960	difficult to demagnetise	168	7.05

The use of DyH_2 powder as a blending agent has proved to be an effective means of improving the magnetic properties of the Philips recycled magnets in particular. There is No EDX analysis of the resultant magnets but it can be assumed that the hydride has disassociated to form Dy which has then substituted for Nd in the matrix phase. The resultant increase in the anisotropy factor (k) has resulted in increase coercivity.

This interpretation can be checked by a careful EDX/SEM study of the magnets which will also establish whether there is an inhomogeneous distribution of the Dy

9.8 Additions and heat treatment of recycling lean rare earth magnets: (IPMni Magnets)

9.8.1 Introduction

These magnets were supplied by Ishu-Chemicals Ltd. in Japan. These magnets in their original un-recycled state had superior magnetic properties over the other 3 commercial magnets. The following table is a reminder of the initial magnetic properties of the IPMni magnet:

Magnet	BHmax (kJ/m^3) ±2%	Inductive Coercivity (kA/m) $_bH_c$ ±1%	Br (mT) ±1%	Intrinsic Coercivity (kA/m) $_jH_c$ ±1%	Squareness factor	Density g/cm^3 ±0.05 g/cm^3
IPM*ni*	359	845	1370	849	0.99	7.65

ICP of the IPMni magnet:

	Nd+Pr	Dy	Fe	Co	B	Al	O (ppm)
IPM*ni*	12.8	0.79	77.09	2.57	6.19	0.56	2565

It was decided therefore to pay special attention to the recycling of these magnets.

To study the effects of the addition of additional elements, consisting of Nb, Co, Dy and Nd, the resulting magnetic properties were investigated along with the microstructure. For microstructural studies the samples were etched using Viella's reagent. Elemental data was obtained using a SEM (JOEL 7000) to identify the additional elements and their distribution; i.e. matrix or grain boundary and the overlap of some phases.

The following results, conducted through SEM studies, show where the spectrum analysis took place for elemental mapping studies in an attempt to reveal the location of the additives within the microstructure. Chemical components studied include elements such as Dy, Co and Nd.

The following section will deal with IPM magnets that are lean rare earth with addition of various elements.

9.9 IPMni Samples analysis and characterisation:

9.9.1 Sample A1: Heat treatment and preparation:

Powder from different starting materials was milled for a half hour and sintered at a temperature of 1120 ^{o}C for 1 hour, then annealed for 3 hours at 900 ^{o}C and further annealed at 650 ^{o}C for 1 hour. The blending addition of NdH_2 was 1 at% and $DyH_2$was 0.2 at%. The resulting microstructure from sample A1 is shown in figure 9-29 with the chemical analysis shown in table 9-11.

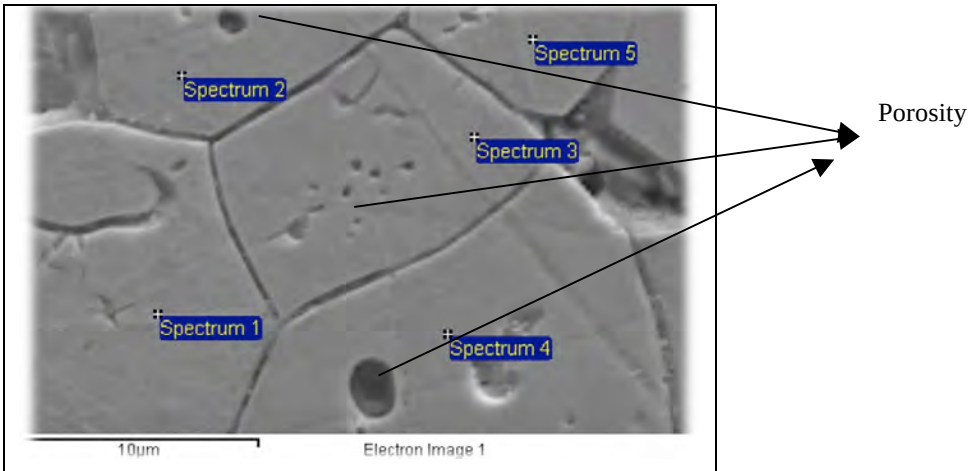

Figure 9-29 Shows SEM image of Sample A1 (matrix). Density = 7.51 g/cm^3.

Table 9-11: Spectrum analysis

Spectrum (at%) ±5%	Fe	Co	Nd	Dy
Spectrum 1	82..58	1.18	14.79	1.45
Spectrum 2	81.34	1.41	14.18	3.08
Spectrum 3	81.79	1.96	15.21	1.05
Spectrum 4	81.06	2.25	14.20	2.50
Spectrum 5	80.11	1.78	14.08	4.03

Although this magnet did shows some porosity, its density at 98% is close to the theoretical original density.

From table 9-11 (and figure 9-32) the highest Fe content was within spectrum 1, whilst the lowest was spectrum 5. The Dy content was higher in spectrums 2, 4 and 5. This shows that there is an inverse relationship between the Fe and Dy contents. The Nd addition is compared with that of the original ICP.

The following figure (figure 9-30) shows an analysis at the grain boundary and how the contents vary when the Nd and Dy are added on:

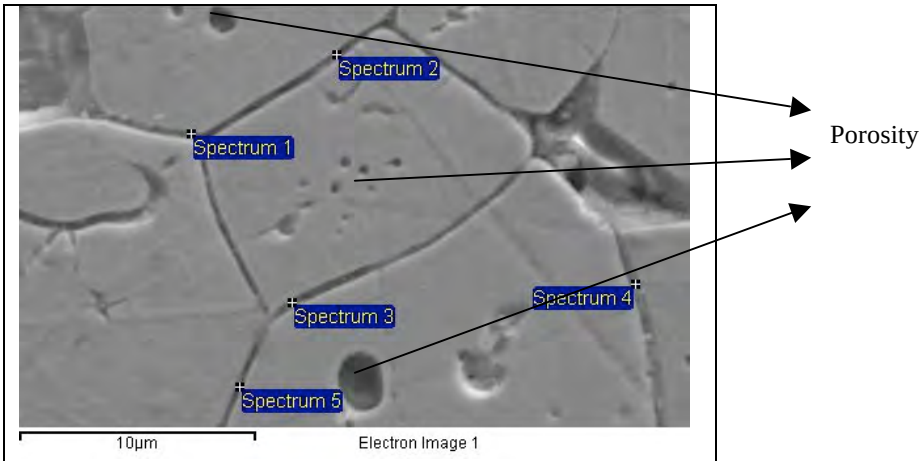

Figure 9-30 Shows SEM image of Sample A1 (grain boundary), Density = 7.51 g/cm^3.

The above figure shows where the spot analysis was taken. This will give a view as to the concentration of the elements added on, such as Nd and Dy. The table below

shows the variations in the elements contents when they are measured at various grain boundaries:

Table 9-12: spectrum analysis

Spectrum (at%) ±5%	Fe	Co	Nd	Dy
Spectrum 1	77.83	1.97	17.03	3.18
Spectrum 2	68.71	0.73	27.26	3.30
Spectrum 3	72.23	0.90	24.12	2.74
Spectrum 4	79.98	1.77	16.66	1.60
Spectrum 5	74.02	2.14	20.99	2.85

The Fe content is significantly less than that of the matrix (see table 9-11). However the Nd is much higher than that of the matrix. The following graph (figure 9-32) shows a comparison between all spectra and their elements contents at each spectrum. This shows a high level of Fe and this is attributed to the overlapping between the narrow grain boundaries and the matrix.

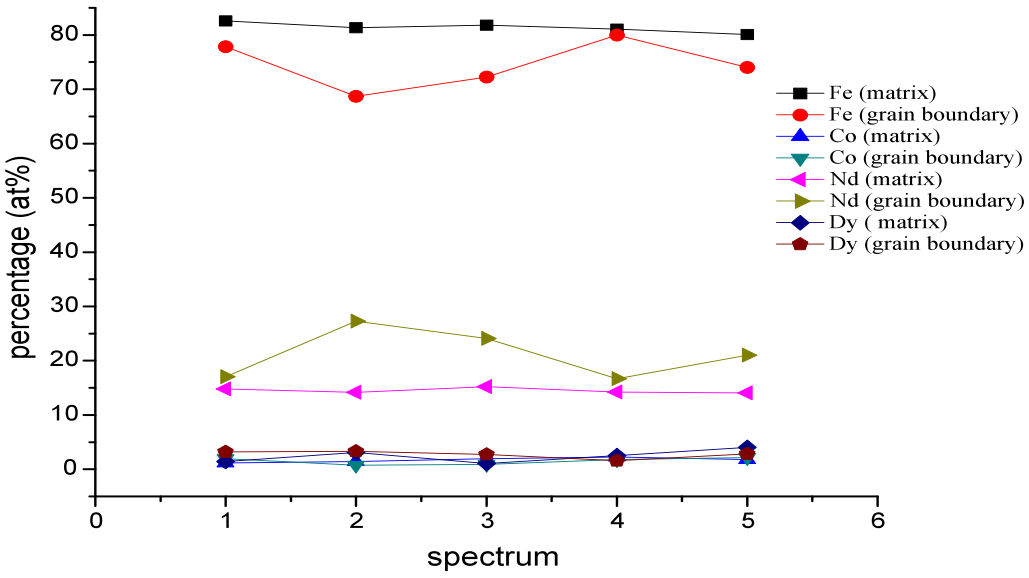

Figure 9-32 Spectrum analysis of the element concentrations (matrix and grain boundary).

9.9.2 Sample A2 (IPMni magnets) preparations

This sample was subjected to high energy milling. This meant that the powder was ground at a much higher speed than in the Pascal roller (using different milling machine for 7 minutes). The addition was 1 at% Nd, 1 at% Co and 0.5 at% Dy.

This sample was subjected to a sintering temperature of 1120 ^{o}C for 1.3 hours followed by an annealing temperature at 800 ^{o}C for 3 hrs and further annealing process at a temperature of 650 ^{o}C for 1 hour. This magnet exhibited little porosity and hence the magnet is denser than the previous magnet. The microstructure is shown in figure 9-33 and chemical analysis shown in table 9-13.

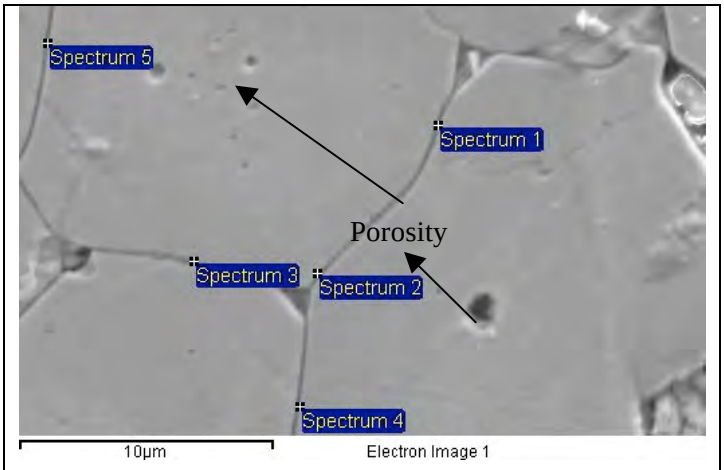

Figure 10-33 Shows SEM of Sample A2- spectrum analysis of the grain boundaries. Density = 7.56 g/cm^3.

The following table shows the elemental concentrations within the grain boundary region.

Table 9-13: spectrum analysis (at%)

Spectrum ±5%	Fe	Co	Nd	Dy
Spectrum 1	75.89	3.33	19.58	1.20
Spectrum 2	82.75	2.66	12.68	1.91
Spectrum 3	80.35	1.08	16.32	2.24
Spectrum 4	82.17	1.97	12.35	3.51
Spectrum 5	83.11	2.23	13.52	1.14

Chemical analysis was also performed with the matrix, shown in figure 9-34 and table 9-14.

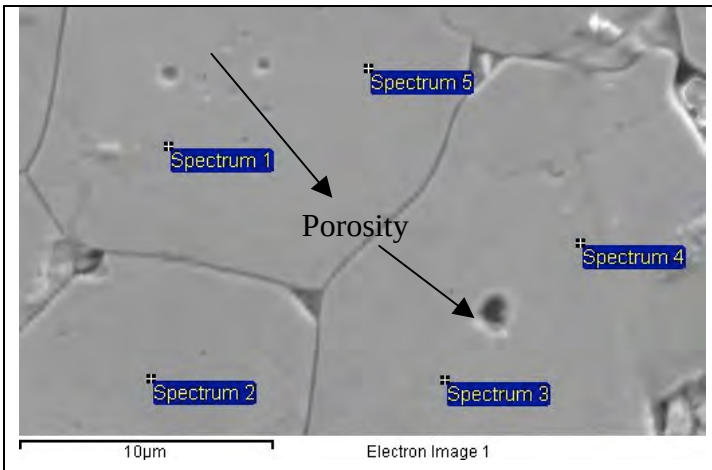

Figure 9-34 Shows SEM image of the matrix of sample A2. Density = 7.56 g/cm^3.

Table 9-14: at% elements contents (matrix)

Spectrum ±5%	Fe	Co	Nd	Dy
Spectrum 1	83.28	2.34	13.02	1.36
Spectrum 2	83.37	1.50	12.97	2.16
Spectrum 3	82.97	2.09	12.18	2.75
Spectrum 4	82.51	2.41	12.92	2.16
Spectrum 5	82.61	2.91	11.67	2.81

The results are summarised in figure 9-35.

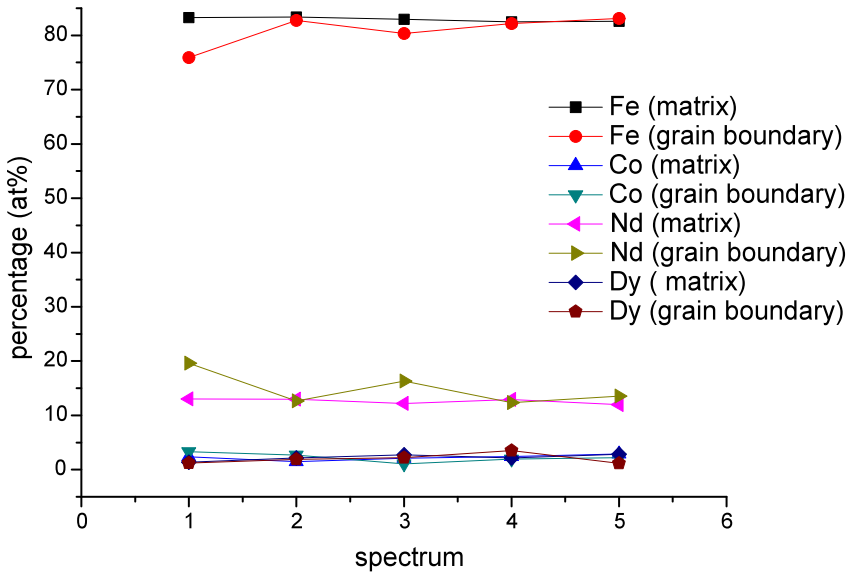

(a)

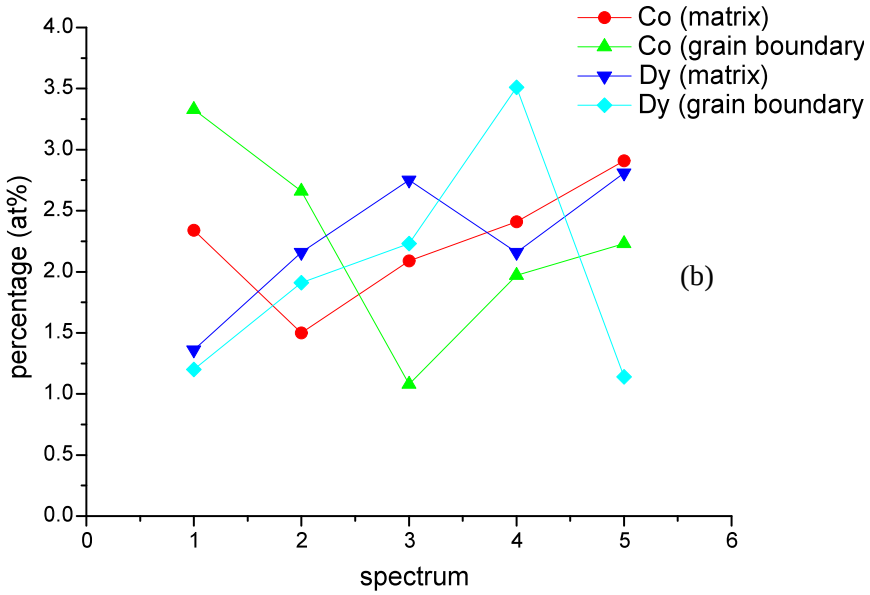

(b)

Figure 9-35 Graphs show the distribution of (a) percentage of at% of Dy, Nd, Fe and Co (grain boundary and matrix) (b) comparison between Co and Dy.

It is likely that there will significant overlap between the compositional analysis at the grain boundary and in the matrix so little significance can be attached to the data shown in figure 9-35 (b). It will be necessary to employ TEM studies in order to establish whether there is any Dy-enrichment at the grain boundaries in this magnet. Any enrichment could have significant commercial interest.

9.9.3 Sample A3 preparations: Heat treatment and additions:

The HD-powder was milled for 1 hour and sintered at a temperature of 1120 ^{o}C for 3 hours, then annealed for 3 hours at 800 ^{o}C and further annealing at a temperature of 650 ^{o}C for 1 hour. The additions to this sample were 2 at% Co, 0.5 at% Dy and 0.2 at% Nb. This sample was further treated with a DyH_2 slurry diffusion treatment at 800 ^{o}C for 1 hour. The resulting microstructure is shown in figure 9-36 and the chemical results are shown in table 9-15.

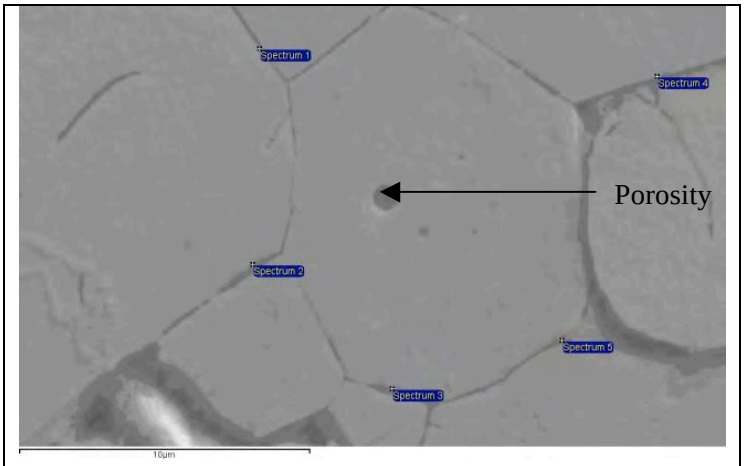

Figure 9-36 SEM grain boundary region of sample A3, density = 7.31 g/cm^3.

The microstructure (figure 9-36) shows a degree of porosity and some of this may be attributed to the process of polishing with diamond paste with the possibility of samples being polished for too long.

Table 9-15: spectrum analysis (at%) of sample A3:

Spectrum ±5%	Fe	Co	Nb	Nd	Dy
Spectrum 1	80.42	2.87	0.06	13.18	3.47
Spectrum 2	85.74	2.55	0.09	10.02	1.60
Spectrum 3	81.73	2.39	0.07	12.93	2.88
Spectrum 4	84.56	2.34	-0.01	11.14	1.97
Spectrum 5	69.40	16.12	2.86	11.80	-0.18

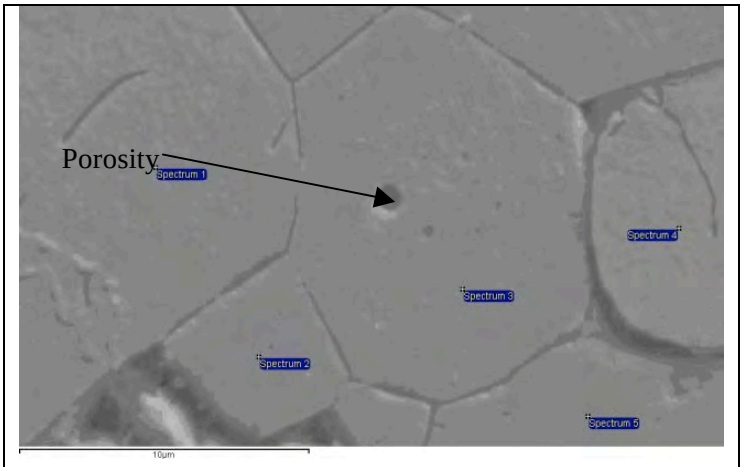

Figure 9-37 SEM image of the matrix of sample A3, density = 7.31 g/cm^3

Table 9-16: spectrum analysis (at%) of sample A3:

Spectrum ±5%	Fe	Co	Nb	Nd	Dy
Spectrum 1	84.78	2.84	0.08	10.90	1.40
Spectrum 2	84.98	3.04	0.16	10.92	0.90
Spectrum 3	85.16	3.12	0.11	11.16	0.45
Spectrum 4	83.98	3.03	0.06	10.84	2.08
Spectrum 5	85.24	2.76	0.06	10.77	1.17

9.9.4 Sample A4: Heat treatment and addition:

The powder was milled for one hour and sintered at a temperature of 1120 ^{o}C for 1.5 hours, then annealed for 3 hours at 800 ^{o}C and a further annealing at a temperature of 650 ^{o}C for 1 hour. The additions were, 0.2 at% DyH_2 and 0.2 at% Nb.

The resulting microstructure is shown in figure 9-38 and 9-39 and the EDX spot analysis is shown in table 9-17 and 9-18.

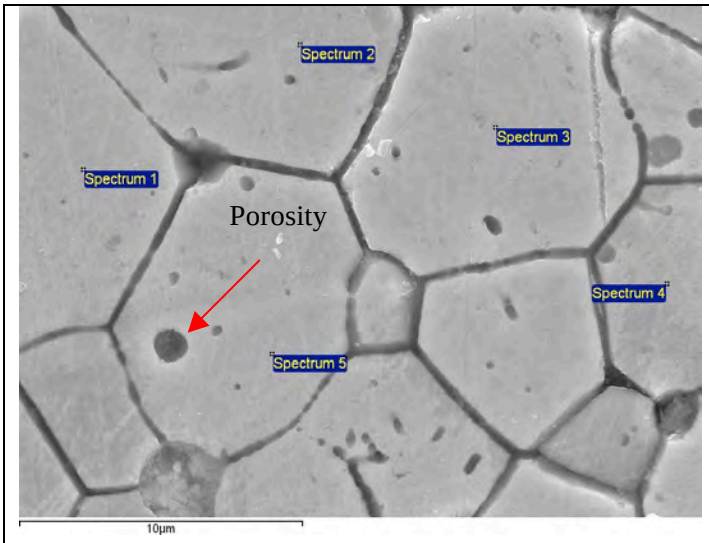

Figure 9-38 SEM image of sample A4 showing matrix, density = 7.52 g/cm^3

Table 9-17: spectrum analysis (at%)

Spectrum ±5%	Fe	Co	Nb	Nd	Dy
Spectrum 1	86.89	1.82	0.03	11.13	0.13
Spectrum 2	88.04	1.05	0.00	10.67	0.24
Spectrum 3	85.79	1.41	0.01	10.04	2.75
Spectrum 4	87.18	1.34	0.03	10.73	0.71
Spectrum 5	87.02	1.07	0.04	9.38	2.48

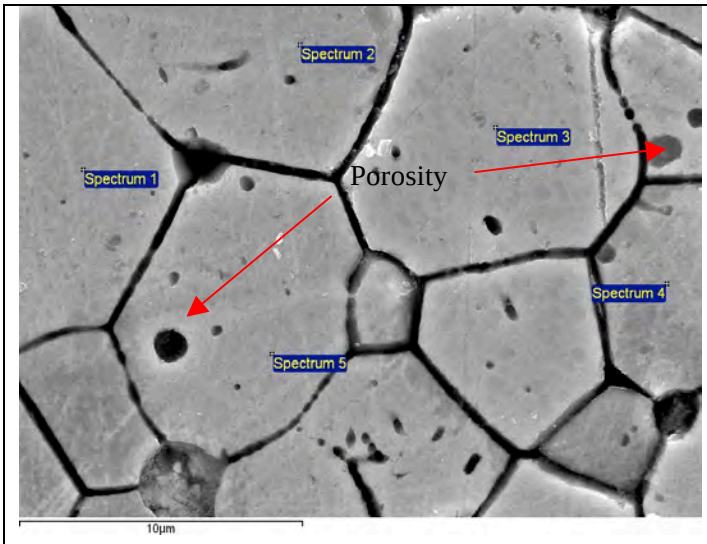

Figure 9-39 SEM image of sample A4 showing matrix, density = 7.52 g/cm^3

Table 9-18: spectrum analysis (at%)

Spectrum ±5%	Fe	Co	Nd	Dy
Spectrum 1	83.97	1.59	11.90	2.54
Spectrum 2	87.17	0.99	9.97	1.87
Spectrum 3	86.20	1.30	12.58	-0.09
Spectrum 4	84.33	1.61	11.24	2.82
Spectrum 5	79.93	2.36	15.25	2.47
Spectrum 6	76.03	2.16	19.13	2.68

This does not seem to be an inhomogeneous distribution of Dy but this does not seem to associated with the grain boundaries. This could be due to variations in the processing of the magnets where some possible synergy associated with the Nb-additives. This clearly requires further investigation.

9.9.5 Sample A5 heat treatment and additions:

The powder was milled for 1 hour and sintered at a temperature of 1120 ^{o}C for 1.5 hours, then annealed for 3 hours at 800 ^{o}C and further annealed at a temperature of 650 ^{o}C for 1 hour. The addition was 1 at% Co, 0.2 at% DyH_2 and 0.2 at% Nb. This sample was subjected to further treatment using the DyH slurry diffusion treatment at 800 ^{o}C for 1 hour. The resulting microstructure is shown in figure 9-40 and 9-41 and the chemical results are summarised in table 9-19 and 9-20.

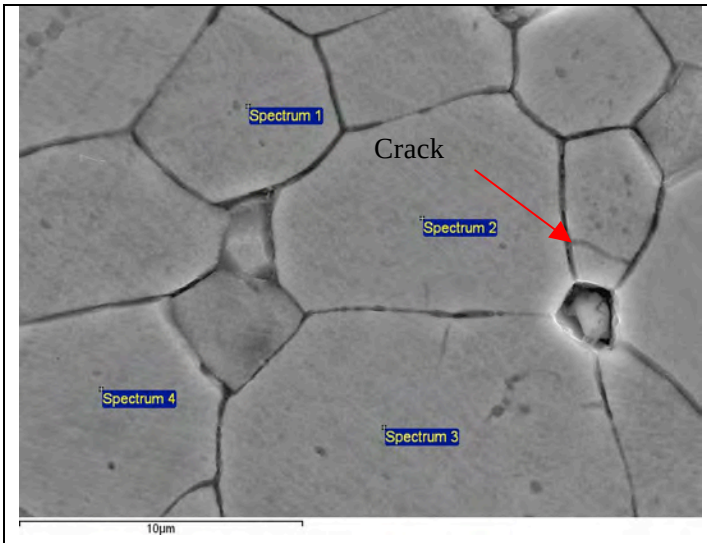

Figure 9-40 SEM image showing spectra at grain boundary regions, density = 7.46 g/cm^3

Table 9-19: spectrum analysis (at%)

Spectrum ±5%	Fe	Co	Nb	Nd
Spectrum 2	86.18	1.65	0.08	12.09
Spectrum 3	83.24	3.54	0.07	13.15
Spectrum 4	80.67	2.45	0.09	16.79
Spectrum 5	86.53	2.36	0.08	11.02
Spectrum 6	87.28	1.82	0.02	10.88

It does not appear to be possible to detect any Dy-content in this magnet, despite the additional diffusion treatment.

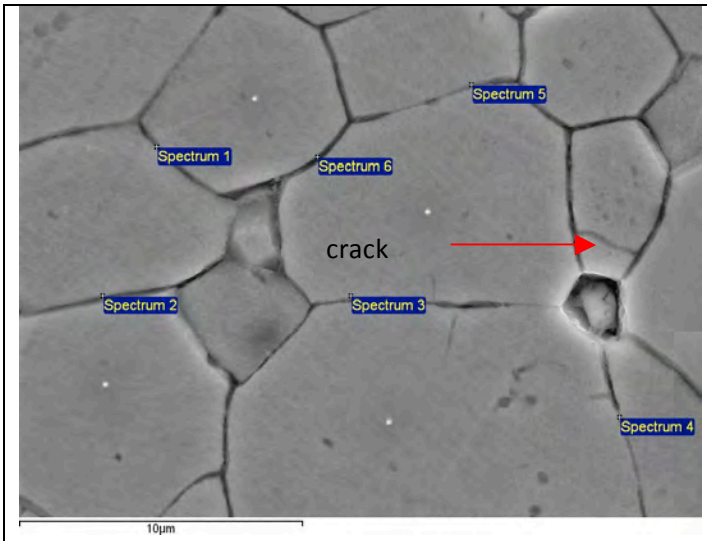

Figure 9-41 SEM image of sample A5 showing spectra at matrix phase, density = 7.46 g/cm^3.

Table 9-20: spectrum analysis (at%)

Spectrum ±5%	Fe	Co	Nb	Nd
Spectrum 1	88.31	1.93	0.03	9.73
Spectrum 2	89.01	1.57	0.11	9.31
Spectrum 3	88.74	1.46	0.05	9.75
Spectrum 4	88.51	1.79	0.08	9.62
Spectrum 5	87.38	2.07	0.05	10.50

9.9.6 Summary of the magnetic properties:

The magnetic properties of all samples prepared by previous blending additions and heat treatments were characterised, the results are shown in figure 9-42 and summarised in table 9-21.

Table 9-21: magnetic properties of all samples

Sample	Br (mT) ±1%	jHc (kA/m) ±1%	BHmax (kJ/m^3) ±2%	ρ (g/cm^3) ±0.05g
A1	1263	373	300	7.51
A2	1283	797	310	7.56
A3	1233	772	256	7.31
A4	1326	763	328	7.52
A5	1295	610	312	7.46
Initial values	***1370***	***849***	***359***	***7.65***

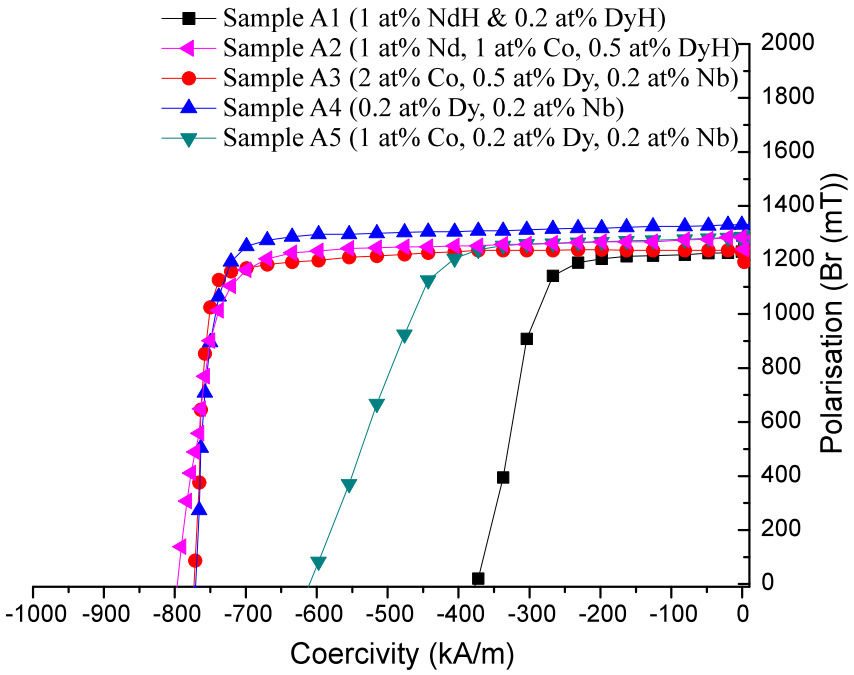

Figure 9-42 Comparison of IPMni samples with various at% additions of Dy, Co, Nd and Nd.

The various heat treatments and additions have had an effect on the magnetic properties of the resultant magnets. Sample A4 exhibited the best overall magnetic properties which were close to the original values but most of the samples produced some good magnetic properties. This shows that, with the correct blending additions and heat treatments, it is possible to recover nearly all the magnetic properties of the starting material through recycling using the HD-process. It remains to be seen whether it is possible to produce an inhomogeneous Dy distribution using DyH_2 blending and/or slurry diffusion.

9.10 Further investigation using additions of same elements with various heat treatments

The following section shows a continuation of the above studies on the effects of various additions on the magnetic properties on the IPM magnets.

The effect of the sintering temperature is shown in figure 9-43, showing an improvement in Br and a decrease in Hcj on increasing the sintering temperature. Similar effects have been previously (McGuiness et al., (1985)) and were ascribed to

an improved alignment giving an increased value in Br but grain growth leading to degradation in Hcj.

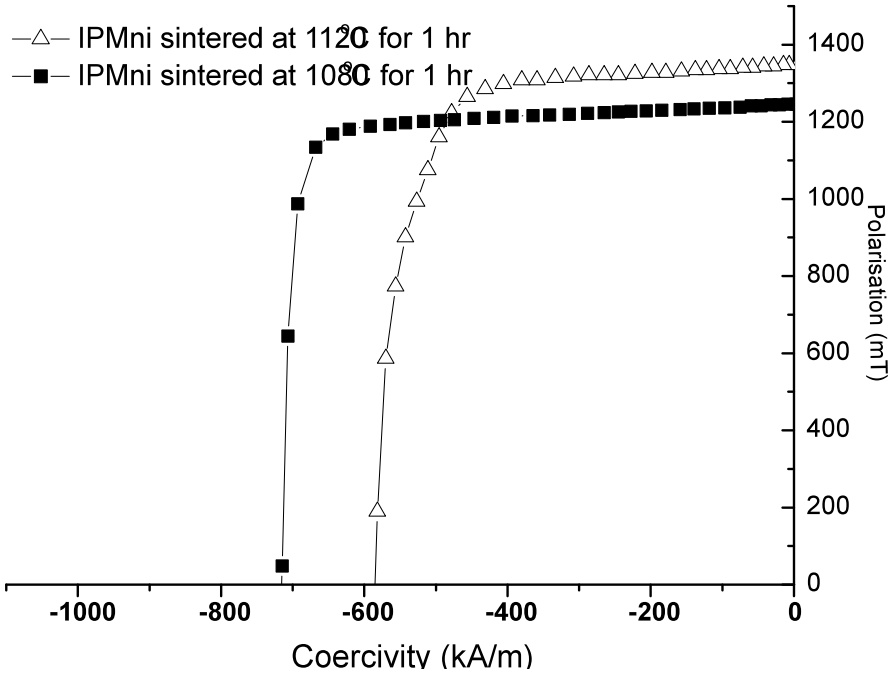

Figure 9-43 Comparison between IPMni sintered at 2 different temperatures.

Because of the improved Br, a sintering temperature of 1120 ^{o}C was selected and the effect of a blending addition of NdH_2 was investigated in an attempt to recover the Hcj value. The results are shown in figure 9-44, For the addition of 1 and 1.5 at% NdH_2 , it can be seen that there has been a progressive increase of Hcj with the addition of NdH_2 without a significant loss in Br. The Hcj for the 1.5 at% NdH2 magnet is now quite close to that of the magnet sintered at the lower temperature.

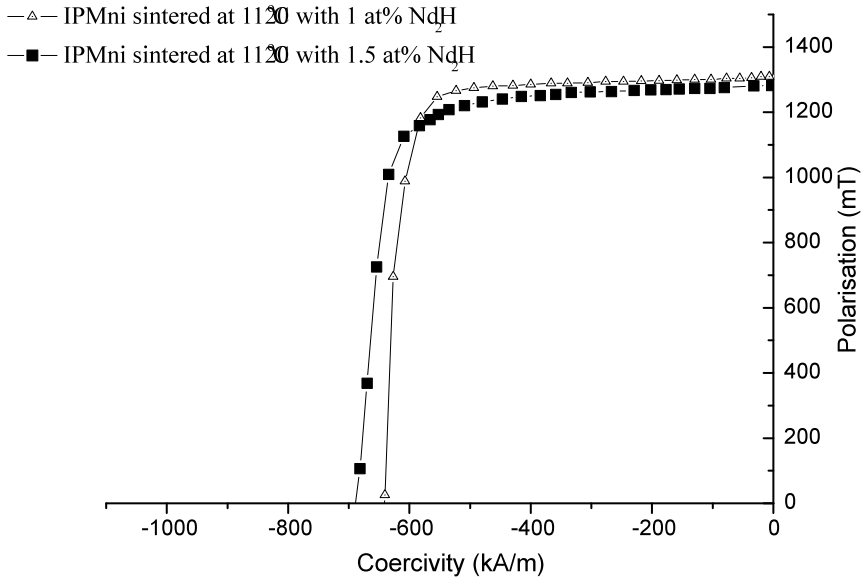

Figure 9-44 demagnetisation measurement, showing the effect of an 1 and 1.5 at% addition of NdH_2

Table 9-22: Magnetic properties of IPMni starting material and Recycled IPMni with 1 and 1.5 at% NdH [1120° C] for 1 h.

	IPMni starting material	IPMni at [1080° C]	IPMni at [1120° C]	IPMni with 1 at% NdH at [1120° C] for 1 h	IPMni with 1.5 at% NdH at [1120° C] for 1 h
Br (mT)±1%	1370	1250	1339	1310	1282
iHc (kA/m)±1%	849	721	593	660	692
BH(max) (kJ/m³)±2%	359	289	321	323	282
ρ (g/cm³)±0.05 g	7.65	7.31	7.47	7.58	7.44

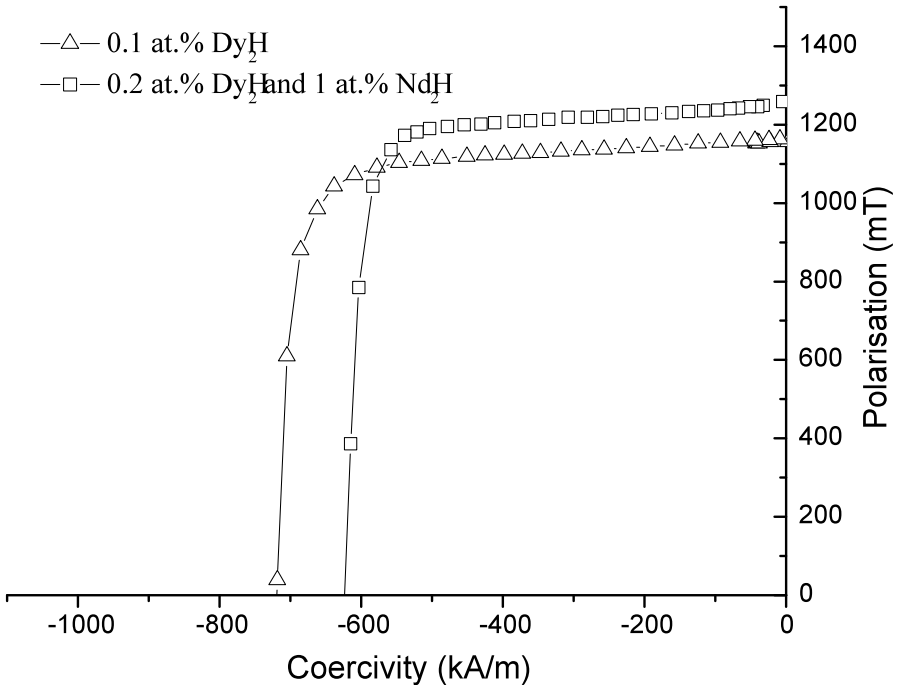

Figure 9-45 Demagnetisation graph of various blends of NdH_2 and DyH_2.

Table 9-23: magnetic properties of IPMni starting material and addition of 1 at% NdH_2 and annealed for 2 hr at 950 ^oC and 1hr at 650 ^oC.

	IPMni starting material	IPMni with 0.1 at% DyH [1115 ^oC]	IPMni with 1 at% NdH and 0.2 at% DyH [1115 ^oC] ½ h mill
Br (mT) ±1%	1370	1152	1253
iHc (kA/m) ±1%	849	732	625
BH(max) ***(kJ/m³) ±2%***	359	250	286
ρ (g/cm³) ***±0.05g***	7.65	7.1	7.61

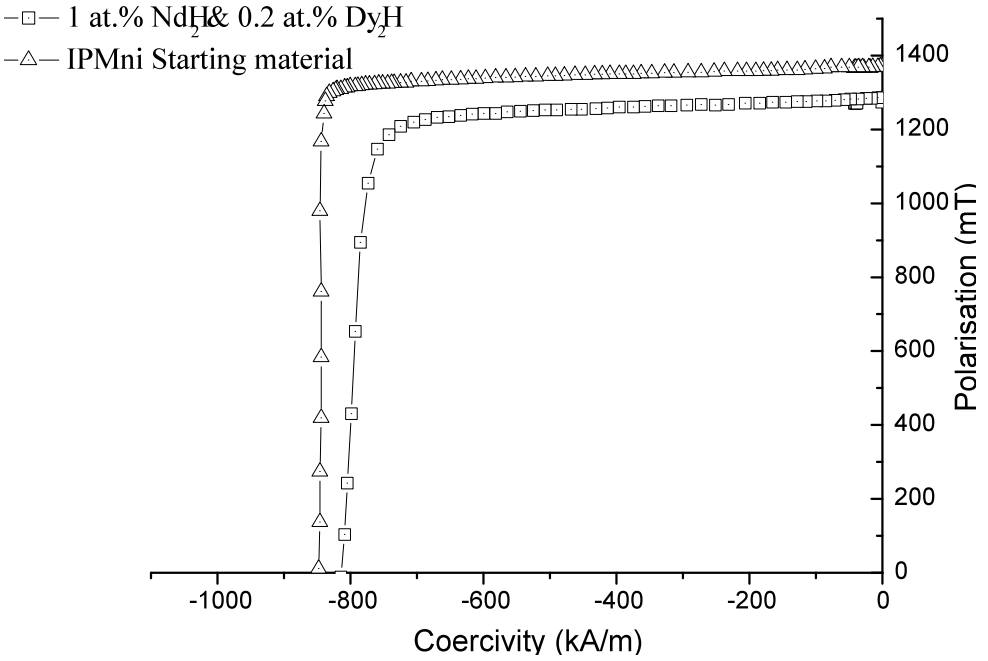

Figure 9-46 Demagnetisation graph of 1at. % NdH_2 and 0.2 at. % DyH_2 versus IPMni (Starting Material).

Table 9-24: magnetic properties of various additions of Nb, Nd,

	IPMni starting material	IPMni with 1 at.% NdH & 0.2 at.% DyH (1 h)[1] 5 h anneal 900° C	IPMni with 1 at.% NdH, 0.2 at.% DyH & 0.2 at% Nb (2hrs)[2] SQM (2 hrs at 1120 ºC)	SQM at 1165 ºC for 1 h & 3 h at 850 ºC (1 at% NdH-0.2 at%DyH- 0.2 at%Nb)
Br (mT) ±1%	1370	1291	1194	1205
iHc (kA/m) ±1%	849	814	806	634
BH(max) (kJ/m³) ±2%	359	312	250	256
ρ (g/cm³) ±0.05g	7.65	7.6	7.22	7.58

[1]IPMni powder recycled from initial IPM material with additions of 1 at% NdH_2 & 0.2 at. % DyH_3 1120 ºC, annealed for 5 hr at 900 ºC and 1hr at 650 ºC.

[2] addition of 1 at% NdH_2, 0.2 at. % DyH_3 & 0.2 at% Nb at 1120 ºC, annealed for 3 h at 900 ºC and 1h at 650 ºC

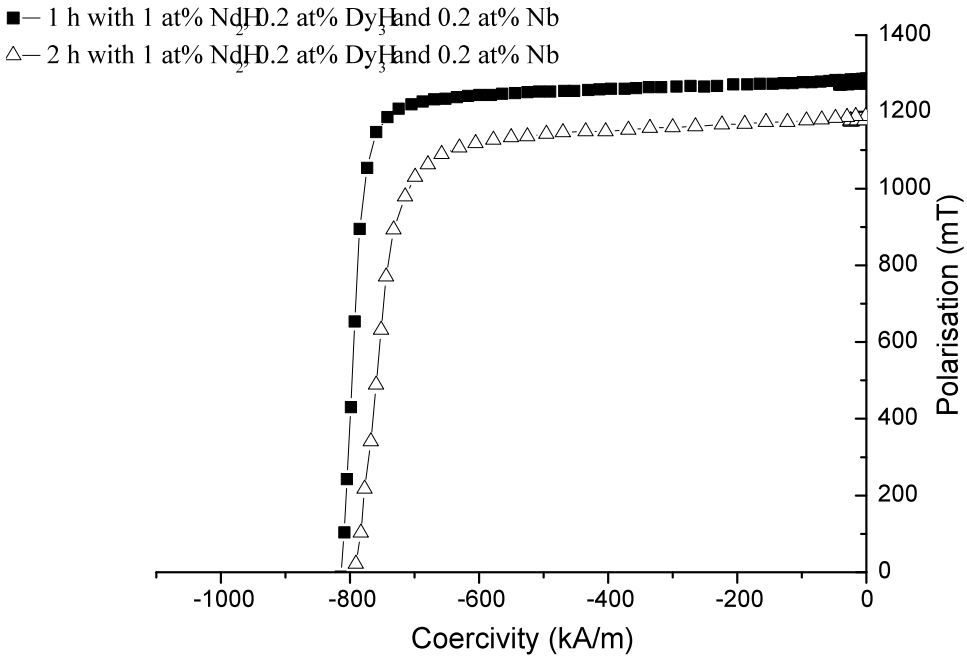

Figure 9-47 Demag-Loop of the magnetic properties shown in table 9-22.

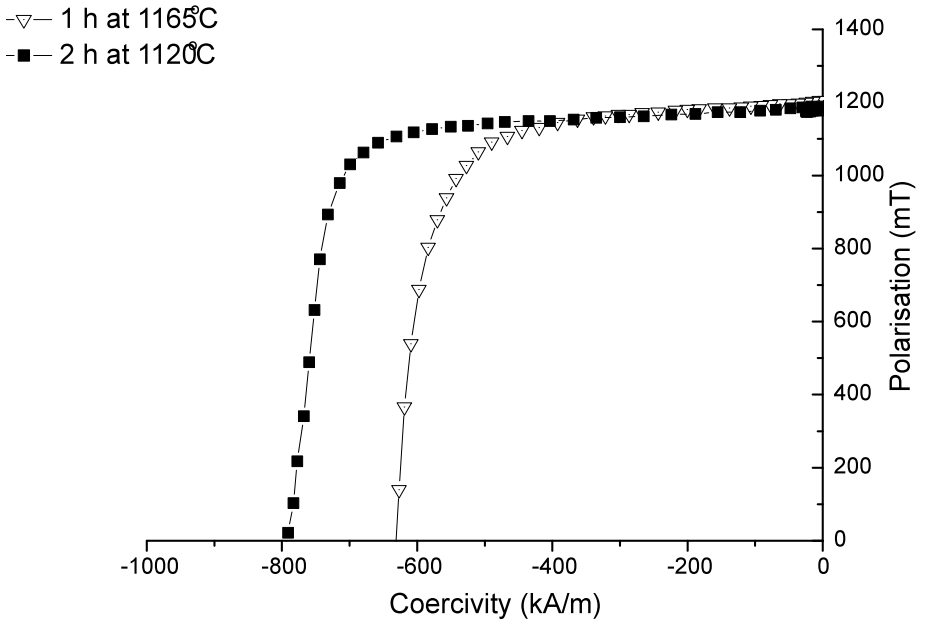

Figure 9-48 Composition of: 1 at% NdH_2, 0.2 at% DyH_3 and 0.2 at% Nb recycled magnets as a function of sintering times and temperatures.

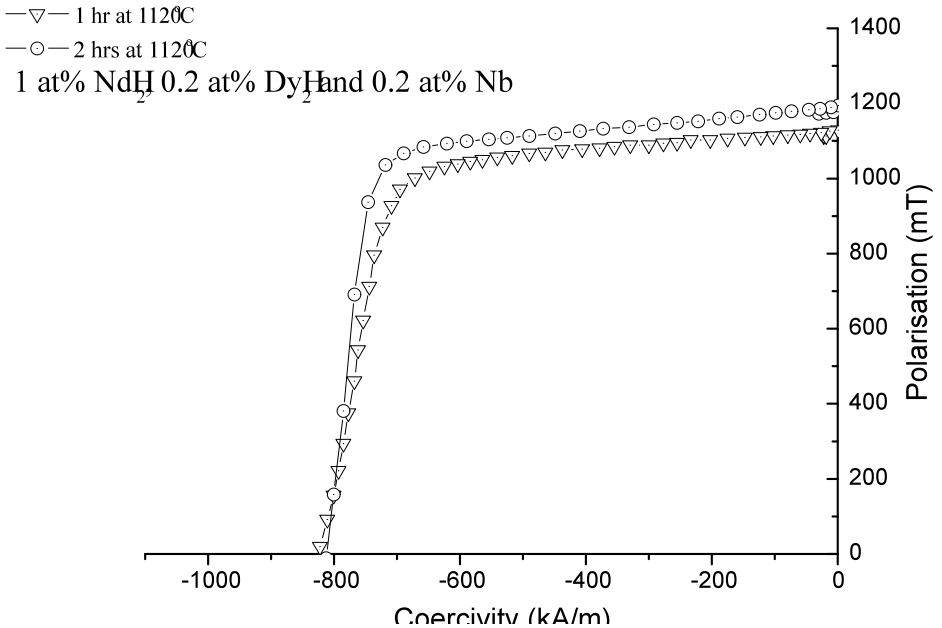

Figure 9-49: Comparison of 2 different temperatures with composition of 1 at% NdH_2, 0.2 at% DyH_2 and 0.2 at% Nb.

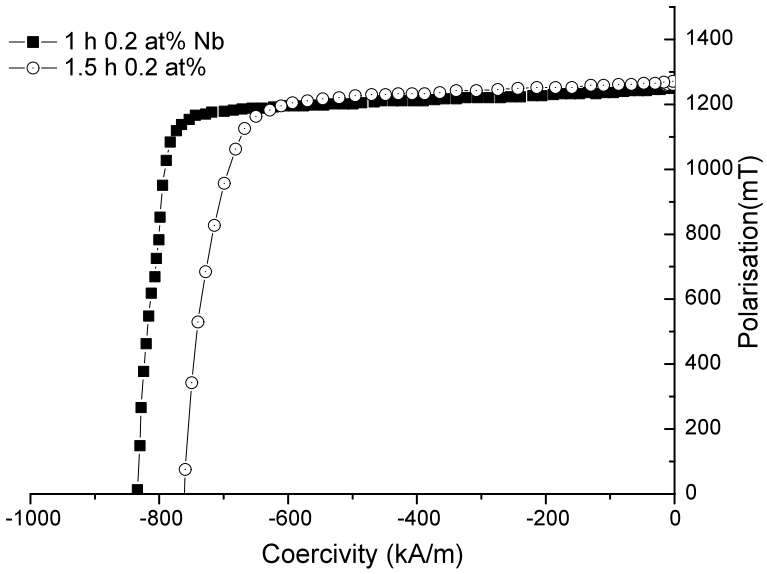

Figure 9-50 IPMni magnets sintered at 1120 ºC for 1hr & 1.5 h, 3 h at 800 ºC and 1h at 650 ºC. Composition of, 0.2 at% DyH_3 and 0.2 at% Nb (1 hour mill).

Table 9-25: IPMni magnets sintered at 1120º C for 1 h & 1.5 h, 3 h at 800 ºC and 1 h at 650 ºC. Composition of, 0.2 at% Dy and 0.2 at% Nb (one hour mill).

	IPMni starting material	IPMni with 0.2 at.% DyH_3 & 0.2 at.% Nb (1h at 1120`ºC)	IPMni with 0.2 at.% DyH_3 & 0.2 at.% Nb (1.5 h at 1120 ºC)
Br (mT) ***±1%***	1373	1249	1271
iHc (kA/m) ***±1%***	847	834	763
BH(max) ***(kJ/m³)*** ***±2%***	359	291	300
ρ (g/cm³) ***±0.05g***	7.71	7.45	7.5

It can be seen from this data that the modified sintering conditions and blending agents have resulted in a Hcj value close to the original value in the case of the 1 hr sinter but there is a significant reduction in the value of Br.

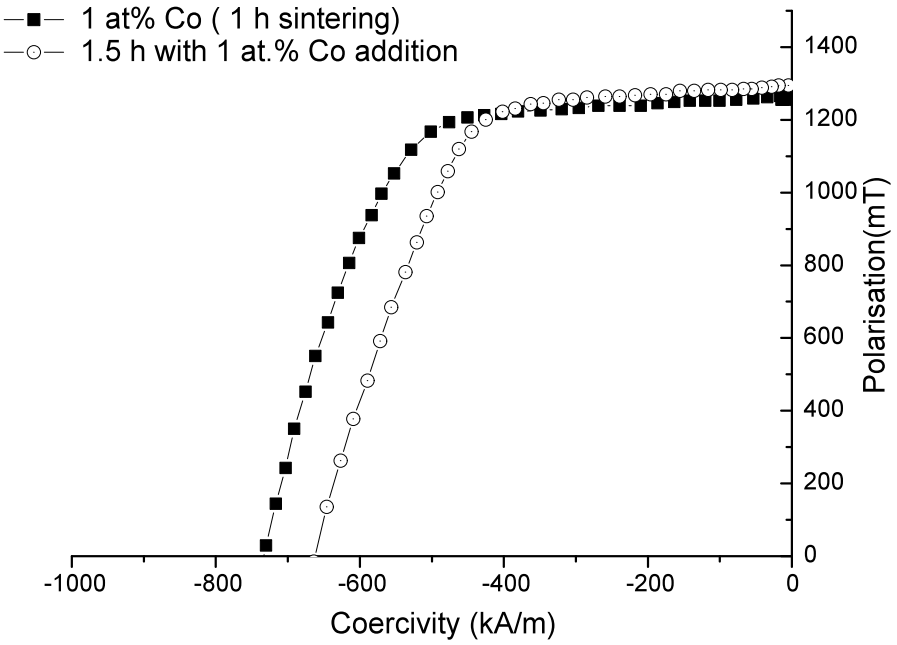

Figure 9-51: IPMni magnets sintered at 1120 ºC for 1 h & 1.5 with same additions (1 hour mill)

The addition of cobalt follows on from the work of Sagawa et al., (1985) where they determined that the main effect of cobalt upon the NdFeB magnets is the improvement in the remanence temperature coefficient. This improvement is due to the increase in the Curie point which occurred as Co substitutes the Fe in the matrix phase. In the case of Nb when it is added to the NdFeB based magnets, there was an improvement in the magnet's impact toughness and in the coercivity. This improvement was achieved by the additions of 1.5 at% Nb to the alloy (Hu et al., 2008). The Nb addition resulted in the grain size of the main phase becoming more regular, and the grain boundaries become clear and smooth, so that the intrinsic coercivity of the sintered magnets is increased

Table 9-26: IPMni magnets sintered at 1120 ºC for 1 hr & 1.5 h, 3 h at 800 ºC and 1 h at 650 ºC. Composition of 1 at.% Co, 0.2 at.% DyH_2 and 0.2 at.% Nb (1 hour mill).

	IPMni starting material	IPMni sintered at 1120^{o}C for 1 h, 800 ^{o}C for 3 h & 1 h at 650 ^{o}C **(1 at.% Co, 0.2 at% Dy and 0.2 at.% Nb)**	IPMni sintered at 1120 ^{o}C for 1.5 h, 800 ^{o}C for 3 h & 1 h at 650 ^{o}C **(1 at.% Co, 0.2 at% Dy and 0.2 at.% Nb)**
Br (mT) ***±1%***	1373	1269	1296
iHc (kA/m) ***±1%***	847	738	655
BH(max) (kJ/m³) ***±2%***	359	289	288
ρ (g/cm³)***)±0.05 g***	7.71	7.4	7.43

Summary of the effect of the blending additions and the various heat treatments:

The IPMni sintered magnet has excellent initial magnetic properties and this magnet has been recycled by means of the HD-process using a combination of blending using HD/milled powder with various elements and by diffusing DyH_2 using the diffusion heat treatment process.

The EDX/SEM studies indicate the presence of the introduced elements. The resolution of the SEM measurements did not allow an accurate determination of the partitioning of the elements between the grain boundaries and the matrix. The problem of “beam overlap” prevented such measurements but, as expected they did indicate less Fe and more Nd/Dy in the grain boundary regions.

The magnetic properties of the recycled magnets indicated a very good degree of retention of the initial properties and the data indicates that further improvements could be achieved by optimisation of the heat treatment procedure (temperature and

time). The density measurements also indicated values close to that of the initial density of the magnet.

9.11 The effect of coating using Tb or Dy hydride on the magnetic properties of NdFeB–type sintered magnets with associated heat treatment.

9.11.1 Introduction

The various process steps are summarised in the following flowchart:

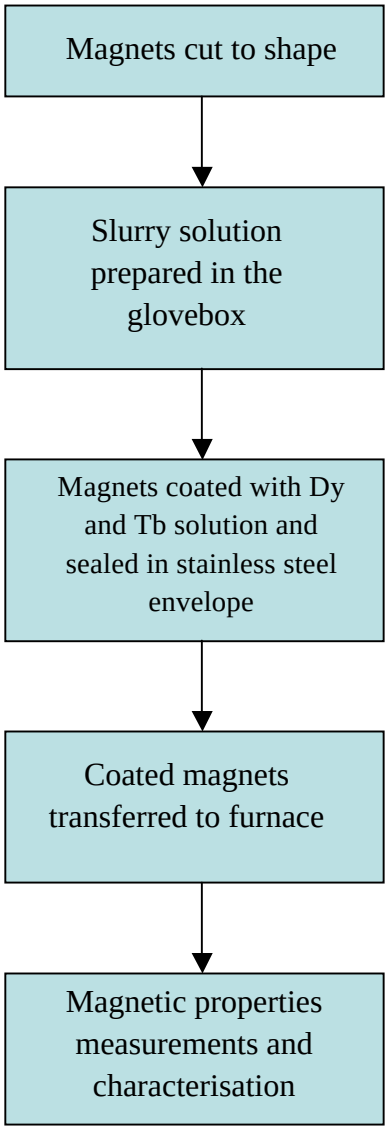

Figure 9-52: Coating process flow chart

Past work on the recycling of permanent magnets based on NdFeB has indicated the possibility of enhancing the magnetic properties whilst conserving the amount of Tb and or Dy required to improve the coercivity and hence the elevated temperature performance. Consequently, the author prepared the magnet samples from the starting materials which, in the present work were in the form of sintered segments obtained from VCMs (voice coil motors) of hard disc drives. Each segment weighed ~10 g and the nickel coating was:

(1) Removed by grinding off the coating by hand.

(2) Square sections of the NdFeB magnets were then prepared with dimensions of 14 mm x 15 mm x 2 mm.

(3) The TbH_2 or DyH_2 powder was prepared and then mixed with cyclohexane to form a suspension. This mixture was in the ratio of 2:1 in weight (2 parts of powder to 1 part of cyclohexane), with a mean particle size of 3−5 μm.

(4) The sintered magnets were coated with this slurry and;

(5) dried in a glove box and housed in a stainless steel envelope and

(6) placed in a furnace. The magnets were heated at 800 ^{o}C for 0.5 h, 1 h, 3 h and 10 hours under vacuum of $6x10^{-2}$ Pa. The magnetic properties were measured using a permeameter after applying a pulse of ~4T. Preliminary microstructural analyses of these magnets have been performed using a SEM JEOL 7000 and these studies have been made to establish if the heavy rare earth elements (Dy and Tb) are concentrated within the grain boundary regions. Such a microstructure would enable these elements to enhance the coercivity whilst minimising the amount required and without diminishing the remanence by substituting for Nd within the matrix 2-14-1 phase.

9.11.2 Results and Discussions

A typical second quadrant demagnetisation curve obtained as a result of this treatment is shown in figure 9-53. The coercivity of the 0.5 h, 1 h, 3 h and 10 h, heat treated sintered magnets with a DyH_2 slurry resulted in an increase in coercivity by about 232, 391, 229, 232 kA/m, respectively.

As expected therefore, the addition of Dy resulted in a significant increase in the intrinsic coercivity, which can be attributed to the increased magnetocrystalline anisotropy (See chapter 4). The remanence after the heat treatment process (HTP) was, on an average, reduced by 50 mT. When the DyH_2 –slurry heat treatment process is compared with the (blending) of the DyH_2 with the sintered magnets, the latter results indicate a dramatic decrease of the remanence (refer to chapter 8). The loss of remanence is ascribed to the antiparallel coupling with the Fe/Nd of the Dy atoms in the ϕ-phase ($Nd_2Fe_{14}B$), this has a dramatic impact when DyH_2 is blended into the virgin material which is due to the large Dy magnetic moment of 10μB* ((*Dy (10μB), Nd (3.4μB) Fe(2.2μB)) and to the more homogeneous distribution of the Dy within the ϕ-phase. These results are in agreement with previous work on DyH_2 blending additions to sintered magnets; see for example (Mottram et al., (1999), Mottram et al., (2001), M. Zakotnik, (2008) and Pan et al., (2010)).

Figure 9-54 show a typical second quadrant demagnetisation curves for the TbH_2 HTP sintered magnet. The coercivity of the 0.5 h, 1 h, 3 h and 10 h, heat treated sintered magnets which resulted in an increase of about 267, 370, 406, kA/m, respectively and, after the 10 hours anneal, the magnet could not be measured due to insufficient demagnetising field. The coercivities of the heat treated sintered magnets with TbH_2 are generally higher than those of heat treated sintered magnets with DyH_2 because of the magnetic anisotropy field of $(Nd_{1-x}, Tb_x)_2Fe_{14}B$, which is higher than that of $(Nd_{1-x}, Dy_x)_2Fe_{14}B$ (Hirosawa et al., 1986).

A summary of the magnetic properties for the Dy and Tb heat-treated magnets are summarised in figure 9-55. Generally it can be seen that, with the increasing values in the coercivity, there is also a small fall in the remanence. It can be seen that the one hour heat treated sintered magnets with DyH_2 slurry resulted in the optimum magnetic properties. The decrease in the remanence value was insignificant while the coercivity was increased by 390 kA/m.

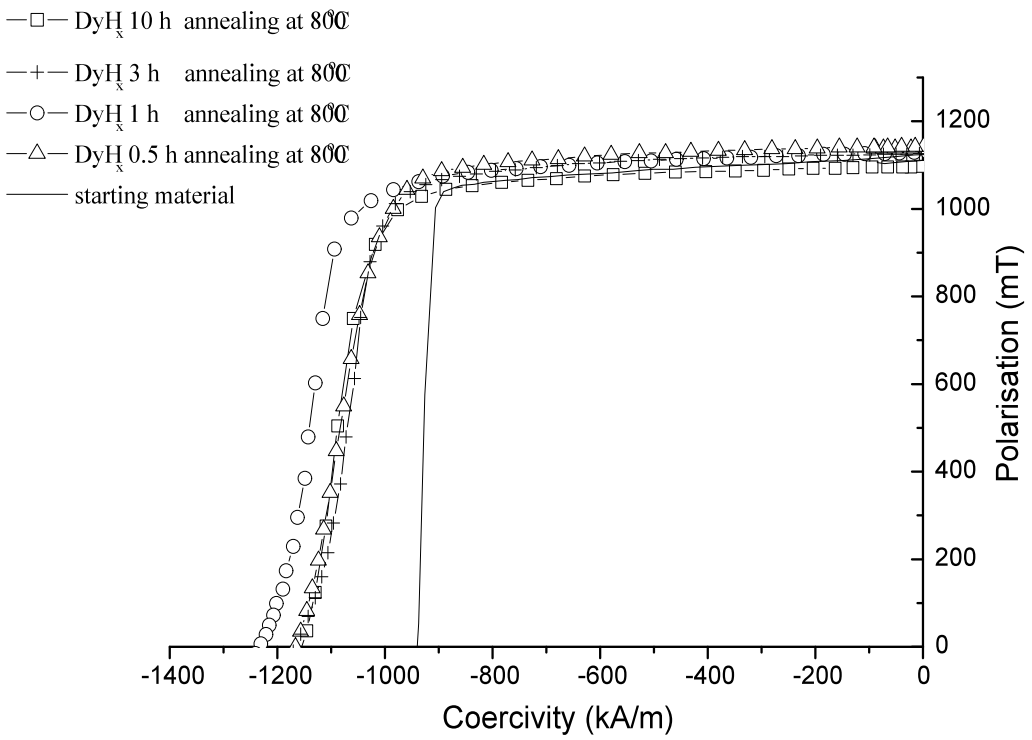

Figure 9-53: Demagnetising curves for DyH_2-slurry heat treated magnets at 800 ^oC, with annealing various times.

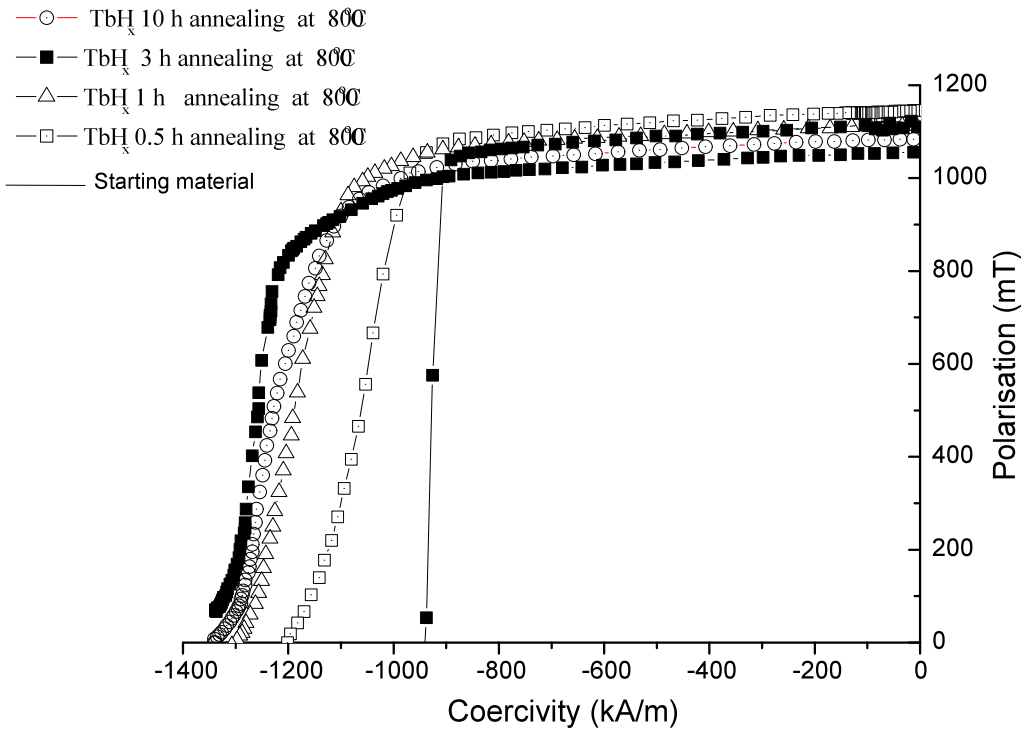

Figure 9-54. Demagnetising curves for TbH_2 heat treated magnets at 800 ^oC, with various times.

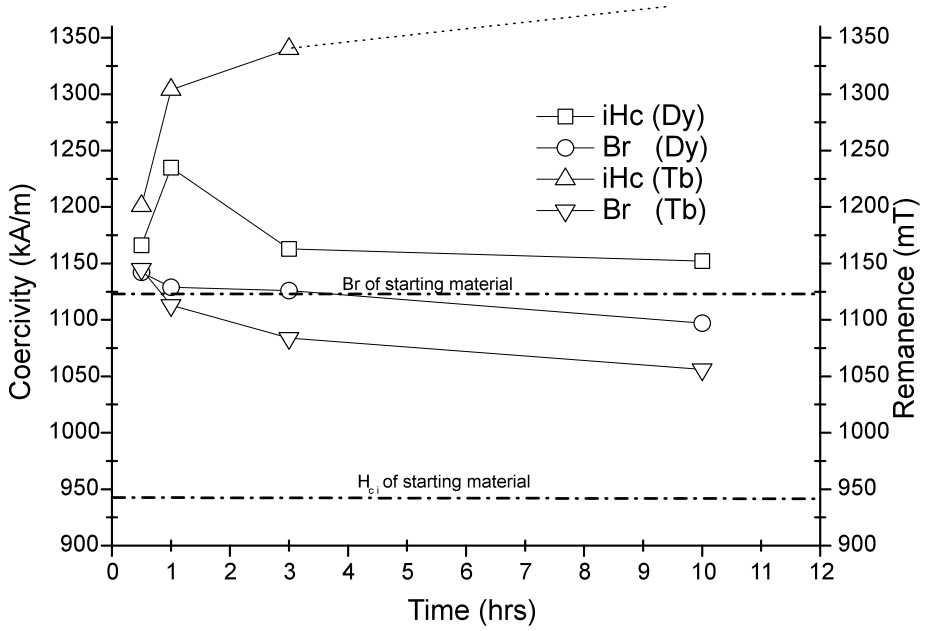

Figure 9-55. Summary of the magnetic properties of the heat treated sintered magnets with Dy/Tb hydrides versus heat treatment times.

9.11.3 The grain size analysis

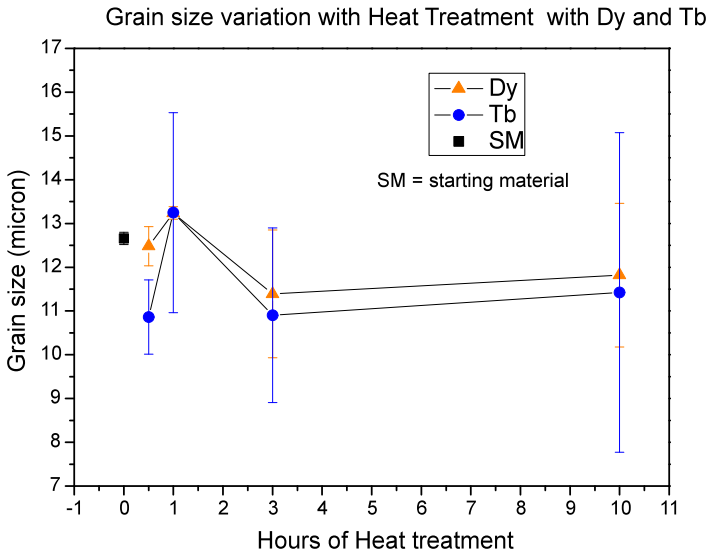

Figure 9-56: grain sizes after heat treatment with Dy and Tb additions.

From figure 9-56 there is an indication that both Dy and Tb have very similar effects on the grain size variation with various heat treatment times. Both of them exhibit grain growth. With the maximum effect obtained after 1 hour heat treatment. If the significant error bars are taken into account then the heat treatment have little effect on the grain size.

9.11.4 Dy line-scanning using SEM:

An elemental line scan for Dy was performed on the sample after it had been subject to the 0.5 hour of heat treatment and those measurements indicate that the Nd-rich phase contains ~2.7±1.4 at% of Dy whereas the matrix contain about 0.7±0.2 at%. These studies indicate a distinct segregation between the grain boundaries and the matrix and this would be consistent with the small changes in the Br-values. Clearly these measurements require confirmation.

A line scan was also performed for Nd, after a heat treatment of 1 h EDX line-scanning indicates that the Nd-rich phase contains ~3 at% of Dy.

In the case of the Tb additions, the Nd rich region also exhibits an enhanced level compared with that of the matrix. This is also be reflected in the Br values which also exhibit a small reduction in the case of the Tb magnets. It is important to note that the concentration of the Dy or Tb at the grain boundaries would result in an increase in Hcj without any degradation in the value of Br.

9.12 DSC measurements: Thermal Characterisation

Thermal characterisations were performed in order to measure important parameters such as the crystallisation temperature, Curie temperature and melting temperature. These parameter values may help when selecting particular sintering conditions necessary to obtain a magnet with an optimised microstructural and hence, magnetic property. Differential Scanning Calorimetry (DSC) was performed on 50-60 mg samples of the NdFeB-type sintered magnets (all four compositions) investigated in the present work.

Thermal characterisation (see figures 9-57→9-60(a)) was carried out by heating the magnetic material under a protective Ar atmosphere which resulted in four endothermic peaks for all the magnets. The first peak (lambda) marked A, at about 320 ^{o}C corresponds to the Curie temperature (Tc) of the $Nd_2Fe_{14}B$ phase, the second peak (marked T_1) at about 690 ^{o}C corresponds the melting temperature of the intergranular Nd-rich phase (ε-Nd), the third peak marked T_2 at 1080 ^{o}C corresponds to the peritectic reaction of the Φ-phase ($Nd_2Fe_{14}B$) and liquid, and the fourth peak marked T_3 represents a complete melting point of the NdFeB sintered magnet.

The thermal characterisation during cooling indicates five exothermic peaks, where the peak marked T_3 on heating indicated two reactions on cooling at a slow rate. The solidification of the molten NdFeB magnet is represented in figures 9-57→9-60(b). Here the first peak (E) represents the formation of the stable γ-Fe at 1220 ^{o}C + Liquid. Further solidification yields a crystallisation peak (D), at 1120 ^{o}C for the liquid + Φ-phase ($Nd_2Fe_{14}B$) with rhombohedral crystal structure (Volkmann et. al., (2004)). Further cooling leads to the stable ternary eutectic φ-phase ($Nd_2Fe_{14}B$), + η ($NdFe_4B_4$) + liquid which are detected when the sample is cooled to 1090 ^{o}C, marked (C).

Further cooling should lead to an increase in the amount of the $Nd_2Fe_{14}B(s)$ + $NdFe_4B_4(s)$ + L (marked (B) table 10-26) at temperatures lower than the temperature of the ternary eutectic, where the liquid phase will have solidified in the form of the three main phases $Nd_2Fe_{14}B$, $NdFe_4B_4$ and ε-Nd, below 700 ^oC.

The excess Nd is indicated by a eutectic reaction at around 695 ^oC (marked B); the presence of small amounts of the Nd-rich material in the permanent magnet has serious consequences for the corrosive behaviour of the magnets (see later). On further cooling, the NdFeB system reaches the Curie temperature, marked (A). These results are in a good agreement with the work reported by Hallemans et al, (1995), Chaban et al., al., (1979), Matsuura et al., (1985 a and b), Buschow et al., (1985) and Buschow et al., (1986).

Table 10-26: Summary of the reactions which occurred on heating and cooling of the NdFeB sintered magnet using Differential Scanning Calorimetry.

Point	**Description**
A: ≈320 ^oC	Curie temperature
B: ≈700 ^oC	Liquid + Φ phase+ η phase
C: ≈1090 ^oC	Liquid + Φ phase
D : ≈1115 ^oC	Liquid + γ phase
E: ≈1210 ^oC	Liquid
T_1: ≈ 690 ^oC	Liquid + Φ phase+ η phase
T_2: ≈ 1090 ^oC	Liquid + Φ phase
T_3: ≈ 1210 ^oC	Liquid

Legend:

Φ phase: (peritectic) $Nd_2Fe_{14}B$	γ Fe phase: Austenite (or gamma phase iron)	η Fe phase

9.12.1 DSC of China magnets:

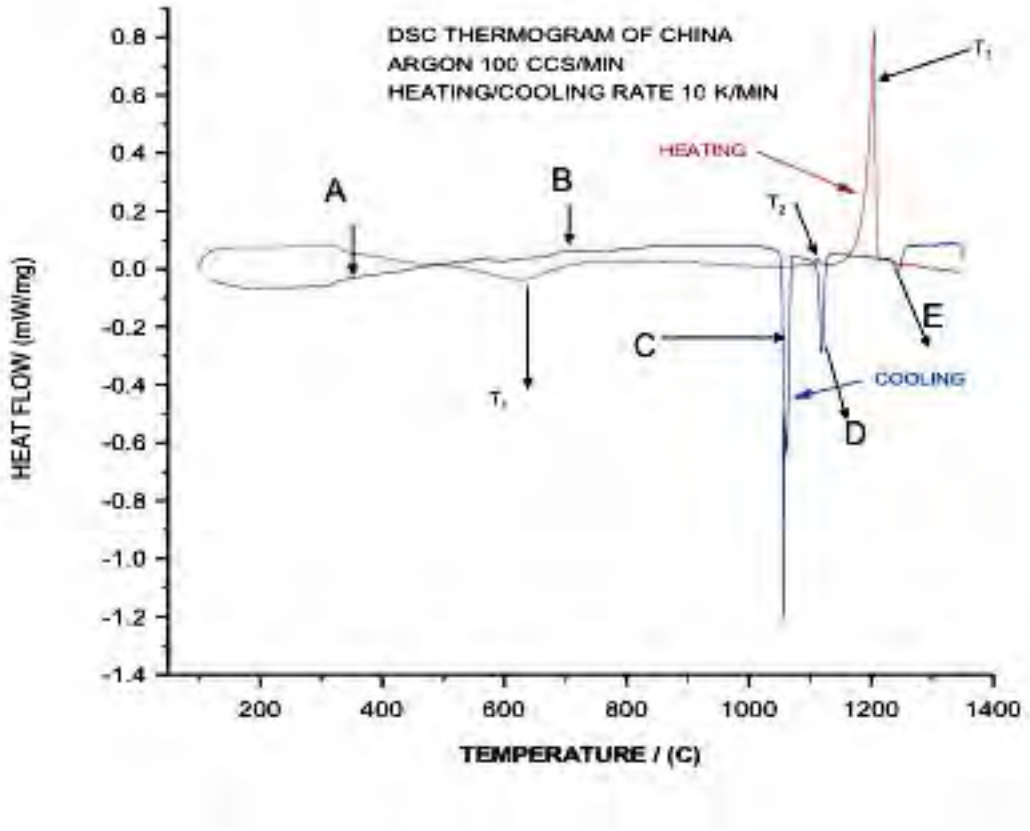

Figure 9-57: DSC diagrams showing the behaviour of the initial China magnet with endothermic and exothermic reactions: a) heating (10 ^{o}C/min) and b) cooling (10 ^{o}C/min). A = Curie temperature, B = Liquid + Φ phase+ η phase, C = Liquid + Φ phase, D = Liquid + γ phase, E = liquid, T_1 = Liquid + Φ phase+ η phase, T_2 = Liquid + Φ phase, T_3= liquid

9.12.2 DSC of Philips magnet:

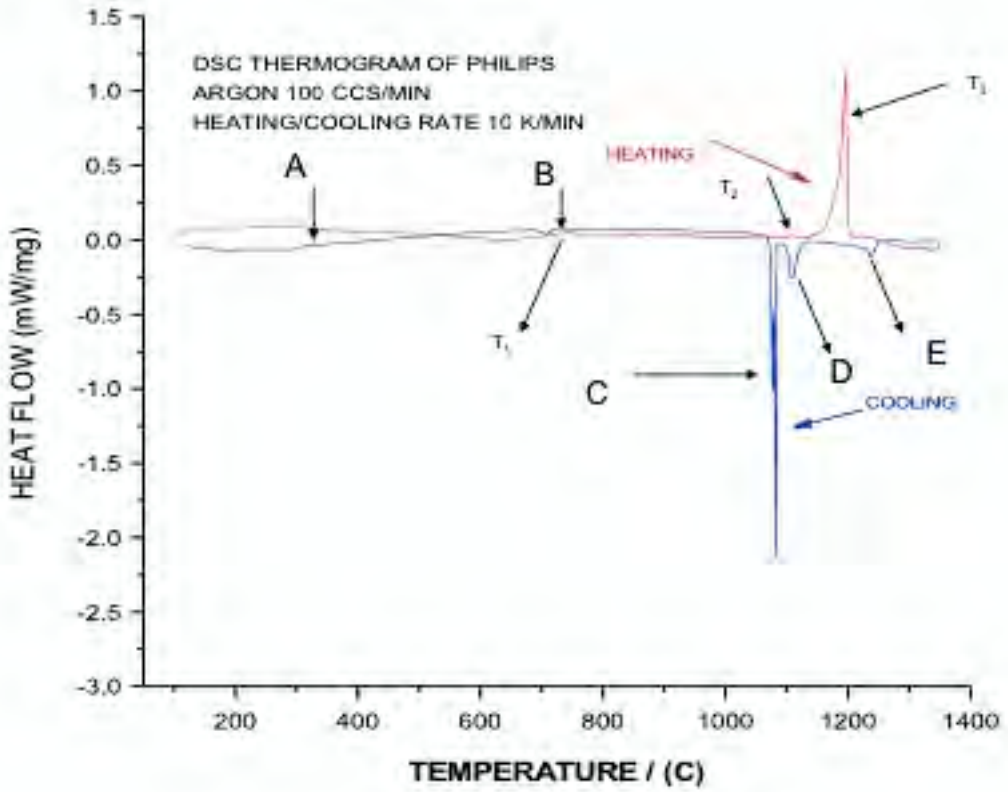

Figure 9-58: DSC diagrams showing initial Philips magnet with endothermic and exothermic reactions: a) heating (10 ^{o}C/min) and b) cooling (10 ^{o}C/min). A = Curie temperature, B = Liquid + Φ phase+ η phase, C = Liquid + Φ phase, D = Liquid + γ phase, E = liquid, T_1 = Liquid + Φ phase+ η phase, T_2 = Liquid + Φ phase, T_3= liquid

9.12.3 DSC of USA magnet:

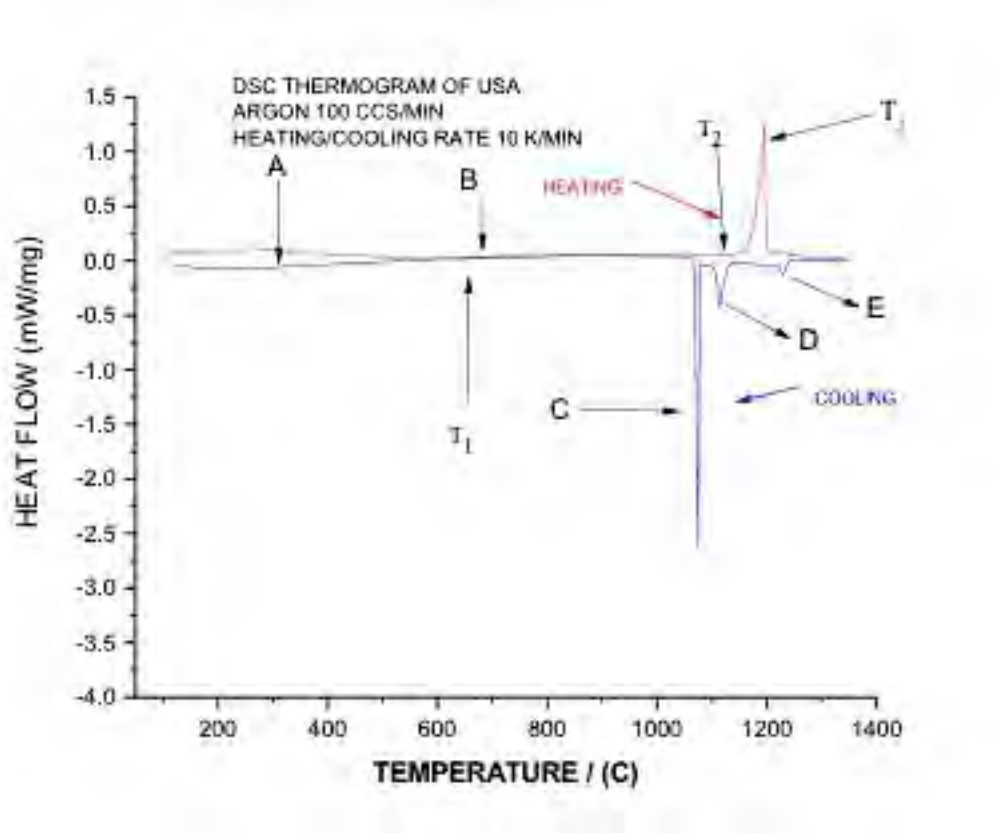

Figure 9-59: DSC diagrams showing initial China magnet with endothermic and exothermic reactions: a) heating (10 ^{o}C/min) and b) cooling (10 ^{o}C/min). A = Curie temperature, B = Liquid + Φ phase+ η phase, C = Liquid + Φ phase, D = Liquid + γ phase, E = liquid, T_1 = Liquid + Φ phase+ η phase, T_2 = Liquid + Φ phase, T_3= liquid

9.12.4 DSC of IPM magnets:

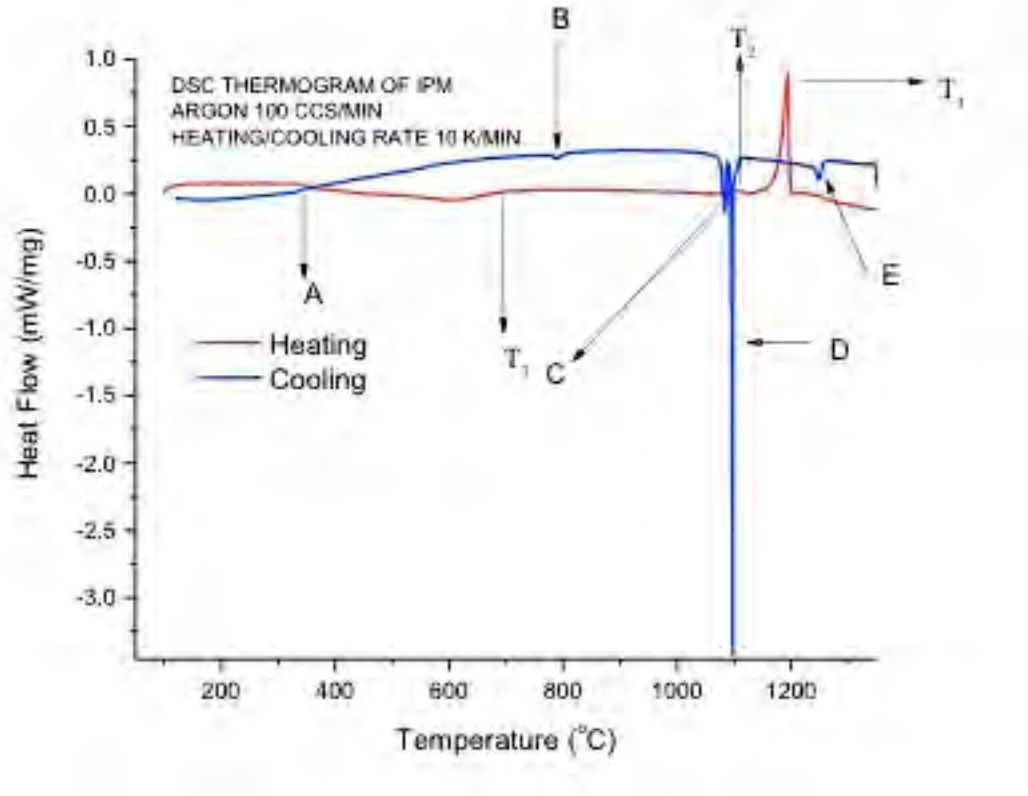

Figure 9-60: DSC diagrams showing initial IPM (Japanese composition) magnet with endothermic and exothermic reactions: a) heating (10 ^{o}C/min) and b) cooling (10 ^{o}C/min). A = Curie temperature, B = Liquid + Φ phase+ η phase, C = Liquid + Φ phase, D = Liquid + γ phase, E = liquid, T_1 = Liquid + Φ phase+ η phase, T_2 = Liquid + Φ phase, T_3= liquid.

10 The effectiveness of corrosion protection coatings on NdFeB sintered magnets

The procedure followed to establish the effectiveness of the corrosion coating is shown in figure 10-1.

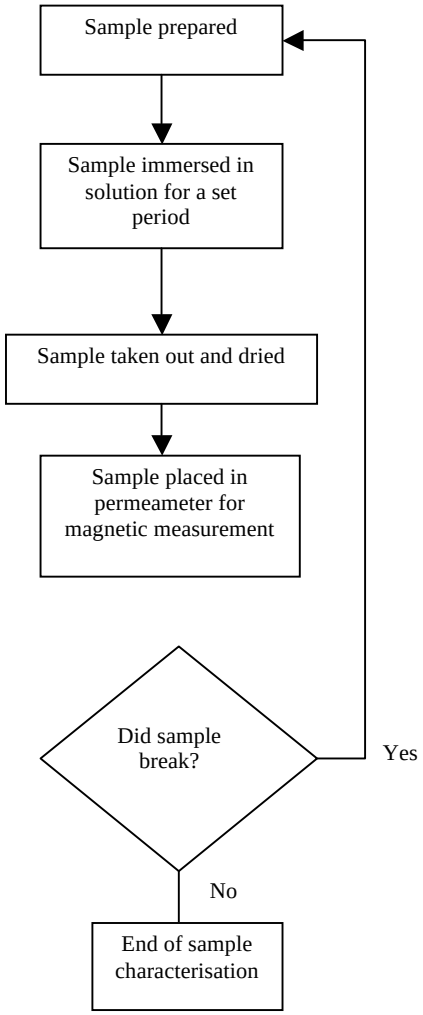

Figure 10-1: Flow chart of corrosion experiments.

10.1 Introduction

The "Archilles Heel" of NdFeB magnets is their poor corrosion resistance and since the early days of NdFeB sintered magnets, research has focussed on the effects of oxidation and corrosion. These have been identified as major obstacles to a much wider application of such magnets. (Willman et al., 1987, Kim et al., 1987, Jacobson et al., 1987). The tendency to attract electrons (electronegativity) between the $Nd_2Fe_{14}B$ matrix phase and the $Nd_{1+\varepsilon}Fe_4B_4$ and Nd-rich grain boundary phases, leads to the localised attack of the grain boundary material, particularly in humid

environments (Block et al., 1990). Many researches have investigated how to tackle this problem, including additions to the NdFeB microstructure to stabilise the grain boundary phases (Tenaud et al., 1990, Tokuhara et al., 1991, Hirosawa et al., 1990) and by metallic or polymeric coating (Cheng et al., 1997, Man et al., 1997, Mitchell, 1990). According to Sugimoto et al., 1987, the order of corrodibility among these phases is as follows:

$Nd_{1+\epsilon}Fe_4B_4$ (η-phase) > Nd-rich eutectic phase > $Nd_2Fe_{14}B$ (ϕ-phase)

Therefore, the $Nd_{1+\epsilon}Fe_4B_4$ and Nd-rich phases become anodes with regard to the $Nd_2Fe_{14}B$ matrix grains. Furthermore, since the matrix phase dominates the alloy volume, then the anodic metal carries a large anode current. As a result, grain boundary material corrodes rapidly (Walton, 2002).

Previous researches published on the subject of humid corrosion, used different NdFeB magnet compositions and a variety of corrosion tests. There is a need to be cautious when dealing with this subject and to be wary of various factors that may affect the corrosion mechanism and rate. These factors include: -

- Composition of the starting magnet.
- Surface preparation – roughness, cleanliness.
- Microstructure – surface oxides, dispersion of grain boundary material.
- Surface coating – metallic or polymeric.
- Conditions of the corrosion test – Temperature, pressure, humidity, composition of fluid used.
- Water droplets forming on samples placed in corrosive environments.
- Monitoring of corrosion rate during testing – Simple observation, gravimetrically, loss in magnetic properties, oxygen concentration, onset of detectable corrosion products by EDX or XRD, metallographic cross section (thickness of corroded layer). (Walton, 2002)

Polarisation curves have been investigated for coated and uncoated (recycled and initial NdFeB magnets) salty condition to assess the factors effecting the corrosion rate (Bala et al., 1990; Attannasio et al., 1995; Assiss et al., 1995; Nozieres et al., 1992). However, for the magnets to withstand automotive environments they need to

be protected against humid environments at elevated temperatures. This has led to standard tests such as the autoclave (or pressure cooker test-PCT) which was initially employed by Crucible Corporation to evaluate the long term stability of $SmCo_5$ alloys (Willman et al., (1987). Sueptitz R. et al., 2011) used other solutions such as H_2SO_4 to investigate the effect of corrosion. The corrosion behaviour of uncoated NdFeB permanent magnets in the unmagnetised and magnetised state was studied using a H_2SO_4 solution by potentio-dynamic and potentiostatic polarisation experiments. Depth profiling measurements were carried out on the corroded surfaces. The anodic behaviour was as a result of the corrosion of neodymium and iron and on the influence of the magnetic forces acting on the electrochemical system. (Sueptitz R. et al., 2011).

The anodic polarisation was attributed to the Lorentz force driven convection which enhanced the mass transfer in the electrolyte (Kishioka, S. et al., 1999; and Tang, Y.C. et al., 2003. Costa et al., 2004) observed enhanced dissolution rates of magnetised NdFeB sample in comparison to unmagnetised state when exposed to NaCl solutions for the long-term and showed that the magnetic field effect amount of two time-dependent mechanisms. At the start of the exposure, the corrosion reaction was enhanced by the action of the magnetic field which attracted paramagnetic O_2 molecules of the solution to the magnet surface and increased the cathodic partial reaction rate. After lengthy exposure, the dissolution of the Nd-rich intergranular phase lead to a detachment of $Nd_2Fe_{14}B$ grains from the microstructure. In the case of the magnetised samples, the ferromagnetic grains were magnetically attached to the surface.

10.2 The corrosion effect on mass:

10.2.1 Recycled magnets coated with zinc

Weight measurements of samples coated with zinc were taken at set intervals (a reading is taken every 2 weeks: 336 hours) and the effect of corrosion on the weight and then on the magnetic properties are reported later in this chapter. The table below shows the recordings of mass measurement taken over a period of 3360 hours (20 weeks) of magnets immersed in salty solution (NaCl). This is of particular significance since a major use of NdFeB magnets is in off-shore wind generators and

this involves prolonged exposure to a salt-air environment. The following picture shows how the experiments were carried out:

Figure 10-2: magnets immersed in a NaCl solution in glass tubes.

10.2.1.1 Images before the start of the corrosion testing:

1) Initial material

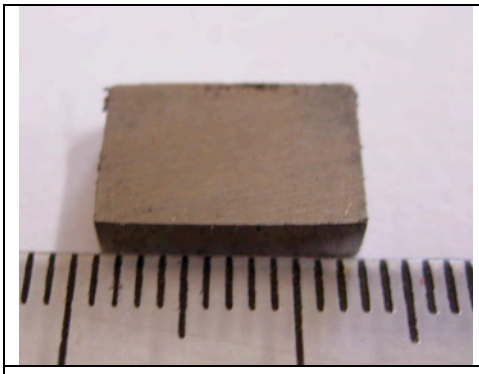	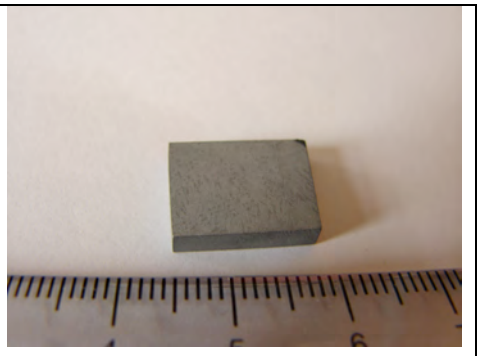
China Uncoated	China – Zinc Coated
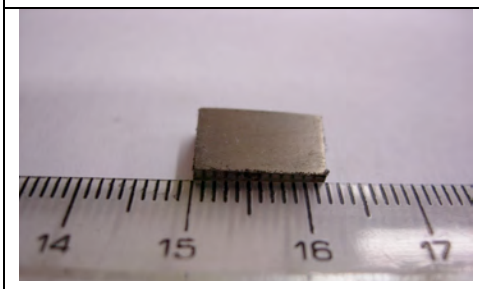	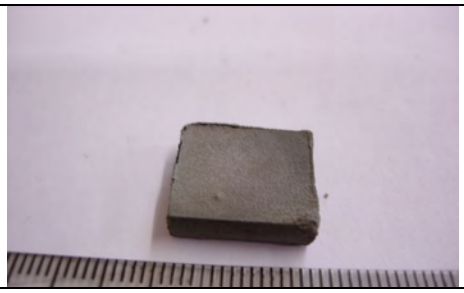
Philips Uncoated	Philips Zinc Coated
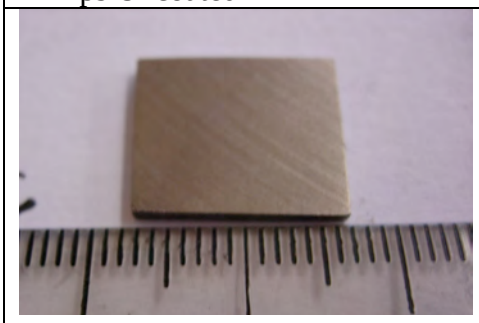	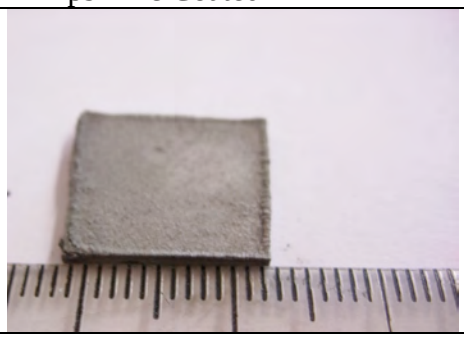
USA Uncoated	USA Zinc Coated
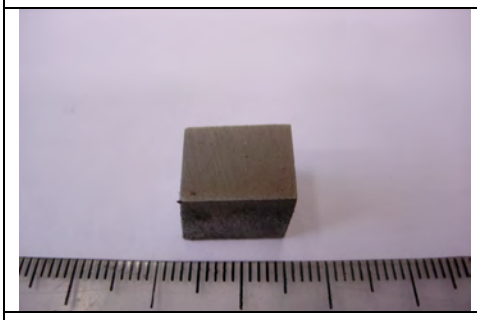	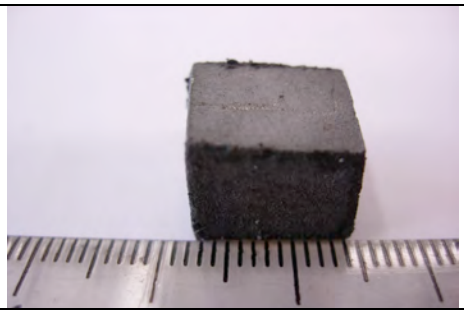
IPM Uncoated	IPM Zinc Coated

Figure 10-3: images of magnets prior to corrosion testing.

2) Recycled magnets:

	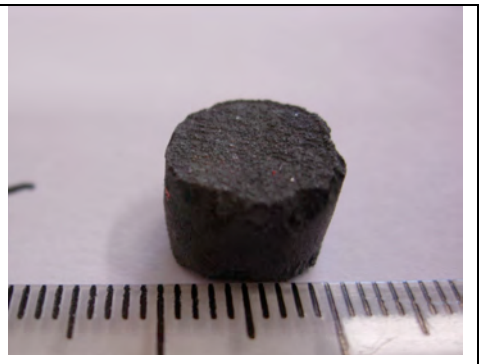
China Uncoated Magnet	China Zn coated Magnet
	
Philips Uncoated Magnet	Philips Zn coated Magnet
	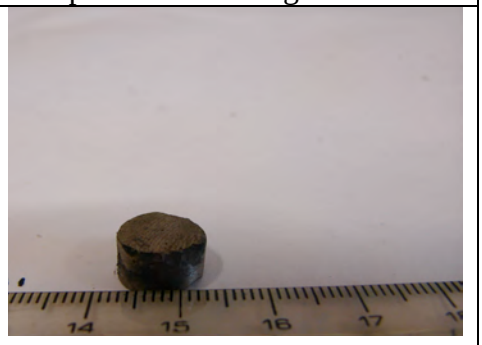
USA Uncoated Magnet	USA magnet Zn coated
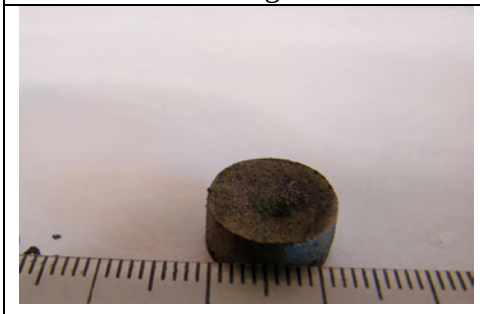	
IPM Uncoated	IPM Zn Coated magnet

Figure 10-4: Images of recycled magnets before corrosion testing.

Images of magnets after 16 weeks: Initial magnets

	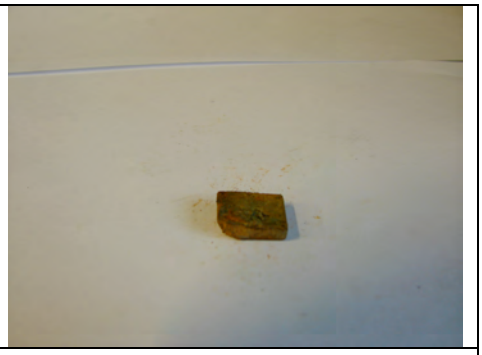
China uncoated	China Zn coated
	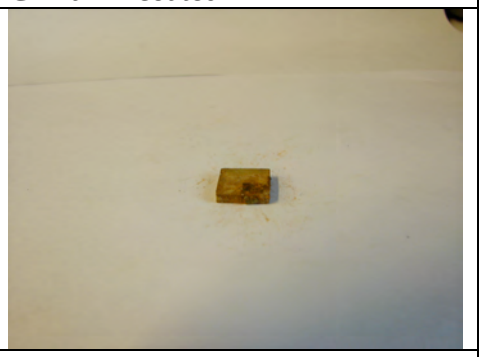
Philips uncoated	Philips Zn coated
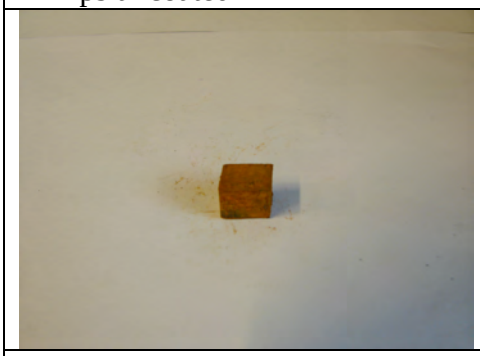	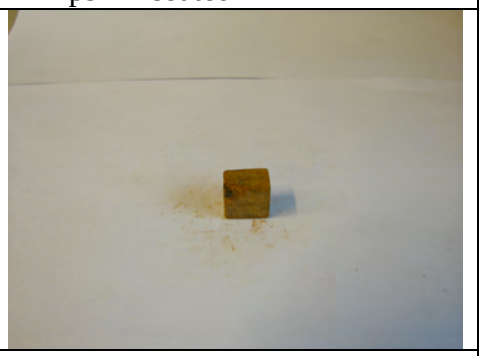
IPM uncoated	IPM zinc coated

Recycled magnets

	
China uncoated	China Zn-coated
	
Philips uncoated	Philips Zn-coated
	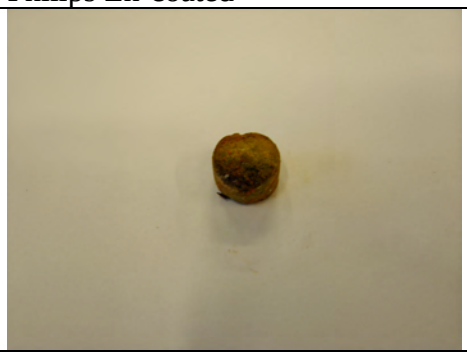
USA uncoated	USA Zn-coated
	
IPM uncoated	IPM Zn coated (destroyed completely)

Figure 10-5: Images of Initial and Recycled magnets after testing (16 weeks).

After 20 weeks: starting materials

	
China uncoated	China Zn-coated
	
Philips uncoated	Philips Zn-coated
	
IPM uncoated	IPM Zn-coated

Figure 10-6A: Initial magnets after testing (20 weeks).

After 20 weeks: Recycled magnets

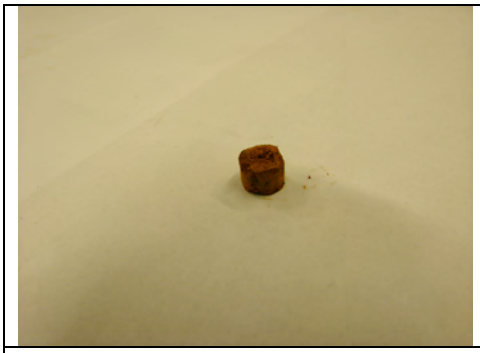	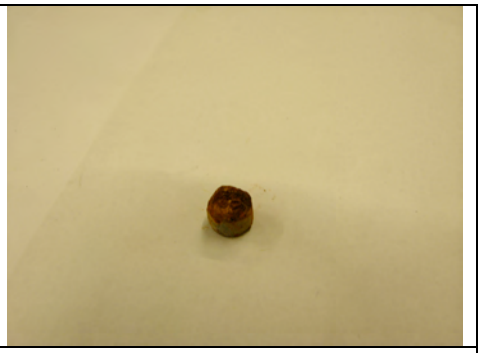
China uncoated	China Zn-coated
	
Philips uncoated	Philips Zn-coated
	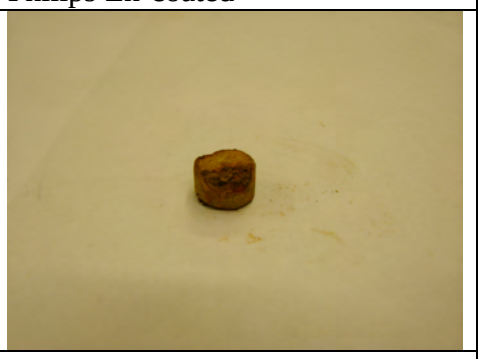
USA uncoated	USA Zn-coated

Figure 10-6B: Images after 20 weeks: Recycled magnets.

Starting materials

	
China uncoated	China Zn-coated
	
Philips uncoated	Philips Zn-coated
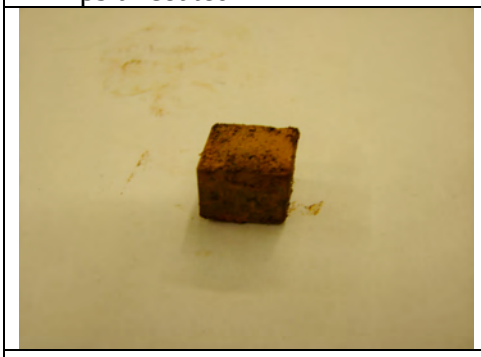	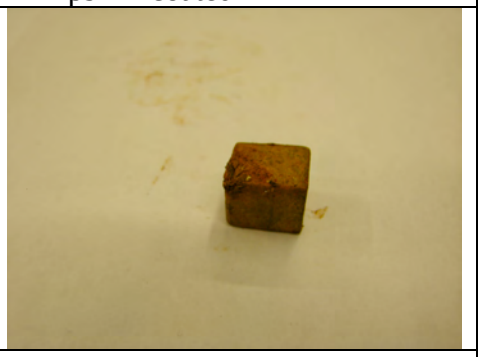
IPM uncoated	IPM Zn-coated

Figure 10-7 Images after 20 weeks: Recycled magnets.

The corrosion progression measurements were taken every 2 weeks and the corrosion images are shown in the following pages for; 2 weeks (336 hrs), 4 weeks, 8 weeks, 12 weeks, 16 weeks and 20 weeks (maximum).

The evidence of craters and pitting is apparent. There are a number of cases of fracture of these magnets. This is due partly to the corrosive environment and the magnets becoming increasingly weak because of the NaCl reaction, as well as the hydrogen effect (HD) and oxygen reaction.

10.3 The corrosion effect on initial magnets' weight: initial magnets:

10.3.1 The effect of corrosion on weight

Each magnet was analysed for the effect of corrosion and compared with other magnets to study the behaviour of each magnet under the same set of conditions:

Each magnet was analysed to study the effect of corrosion and make a comparison with other magnets under the same set of conditions.

The magnets were subjected to a salty environment (3% NaCl). This should indicate the performance of an unprotected and protected (Zn) magnet when subjected to such conditions. All the magnets are in their fully magnetised state.

10.3.1.1 Initial materials: starting with uncoated magnets;

This shows how the initial material behave when subjected to the same corrosive conditions. The following numbered sections present analyses of each magnet under the same corrosive conditions:

1) China magnet:

The following figure (figure 10-8) shows a comparison between uncoated and coated starting material.

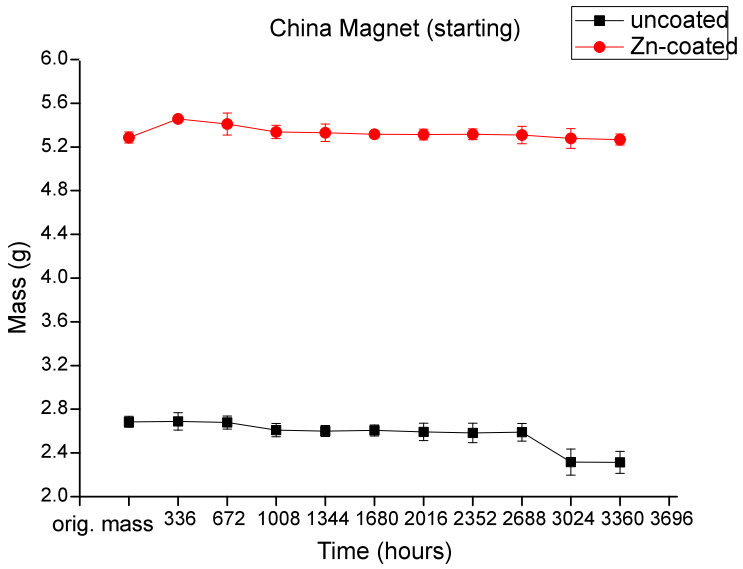

Figure 10-8: 2 China magnets.

The uncoated magnet behaviour indicated a rapid loss in weight after 2688 hours. No evidence of this effect was observed for the coated magnet throughout the test. The rapid loss of weight could be due to the creation of hydrogen and then flaking of the surface material.

2) Philips magnet:

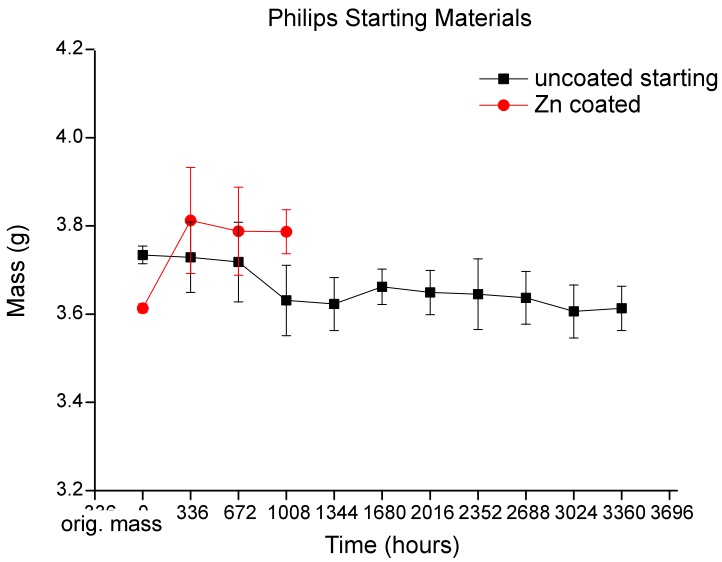

Figure 10-9: 2 Philips magnets.

Limited data on the Zn-coated magnets means that a detailed comparison cannot be made. Loss of weight of the uncoated magnet indicates severe flaking. Weight gain could be due to attraction of the decrepitated powder (see later).

3) USA magnet:

This magnet had been destroyed when placed in permeameter in a magnetic field for the last measurement.

4) IPM magnet;

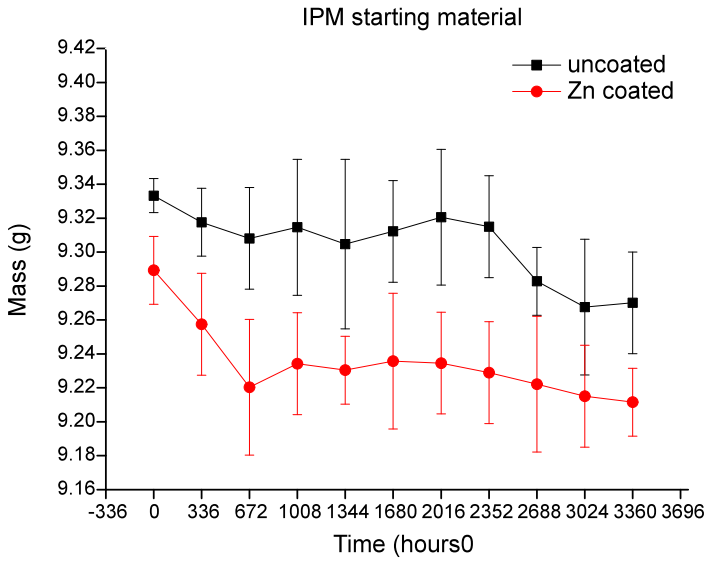

Figure 10-10: 2- IPM magnets.

Similar losses are observed for both the uncoated and coated magnets.

Summary:

The behaviour of the initial magnets (Zn-coated or uncoated) after some period exhibited similar reactions at same time (e.g. IPM magnets at 1680 hours) where there was a gain in weight (from its previous period) in terms of percentage mass change this was 0.4%. However both magnets (Zn-coated and uncoated) behaved in a similar manner. The Chinese magnet (Zn-coated and uncoated) followed a similar trend (weight reduction over the period of the corrosion test). In the case of Philips magnets, the Zn-coated magnet failed after 6 weeks (or 1344 hours) and the uncoated measurements continued throughout the life of the corrosion test. The USA magnets (Zn-coated and uncoated) both were broken after 6 weeks (or 1344 hours). These indicated severe corrosion and significant hydrogen expansion and hence fracture. It will be a good idea to establish that H_2 production is the problem, and it is proposed to study the magnets with XRD and by vacuum desorption linked to a mass spectrometer.

10. 4 Recycled magnets:

1) Recycled China magnets (uncoated):

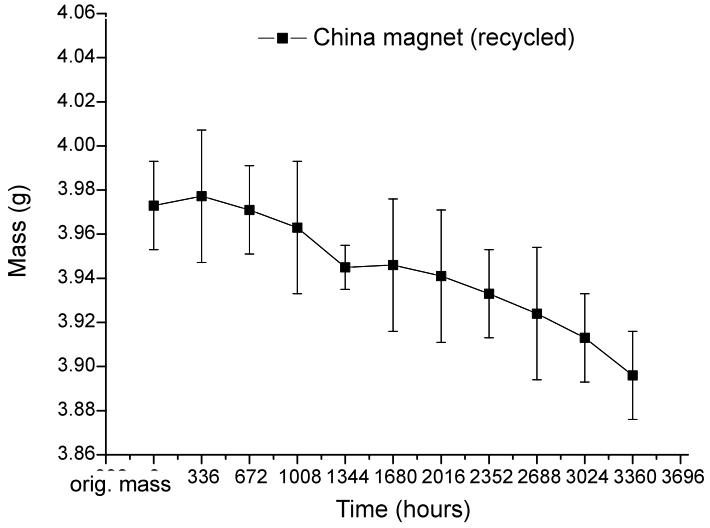

Figure 10-11: China magnet weight change

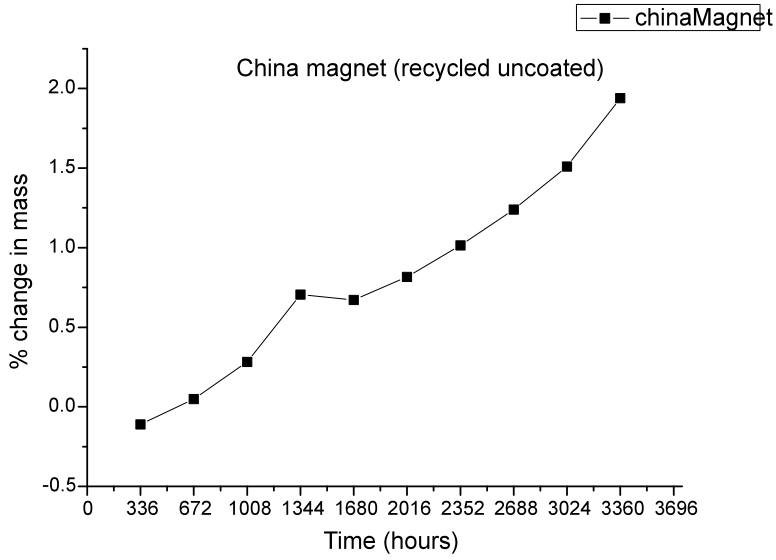

Figure 10-12: percentage loss in weight in China recycled magnet.

This magnet indicated that there is a regular weight loss over the test periods with some evidence of a change of slope in the variation of 1344 hours.

2) Comparison between 2 magnets:

3) Philips magnets

The weight of the following 2 magnets is compared, each against the other shows how their weights change due to the corrosion effect.

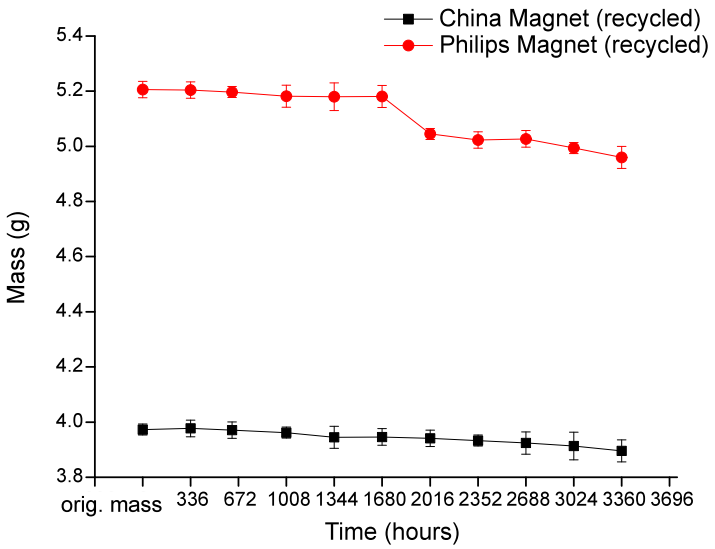

Figure 10-13: China and Philips magnets weight change comparison.

In the above variation, the Philips magnet followed a similar pattern to the China magnet. There is evidence that the magnet decrepitated which is probably due to the hydrogen reaction with the magnet. There is evidence for a discontinuing in the weight loss which occurs around 1680 hours. The origin of this effect requires further investigation.

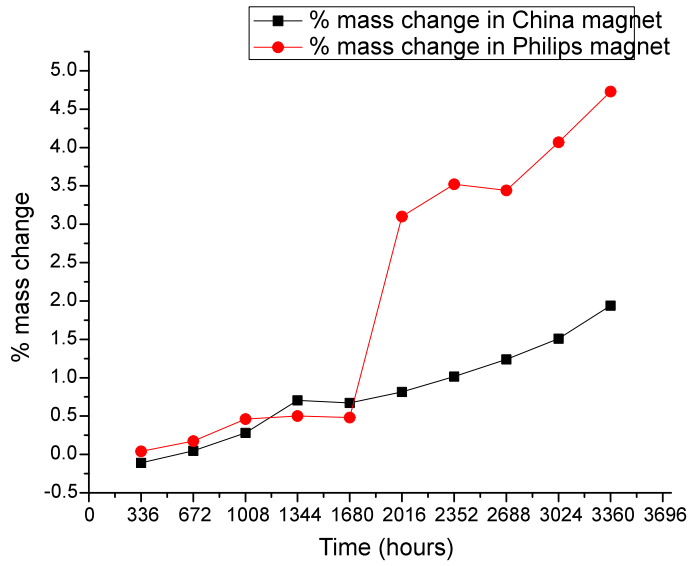

Figure 10-14: % weight loss in recycled Philips and China magnets. There is weight loss after 1680 hours.

For the Philips magnet which is clearly more evident on this plot and occurs around 1680 hours. More detailed measurements are required to establish this effect and to study its precise characteristics

4) USA magnets

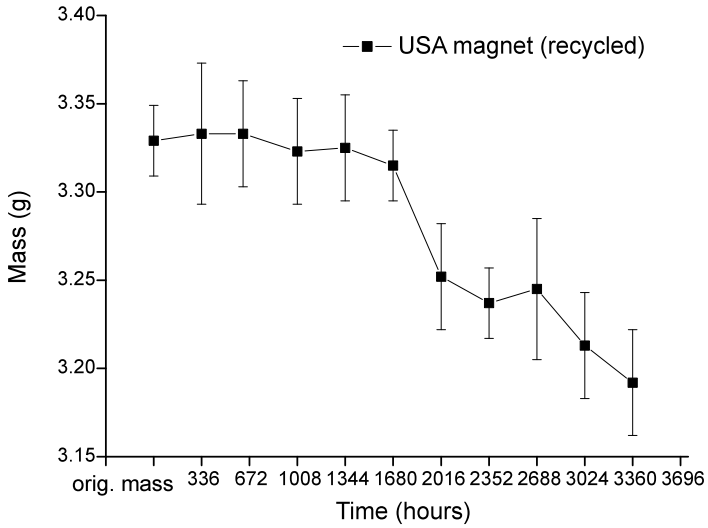

Figure 10-15: USA magnet mass change. Rapid weight loss around 1680 hours is observed and further studies are required to establish if this is a real effect and if so, why it occurs.

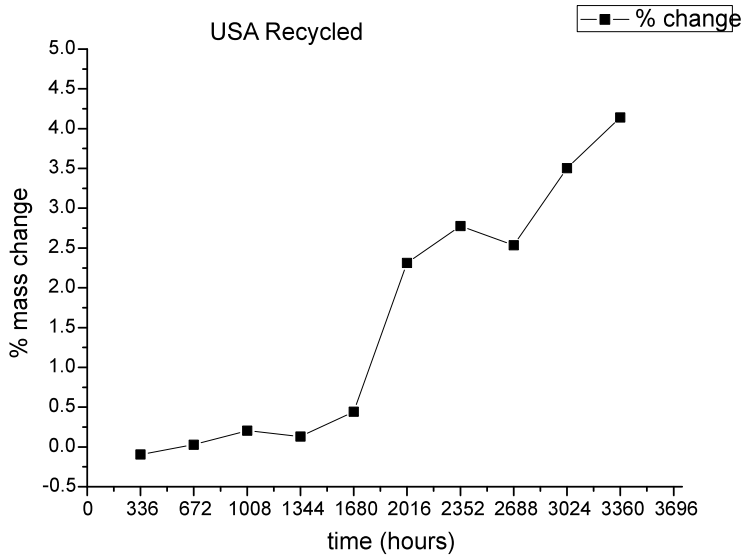

Figure 10-16: percentage weight loss in recycled USA magnet. Exhibits a very similar shape to the plot for the Philips magnet. Both exhibit an accelerated weight loss after 1680 hours.

The corrosion studies on this magnet showed that after 10 weeks there was a large loss in weight and this continued until the test ended.

The following graph shows a lean rare earth magnet and its behaviour when subject to the same conditions of a severe salty environment.

5) IPM magnets

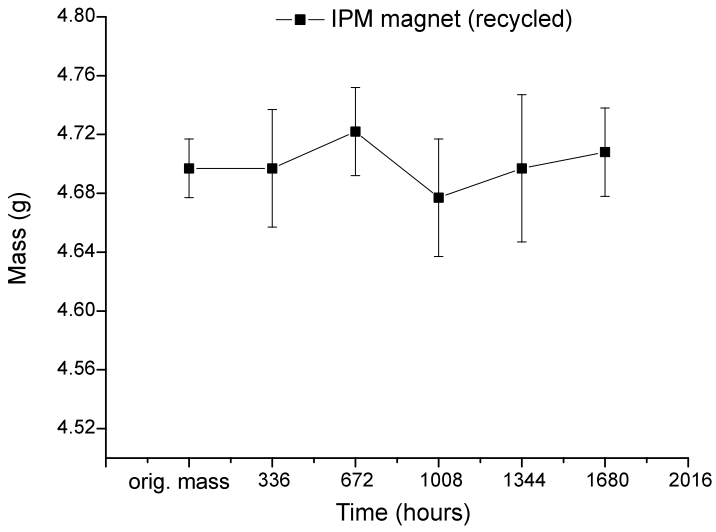

Figure 10-17: IPM magnet mass change. This exhibits only a very small change in weight and taking the error bars into account the behaviour could be said to be invariant.

LPPS-Zn coated recycled magnets:

Similar recycled magnets were subjected to the same conditions (3% salt bath) and were LPPS zinc coated for additional protection. The zinc coating was performed by the LPPS process (see chapter 7 for LPPS process details). This process formed coatings on the NdFeB magnets (at 390 ^{o}C for 2 hours) with a zinc layer thickness of ≈20 μm. Previous work has shown that coatings of this thickness had a better performance in terms of coating adhesion and weight change during previous corrosion tests when compared to the uncoated magnets (Walton et al., 2000).

6) China Zinc coated magnet (recycled):

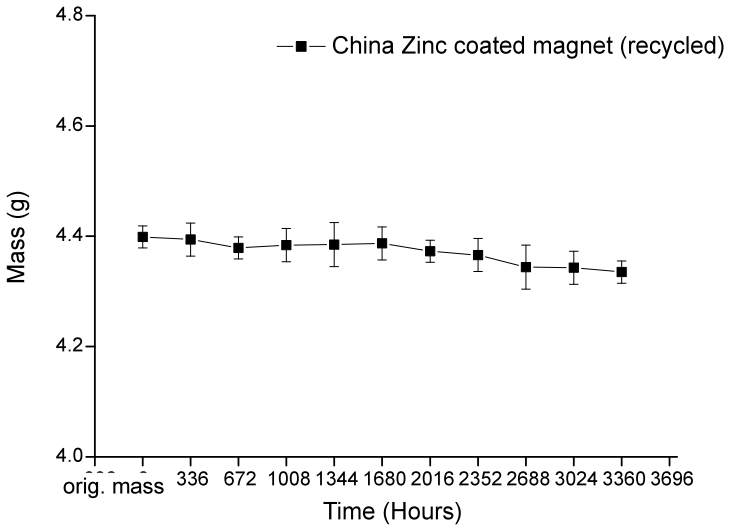

Figure 10-18: China magnet mass change

The addition of the zinc layer had affected the initial performance of this magnet (see figure 10-19). Although the Zn-coating had the effect of apparently enhancing the magnet's corrosion resistance, it lowered the magnetic properties (see later). The weight loss here compared with the original value increased over time and these measurements show that there is a fluctuation in the weight value at certain intervals. This may be explained by the hydrogen decrepitation and oxygen and hydrogen uptake by the magnet. With the salt bath, there is degenerative behaviour due to these uptakes as well as the hydrogen decrepitation which eventually leads to the total loss of the magnet. Images of these magnets are shown previously.

The following graph shows the percentage change in weight in this magnet compared to that of the uncoated magnet:

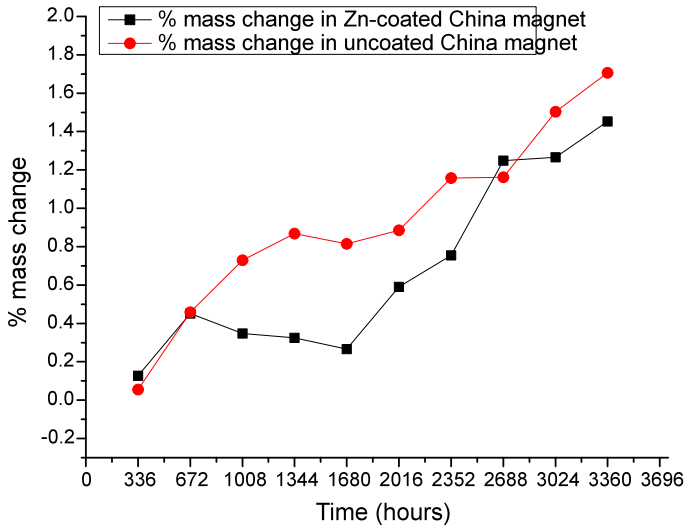

Figure 10-19: showing percentage change in weight in China magnets (Zn-coated and uncoated).

This variation indicates that the Zn coating appears to inhibit the early stages of corrosion but there is again a rapid decrease after around 1680 hours. This seems to be a consistent feature of a large proportion of the magnets. But clearly requires more study to establish if this is a real phenomenon and if established, then the precise nature of this effect.

7) Philips Zinc coated magnet (recycled):

This magnet sustained a more resilient behaviour within a corrosive environment. The weight loss was small in comparison with the previous non-coated magnets. As the corrosion continues with time, the magnet probably absorbs more hydrogen and this would be in agreement with previous authors (Yan et al., 1999). After 16 weeks (2688 hours) there is an increase in the weight which can be attributed to the hydrogen being absorbed by the $Nd_2Fe_{14}B$ phase and the by the Nd-rich phase to form $Nd_2Fe_{14}BH_x$ and NdH_2.

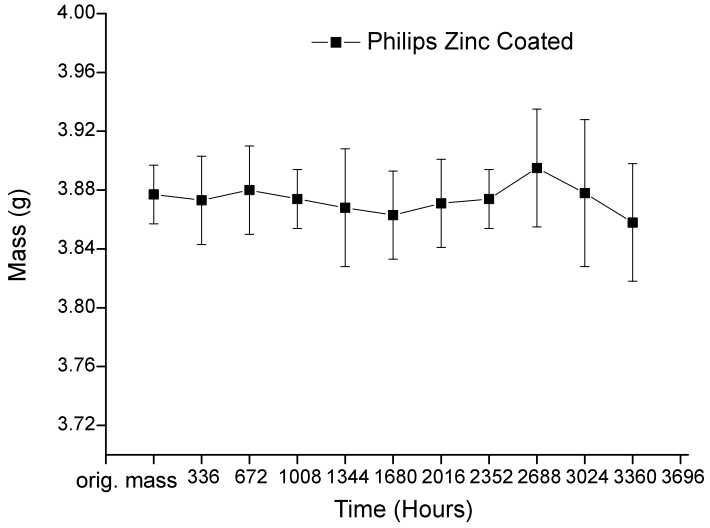

Figure 10-20: Zn-coated, Philips magnet weight change.

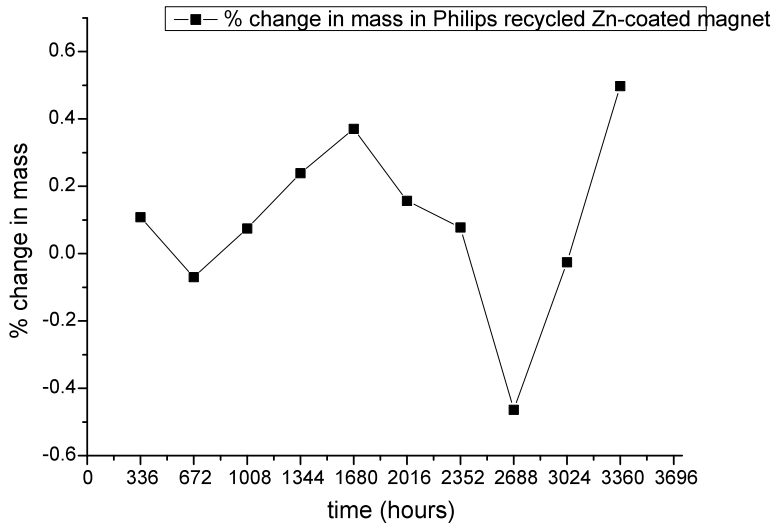

Figure 10-21: % weight change in Recycled Philips Zn-coated magnet. Again there is a possible effect observed at 1680 hours interval. It should be noted, however, that this is a very expanded scale compared with that shown in figure 10-14 and this behaviour shown here can be regarded as essentially invariant.

8) USA Zinc coated magnet (recycled):

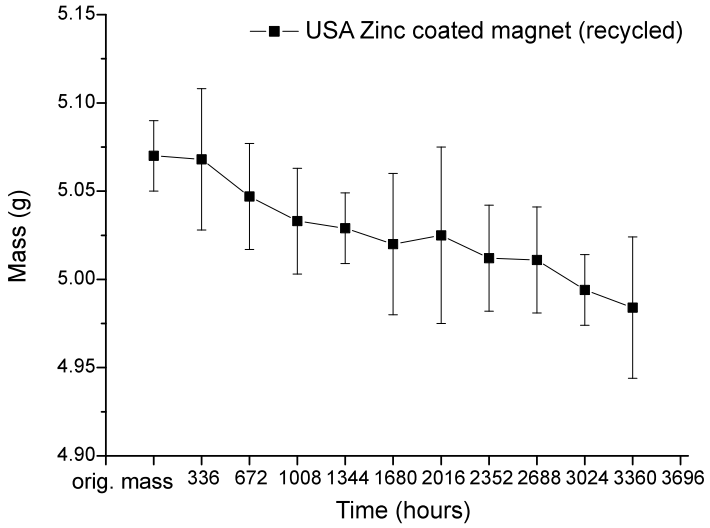

Figure 10-21: Zn-coated USA magnet weight change

The weight of this magnet exhibited a regular decrease over a period 3360 hours and the corrosive environment leads to a total loss of all the magnetic properties (see later). The zinc layer did provide some corrosion protection in the initial stages of the corrosion measurements.

.

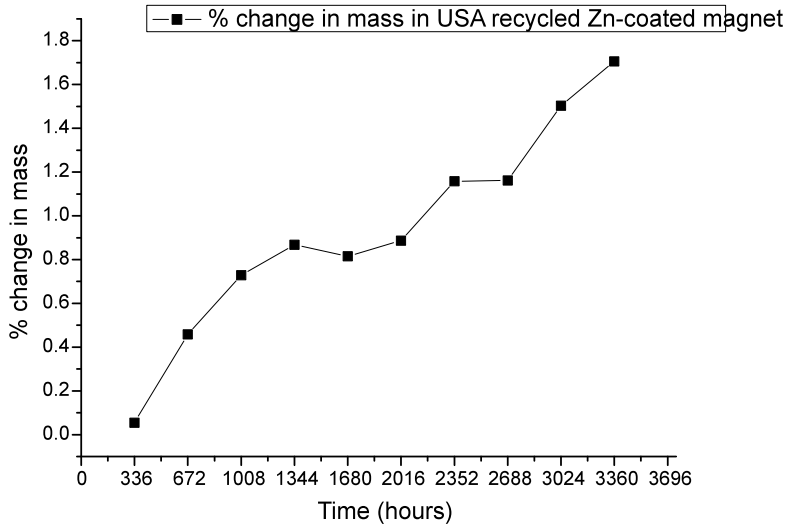

Figure 10-22: percentage weight change in recycled USA Zn-coated magnet.

From figure 10-22 there again appears to be an effect around the 1680 hours period bur further studies are required.

9) IPM Zinc coated magnet (recycled):

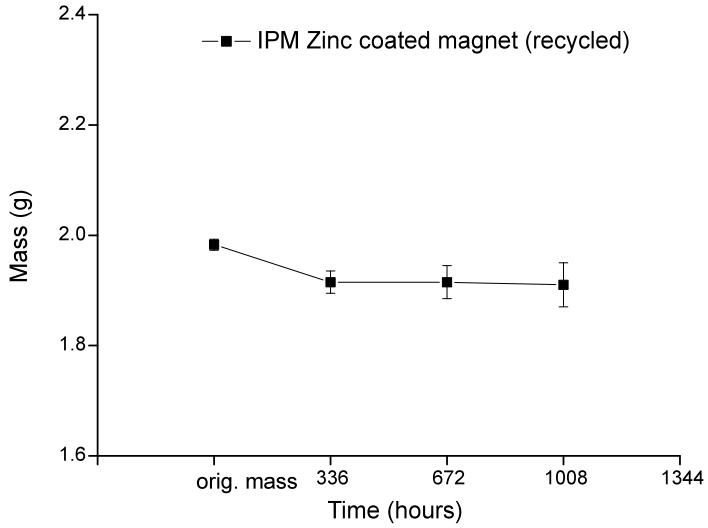

Figure 10-23; IPM zinc coated magnet (recycled).

This magnet was smaller than the rest. It had a thickness of only 4 mm. The graph shows less data than other magnets as this magnet could not withstand the permeameter field and was broken after 3 readings. This magnet was subject to the corrosive environment for over 11 weeks before the permeameter field destroyed it, and the initial results indicate a much higher corrosion stability for this magnet which would be consistent with its other properties.

Summary of gravimetric corrosion studies:

All the magnets exhibited weight loss when submerged in a 3% saline solution. The recycled magnets exhibited greater reactivity and this can be ascribed to their lower densities when compared with those of the initial magnets. The Zn coating provided some initial corrosion resistance but many of the magnets exhibited what appeared to be a an increased weight loss phenomenon after a period of around 1680 hours. The

exact corrosion mechanism has not been established but there is the possibly that the effect is related to the HD-process resulting in the decrepitation of the surface layers.

Overall, the data indicates that NdFeB magnets will require long term protection in a marine environment. Degassing studies should provide useful additional information on the nature of the corrosion process.

The following graphs give an illustration to the percentage mass change in all the magnets (starting and recycled, coated and uncoated)

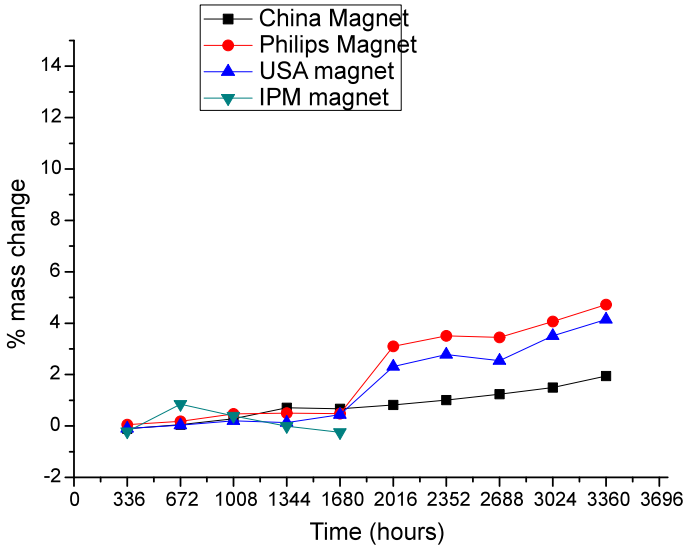

Figure 10-24: percentage weight loss in uncoated recycled magnets

The China, USA and Philips magnets behaved differently from the IPM. The IPM magnet was broken after 8 weeks of being in the saline environment and the Philips and USA magnets presented an erratic behaviour and there was evidence that the magnets had swelled up, consistent with extensive hydrogen absorption.

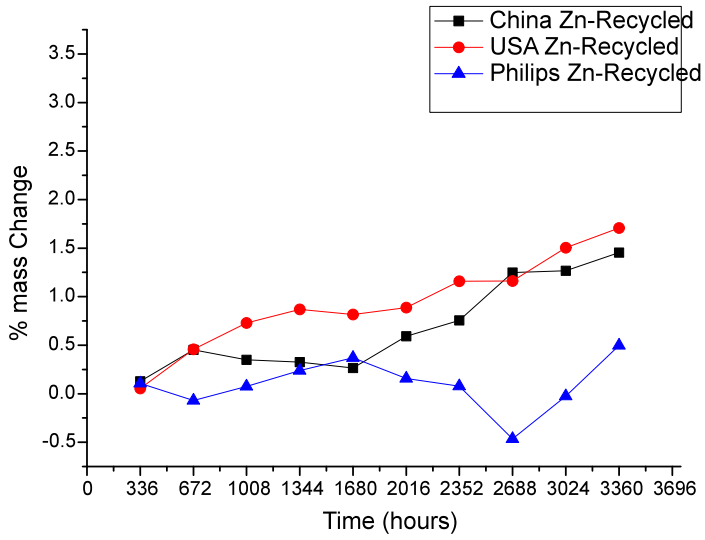

Figure10-25: Percentage mass change in Zn coated recycled magnet

The Philips magnet, exhibited an inconsistent behaviour, unlike the other magnets. Overall, there is a significant reduction in the percentage losses compared with the uncoated magnets but there is evidence of slow corrosion of these magnets in the saline conditions.

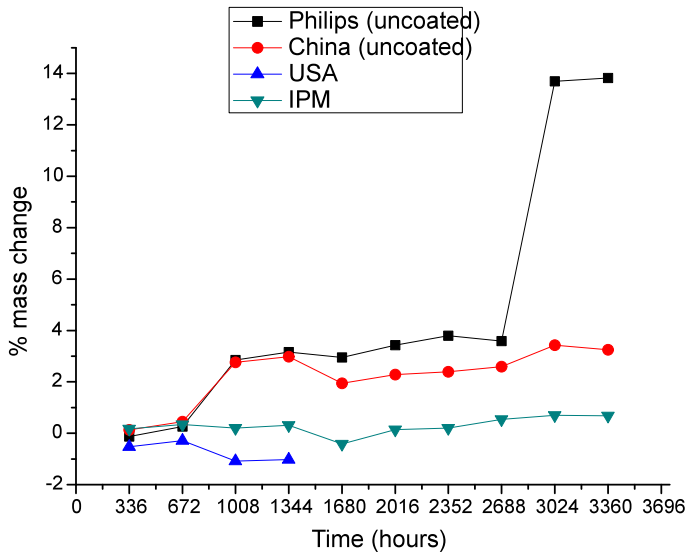

Figure 10-26: Uncoated (starting material) magnets percentage weight change.

The USA magnet was broken after 8 weeks. The size of the magnets led to its destruction as it could not withstand the effect of the magnetic field of the permeameter. The Philips magnet again behaved erratically after around 16 weeks and indicated that the magnet had lost a great deal of weight. The IPM magnet continued to resist the saline corrosive environment and maintained good magnetic properties (see later) until the test was terminated. This emphasise the importance of the initial state of the magnet in terms of its density.

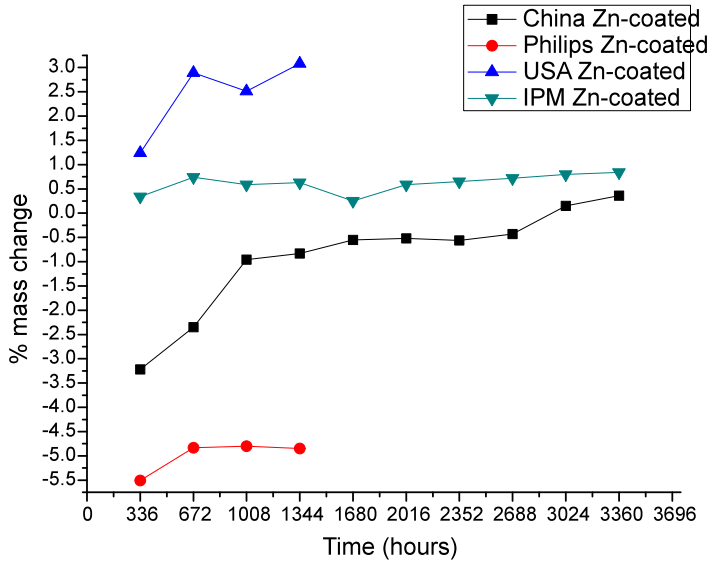

Figure 10-27: Percentage weight change in all four (starting material) magnets (Zn-coated)

10.5 The effect of exposure of magnets to saline liquid corrosion on the magnetic properties

The corrosion study was carried out on using a direct comparison between the starting material which is divided into 2 groups: uncoated and zinc coated. The initial magnetic properties of the starting materials prior to corrosion testing (original magnets) are given in table 10-1:

10.5.1 Initial magnetic properties of initial material before the corrosion studies:

Table 10-1: Initial magnetic properties of initial material:

Magnet	Br (mT)	$_jH_c$ (kA/m)	BH_{max}
China Uncoated	1248	1219	296
China Zn-Coated	1011	1188	191
Philips Uncoated	1123	1020	237
Philips Zn-Coated	1100	1087	229
USA Uncoated	1238	1024	292
USA Zn-Coated	948	957	164
IPM Uncoated	1412	831	376
IPM Zn-Coated	1290	771	308

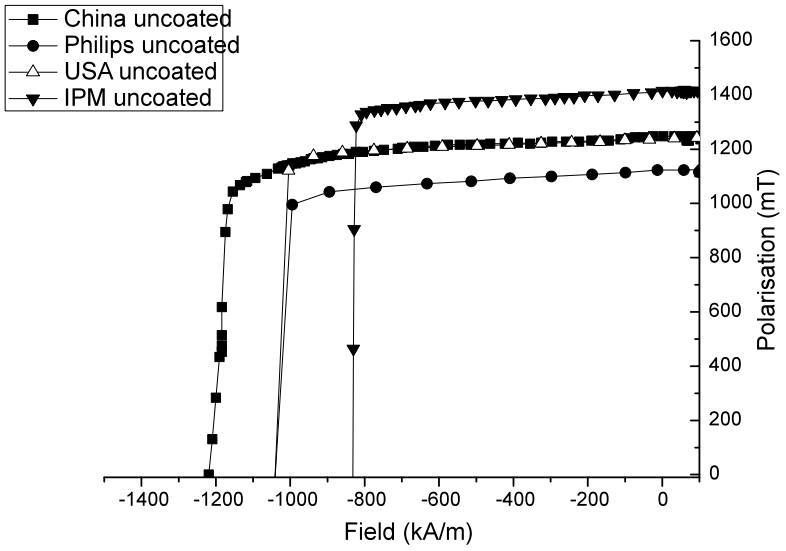

Figure 10-28: Hysteresis loops of uncoated initial material of all magnets (uncoated).

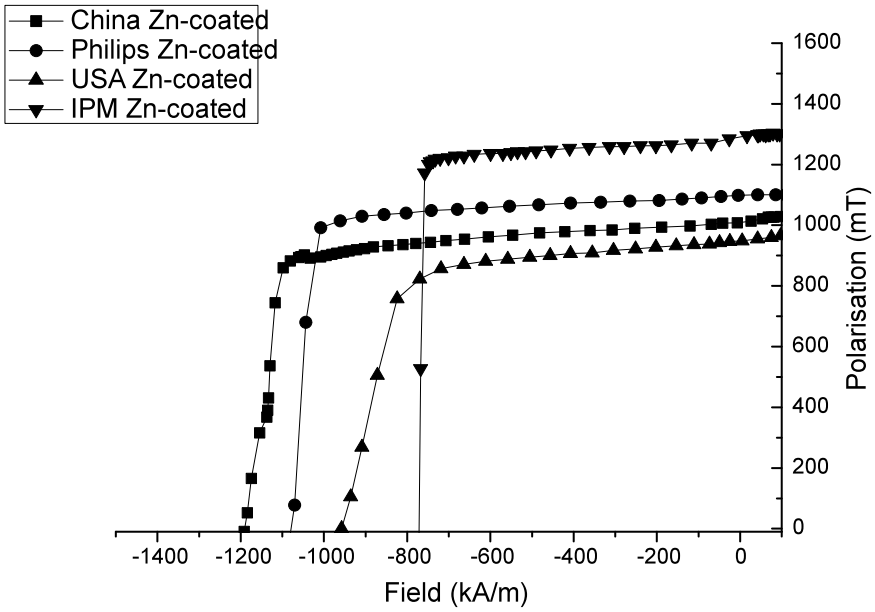

Figure 10-29: Hysteresis loops of coated of initial material of all magnets (Zn-coated)

10.5.2 Recycled magnets initial magnetic properties prior to corrosion testing:

Table 10-2: Magnetic properties before corrosion.

Magnet	Br (mT)	$_jH_c$ (kA/m)	BH_{max}
China Uncoated	1157	966	246
China Zn-Coated	1028	854	186
Philips Uncoated	1178	586	249
Philips Zn-Coated	1177	603	244
USA Uncoated	1195	604	250
USA Zn-Coated	1091	503	198
IPM Uncoated	1184	530	223
IPM Zn-Coated	742	342	33

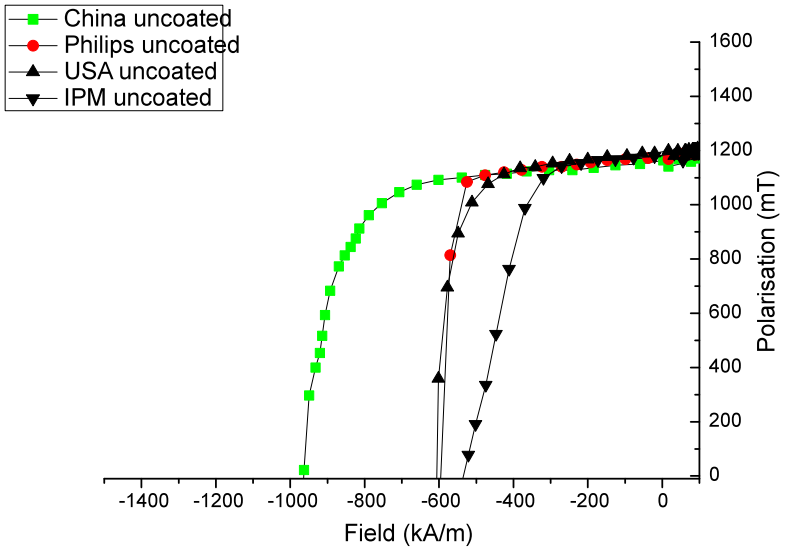

Figure 10-30: Recycled magnets uncoated.

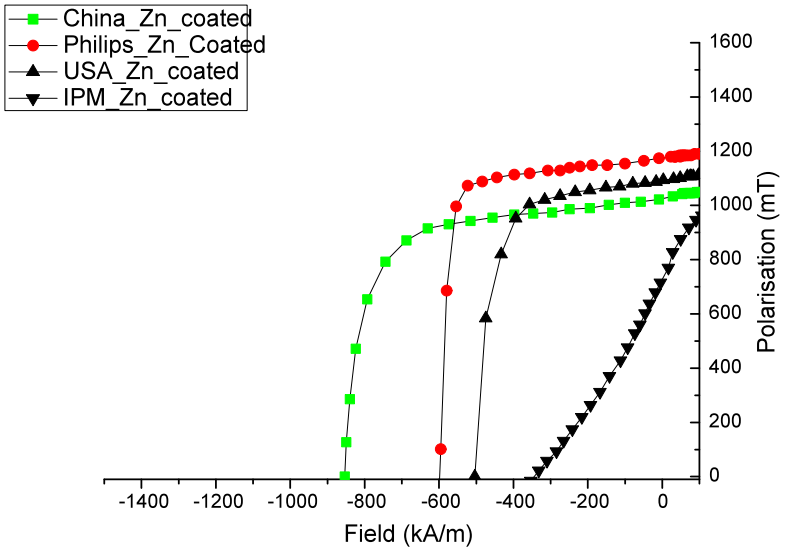

Figure 10-31: Recycled magnets Zinc coated.

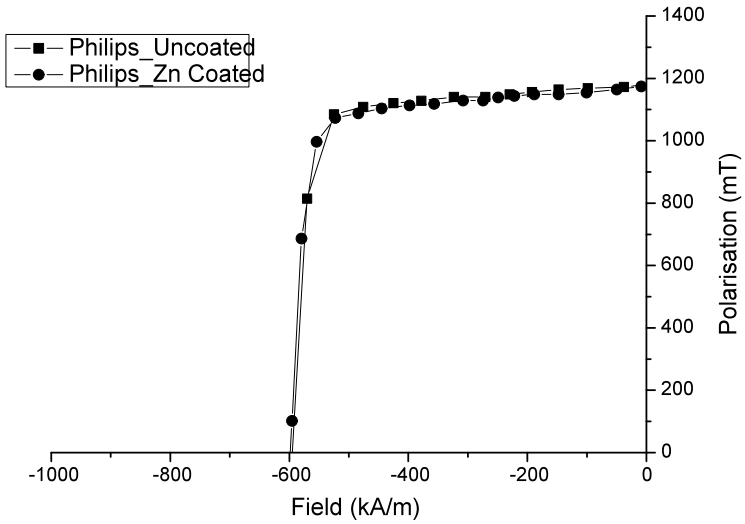

Figure 10-32: Initial comparison between Uncoated and Zn coated Philips magnets.

These magnetic properties of zinc coated Philips magnets were closely similar to those of the uncoated magnet, and hence it appeared that the zinc coated layer on the Philips magnet did not have any detrimental effect on its magnetic properties. This is not so for the Zn-coated IPM magnet (see figure 10-31)

General comments on the magnetic measurements conducted during corrosion trials

The various samples are shown in figure 11-3 and 11-4. The samples were immersed in the aqueous saline solution (3%) and in the magnetised state they were removed at regular intervals, dried and measured in the permeameter (see chapter 8). After each measurement, the samples were re-immersed in the saline solution. It should be noted that, as the corrosion trials progressed, the surface of the magnets become progressively more irregular and there would be dimensional changes associated with the corrosion process.

These changes will affect the accuracy of the permeameter measurements and material may will be removed from the surface of the magnets during the magnetisation process. The magnetic measurements, therefore, provide a general indication of changes during the corrosion process but some of the details may well be a consequence of the measurement process.

It should also be noted that only up to 336 hours would the samples be in the magnetised state and subsequently apart from some residual magnetism, they would be as the demagnetised condition. This could well have an important bearing on the corrosion rates reported in this work and will be the subject of further investigation.

10.6 The effect of corrosion on the magnetic properties.

Introduction:

The following section will examine the effect of corrosion on the magnetic properties. The magnets have been studied and the magnetic properties are shown in the following graphs. Each initial material will be discussed and compared with the corresponding recycled magnets and provide an indication of how the NaCl solution affected the magnetic properties.

10.6.1 Initial material (China magnets):

10.6.1.1 The effect of corrosion on the values of BH_{max}:

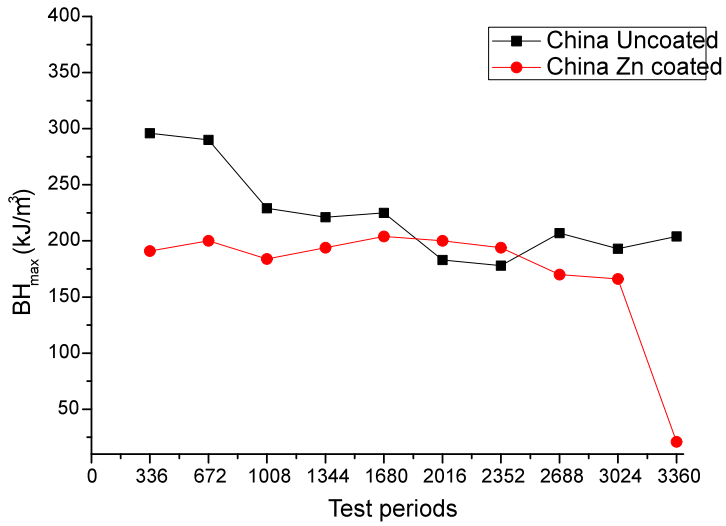

Figure 10-33: Corrosion effect on (BH)max.

Zn coated BHmax results indicated that these magnets may be more prone to corrosion than the uncoated magnets, but the comments made at the beginning of this section should also be noted.

10.6.1.2 The effect of corrosion on the remanence (B_r):

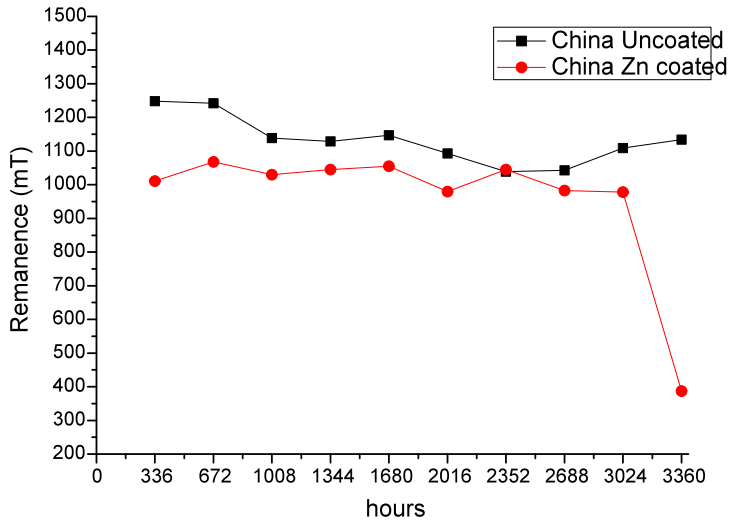

Figure 10-35: Corrosion effect on Br.

10.6.1.3 The effect of corrosion on the Coercivity (jHc):

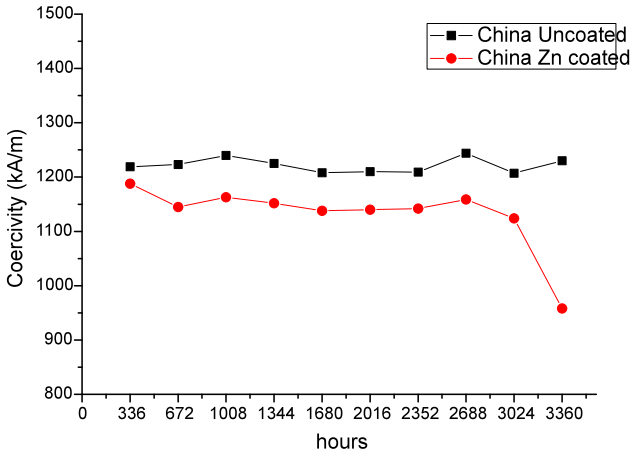

Figure 10-34: Corrosion effect on Hcj.

As can be seen from the above graph, as expected, the remanence decreased over the period of the corrosion testing (20 weeks). This behaviour is shown in both graphs for the remanence and BHmax. The coercivity exhibited a steady decline over the corrosion testing period with a dramatic drop of around 400 kA/m in coercivity after an exposure of 2016 hours exposure.

10.6.2 Recycled magnets (China):

10.6.2.1 The effect of corrosion on the BH_{max}:

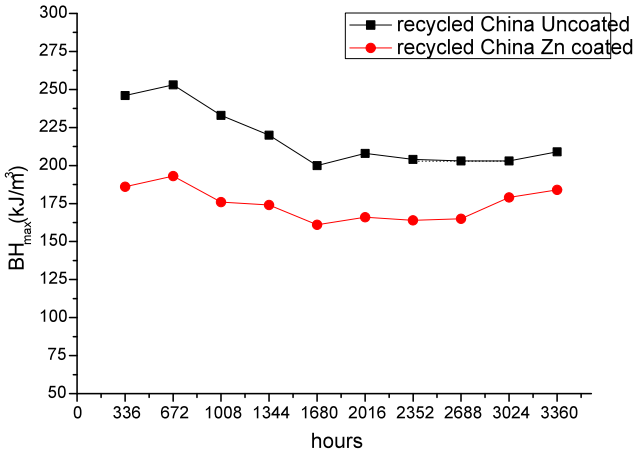

Figure 10-36: Corrosion effect on (BH)max.

10.6.2.2 The effect of corrosion on the remanence (B_r):

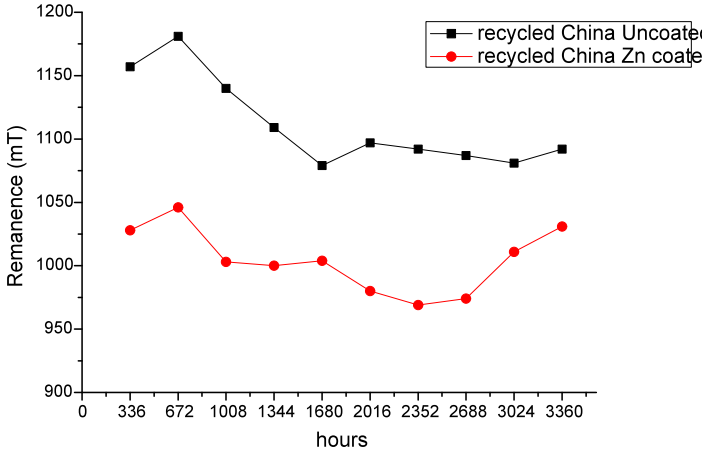

Figure 10-37: Corrosion effect on Br.

10.6.2.3 The effect of corrosion on coercivity (jHc):

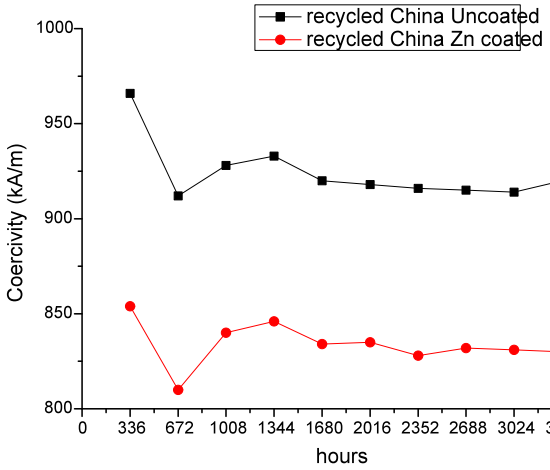

Figure 10-38: Corrosion effect on Hcj.

As the corrosion period increases, the remanence decreases but there appears to be a steeper fall for the uncoated magnet. There is, however, a small increase towards the end of the test period. This can be attributed to the hydrogen uptake and hence a lattice expansion. The coercivity exhibited a rapid initial fall and then removed relatively steady throughout.

10.7 The effect of corrosion on initial Philips magnets

10.7.1 The effect of corrosion on coercivity (jHc):

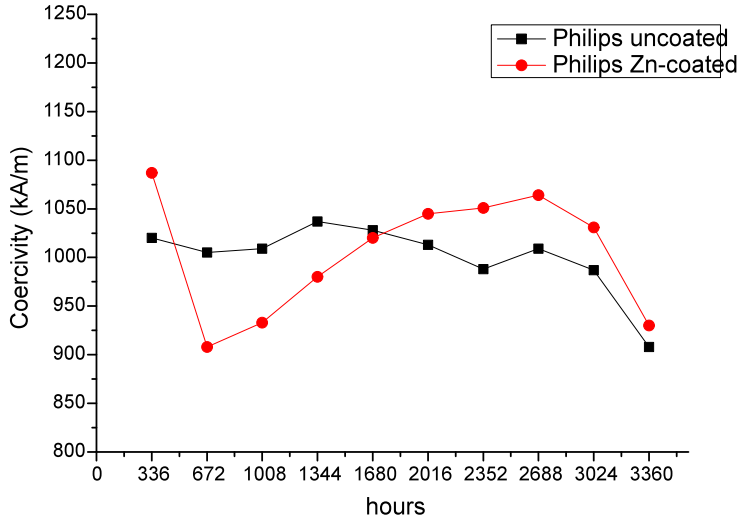

Figure 10-38: Corrosion effect on $_jH_c$.

10.7.2 The effect of corrosion on BHmax:

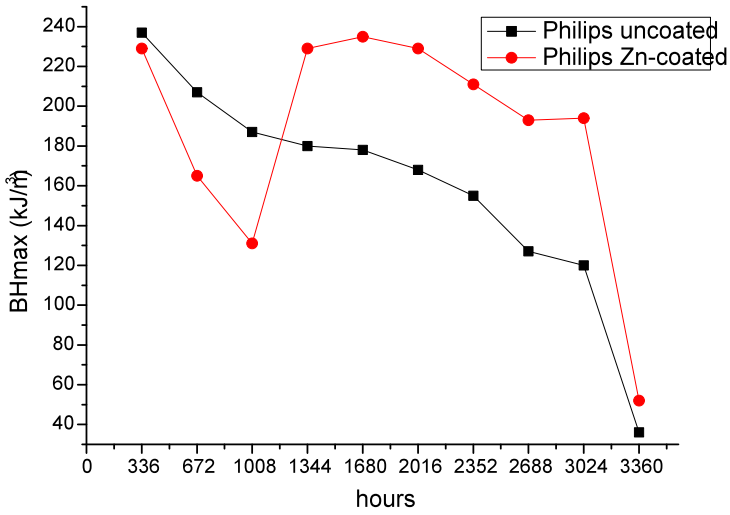

Figure 10-39: Corrosion effect on BHmax.

10.7.3 The effect of corrosion on remanence (Br):

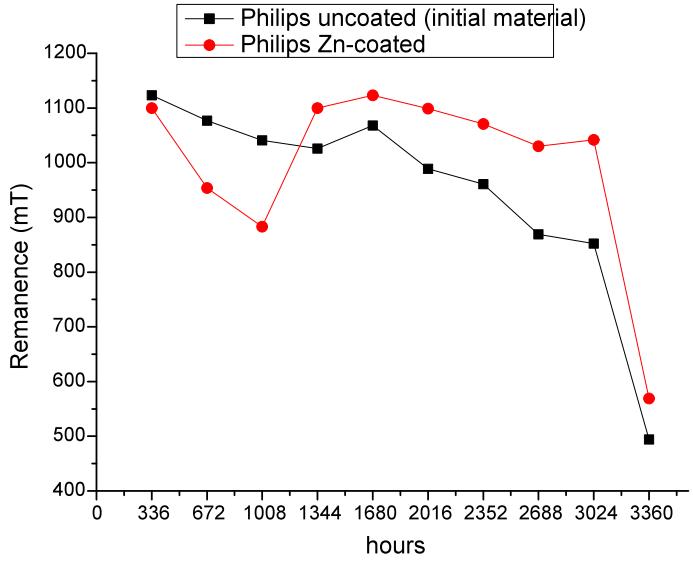

Figure 10-40: Corrosion effect on Br.

The zinc coated magnets exhibited consistently higher Br and (BH)max values after an initial steep fall. As the corrosion period continued, the magnetic properties declined steeply until the magnet reached its lowest value of remanence as indicated in the above graph. These effects are consistent with the progressive influence of hydrogen on the properties and it would be interesting to study the effect of vacuum degassing on this behaviour.

10.8 The effect of corrosion on recycled Philips magnets

10.8.1 The effect of corrosion on the Remanence (Br):

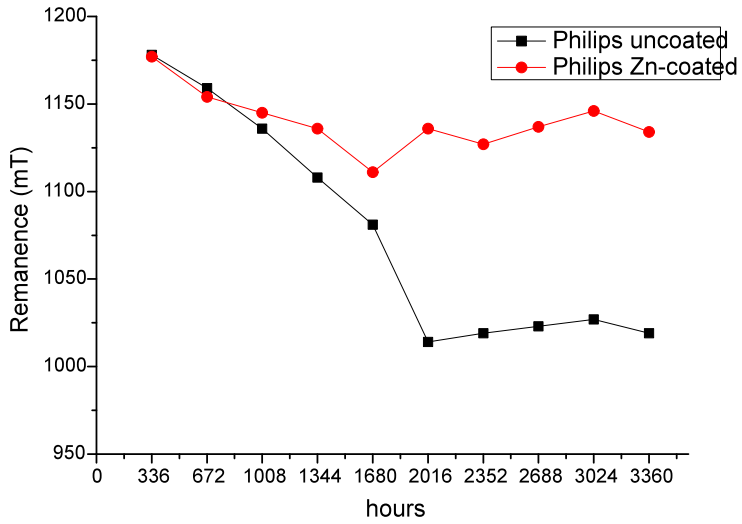

Figure 10-41: Shows the effect of corrosion on the Remanence (Br).

10.8.2 The effect of corrosion on the Coercivity (jHc):

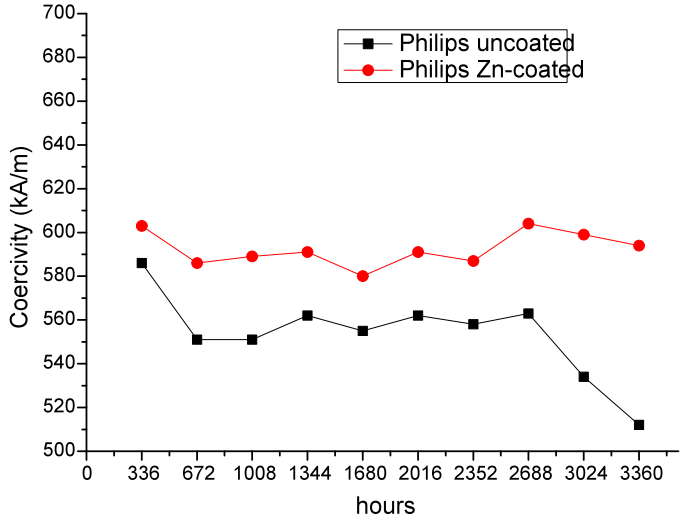

Figure 10-42: Shows the effect of corrosion on Coercivity (jHc)

10.8.3 The effect of corrosion on the BHmax:

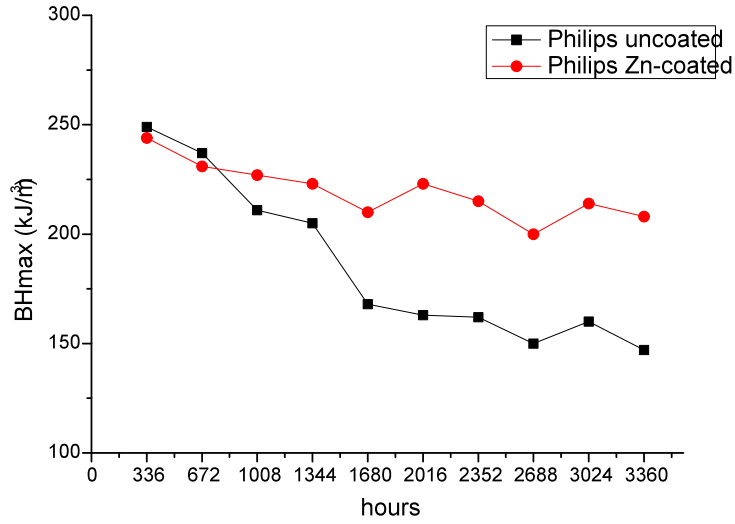

Figure 10-43: Shows the effect of corrosion on BHmax.

This data indicates an improved performance for the Zn-coated magnet and much smaller changes than in the previous case. Again it would be interesting to study the effect of vacuum degassing to see if any of these changes reversible.

10.9 The effect of corrosion on the initial USA magnet

10.9.1 The effect of corrosion on the Br:

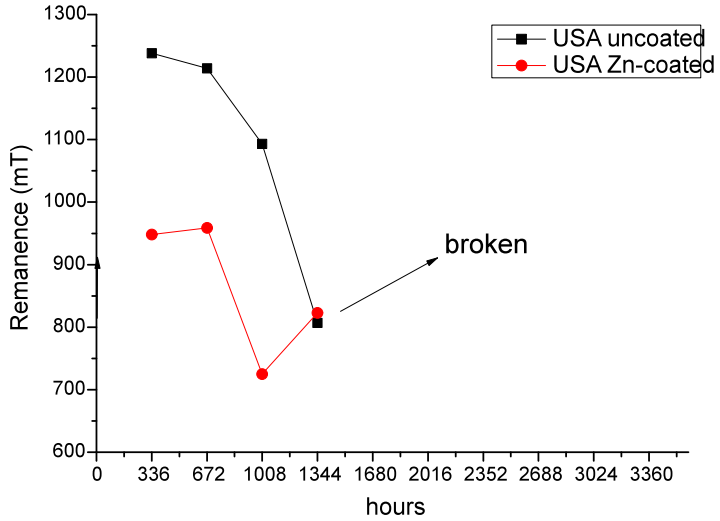

Figure 10-44: Shows the effect of corrosion on B_r.

10.9.2 The effect of corrosion on the Coercivity:

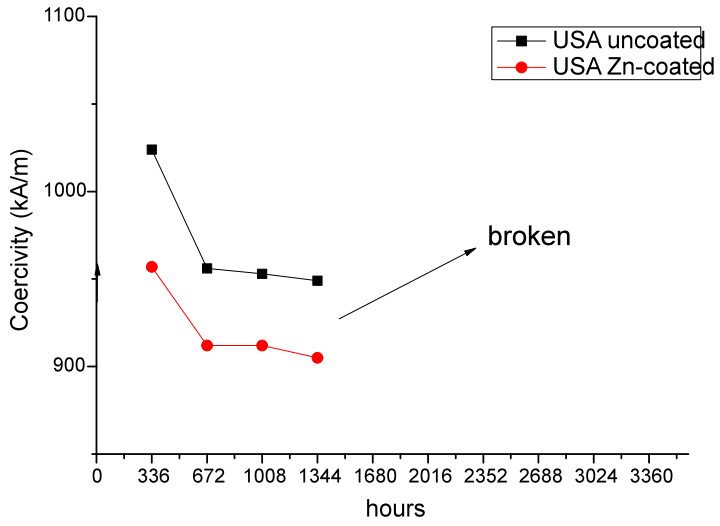

Figure 10-45: Shows the effect of corrosion on Hcj.

10.9.3 The effect of corrosion on the BHmax:

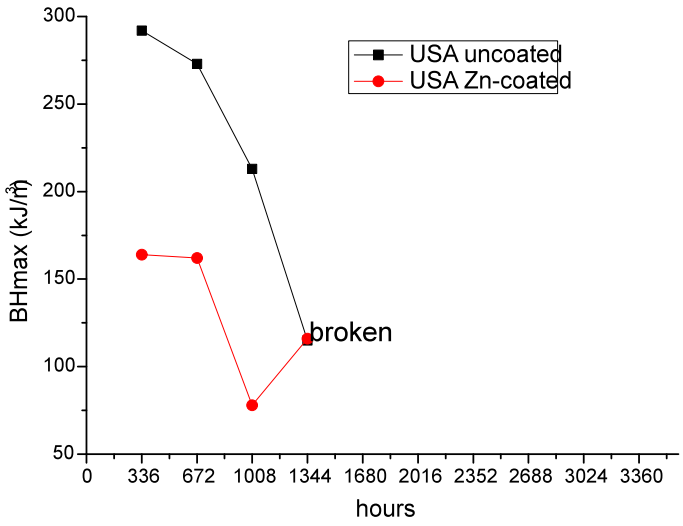

Figure 10-46: Shows the effect of corrosion on BHmax.

The exposure to the saline solution has rapidly affects the magnetic properties with a rapid decline in Br, (BH)max and Hcj

10.10 The effect of corrosion on the recycled USA magnets.

10.10.1 The effect on Br, coercivity and BHmax:

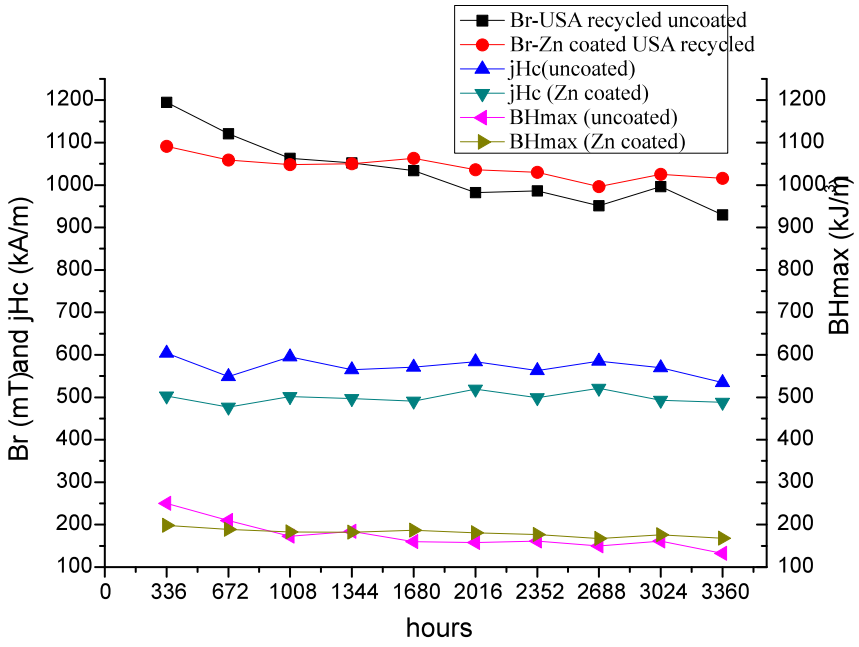

Figure 10-47: Shows the corrosion effect on Br, coercivity and BHmax.

The rapid decline in the properties of the initial magnet is not observed in the case of the recycled magnet, either coated or uncoated.

10.11 The effect of corrosion on the IPM initial magnet.

10.11.1 The effect on Br, coercivity and BHmax:

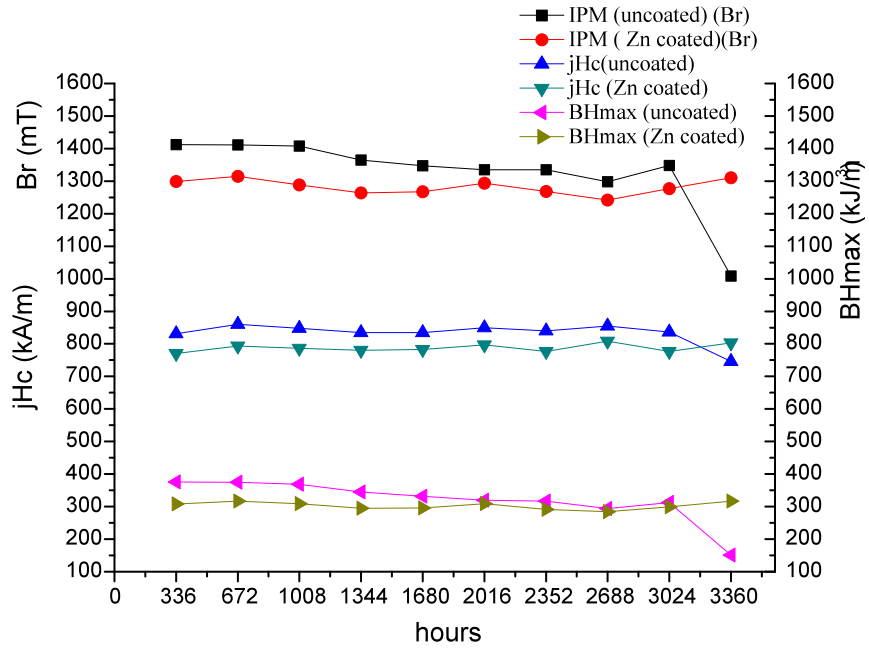

Figure 10-48: Shows the corrosion effect on Br, coercivity and BHmax

This magnet possessed by far the best initial magnet properties compared with the other initial and recycled magnets. It also shows a greater resilience and resistance to salt-bath corrosion. This magnet had an energy product loss of 22% and 8% (uncoated and Zn coated respectively) over the testing period of 24 weeks. It would be interesting and informative to study the behaviour of this magnet after vacuum degassing. Zn-coating did not appear to impart any additional corrosion protection until after 3360 hours, there appeared to be a more rapid fall in the properties of the uncoated magnet. This effect requires further investigation.

10.12 The effect of corrosion on the IPM recycled magnet

10.12.1 The effect on Br, coercivity and BHmax:

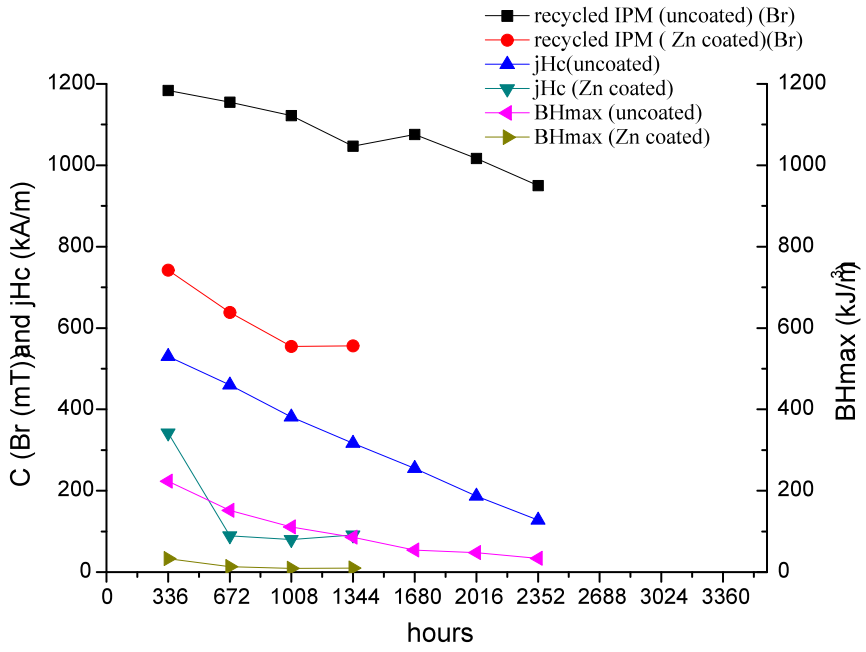

Figure 10-49: shows the corrosion effect on the IPM magnetic properties.

This magnet deterioted more rapidly in comparison with the behaviour of the initial material (see figure 10-48). This would be due to its size as it was much thinner than the initial material (5mm). The corrosive environment was very aggressive etched its way into the surface and then the substrate of the magnet causing disintegration of the grains and ultimately the loss of the magnetic properties. The energy product loss over the testing period is 85% and 73% (uncoated and Zn coated respectively). This shows that although the Zn coating affects the magnetic properties, it does provide some protection against a corrosive environment. The coercivity ($_jH_c$) exhibited a similar loss (76% uncoated & 77% Zn coated). Finally, this magnet was broken as it could not withstand the effect of the magnetic field of the permeameter.

10.13 Conclusions:

All the magnets consisted of Nd-rich material at the grain boundaries and a matrix phase of $Nd_2Fe_{14}B$. The Nd-rich material contains around 6 at% Fe in solution. The magnets had corroded rapidly under the present conditions and the magnets probably contained significant amounts of hydrogen as a result of the corrosion process. It can

be assumed that the hydrogen dissolved in the $Nd_2Fe_{14}B$ phase and existed as $NdH_{2.7}$ at the grain boundaries. These suppositions should be tested by XRD and degassing studies linked to mass-spectrometer.

The Nd-rich areas in these magnets provided an anodic reaction with water with the formation of $Nd(OH)_3$ along with some other corroded iron products. As the water evaporates over a period of time, the saline solution becomes more concentrated and more effective in etching into the magnet's surface. The matrix phase ($Nd_2Fe_{14}B$) provides the cathode where, the hydrogen (as H^+ ions) is absorbed by this phase and by the Nd-rich material resulting in the formation of $Nd_2Fe_{14}BH_x$ and $NdH_{2.7}$ (where x ~ 3).

The coupling effects of the lattice expansion of the phase $Nd_2Fe_{14}BH_x$ and the volume increase on formation of $Nd(OH)_3$, can lead to the eventual destruction of the magnet. All these effects also lead to a deterioration in the magnetic properties.

In the case of the Zn-coated magnets, there could be an additional galvanic coupling effect which could, in some circumstances, accelerate corrosion in salt solution. . (This effect would be exacerbated if there is incomplete coverage of the Zn coating). The zinc also reacts readily with oxygen to produce ZnO and this would provide additional protection.

A confocal study (S. Adrwish to be published) of the magnet surfaces as a result of the corrosion process illustrates very clearly the irregular nature of these surfaces. This means that the magnetic measurements should be regarded with some caution (particularly at the later stages of corrosion process) as it is not clear how much actively magnetic material is contributing towards Br and (BH)max values. Further studies need to be undertaken in order to evaluate the precise nature of the corrosion process. It is clear however, that the initial composition and density of the magnet are of particular significance (see data on IPM magnet) and, in the long term exposure of the magnets to a saline (marine) environment is likely to cause stability problems.

11 General Conclusions

- Some of the recycled magnets have produced magnetic properties close to those of the initial magnets. Long milling time and/or higher oxygen content produced poor values for (BH)max, Hcj and Br. Half hour milling time on the other hand, for the recycled USA and China magnets produced good values of (BH)max and Br. However, the Philips and the Neomax magnets gave rather poor magnetic properties after half hour milling and longer times were required. This also indicates that the 3 h sintering process is not applicable to the Philips, or Neomax magnets due to the oxygen uptake and the oxygen content relative to the RE content.

- By ICP, it was shown that the China magnet had a much higher content of Dy than the others and this resulted in it having a much higher coercivity, but a reduced Br due to anti-coupling of the Dy atoms.

- As expected, the lower the content of the RE (namely Nd) the higher is the Br. This is true in the case of the USA and IPM magnets.

- Lower oxygen content can affect the magnetic properties and the grain size and there is evidence that a certain oxide content has the beneficial effect of minimising the grain size.

- Milling time and oxygen content are closely related in the sense that the longer the milling the greater is the oxygen content and this can be detrimental to the sintering process and hence to the density and the magnetic properties of the sintered magnet.

- The ½ hour milling time proved to be the best compromise where there was sufficient powder packing but what is more important is the minimisation of the oxygen contamination.

- The best magnetic properties were produced by the IPM (Japanese) magnets and the China magnets. The advantage of the recycled powder is that the grains within multi-grained particles are all aligned.

- The best magnetic properties were produced by the IPM (Japanese) magnets and the China magnets.

- It was found that on recycling all these magnets exhibited a drop in BHmax, Br, intrinsic coercivity ($_jH_c$) and Inductive coercivity ($_bH_c$) as was expected in comparison with the initial magnet. This can be rectified to certain extent by blending with small additions of Dy (hydride), Nb, Nd (hydride), Co or Tb (hydride).

- Recycling of the IPM magnet by means of HD-process yielded good magnetic properties which were close to the initial material. The initial material also exhibited a high corrosion resistance. In the case of the recycled material, the corrosion resistance was not as good as the initial material. This was due partly to the thickness of the recycled material being less than that of the initial material and it was coated with zinc which reduced its magnetic properties.

- The IPM magnets had better corrosion resistance when subjected to a salt-solution (3% saline solution) environment than that exhibited by other magnets. This can be ascribed to the magnet having a higher content of Co than any of the other compositions (Table 11-1). It was noted that all magnets has corroded along the c-axis.

- **Table 11-1 ICP measurements of composition of magnets (± 0.008-0.073)**

	Nd+Pr	Dy	Fe	Co	B	Al	O (ppm)
USA	13.55	0.889	78.27	0.056	6.37	0.859	4068
China	12.56	1.8	77.51	1.17	6.14	0.812	3883
Philips	14.04	0.63	77.81	-	6.44	0.69	4670
IPM*ni*	**12.8**	**0.79**	**77.09**	**2.57**	**6.19**	**0.56**	**2565**

- The heat treatment of heavy rare earth (Dy and Tb) hydride slurry coating could provide an effective means of increasing the coercivity of the sintered NdFeB-type magnets, but might be limited to the particular thickness of the sintered magnets. Such a process results in a slight drop in the remanence when compared to those magnets produced by the blending process (using additives such Nd, Dy Tb etc.) During the heat treatment, the Dy/Tb element diffused into the magnet along the grain boundaries, and, appeared to form heavy rare earth-rich shells around the grain boundary of the $Nd_2Fe_{14}B$ phase, which was similar effectto the outcome of using coating with Dy or Tb oxides and fluorides (Park, K. T. et al., 2000; Machida, K. at el., 2004; Nakamura, H. et al., 2004; and Hirota, K. et al., 2006).

- It can be seen from the diffusion studies of Dy and Tb that the amount of diffused Tb and Dy varies according to the distance. This can be seen at a depth of 60 μm which is due to the difference in chemical reaction during heat treatment. The detection of Dy proved to be much easier to identify using the Joel 7000 and EDX. This type of diffusion process could provide an alternative route to modify the composition after sintering which might provide a practical means of tailoring the magnetic properties. The SEM/EDX studies indicated that:

- The SEM characterisation of the grain boundary diffusion indicated that the Dy diffused along the grain boundary. With longer time, the diffusion became more apparent with a corresponding improvement in the magnetic properties.

- The Tb diffusion within the grain boundary was more difficult to trace with longer times (1, 3 and 10 hours). The studies indicated that the Tb had diffused within the grain boundary and there was little evidence of Tb as the treatment time became longer.

- There were indications of Dy and Tb in the matrix phases. This was attributed to the complete coating of the magnets. there was also tentative evidence for Dy(Tb) enrichment at the grain boundaries

- The BEI image shows the Nd-rich and $Nd_2Fe_{14}B$ phases in the Dy-containing sample after 1 hour of heat treatment. The EDX line-scanning showed that the

Nd-rich phase contains ~3 at% of Dy which implies some segregation of this element.

- The BEI image also revealed the Nd-rich and $Nd_2Fe_{14}B$ phases in the Dy-containing sample with 10 hours of heat treatment. EDX line-scanning indicated that both the matrix and the Nd-rich phase contain ~2 at% of Dy. This shows that the following was determined using the SEM (JOEL 7000) analysis:

1. Chemical analysis from these heat treatment samples revealed that, initially the Dy is concentrated in the Nd-rich phase and subsequently diffuses into the matrix with increasing heat treatment time.

2. As the annealing time increases to more than 3 hours, a consistent level of Dy was observed within the matrix. These measurements are supported by the magnetic properties.

- Overall results from this research indicated that IPM magnets (from Japan) had performed better in retaining its magnetic properties (and density) during recycling and corrosion studies. With small additions of elements such Nd, Dy, Nb or Tb, will enhance its magnetic properties and can function for longer period when subjected to aggressive environments. These magnets can work well in wind turbines or be part of marine applications (on-shore or off-shore). The China magnets had came close to the IPM magnets followed by the USA and then Philips magnets.

12 Future works and challenges

Recycling is an important vehicle in order to sustain the RE elements that exist in this world and the continued growth in the use of these vital raw materials can lead to more environmental complications in the future. Therefore, future development and adoption of magnet recycling is crucial.

- Future work must seek to identify important parameters and produce a model to predict the optimum processing parameters from analysis of the scrap. With this in mind, future work will characterise further the currently available scrap (i.e. different sintering conditions and scrap form various sources).

- In addition, other methods of recycling will be attempted that may allow all types of scrap to be processed under the same conditions, thus making recycling a more viable option. These processes will include blending RE hydrides and /or using spark plasma sintering (SPS).

- The HD powder generated from the scrap magnets has a high oxygen content thus reducing the amount of liquid phase during sintering. SPS may overcome the problem of insufficient liquid phase and also reduce the subsequent grain growth.

- It is possible with further research with dilatometery could identify optimum sintering conditions and allow prediction of the appropriate time and temperature for particular batches of magnet scrap.

- Preliminary studies (in this work) on bonded magnet using tin as a binder proved that there is considerable scope for future work on these materials. This can provide a sustainable source of powder for certain bonded magnet applications.

- The sintering characterisation of recycled NdFeB based magnets using high energy milling. Attempts have been made to run some experiments to investigate the use of a RETSCH PM400 planetary ball-milling machine.

There seems to be room for development producing good magnetic properties. One obstacle to overcome is the oxygen contamination.

- Future follow up research activities based on the current work reported in this thesis (Tb & Dy diffusion, further corrosion studies)

- Study of XRD and the out-gassing of magnets to establish that H_2 has been absorbed as part of the saline corrosion process. Study the possible origins of accelerated corrosion phenomenon reported in this work.

- Progressive surface studies using the confocal microscope to study the corrosion process develops.

- Detailed study and optimisation of Zn coatings (by means of the LPPS process) and the effect of saline corrosion and other conditions.

Regarding to the future challenges, meeting the demand for NdFeB should concentrate on future demands for such applications as wind and tidal- turbines. There is here a potential competition from automotive and electric vehicles. The current researches should concentrate on commercialisation of the recycling of permanent magnets to meet local and international demands.

There is a concern about the “in-house” Chinese demand in the future for rare earths as China is expected to have more vehicles than the rest of the world put together. This could have a negative impact upon carbon emission and on natural resources. Their enormous demand for PM-wind generators could also present problems and point to the need to develop alternative rare earth source outside China. This would have an effect on the price of Nd-Fe-B and related magnets and this may raise concerns of further future risk exposure via geopolitics.

Appendix A1

1. Complete desorption of the ϕ phase (room temperature to 300 ^{o}C):

$Nd_2 Fe_{14} BH_{2.9} \rightarrow Nd_2Fe_{14} B + 1.45H_2$ **(1)**

2. Conversion of the Nd ‘trihydride’ ($NdH_{2.7}$) to Nd ‘dihydride’ ($NdH_{1.9}$) (250 ^{o}C to 400 ^{o}C)

$NdH_{2.7} \rightarrow NdH_{1.9} + 0.4H_2$ **(2)**

3. Complete desorption of the Nd ‘dihydride’ (550 ^{o}C to 650 ^{o}C):

$NdH_{1.9} \rightarrow Nd + 0.95H_2$ **(3)**

Ahmed, F. M., Edgley, D. S., Harris, I.R. (1994). "Effect of niobium addition on the Nd-Fe-B alloy and magnet." journal of Magnetism and Magnetic Materials **209**: 363-368.

Ahmed, F. M. and Harris, I. R. (2008). "Improvement of microstructure and magnetic properties of NdFeB alloys by Nb and Co additions." Journal of Magnetism and Magnetic Materials **320**: 2808-2813.

Ali, A., Ahmad, A., Deen, K. M. (2009). "Multilayer ceramic coating for impeding Corrosion of sintered NdFeB magnets." Journal of Rare Earths 27(6): 1003-1007.

Asabe, K., Saguchi, A., Takahashi, W. Suzuki, R. O. Ono, K. (2001). "Recycling of rare earth magnet scraps: part 1 carbon removal by high temperature oxidation." Materials Transactions recycling and high performance waste processing **42**(12): 2487-2491.

Assis, O. B. G., Sinka, V., Ferrante, M., Oliveira, I. L. (1995). "Electrochemical aspects of corrosion in sintered and hot-deformed Nd-Fe-B magnets." Journal of Alloys and Compounds **218**(2): 263-266.

Attanasio, S. A. and Latanision, R. M. (1995). "Corrosion of rapidly solidified neodymium-iron-boron (Nd---Fe---B) permanent magnets and protection via sacrificial zinc coatings." Materials Science and Engineering A **198**(1-2): 25-34.

Bai, G., Gao, R. W., Sun, Y., Han, G. B., Wang, B. (2007). "study of high-coercivity sintered NdFeB magnets." Journal of Magnetism and Magnetic Materials **308**(2007): 20-23.

Bai, Q., H. Xu, Tan, X. H., Zhang, S. Y. (2007). "Effect of boron addition on the magnetic properties of the Fe-Nd-Al alloys prepared by suction casting." Materials Science and Engineering **A 445-446**(2007): 513-516.

Bala, H., Pawlowska, G., Szymura, S., Sergeev, V. V., Rabinovich, Yu M., (1990). "Corrosion characteristics of Nd-Fe-B sintered magnets containing various alloying elements." Journal of Magnetism and Magnetic Materials **87**(3): L255-L259.

Bala, H., Szymura, S., Sergeev, V. V., Pokrovskii, D. V., Pawlowska, G., Potapova, L.V. (1992). "Properties of terbium-doped (Nd, Dy)-(Fe,Co)-B sintered magnets." Journal of Magnetism and Magnetic Materials **103**(1-2): 58-64.

Block, W., Grendel, K., Staubach, H. (21-24 October 1990). corrosion protection of NdFeB magnets by zinc coating. 11th Int Workshop on RE Magnets and Applications, China.

Bollero, A., Gebel, B., Gutfleisch, O., Müller, K. H., Schultz, L., McGuiness, P. J., Drazic, G., Kobe, S., (2001). "NdDyFeBZr high-coercivity powders prepared by intensive milling and the HDDR process." Journal of Alloys and Compounds **315**(1-2): 243-250.

Burns, V. S. J., Williams, A. J., Harris, I.R. (2000). Proceedings of the 16th international workshop on Rare-Earth Magnets and their applications, Sendai, Japan.

Buschow, K. H. J., Cahn, R.W., Flemings, M. C., Ilschner, B., Kramer, E. J., Mahajan, S., Veyssière, P. (2002). Magnets: Bonded Permanent Magnets. Encyclopaedia of Materials: Science and Technology. Oxford, Elsevier**:** 1-5.

Buschow, K. H. J., De Mooij, D. B., Van Noort, H.M., (1985). "Fe-RICH ISOTHERMAL SECTION OF Nd-Fe-B AT 900 degree C. " Philips Journal Research , Eindhoven, Neth, Philips Research Lab, Eindhoven, Netherlands

Buschow, K. H. J., De Mooij, D. B.,Van Noort, H.M.,(1986). "Properties of metastable ternary compounds and amorphous alloys in the Nd-Fe-B system." Journal of the Less Common Metals **125**: 135-146.

Cahn, V. W. and Heady, R. B. (1970). "Analysis of capillary forces in liquid-phase sintering of jagged particles." Journal of American ceramic Society **53**: 406-409.

CEAM: Concerted European Action on Magnets report, 1995.

Chaban, N. F., Kuzma. Y.B., Bolinizhko N.S., Kachmar O., Petrov N.U., Dopov (1979). "In situ TEM study of Nd-rich phase in NdFeB magnet." A. Fiz-Mat. Tekh. Nauk:Akad. Nauk SSSR, **10**: 873.

Chen, C. W. (1986). Magnetism and Metallurgy of Soft Magnetic Material, Dover, New York.

Chen, W., Zhao, X., Hu, J. J., Li, A. J., Tian, Y., Tang, G. D., Gao, R. W., Zhu, M. G., Li, X. M., LI, W., (2006). "refinement of the microstructure and enhancement of the magnetic properties in α Fe $(Nd, Dy)_2Fe_{14}B$ nanocomposite using the two-step annealing technique." Journal of Magnetism and Magnetic Materials **306**(2006): 51-54.

Cheng, C. W., Man, H. C., Cheng, F. T., (1997). "Magnetic and corrosion characteristics of Nd-Fe-B magnet with various surface coatings." Magnetics, IEEE Transactions on **33**(5): 3910-3912.

Corfield, M. R., Williams, A. J., Harris, I. R., (2000). "The effects of long term annealing at 1000 °C for 24 h on the microstructure and magnetic properties of Pr-Fe-B/Nd-Fe-B magnets based on $Nd_{16}Fe_{76}B_8$ and $Pr_{16}Fe_{76}B_8$." Journal of Alloys and Compounds 296(1-2): 138-147.

Croat, J. J. (1981). "Crystallization and magnetic properties of melt-spun neodymium-iron alloys." Journal of Magnetism and Magnetic Materials **24**(2): 125-131.

Croat, J. J. (1981). "“Magnetic hardening of Pr." Journal of Applied Physics letters **39**: 35

Croat, J. J. (1982b). ""Melt-spun $R_{0.4}Fe_{0.6}$ alloys: Dependence of coercivity on quench rate alloys: Dependence of coercivity on quench rate," " Journal of Applied Physics **53**: 2404.

Croat, J. J. (1989). "Manufacture of Nd-Fe-B permanent magnets by rapid solidification." Journal of the Less Common Metals **148**(1-2): 7-15.

Croat, J. J., Chraplyvy, A. R., Herbst, J. F. (1980). "Crystallization of amorphous Pr0.27 Co0.73: Magnetic properties and laser-induced coercivity." Applied Physics Letters **37**: 962.

Croat, J. J., Herbst, J. F., Lee, R.W. (1984). "Pr-Fe and Nd-Fe-based materials - A new class of high-performance permanent magnets (Invited)." Journal of Applied Physics **55**: 2078.

Cui, J. and Forssberg, E. (2003). "Mechanical recycling of waste electric and electronic equipment: a review." Journal of Hazardous Materials **99**(3): 243-263

David, S. and Givord, D. (1998). "Coercivity in lean rare earth NdFeB and PrFeB nanocomposite hard magnetic materials." Journal of Alloys and Compounds **281**: 6-11.

Davies, B. (2004). Sintering characteristics of NdFeB permanent magnets produced by powder blending. Metallurgy and Materials, University of Birmingham. **PhD**.

Davies, B. E., Mottram, R. S., Harris, I. R. (2001). "Recent developments in the sintering of NdFeB." Materials Chemistry and Physics 67(1-3): 272-281.

Durst, K., -D., Kronmüller, H, Ervens, W. (1988). "Investigations of the magnetic properties and demagnetization processes of an extremely high coercive Sm(Co, Cu, Fe, Zr)7.6 permanent magnet. I. Determination of intrinsic magnetic material parameters." Physica Status Solidi **108**(1): 403 - 416.

El-Moneim, A. A., Gebert, A., Uhlemann, M., Gutfleisch, O., Schultz, L. (2002). "The influence of Co and Ga additions on the corrosion behaviour of nanocrystalline NdFeB magnets." Corrosion Science 44(8): 1857-1874.

Endoh, M. and. Shindo, M. (1994). Proceedings on the 13th International workshop on RE magnets, Birmingham, UK." 237.

Eremenko, V. N., Naidich, Y. V. Lavrinenko, I.A. (1970). Liquid-phase sintering. C. Bureau. New York.

Exner, H. E., Arzt, E., Cahn, R. W., Haasen, P. (1996). Sintering Processes. Physical Metallurgy (Fourth Edition). Oxford, North-Holland**:** 2627-2662.

Fang, X., Jiles, D. C., Shi, Y. (1998). "Modelling of magnetic properties of Nd-Dy-Fe-B particulate composites with different compacting processes." Journal of Magnetism and Magnetic Materials **187**(1): 79-82.

Fidler, J., Bernardi, J. Schrefl, T. (1995). "Permanent magnets -- New microstructural aspects." Scripta Metallurgica et Materialia **33**(10-11): 1781-1791.

Fidler, J., Schrefl, T., Hoefinger, S., Hajduga, M. (2004). "Recent developments in hard magnetic bulk materials." Journal of Physics: Condensed Matter **16**: S455-S470.

Fidler, J., Schrefl, T., Hoefinger, S., Suess, D. (1999). "Grain boundaries in high performance magnets, reasons for poor or excellent properties?" Proc. of Workshop on Grain Boundaries: Their Characterisation and influence on properties, Birmingham, UK, Sept. 1999, edited by I.R. Harris and I.P. Jones,(The University Press, Cambridge): 147-163.

Gang, S., Lianxi, H., Erde, W. (2006). "Preparation, microstructure, and magnetic properties of a nanocrystalline Nd12Fe82B6 alloy by HDDR combined with mechanical milling." Journal of Magnetism and Magnetic Materials **301**(2): 319-324.

Gao, J., Volkmann, T., Strohmenger, J. Herlach, D. M. (2004). "Phase selection in undercooled Nd-Fe-Co-B alloy droplets." Materials Science and Engineering A **375-377**: 498-501.

Gao, J.-r., Song, X.-p., Wang, X-t. (1997). "Effects of Co and Zr additions on microstructure and anisotropy of HDDR-treated NdFeB alloy powders." Journal of Alloys and Compounds **248**: 176-179.

German, R. M. (1985). "Liquid Phase Sintering", New York, Plenum Press.

German, R. M. (1996). "Sintering Theory and Practices". New York. Plenum Press.

Gessinger, G. H. and Fischmeister, H. F. (1972). "A modified model for the sintering of tungsten with nickel additions." Journal of the Less Common Metals **27**(2): 129-141.

Gessinger, G. H., Fischmeister, H. F., Lukas, H. L. (1973). "A model for second-stage liquid-phase sintering with a partially wetting liquid." Acta Metallurgica **21**(5): 715-724.

Ghandehari, M. H. and Fidler, J. (1987). "Microstructural evidence for the magnetic surface hardening of Dy2O3-doped Nd15Fe77B8 magnets." Materials Letters **5**(7-8): 285-288.

Givord, D., Rossignol, M., Barthem, V.M.T.S. (2003). "The physics of coercivity." Journal of Magnetism and Magnetic Materials: 258-259.

Gutfleisch, O. "Magnetic materials in sustainable energy", IEEE Magnetics Society Distinguished Lecture Series 2011, National Tsing-Hua University, HsinChu/ Taiwan, 2.5.11 (2011)

Hadjipanayis, G. C., Hazelton, R. C., Lawless, K. R. (1984). "Cobalt-free permanent magnet materials based on iron-rare-earth alloys (invited)." Journal of Applied Physics **55**(6): 2073-2077.

Hall, M. G. (1990). “Wavelength Dispersive X-ray Analysis”. Internal Report. Birmingham, School of Metallurgy and Materials, University of Birmingham, UK.

Hallemans, B., Wollants, P., Roos, J.R. (1995). "Thermodynamic assessment of the Fe-Nd-B phase diagram” Journal of Phase Equlibria **16**(2): 137.

Hamano, M. (1995). "Overview and outlook of bonded magnets in Japan." Journal of Alloys and Compounds **222**(1-2): 8-12.

Harland, C. L. and Davies, H. A. (1998). "Magnetic properties of melt-spun Nd-rich NdFeB alloys with Dy and Ga substitutions." Journal of Alloys and Compounds **281**: 37-40.

Harris, I. R. (1987). "The potential of hydrogen in permanent magnet production." Journal of the Less Common Metals **131**(1-2): 245-262.

Harris, I. R. and McGuiness, P. J. (1991). "Hydrogen: its use in the processing of NdFeB-type magnets." Journal of the Less Common Metals **172-174**(Part 3): 1273-1284.

Harris, I. R., Noble, C., Bailey, T. (1985). "The hydrogen decrepitation of an Ndi15Fe77B8 magnetic alloy." Journal of the Less Common Metals **106**(1): L1-L4.

Harris, I. R., Evans, J. and Nyholm, P. S., U.K. Patent 1554384 (October 1979).
Herbst, J. F. (1991). "R2Fe14B materials: Intrinsic properties and technological aspects." Reviews of Modern Physics **63**(4): 819.

Hatch, G.,”The sustainability of the rare-earth permanent magnets-materials and applications”, The UK Magnetic Society Seminar, TRW Conket, Solihull, UK, 2nd December, 2010

Herbst, J. F. and Croat, J. J. (1991). "Neodymium-iron-boron permanent magnets." Journal of Magnetism and Magnetic Materials **100**(1-3): 57-78.

Herbst, J. F., Croat, J. J., Pinkerton, F. E., Yelon, W. B. (1984). "Relationships between crystal structure and magnetic properties in Nd2Fe14B." Physical Review B **29**(7): 4176.

Hirosawa, S., Matsuura, Y., Yamamoto, H., Fujimura, S. (1986). "Magnetization and magnetic anisotropy of R Fe B measured on single crystals." Journal of Applied Physics **59**(3): 873–879.

Hirosawa, S., Mino, S., Tomizawa, H. (1991). "Improved corrosion resistance and magnetic properties of Nd Fe B type sintered magnets with Mo and Co." journal of Applied Physics **69**(8): 5844.

Hirota, K., Nakamura, H., Minowa, T., Honshima, M.(2006). "Coercivity enhancement by the grain boundary diffusion process to Nd-Fe-B sintered magnets." IEEE Transactions on Magnetics **42**(10): 2909-2911.

Hong, Y. G., Nakamura, H., Sugimoto, S., Kagotani, T., Okada, M. Homma, M. (1995). "3rd ISPMM, Seoul, South Korea." 665.

Honkura, Y. (2006). "Automotive Motor Innovation With Anisotropic Bonded Magnet - MAGFINE." Journal of Iron and Steel Research, International **13**(Supplement 1): 231-239.

Horikawa, T., Itoh, M., Suzuki, S., Machida, K. (2004). "Magnetic properties of the Nd-Fe-B sintered magnet powders recovered by Yb metal vapour sorption." Journal of Magnetism and Magnetic Materials **271**(2-3): 369-380.

Horikawa, T., Miura, K., Itoh, M., Machida, K-i. (2006). "Effective recycling for Nd-Fe-B sintered magnet scraps." Journal of Alloys and Compounds **408-412**: 1386-1390.

Hu, Z. H., Lian, F. Z., Zhu, M. G., Li, W. (2008). "Effect of Tb on the intrinsic coercivity and impact toughness of sintered Nd-Dy-Fe-B magnets." Journal of Magnetism and Magnetic Materials **320**: 1735-1738.

Hu, Z. H., Zhu, M. G., Li, W., Lian, F. Z. (2008). "Effects of Nb on the coercivity and impact toughness of sintered Nd-Fe-B magnets." Journal of Magnetism and Magnetic Materials **320**(3-4): 96-99.

Hua, Z., Han, Z., Wang, D., Gu, B., Du, Y.(2007). "Influence of a small addition of Nd on structure and magnetic properties of nanocrystalline Fe_b alloys." Journal of Magnetism and Magnetic Materials **312**(2007): 48-52.

Itoh, M., Masuda, M., Suzuki, S., Machida, K-i. (2004). "Recycling of rare earth sintered magnets as isotropic bonded magnets by melt-spinning." Journal of Alloys and Compounds **374**(1-2): 393-396.

Itoh, M., Miura, K., Machida, K-i. (2009). "Novel rare earth recovery process on Nd-Fe-B magnet scrap by selective chlorination using NH4Cl." Journal of Alloys and Compounds **477**(1-2): 484-487.

Jacobson, J. and Kim, A. (1987). "Oxidation behaviour of NdFeB magnets." Journal of applied Physics **61**(8): 3763-3765.

Jay, F., Gauthier-Brunet, V., Pailloux, F., Mimault, J., Bucher, S., Dubois, S. (2008). "Al-coated iron particles: Synthesis, characterization and improvement of oxidation resistance." Surface and Coatings Technology **202**(17): 4302-4306.

Jezek, G. (2006). "The history of magnets." how magnets work website: http://www.howmagnetswork.com/history.html

Bostock, J. J and Riley H. T. (1855). Natural History of Pliny, London, UK.

Jones, D. G. R., McGuiness, P. J., Abell, J. S., Harris, I. R. (1990). "Hydrogen absorption studies on $Tb_{0.27}Dy_{0.73}Fe_{1.9}$." Journal of the Less Common Metals **158**(1): 153-162.

Kaneko, Y. and Ishigaki, N. (1994). "Recent developments of high-performance NEOMAX magnets" Journal of Materials Engineering Performance **3(2)**: 228.

Kaneko, Y., Kuniyoshi, F., Ishigaki, N. (2006). "Proven technologies on high-performance Nd-Fe-B sintered magnets." Journal of Alloys and Compounds **408-412**: 1344-1349.

Kaneko, Y., Tokuhara, K., Ishigaki, N. (1996). "Research on high performance Nd-Fe-B sintered magnets." Vacuum **47**(6-8): 907-910.

Kennedy, D., Great Western Minerals Group (GWMG). The UK Magnetic Society Seminar, TRW Conket, Solihull, UK, 2nd December, 2010

Kianvash, A. and Harris, I. R. (1985). "Hydrogen decrepitation as a method of powder preparation of a 2:17-type, Sm(Co, Cu, Fe, Zr)_{8.92} magnetic alloy." Journal of Materials Science 20(2): 682-688.

Kianvash, A. and Harris, I. R. (1999). "The production of a Nd16Fe76B8 sintered magnet by the hydrogen decrepitation/hydrogen vibration milling route." Journal of Alloys and Compounds **282**(1-2): 213-219.

Kianvash, A., Mottram, R. S., Harris, I. R. (1999). "Densification of a $Nd_{13}Fe_{78}NbCoB_7$-type sintered magnet by (Nd, Dy)-hydride additions using a powder blending technique." Journal of Alloys and Compounds **287**(1-2): 206-214.

Kim, A. and. Jacobson, J. (1987). "Oxidation and oxidation protection of Nd-Fe-B magnets." IEEE Transactions on Magnetics **23**(5): 2509-2511.

Kim, A. S., Buschow, K. H. J., Cahn, R. W., Flemings, M. C., Ilschner, B., Kramer, E. J., Mahajan., S., Patrick, Veyssière, P. (2001). Permanent Magnets: Corrosion Properties. Encyclopaedia of Materials: Science and Technology. Oxford, Elsevier**:** 6812-6815.

Kim, A. S. and Camp, F. E. (1996). "High performance NdFeB magnets (invited)." journal of Applied Physics **79**(8): 5035.

Kim, A. S., Camp, F. E., Lizzi, T. (1996). "Hydrogen induced corrosion mechanism in NdFeB magnets." Journal of Applied Physics **79**(8): 4840

Kim, A.S.; Camp, F. E. (11/1995) "Effect of minor grain boundary additives on the magnetic properties of NdFeB magnets". Crucible Res. Centre, Crucible Mater. Corp., Pittsburgh, PA. USA. IEEE transitions on Magnetics. Pages: 3620 - 3622, volume: 31 issue: 6, ISSN: 0018-9464.

Kingery, W. D. and Narasimhan, M. D.(1959). "Densification during Sintering in the Presence of a Liquid Phase. II. Experimental." Journal of applied Physics **30**(3): 307-310.

Kinsey, D. J., Lillywhite, S . J., Jewell, G. W., Ede, J. D., Williams, A. J., Howe, D., Harris, I. R. (2002). "Design of powder aligning systems for the compression molding of radially anisotropic permanent magnet rings." Journal of applied Physics **91**(10): 8837-8839.

Koon, N. C., Das, B. N., Rubinstein, M., Tyson, J. (1985). "Magnetic properties of R Fe B single crystals." Journal of Applied Physics: 4091–4093.

Koon, N. C. and Das, B. N.(1984). "Crystallization of FeB alloys with rare earths to produce hard magnetic materials (invited)." Journal of Applied Physics **55**(6): 2063-2066.

Kwon, H. W., Jeong, I. C., Kim, A. S., Kim, D. H., Namkung, S., Jang, T. S., Lee, D. H. (2006). "restoration of coercivity in crushed Nd-Fe-B magnetic powder." Journal of Magnetism and Magnetic Materials **304**(2006): e219-e221.

Kwon, H. W., Zhang, Y., Hadjipanayis, G. C. (2006). "Effect of host and added alloy composition on magnetic properties of $Nd_2Fe_{14}B$ + $Nd_2Fe_{14}B$/Fe hybrid magnets." Journal of Magnetism and Magnetic Materials **303**(2006): e410-e414.

Li, J., Liu, Y., Gao, S. J., Li, M., Wang, Y. Q., Tu, M. J. (2006). "Effect of process on the magnetic properties of bonded NdFeB magnet." Journal of Magnetism and Magnetic Materials **299**(1): 195-204.

Li, L., Yi, J., Peng, Y., Huang, B. (2007). "The effect of compound addition Dy_2O_3 and Sn on the structure and properties of NdFeB magnets." Journal of Magnetism and Magnetic Materials **308**(2007): 80-84.

Li, W. F., Ohkubo, T., Hono, K., Sagawa, M. (2009). "The origin of coercivity decrease in fine grained Nd-Fe-B sintered magnets." Journal of Magnetism and Magnetic Materials **321**: 1100-1105.

Li, Y., Kim, Y. B., Yoon, T. S., Suhr, D. S., Kim, T. K., Kim, C. O. (2002). "Coercivity enhancement by Zn addition in hot deformed NdFeB magnets." Journal of Magnetism and Magnetic Materials **242-245**: 1369-1371

Liesert, S., Kirchner, A., Gru¨nberger, W., Handstein, A., De Rango, P., Fruchart, D., Schultz, L., Mu¨ller, K.-H. (1998). "Preparation of anisotropic NdFeB magnets with different Nd contents by hot deformation (die-upsetting) using hot-pressed HDDR powders." Journal of Alloys and Compounds **266**: 260-265.

Liszkowski, P., K. Turek, Figiel, H. (2000). The influence of decrepitation on the diffusion kinetics of hydrogen in Nd-Fe-B. Journal of Alloys and Compounds. **307:** 297-303.

Liu, Z. W. and Davies, H. A. (2007). "The practical limits for enhancing magnetic property combinations for bulk nanocrystalline NdFeB alloys through Pr, Co and Dy substitutions." Journal of magnetism and magnetic materials **313**(2007): 337-341.

Lukin, A. A., Szymura, S., Zhuravlyev, A. A., Margaryan, S. M., Bala, H. (2000). "Post-sintering heat treatment effect on the coercivity of sintered (Nd, $Dy)_{15}(Fe,Co,Mo,Al)_{77}B_8$ permanent magnets." Materials Chemistry and Physics **65**(1): 74-78.

Lyman, J. W. and Palmer, G. R. (1993). "Recycling of rare earths and iron from NdFeB magnet scrap." High Temperature Materials and Processes **11**(1-4): 175-187

Ma, B. M., Herchenroeder, J. W., Smith, B., Suda, M., Brown, D. N., Chen, Z. (2002). "Recent development in bonded NdFeB magnets." Journal of Magnetism and Magnetic Materials **239**(1-3): 418-423.

Ma, B. M., Liu, W. L., Liang, Y. L., Scott, D. W., Bounds, C. O. (May, 1994) "Comparison of the improvement of thermal stability of NdFeB sintered magnets: Intrinsic and/or microstructural."; Journal of Applied Physics, Rho□ne-Poulenc Basic Chemicals, CN 7500, Cranbury, New Jersey 08512, Volume: 75 Issue: 10, pages: 6628 – 6630. ISSN: 0021-8979.

Machida, K., Kawasaki, T., Suzuki, S., Ito, M., Horikawa, T. (2004). "Abstracts of Spring Meeting of Japan Society of Powder and Powder Metallurgy." 202.

Man, H. H., Man, H. C., Leung, L. K. (1996). "Corrosion protection of NdFeB magnets by surface coatings - Part 2: Electrochemical behaviour in various solutions." Journal of Magnetism and Magnetic Materials **152**(1-2): 47-53.

Matsuura, Y. (2006). "Recent development of Nd-Fe-B sintered magnets and their applications." Journal of Magnetism and Magnetic Materials **303**(2006): 344-347.

Metal-pages website, (2011), www.metal-pages.com.

McGuiness, P. J., Fitzpatrick, L., Yartys, V. A., Harris, I. R. (1994). "Anisotropic hydrogen decrepitation and corrosion behaviour in NdFeB magnets." Journal of Alloys and Compounds **206**(2): L7-L10.

McGuiness, P. J. and Harris, I. R. (1989). "A study of Nd-Fe-B magnets produced using a combination of hydrogen decrepitation and jet milling" Journal of Materials Science **24**(number 7): 2541-2548.

McGuiness, P. J., Zhang, X. J., Forsyth, H., Harris, I. R. (1990). "Disproportionation in $Nd_{16}Fe_{76}B_8$-type hydrides." Journal of the Less Common Metals **162**(2): 379-387.

Mishima, C., Hamada, N., Mitarai, H., Honkura, Y. (2001). "development of Ga Co-Free NdFeB Anisotropic Bonded Magnet Produced from the d-HDDR Processed Powder." IEEE Transactions on Magnetics, **37**(4): 2467-2470.

Mitchell, P. (1990). "CORROSION PROTECTION OF NdFeB MAGNETS." IEEE Transactions on Magnetics **VOL. 26**(NO. 5): 1933.

Miura, K., Itoh, M., Machida, K-i. (2008). "Extraction and recovery characteristics of Fe element from Nd-Fe-B sintered magnet powder scrap by carbonylation." Journal of Alloys and Compounds **466**(1-2): 228-232.

Morgan, V. T. (1978). "Bearing materials by powder metallurgy." Powder Met **21**: 80-85.

Mottram, R. S., Davis, B., Yartys, V. A., Harris, I. R. (2001). "The use of metal hydride powder blending in the production of NdFeB-type magnets." International Journal of Hydrogen Energy **26**(5): 441-448.

Mottram, R. S., Kianvash, A., Harris, I. R. (1999). "the use of metal hydrides in powder blending for the production of NdFeB-type magnets." Journal of Alloys and Compounds **283**: 282-288.

Mottram, R. S., Williams, A. J., Harris, I. R. (2001). "The effects of blending additions of copper and cobalt to Nd16Fe76B8 milled powder to produce sintered magnets." Journal of Magnetism and Magnetic Materials **234**(1): 80-89.

Mottram, R. S. and Harris, I.R. (1998) "production of sintered NdFeB magnets by a powder blending techniques" proceedings of the 15th International Workshop on Rare-Earth Magnets and their applications. Dresden, 1998.

Murase, K.,. Machida, K-i, Adachi, Gin-ya (1992). "Recovery of Rare Metals from the Sludge of Samarium-Cobalt Magnetic Alloy by a Chemical Vapor Transporting Method." Chemistry Letters **21**(8): 1555.

Nakamura, H., Hirota, K., Shimao, M., Minowa, T., Honshima, M. (2005). "Magnetic properties of extremely small NdFeB sintered magnets." IEEE Transactions on Magnetics **41**(10): 3844-3846

Ni, J. J., Ma, T. Y., Cui, X. G., Wu, Y. R., Yan, M. (2010). "Improvement of corrosion resistance and magnetic properties of Nd-Fe-B sintered magnets by $Al_{85}Cu_{15}$ intergranular addition." Journal of Alloys and Compounds 502(2): 346-350.

Nozières, J. P., Taylor, D. W., Bala, H., Malik, M., Szymura, S., Stoklosa, H. et al. (1992). "Corrosion behaviour of hot-worked Nd-Fe-B and Nd-Fe-Cu-B permanent magnets." Journal of Alloys and Compounds **186**(2): 201-208.

Okabe, T. H. A., Takeda, O. B., Fukuda, K.C., Umetsu, Y.C. (2003). "Direct extraction and recovery of neodymium metal from magnet scrap." Materials Transactions **44**(4): 798-801

Ozawa, S., Kuribayashi, K., Hirosawa, S., Reutzel, S., Herlach, D. M. (2006). "Heat treatment of metastable Nd[sub 2]Fe[sub 17]B[sub x] phase formed from undercooled melt of Nd--Fe--B alloys." Journal of Applied Physics 100(12): 123906-8.

Pandian, S., Chandrasekaran, V., Markandeyulu, G., Iyer, K. J. L., Rama Rao, K. V. S. (2004). "Effect of Co, Dy and Ga on the magnetic properties and the microstructure of

powder metallurgically processed Nd-Fe-B magnets." Journal of Alloys and Compounds **364**(1-2): 295-303.

Park, K. T., Hiraga, K., Sagawa, M. (2000). proceedings of the 16th International RE magnets and their applications, Sendai, Japan.

Price, O. R., Stork, D. H., Ticho, H. K. (1958). "K+ Meson-Nucleon Scattering Phase Shift Analysis." Physical Review Letters **1**(6): 212.

R. Pollard and Oesterreicher, H., Internat. Magn. Conf., Phoenix, Arizona, April, 1986. IEEE Trans Magn. MAG 22, 735, (1986).

Ragg, O. M. and Harris, I. R. (1994). "A study of the effects of heat treatment on the microstructures and magnetic properties of Cu-added Nd---Fe---B type sintered magnets." Journal of Alloys and Compounds **209**(1-2): 125-133.

Rivoirard, S., Noudem, J. G. (2000). Proceedings of the 16th International workshop on rare earth magnets and their applications, Sendai. Japan.

Rodewald, W. (1985). "Magnetization and aging of sintered Nd---Fe---B magnets." Journal of the Less Common Metals **111**(1-2): 77-81

Rodewald, W., Blank, R., Wall, B., Reppel, G.W., Zilg, H.D. (2000). Production of Sintered Nd-Fe-B Magnets with a Maximum Energy Density of 53 MGOe. Proceedings 16th Int. Workshop on RE Magnes and Their Applications, Sendai, Japan.

Rodewald, W. and Wall, B. (1989). "Structure and magnetic properties of sintered Nd-Fe-Nb-B magnets." Journal of Magnetism and Magnetic Materials **80**(1): 57-60.

Rodewald, W. and Wall, B. (1991). "Temperature stability and magnetizing behaviour of sintered Nd-Dy-Fe-Co-Mo-Al-B-magnets." Journal of Magnetism and Magnetic Materials **101**(1-3): 338-340.

Ronghai Qu, (May 2010). “The workshop on next generation wind power lecture” - GE Global Research Centre, (Rensselaer Polytechnic Institute-, France.

Rupp, B. and Wiesinger, G. (1988). "Magnetic and structural properties of a novel ternary hydride: $Nd_2Fe_{17}H_{x(0<x<5)}$." Journal of Magnetism and Magnetic Materials **71**(3): 269-278.

Sagawa, M., Fujimura, S., Togawa, N., Yamamoto, H., Matsuura, Y.(1984). "Nd–Fe–B Permanent Magnet Materials." Journal of Applied Physics **55**(2083).

Sagawa, M., S. Fujimura, Togawa, N., Yamamoto, H., Matsuura, Y. (1984). "New material for permanent magnets on a base of Nd and Fe (invited)." Journal of Applied Physics **55**(6): 2083-2087.

Saguchi, A., Asabe, K., Fukuda, T., Takahashi, W., Suzuki, R. O. (2006). "Recycling of rare earth magnet scraps: Part II: Carbon and oxygen removal from Nd magnet scraps." Journal of Alloys and Compounds **408-412**: 1377-1381.

Saguchi, A., Asabe, K., Takahashi, W., Suzuki, R.O., Ono, K.(2002). "Recycling of rare earth magnet scrap: part III: carbon removal from Nd magnet grinding sludge under vacuum heating." Materials Transactions **43**(2): 256-260.

Saito, T. (2006). "Structures and magnetic properties of Nd-Fe alloys produced by the glass slag method." Journal of Alloys and Compounds **414**(1-2): 88-93.

Saito, T., Wang, W. Q., Kamagata, Y. (2005). "Extraction of Sm from Sm-Fe alloys by the glass slag method." Journal of Alloys and Compounds **387**(1-2): 274-278.

Saito, T., Sato, H., Motegi, T. (2006). "Recovery of rare earths from sludges containing rare-earth elements." Journal of Alloys and Compounds **425**(1-2): 145-147.

Saito, T., Sato, H., Motegi, T., Kobayashi, K. (2005). "Extraction of Sm from Sm-Fe-N magnets by the glass slag method." Journal of Alloys and Compounds **403**(1-2): 341-344.

Saito, T., Wang, W. Q., Kamagata, Y. (2005). "Structures and magnetic properties of Nd-Fe-Ti alloys produced by melt-spinning technique." Journal of Alloys and Compounds **402**(1-2): 242-245.

Schneider, J. and Knehans-Schmidt, R.(1996). "Bonded hybrid magnets." Journal of Magnetism and Magnetic Materials **157-158**: 27-28.

Schüler, D., Buchert, M., Liu, R., Dittrich, G., Merz, C. **"**Study on Rare Earths and Their Recycling**"-** Final Report for The Greens/EFA Group in the European parliament- Öko-Institut, Germany, January, 2011

Shimizu, K., Ichinose, K., Fukuda, Y., Shimotomai, M. (1995). "143Nd NMR study of 3d and 4f magnetism in $Nd_2(Fe_{1-x}Co_x)_{14}B$ and $Nd_2(Fe_{1-y}Ni_y)_{14}B$." Solid State Communications **96**(9): 671-674.

Silman. H, Isserlis. G, Averill. A. F, (1978). "Protective and Decorative Coatings." Book (Finishing Publications Ltd): 325.

Skulj, I., A. P. Douvalis, Harris, I. R.. (2006). "Characterisation of oxidation products of modified Nd-Fe-B type magnets." Journal of Alloys and Compounds **407**(1-2): 304-313.

Skulj, I., H. E. Evans, Harris, I. R. (2008). "oxidation of NdFeB-type magnets modified with additions of Co, Dy, Zr, and V." Journal of Material Science **43**: 1324-1333.

Speight and Harris, UK Patent Applications (1994).

Speight, J.D. – Private communication, University of Birmingham, (2010)

Sprengel, W., Herth, S., Barbe, V., Schaefer, H. E., Wejrzanowski, T., Gutfleisch, O., Wurschum, R.(2005). "Grain-boundary diffusion of Nd in nanocrystalline Nd2Fe14B." Journal of Applied Physics **98**(074314).

Stadelmaier, H. H., Elmasry, N. A., Cheng, S. (1983). "Cobalt-free and samarium-free permanent magnet materials based on an iron-rare earth boride." Materials Letters **2**(2): 169-172.

Strnat, K. (1967). "A family of new cobalt-base permanent magnet materials." Journal of Applied Physics **38**(3): 1001-1002

Strnat, K. J. (1988). In Ferromagnetic Materials,. Journal of Less Common Metals E. P. W. a. K. H. J. Buschow. North Holland, Amsterdam. **4:** 131.

Strnat, K. J., E. P. Wohlfarth, Buschow, K. H. J. (1988). Chapter 2 Rare earth-cobalt permanent magnets. Handbook of Ferromagnetic Materials, Elsevier. **Volume 4:** 131-209.

Sugimoto, K., Sohma, T., Minowa, T., Honshima, M. (1987). Japan Metal Society Fall Meeting. J. M. Soc. Japan**:** 604

Sugimoto, T. and Matijevic, E. (1980). "Formation of uniform spherical magnetite particles by crystallization from ferrous hydroxide gels." Journal of Colloid and Interface Science **74**(1): 227-243.

Sueptitz, R., Uhlemann, M., Gebert, A., Schultz, L. (2010). "Corrosion, passivation and breakdown of passivity of neodymium." Corrosion Science 52(3): 886-891.

Suzuki, R. O., Saguchi, A., Takahashi, W., Yagura, T., Ono, K. (2001). "Recycling of rare earth magnet scraps: Part II oxygen removal by Calcium." Materials Transactions **42**(12): 2492-2498.

Szymura, S., Wyslocki, J. J., Bala, H., Rabinovich, Yu M. (1998). "High-coercivity sintered Nd14.5Dy1.5Fe68Co5Al1.5Cr2B7.5 permanent magnet." Materials Chemistry and Physics 52(2): 147-151.

Takahashi, M., Uchida, K., Taniguchi, F., Mikamoto, T.(1998). "High performance Nd–Fe–B sintered magnets made by the wet process." Journal of Applied Physics **83**(11): 6402

Takahashi, S., Zakotnik, L., Ueda, T. (2003). "Magnetic hysteresis minor loops in Fe single crystal." Journal of Physics: Condensed Matter **15**: 7997-8002.

Takeda, O., Okabe, T. H., Umetsu, Y. (2004). "Phase equilibrium of the system Ag-Fe-Nd, and Nd extraction from magnet scraps using molten silver." Journal of Alloys and Compounds **379**(1-2): 305-313.

Takeda, O., Okabe, T. H., Umetsu, Y. (2005). "Phase Equilibria of the system Fe-Mg-Nd at 1076 K." Journal of Alloys and Compounds **392**(1-2): 206-213.

Takeda, O., Okabe, T. H. Umetsu, Y. (2006). "Recovery of neodymium from a mixture of magnet scrap and other scrap." Journal of Alloys and Compounds **408-412**: 387-390.

Taylor, Mark Geoffrey, “A comparison of the sintering behaviour of powders based on the alloys $Nd_{16}Fe_{76}B_8$ and $Pr_{16}Fe_{76}B_8$ and produced by the roller milling or hydrogen vibration milling”. Thesis (MPhil)-University of Birmingham, School of Engineering, Department of Metallurgy and Materials. 2004

Tang, W., Dennis, K. W., Kramer, M. J., Anderson, I. E., McCallum, R. W. (2012). "Studies of sintered MRE-Fe-B magnets by DyF[sub 3] addition or diffusion treatment (MRE = Nd + Y + Dy)." Journal of Applied Physics 111(7): 07A736-3.

Tao, S., J. Tian, Lu, X., Qu, X., Honkura, Y., Mitarai, H., Noguchi, K. (2009). "Anisotropic bonded NdFeB magnets with radial oriented magnetization by 2-step warm compaction process." Journal of Alloys and Compounds **477**(1-2): 510-514.

Tattam, C., Williams, A. J., Hay, J. N., Harris, I. R., Tedstone, S. F., Ashraf, M. M. (1996). "Improvement in the mechanical properties of PTFE bonded Nd---Fe---B magnets by heat treatment." Journal of Magnetism and Magnetic Materials **154**(3): 328-332.

Tattam, C., Williams, A. J., Hay, J. N., Harris, I. R., Tedstone, S. F., Ashraf, M. M. (1996). "The corrosion behaviour of uncoated bonded Nd---Fe---B magnets in humid environments." Journal of Magnetism and Magnetic Materials **152**(3): L275-L278.

Tenaud, P., Vial, F., Sagawa, M. (1990). "Improved corrosion and temperature behaviour of modified Nd-Fe-B magnets." Magnetics, IEEE Transactions on **26**(5): 1930-1932

Thummler, F. and Thomma, W. (1967). "The sintering process." Met. Rev **12**: 69-108.

Tokuhara, K. and Hirosawa, S. (1991). "Corrosion resistance of Nd-Fe-B sintered magnets." Journal of Applied Physics **69**(8): 5521

Torrance, T. F. (1996). "Maxwell James C. :A dynamical Theory of the Electromagnetic Field."

Uda, T. (2002). "Recovery of rare earths from magnet sludge by FeCl2." Materials Transactions **43**(1): 55-62.

Vial, F., Joly, F., Nevalainen, E.,Sagawa, M., Hiraga, K., Park, K. T. (2002). "Improvement of coercivity of sintered NdFeB permanent magnets by heat treatment." Journal of Magnetism and Magnetic Materials **242-245**(Part 2): 1329-1334.

Waldron, M. B. and Daniell, B. L., Eds. (1978). Sintering. London, Haydon & Sons.

Walton, A., Speight, J. D., Williams, A. J., Harris, I. R. (2000). "A zinc coating method for Nd-Fe-B magnets." Journal of Alloys and Compounds **306**(1-2): 253-261.

Walton, A., Speight, J. D., Williams, A. J., Harris, I. R (2002). "Proceedings of the 17th International Workshop on RE magnets.", **2**: P.925, Delaware, USA.
Walton, A, (2002) "Corrosion Protection for Rare Earth Permanent Magnets" PhD Thesis. School of Metallurgy and Materials, University of Birmingham, Birmingham, UK.

Wang, H., Li, A., Li, W. (2006). "Effect of Pr and Dy substitution on the impact resistance of sintered Nd-Fe-B magnets." Intermetallics **15**(2006): 985-988.

Watanabe, N., Umemoto, H., Itakura, M., Nishida, M., Machida, K. (2009). Grain boundary structure of high coercivity Nd-Fe-B sintered magnets with Tb-metal vapor sorption. Rare-earth related material processing and functions, Japan, IOP.

Wenjian, M., Lanting, Z., Qiongzhen, L., Aidang, S., Jiansheng, W., Matahiro, K. Liping, S. (2008). "Microstructure and corrosion resistance of sintered NdFeB magnet modified by intergranular additions of MgO and ZnO." journal of rare earths **26**(2): 268-273.

Williams, A. J. (2000). University website about "www.magnets.bham.ac.uk"

Williams, A. J., McGuiness, P. J., Harris, I. R. (1991). "Mass spectrometer hydrogen desorption studies on some hydrided NdFeB-type alloys." Journal of the Less Common Metals **171**(1): 149-155.

Willman, C. J. and Narasimhan, K. S. V. L. (1987). "Corrosion characteristics of RE-Fe-B permanent magnets." Journal of Applied Physics **61**: 3766.

Xianglian, L. and Shouzeng, Z. (2007). "Grain growth behaviour in sintered Nd-Fe-B-magnets." Journal of Rare Earths **25**(2007): 329-335.

Xie, H.-z., Zhao, J.-t., Yu, Y.-j. (2006). New achievements in NdFeB mass production. 19th international workshop on rare earth permanent magnets and their applications, Shandong, China.

Xu, Y., Chumbley, L. S., Lin, Z., LÜ, B., MA, C., Gao, X. (2000). "Liquid metal extraction of Nd from NdFeB magnet scrap." Journal of Materials Research **15**(11): 2296-2304

Yan, A., Chen, Z., Song, X., Wang, X. (1996). "The influence of MgO/Mg and Al2O3 additives on coercivity, thermal stability, and microstructure of Nd-Fe-B magnets." materials Research Bulletin **31**(10): 1171-1177.

Yan, G., McGuiness, P. J., Farr, J.P.G., Harris, I.R. et al. (1999). "Optimisation of the processing of Nd–Fe–B with dysprosium addition." Journal of Alloys and Compounds **L20**-**L24**(1999): 5.

Yan, G., McGuiness, P. J., Farr, J.P.G., Harris, I.R. (2009). "Environmental degradation of NdFeB magnets" Journal of Alloys and Compounds **478**: 188-192.

Yan, G., Williams, A. J., Farr, J.P.G., Harris, I.R. (2009). "The effect of density on the corrosion of NdFeB magnets." Journal of Alloys and Compounds **292**: 266-274.

Yan, M., Yu, L. Q. Wu, J. M., Cui, X. G. (2006). "Improved magnetic properties and fracture strength of NdFeB by dehydrogenation." Journal of Magnetism and Magnetic Materials **306**(2): 176-180.

Yang, L. (2006). Development of NdFeB magnet industry in new century. 19th international workshop on rare earth permanent magnets & their applications, Beijing, China, Journal of Iron and steel research.

Yang, L. (2008). The marvellous development of the rare earth magnet industry. Magnews, Magnews**:** 32-35.

Yin, X. J., Hall, M. G., Jones, I. P., Faria, R. N., Harris, I. R. (1993). "The microstructural characterisation of Nd-Fe-B alloys. I: Light element microanalysis." Journal of Magnetism and Magnetic Materials **125**(1-2): 78-90.

Zakotnik, M. (2008). Recycling Rare Earth Transitional Permanent Magnets. PhD Thesis. Birmingham, University of Birmingham. **PhD:** 280.

Zakotnik, M., Devlin, E., Harris, I. R., Williams, A. J. (2006). "Hydrogen Decrepitation and Recycling of NdFeB-type Sintered Magnets." Journal of Iron and Steel Research, International **13**(Supplement 1): 289-295.

Zakotnik, M., Harris, I. R., Williams, A. J. (2007). "Possible methods of recycling NdFeB-type sintered magnets using the HD/degas process." Journal of Alloys and Compounds Vol.450(1), pp.525-531.

Zakotnik, M., Harris, I. R., Williams, A. J. (2008). "Multiple recycling of NdFeB-type sintered magnets." Journal of Alloys and Compounds **450**: 525-531

Zakotnik, M., Prosperi, D., Williams, A. J. (2009). "Kinetic studies of hydrogen desorption in SmCo 2/17-type sintered magnets." Thermochimica Acta **486**(1-2): 41-45.

Zakotnik, M., Williams, A. J., Martinek, G., Harris, I. R. (2006). "Hydrogen decrepitation of a 2/17 sintered magnet at room temperature." Journal of Alloys and Compounds. Vol.13 (2006), pp.289-295

Zhang, M., Sun, G., Guo, D., Jin, Z. (2002). "Improvement of the magnetic properties of nanocomposite permanent magnetic alloys with Dy and Ga substitutions." Journal of materials processing technology **120**(2002): 265-269.

Zhang, S. Y., Xu, H., Ni, J. S., Wang, H. L., Hou, X. L., Dong, Y. D.(2007). "Microstructure refinement and magnetic property enhancement for nanocomposite $Nd_2Fe_{14}B$/[alpha]-Fe alloys by Co and Zr additions." Physica B: Condensed Matter 393(1-2): 153-157.

Zheng, Q., Peng, M., Yi, X. (1999). "Crystallization of high density polyethylene: effect of contact with NdFeB magnetic powder substrates." Materials Letters **40**(2): 91-95.